

University of Bath



PHD

Experimental Assessment and Thermal Characterisation of Lightweight Co-Polymer Building Envelope Materials

Dimitriadou, Eleni

Award date:
2015

Awarding institution:
University of Bath

[Link to publication](#)

General rights

Copyright and moral rights for the publications made accessible in the public portal are retained by the authors and/or other copyright owners and it is a condition of accessing publications that users recognise and abide by the legal requirements associated with these rights.

- Users may download and print one copy of any publication from the public portal for the purpose of private study or research.
- You may not further distribute the material or use it for any profit-making activity or commercial gain
- You may freely distribute the URL identifying the publication in the public portal ?

Take down policy

If you believe that this document breaches copyright please contact us providing details, and we will remove access to the work immediately and investigate your claim.

**Experimental Assessment and Thermal Characterisation of Lightweight
Co-Polymer Building Envelope Materials**

Eleni Anastasia Dimitriadou

Thesis submitted for the degree of Doctor of Philosophy

University of Bath, United Kingdom
Department of Architecture and Civil Engineering

March 2015

COPYRIGHT

Attention is drawn to the fact that copyright of this thesis rests with its author. A copy of this thesis has been supplied on condition that anyone who consults it is understood to recognise that its copyright rests with the author and that they must not copy it or use material from it except as permitted by law or with the consent of the author.

This thesis may be made available for consultation within the University Library and may be photocopied or lent to other libraries for the purposes of consultation.

Signed on behalf of the Faculty of Engineering and Design.....

Abstract

Co-polymer facade materials have recently become a popular option in the building industry as an alternative to glazing. Ethylene Tetra-Fluoro-Ethylene (ETFE) foil has been successfully used in many projects as an innovative solution to energy-conscious design challenges. In addition, the use of ETFE membrane has resulted in significant savings in cost and structural support requirements, compared with conventional glazing, due to its low weight. There is a lack of detailed published data reporting its thermal behaviour. This study focuses on the examination of heat transfer through the ETFE membrane, and more specifically heat loss and solar gains.

The document examines the impact of the material on the energy use of a building, as well as thermal comfort and interior conditions. Through field-testing and computer simulations the research evaluates the material's thermal properties to obtain results that will assist in estimating the suitability of ETFE foil use in comparison to glass. Field-testing is used to perform a comparison of the thermal and energy behaviour of a fritted double ETFE cushion to a double glazed cover. The two experimental devices under examination present nearly identical energy consumption due to heating requirements. The experimental findings are implemented in Integrated Environmental Solutions (IES) and used to identify the necessary steps to accurately reproduce the thermal and energy behaviour associated with both covering materials. Further simulations were undertaken to provide a comparison of several types of ETFE cushions to various types of double glass. More specifically, the types examined are a clear double ETFE roof cover and a fritted double ETFE roof cover in comparison to a standard double glazed roof and a low-E double glazed roof. The roof covers are examined in relation to energy requirements for both the heating and cooling of a space. Such an assessment of performance will provide information for further investigation to improve the material's features and optimise energy performance.

Acknowledgements

This work would not have been possible without the assistance of a number of people. Prior to all I would like to thank my parents, Nouli Harouli and Dr Dinos Dimitriadis, for encouraging and assisting me through the long process of completing this thesis. I would also like to thank my supervisors, Dr Steve Lo and Dr Andy Shea, for giving me the opportunity to complete this PhD under their guidance. Furthermore, I would like to express my appreciation to the laboratory technicians of the University of Bath Department of Architecture and Civil Engineering – and particularly Will Bazeley; their ongoing help was instrumental to carry through the experimental work.

I would like to dedicate this thesis to my brother, Alexandros Dimitriadis, who has been the quiet force driving my decisions and the motivation for me to carry on.

Contents

Abstract.....	ii
Acknowledgements	iii
Abbreviations	vii
Nomenclature.....	viii
Subscripts	xi
List of Figures / Charts	xi
List of Tables.....	xx
1 Introduction to research.....	1
1.1 Background.....	1
1.2 Literature supporting the research.....	3
1.3 Aims, objectives and research methodology.....	4
1.4 Contribution to knowledge, impact of work	6
1.5 Boundaries and limitations	7
2 Introduction to ETFE.....	9
2.1 Background.....	9
2.2 Information on ETFE foil.....	10
2.3 Manufacturing and assembly of ETFE foil and cushions.....	14
2.4 Comparison of ETFE foil with glass.....	21
2.5 Comparison of ETFE foil with other plastics	25
3 Heat transfer	30
3.1 Background.....	30
3.2 The thermal behaviour of greenhouses	35
3.3 The thermal behaviour of films, glass and ETFE foils and cushions	40
3.4 Material properties – lab based spectral data	48
3.5 Methods for the measurement of heat transfer through ETFE foils and cushions.....	57
4 In-situ experiment.....	65
4.1 Planning of experiment.....	65

4.2	Box calibration.....	72
4.3	Results – Exterior conditions	74
4.4	Long-wave radiation and emissivity	78
4.5	Results and analysis – Interior conditions and energy consumption	81
4.6	Summary and conclusions	94
5	Primary modelling using IES.....	96
5.1	Computational modelling of the energy and thermal behaviour of an ETFE cushion.....	96
5.1.1	Primary modelling using IES	97
5.1.2	IES background calculations	99
5.1.3	Weather file preparation.....	104
5.1.4	Representing the physical model in IES	110
5.1.5	Calibration.....	111
5.1.6	Digital model construction	140
5.1.7	IES model results and accuracy	143
5.1.8	Analysis	144
5.2	Computational modelling of the shape of an ETFE cushion.....	146
5.2.1	Digital model construction	147
5.2.2	IES model results and accuracy	150
5.2.3	Summary and conclusions	153
6	Secondary modelling using IES.....	155
6.1	The energy saving potential of ETFE cushions when used to replace glass as a roofing material	155
6.2	Preparation of secondary modelling using IES	155
6.3	Secondary modelling results	160

6.3.1	Performance comparison of clear double ETFE-covered notional building to standard double glass-covered notional building	161
6.3.2	Results analysis	165
6.3.3	Performance comparison of clear double ETFE-covered notional building to low-E double glass-covered notional building	168
6.3.4	Results analysis	171
6.3.5	Performance comparison of fritted double ETFE-covered notional building to standard double glass-covered notional building	174
6.3.6	Results analysis	177
6.3.7	Performance comparison of fritted double ETFE-covered notional building to low-E double glass-covered notional building	181
6.3.8	Results analysis	184
6.4	Summary and conclusions	189
7	Conclusions.....	195
7.1	Aims and objectives, and degree to which each was met.....	195
7.2	Impact and significance of work.....	198
7.3	Summary and conclusions	200
	References.....	205
	Appendix A: Trade values for construction materials and components.....	213
	Appendix B: Long-wave radiation and emissivity.....	214
	Appendix C: Detailed measurements of experimental interior conditions.....	220
	Appendix D: Calculation of the U-value of the two-layered ETFE cushion.....	223
	Appendix E: East Building drawings, IES default material properties and weather conditions.....	226

Abbreviations

AF:	Aluminum Foil
AHAM:	Association of Home Appliance Manufacturers
ASTM:	(formerly known as) American Society for Testing and Materials
BR:	Building Regulations
BS:	British Standards
BSI:	British Standards Institution
CET:	Central European Time
CFD:	Computational Fluid Dynamics
CIBSE:	Chartered Institution of Building Services Engineers
CO ₂ :	Carbon Dioxide
CWCT:	Centre for Window and Cladding Technology
DIN:	Deutsches Institut für Normung (=German Institute for Standardisation)
EFEP:	Ethylene-Fluorinated Ethylene Propylene
EPD:	Environmental Product Declaration
EPDM:	Ethylene Propylene Diene Monomer
ETFE:	Ethylene Tetra-Fluoro-Ethylene
FEP:	Fluorinated Ethylene Propylene
FIR:	Far Infra-Red
FTIR:	Fourier Transform Infra-Red
HES:	High-Energy Solar
HVAC:	Heat, ventilation and air conditioning
IES:	Integrated Environmental Solutions
IR:	Infra-Red
ISO:	International Organisation for Standardisation
JIS:	Japanese Industry Standards
LAT:	Local apparent time
LBNL:	Lawrence Berkeley National Laboratory
LMT:	Local mean time
Low-E:	Low Emissivity
LWIR:	Long-Wave Infra-Red
MRT:	Mean Radiant Temperature
MWIR:	Mid-Wave Infra-Red
NIR:	Near Infra-Red
NPL:	National Physical Laboratory
NS:	National Statistics
PE:	Poly-Ethylene
PIR:	Poly-Iso-Cyan-Urate
PTFE:	Poly-Tetra-Fluoro-Ethylene

PV-ETFE:	Photo-Voltaic-Ethylene-Tetra-Fluoro-Ethylene
PVC:	Poly-Vinyl Chloride
SWIR:	Short-Wave Infra-Red
TP:	Thermo-Plastics
TPE:	Thermo-Plastic Elastomer
UV:	Ultra Violet
WB:	Polyamide
WUFI:	Wärme und Feuchte instationär (translating from German to: Heat and moisture transient)

Nomenclature

q :	Heat flow (W)
k :	Thermal conductivity (W/m °C)
A :	Heat transfer surface area (m ²)
T :	Temperature (°C or K)
x :	Length (m)
q_c :	Heat flow by convection (W)
h :	Heat transfer coefficient (W/m ² °C)
$T_s - T_\infty$:	Temperature potential difference for heat flow away from surface (°C)
q_r :	Heat flow by radiation (W)
σ :	Stefan-Boltzmann constant (5.67 *10 ⁻⁸ W/m ² K ⁴)
ε :	Emissivity (0< ε <1)
λ_{max} :	Maximum intensity wavelength (nm)
b :	Wien's displacement constant (2.89*10 ⁻³ mK)
E_b :	Blackbody emissive power
$E_{\lambda,b}$:	Spectral black body emissive power
β_1, β_2 :	Constants
λ :	Wavelength (nm)
h_p :	Planck's constant (6.62 x 10 ⁻³⁴ Js)
dF_{d1-d2} :	Fraction of energy that leaves a black body element dA_1 and arrives at a black body element dA_2 (W)
θ :	Angle (°)
θ_i :	The angle normal to a surface dA_i and the length R between two elements dA_i and dA_j (°)
θ_j :	The angle normal to a surface dA_j and the length R between two elements dA_i and dA_j (°)
R :	Length of line joining two elements dA_i and dA_j (m)
Q_h :	Heat supplied/required by the heating system of a greenhouse (W/m ²)
H_S :	Convective heat transfer from soil inside greenhouse (W/m ² K)

$H_{c,i}$:	Convective heat transfer from inside of greenhouse cover (W/m ² K)
$H_{f,s}$:	Exchange of heat due to air leakage in greenhouse (W/m ² K)
$R_{n,e}$:	Net radiation outside the greenhouse (W/m ²)
R_a :	Atmospheric radiation (W/m ²)
$R_{c,e}$:	Radiation emitted by the outer cover surface of greenhouse (W/m ²)
$R_{n,i}$:	Net radiation inside greenhouse (W/m ²)
$R_{c,i}$:	Radiation emitted by greenhouse inner cover surface (W/m ²)
R_s :	Radiation emitted by soil inside greenhouse (W/m ²)
$H_{c,e}$:	Convective heat transfer from greenhouse outer cover surface (W/m ²)
$H_{c,i}$:	Convective heat transfer from greenhouse inner cover surface (W/m ²)
Q_{ai} :	Sensible heat loss due to leakage in a greenhouse (W/m ²)
h_{ai} :	Sensible heat transfer coefficient (W/m ² °C or W/m ² K)
h_r :	Radiative heat transfer coefficient (W/m ² °C or W/m ² K)
ρ_{air} :	Air density (kg/m ³)
c_a :	Specific heat capacity of air (J/kg °C)
N :	Air leakage rate per hour in a greenhouse
V :	Greenhouse air volume (m ³)
A_g :	Ground area (m ²)
Q_i :	Latent heat loss due to air leakage (W)
γ :	Psychrometric constant (0,0667 kPa/K)
e :	Water vapour pressure (kPa)
Q :	Heat loss (W)
U :	U value, the overall heat transfer coefficient (W/m ² K)
ΔT :	Temperature difference (K)
L_d :	Downward long-wave radiation (W/m ²)
L_{net} :	Measured net long-wave radiation (W/m ²)
$T_{a\ ETFE}$:	Interior air temperature of the ETFE- receiving box (°C)
$T_{a\ glass}$:	Interior air temperature of the glass- receiving box (°C)
$T_{bb\ ETFE}$:	Interior black-bulb temperature of the ETFE- receiving box (°C)
$T_{bb\ glass}$:	Interior black-bulb temperature of the glass- receiving box (°C)
$T_w\ ETFE$:	Interior wall temperature of the ETFE- receiving box (°C)
$T_w\ glass$:	Interior wall temperature of the glass- receiving box (°C)
$T_r\ ETFE$:	Interior roof surface temperature of the ETFE- receiving box (°C)
$T_r\ glass$:	Interior roof surface temperature of the glass- receiving box (°C)
RH_{ETFE} :	Interior relative humidity of the ETFE- receiving box (%)
RH_{glass} :	Interior relative humidity of the glass- receiving box (%)
P_{ETFE} :	Recorded pulses for the ETFE- receiving box
P_{glass} :	Recorded pulses for the glass- receiving box

e_{rel} :	Relative error
R_{meas} :	Measured value
R_{pred} :	Predicted value
ρ :	Density of solid (kg/m ³)
c_s :	Specific heat capacity of solid (J/kg*K)
v :	Wind speed (m/s)
f :	Coefficient depending on mean air speed
g :	Coefficient depending on surface orientation
j :	Exponent
$d\omega$:	Element of solid angle
dA :	Element of surface area (m ²)
T_s :	Surface temperature (K)
T_{MRT} :	Mean radiant temperature of enclosure (K)
y :	Auxiliary quantity used in the equations
J :	Number of day of the year
z :	Variable difference in time between the actual culmination of the sun and noon
Λ :	Geographical longitude
w :	Distance between the sun and the meridian
ψ :	Declination. Expresses the distance of the sun from the celestial equator
φ :	Geographical latitude
I_{dir} :	Direct radiation vertically incident on a surface facing the sun
ξ :	Solar altitude
$I_{diffuse_in}$:	Diffuse component scattered by the air and the clouds
P :	Tilt of surface from the horizontal
η :	Azimuth to the surface
η_s :	Solar azimuth
G_o :	Hourly extra-terrestrial radiation (MJ/m ²) (1 MJ=277.78 Wh)
I_{sc} :	Solar constant (1367 kW/m ²)
E_o :	Eccentricity correction
Γ :	Day angle
ω_s :	Sunset-hour angle for a horizontal surface
L_o :	Long-wave radiation under a clear sky (W/m ²)
ε_o :	Clear sky emissivity
T_a :	Air temperature (K)
T_{dp} :	Dew point temperature (°C)
e_s :	Saturated water vapour pressure
μ, ν, δ, ζ :	Experimentally derived coefficients
RH :	Relative humidity

e_w :	Vapour pressure related to wet-bulb temperature
n :	Cloud fraction, the amount of cloud presence (in percentage of unity)
N :	Clearness factor (Okta)
T_c :	Average cloud base temperature (°C)
h_b :	Thermal conductance coefficient of air trapped inside ETFE cushion (W/m ² K)
h_c :	Convective coefficient (W/m ² K)
h_r :	Radiative coefficient (W/m ² K)
h_{ro} :	Radiative coefficient for a black-body surface (W/m ² K)
T_m :	Mean thermodynamic temperature of the surface and its surroundings (K)

Subscripts

i :	Inside / interior
o :	Outside
e :	Exterior

List of Figures / Charts

Figure 1.1: Value of Overseas Trade for the United Kingdom in Materials and Components for Constructional Use: Summary of Imports (cost, insurance, freight) & Exports (freight on board) In Thousand Pounds (Statistics, 2005; Statistics, 2010) ...	2
Figure 2.1: ETFE roof of the Burger's Zoo Desert Hall, Vector Foiltec, 1982 (VectorFoiltec, 2011)	9
Figure 2.2: (Left to right) Eden Project, Nicholas Grimshaw and Partners, 2001; Allianz Arena, Herzog & de Meuron, 2005; Interior of the National Aquatics Centre, PTW Architects and Arup, 2008 (buildingskins, 2010)	10
Figure 2.3: Typical uniaxial stress-strain curves at different orientations (Galliot <i>et al.</i> , 2011).....	12
Figure 2.4: Detail of the framing and wires that protect the material from birds puncturing the cushions (LeCuyer <i>et al.</i> , 2008)	16
Figure 2.5: Air valve embedded on the ETFE foil (LeCuyer <i>et al.</i> , 2008)	17
Figure 2.6: Schematic section of spring-cushion structure (Wu <i>et al.</i> , 2011).....	19
Figure 2.7: Spring-cushion structure (Wu <i>et al.</i> , 2011).....	19

Figure 2.8: Types of air-cushion-membrane structures (Toyoda et al., 2013)	19
Figure 2.9: Flexible photovoltaic construction integrated in an ETFE cushion (Cremers, 2009).....	20
Figure 3.1: Heat radiation from black body - external surroundings at absolute zero temperature (Toolbox, 2013)	32
Figure 3.2: View factor associated with radiation exchange between surfaces of area dA_i and dA_j (Incopera et al., 1985).....	34
Figure 3.3: Solar and terrestrial radiation (UDEL, 2014).	35
Figure 3.4: Calculated comparative total transmission of polymer films for a 0.5 mm thickness (Wu et al., 2008)	41
Figure 3.5: Minimum and maximum values of the coefficient of heat transfer (W/m^2K) for several types of greenhouse covering materials (Papadakis et al., 2000).....	42
Figure 3.6: Experimental structure with ETFE roof built by the Fraunhofer Institut für Bauphysik (Antretter et al., 2011)	43
Figure 3.7: Heat flow distribution within cushion as occurring from the use of CFD (Antretter et al., 2011)	44
Figure 3.8: Experimental Glass and ETFE composite cladding system (Max et al., 2012)	45
Figure 3.9: Hot box setup with open lids (Max <i>et al.</i> , 2012)	46
Figure 3.10: FTIR Perkin Elmer Spectrum 100 spectrophotometer.....	48
Figure 3.11: Electromagnetic radiation spectrum (μm) (Poirazis et al., 2010).	49
Figure 3.12: Tested ETFE samples (Starting from the left: clear, clear fritted, white, matt, white fritted foil)	49
Figure 3.13: Transmission of clear, matt and white ETFE foil	51
Figure 3.14: Treated ETFE samples.....	53
Figure 3.15: Transmission of weighed clear and white fritted ETFE foil	54

Figure 3.16: Transmission of clear and white fritted ETFE foil	55
Figure 4.1: Experimental set-up on the roof of the Department of Architecture and Civil Engineering building.....	65
Figure 4.2: Experimental set-up.....	65
Figure 4.3: The ETFE cushion alongside the double glazed unit	66
Figure 4.4: Figure 4.3: Wall-mounted fan (Fantronix, 2013).....	66
Figure 4.5: Figure 4.2: Wall-mounted exhaust vent (Masters, 2013)	66
Figure 4.6: Schematic plan and section of experimental setup	67
Figure 4.7: Schematic diagram of experimental setup	68
Figure 4.8: Schematic frame detail	69
Figure 4.9: Black bulb thermometers	70
Figure 4.10: Schematic diagram of electrical and electronic devices set-up	71
Figure 4.11: CMP3 Pyranometer by Kipp & Zonen (Kipp&Zonen, 2012)	72
Figure 4.12: CGR3 Pyrgeometer by Kipp & Zonen (Kipp&Zonen, 2012)	72
Figure 4.13: Shortwave radiation (W/m^2).....	75
Figure 4.14: External air temperature ($^{\circ}C$).....	76
Figure 4.15: Downward long-wave radiation (W/m^2).....	78
Figure 4.16: Emissivity ϵ	80
Figure 4.17: Internal air temperatures ($^{\circ}C$) in relation to clear sky long-wave radiation (W/m^2).....	83
Figure 4.18: Internal air temperatures ($^{\circ}C$) in relation to overcast sky long-wave radiation (W/m^2)	84
Figure 4.19: Internal radiant temperatures ($^{\circ}C$) in relation to clear sky long-wave radiation (W/m^2)	85

Figure 4.20: Internal radiant temperatures (°C) in relation to overcast sky long-wave radiation (W/m ²)	86
Figure 4.21: Wall surface temperature (°C) in relation to clear sky long-wave radiation (W/m ²).....	87
Figure 4.22: Wall surface temperature (°C) in relation to overcast sky long-wave radiation (W/m ²)	87
Figure 4.23: Roof interior surface temperature (°C) in relation to clear sky long-wave radiation (W/m ²)	89
Figure 4.24: Roof interior surface temperature (°C) in relation to overcast sky long-wave radiation (W/m ²)	89
Figure 4.25: Interior in relation to exterior relative humidity (%) under a clear sky ...	90
Figure 4.26: Interior in relation to exterior relative humidity (%) under an overcast sky	91
Figure 4.27: Energy consumption (kWh) per interior-external air temperature difference (°C) under a clear sky.....	93
Figure 4.28: Energy consumption (kWh) per interior-external air temperature difference (°C) under an overcast sky	93
Figure 5.1: Equation of time (Stine et al., 1985).....	106
Figure 5.2: Hour angle (Stine et al., 1985).....	107
Figure 5.3: Solar declination (Stine et al., 1985).....	108
Figure 5.4: Primary model built in the IES ModelIT environment	112
Figure 5.5: IES Edit Construction materials palette of the Building Template Manager	112
Figure 5.6: MacroFlo tool of the IES multizone air movement interface	113
Figure 5.7: Mean values of simulated in relation to measured energy consumption (kWh) for the glass covered box, 1 st group of simulations: initial stages of modelling	116

Figure 5.8: Mean values of simulated in relation to measured energy consumption (kWh) for the glass covered box, 2 nd group of simulations: materials refinement ...	118
Figure 5.9: ApacheHVAC tool of the IES HVAC system simulation interface.....	119
Figure 5.10: Edit Thermal tool of the IES Building Template Manager.....	120
Figure 5.11: Mean values of simulated in relation to measured energy consumption (kWh) for the glass covered box, 3 rd group of simulations: Bespoke heating and ventilation system implementation (1 st attempt)	122
Figure 5.12: Mean values of simulated in relation to measured energy consumption (kWh) for the glass covered box, 4 th group of simulations: Bespoke heating and ventilation system implementation (2 nd attempt)	124
Figure 5.13: Mean values of simulated in relation to measured energy consumption (kWh) for the glass covered box, 5 th group of simulations: Bespoke heating and ventilation system implementation (3 rd attempt).....	126
Figure 5.14: Measured and simulated energy consumption for the glass-covered box (kWh)	127
Figure 5.15: Measured and simulated air temperature for the glass-covered box (°C)	127
Figure 5.16: Measured and simulated radiant temperature for the glass-covered box (°C).....	128
Figure 5.17: Schematic annotation of the modelled ETFE layers.....	129
Figure 5.18: Mean values of simulated in relation to measured energy consumption (kWh) for the ETFE covered box, 1 st group of simulations: ETFE membrane representation	131
Figure 5.19: Mean values of simulated in relation to measured energy consumption (kWh) for the ETFE covered box, 2 nd group of simulations: examining the effect of distance between ETFE membranes.....	134
Figure 5.20: Mean values of simulated in relation to measured energy consumption (kWh) for the ETFE covered box, 3 rd group of simulations: air infiltration and heat loss through the ETFE frame (1 st attempt)	136

Figure 5.21: Mean values of simulated in relation to measured energy consumption (kWh) for the ETFE covered box, 4 th group of simulations: heat loss through the ETFE frame (2 nd attempt)	138
Figure 5.22: Measured and simulated energy consumption for the ETFE-covered box (kWh)	139
Figure 5.23: Measured and simulated air temperature for the ETFE-covered box (°C)	139
Figure 5.24: Measured and simulated radiant temperature for the ETFE-covered box (°C).....	140
Figure 5.25: Energy consumption of the ETFE box per air temperature degree difference under clear sky conditions	145
Figure 5.26: Energy consumption of the ETFE box per air temperature degree difference under overcast sky conditions.....	146
Figure 5.27: Representation of ETFE cushion in SketchUp through faceted surfaces	147
Figure 5.28: IES models used for different representation of the ETFE cushion through a number of flat surfaces.....	148
Figure 5.29: Mean values of simulated in relation to measured energy consumption (kWh) for various faceted ETFE covered box	150
Figure 5.30: Measured and simulated energy consumption for the faceted ETFE-covered box (kWh)	151
Figure 5.31: Measured and simulated air temperature for the faceted ETFE-covered box (°C).....	152
Figure 5.32: Measured and simulated radiant temperature for the faceted ETFE-covered box (°C)	152
Figure 6.1: North façade of the East Building, main entrance to the building	156
Figure 6.2: ETFE cushions covering the central atrium as viewed from the building interior.....	156

Figure 6.3: West façade of the East Building	156
Figure 6.4: South façade of the East Building	156
Figure 6.5: East Building modelled in IES: format plan view	157
Figure 6.6: East Building modelled in IES: format axonometric view	157
Figure 6.7: East Building modelled in IES: model viewer South-West 3d view.....	157
Figure 6.8: East Building modelled in IES: model viewer North-East 3d view	157
Figure 6.9: Simulated East Building atrium air temperature: comparison between a clear double ETFE and a standard double glazed roof	162
Figure 6.10: Simulated East Building atrium radiant temperature: comparison between a clear double ETFE and a standard double glazed roof	162
Figure 6.11: Simulated East Building atrium energy consumption due to heating: comparison between a clear double ETFE and a standard double glazed roof.....	163
Figure 6.12: Simulated East Building atrium energy consumption due to cooling: comparison between a clear double ETFE and a standard double glazed roof.....	164
Figure 6.13: Simulated interior air and radiant temperature differences (°C) between the clear double ETFE-covered building and standard double glass-covered building under clear sky L_{\downarrow} (W/m ²)	165
Figure 6.14: Simulated interior air and radiant temperature differences (°C) between the clear double ETFE-covered building and standard double glass-covered building under overcast sky L_{\downarrow} (W/m ²)	166
Figure 6.15: Simulated heating energy consumption difference (kWh) between the clear double ETFE-covered building and standard double glass-covered building under clear sky L_{\downarrow} (W/m ²)	167
Figure 6.16: Simulated cooling energy consumption difference (kWh) between the clear double ETFE-covered building and standard double glass-covered building under clear sky L_{\downarrow} (W/m ²)	167
Figure 6.17: Simulated East Building atrium air temperature: comparison between a clear double ETFE and a low-E double glazed roof	168

Figure 6.18: Simulated East Building atrium radiant temperature: comparison between a clear double ETFE and a low-E double glazed roof 169

Figure 6.19: Simulated East Building atrium energy consumption due to heating: comparison between a clear double ETFE and a low-E double glazed roof 170

Figure 6.20: Simulated East Building atrium energy consumption due to cooling: comparison between a clear double ETFE and a low-E double glazed roof 170

Figure 6.21: Simulated interior air and radiant temperature differences (°C) between the clear double ETFE-covered building and low-E double glass-covered building under clear sky L_{\downarrow} (W/m²)..... 171

Figure 6.22: Simulated interior air and radiant temperature differences (°C) between the clear double ETFE-covered building and low-E double glass-covered building under overcast sky L_{\downarrow} (W/m²)..... 172

Figure 6.23: Simulated heating energy consumption difference (kWh) between the clear double ETFE-covered building and low-E double glass-covered building under clear sky L_{\downarrow} (W/m²) 173

Figure 6.24: Simulated cooling energy consumption difference (kWh) between the clear double ETFE-covered building and low-E double glass-covered building under clear sky L_{\downarrow} (W/m²) 174

Figure 6.25: Simulated East Building atrium air temperature: comparison between a fritted double ETFE and a standard double glazed roof..... 175

Figure 6.26: Simulated East Building atrium radiant temperature: comparison between a fritted double ETFE and a standard double glazed roof 175

Figure 6.27: Simulated East Building atrium energy consumption due to heating: comparison between a fritted double ETFE and a standard double glazed roof 176

Figure 6.28: Simulated East Building atrium energy consumption due to cooling: comparison between a fritted double ETFE and a standard double glazed roof 177

Figure 6.29: Simulated interior air and radiant temperature differences (°C) between the fritted double ETFE-covered building and standard double glass-covered building under clear sky L_{\downarrow} (W/m²)..... 178

Figure 6.30: Simulated interior air and radiant temperature differences (°C) between the fritted double ETFE-covered building and standard double glass-covered building under overcast sky L_{\downarrow} (W/m²) 179

Figure 6.31: Simulated heating energy consumption difference (kWh) between the fritted double ETFE-covered building and standard double glass-covered building under clear sky L_{\downarrow} (W/m²) 180

Figure 6.32: Simulated cooling energy consumption difference (kWh) between the fritted double ETFE-covered building and standard double glass-covered building under clear sky L_{\downarrow} (W/m²) 180

Figure 6.33: Simulated East Building atrium air temperature: comparison between a fritted double ETFE and a low-E double glazed roof 182

Figure 6.34: Simulated East Building atrium radiant temperature: comparison between a fritted double ETFE and a low-E double glazed roof 182

Figure 6.35: Simulated East Building atrium energy consumption due to heating: comparison between a fritted double ETFE and a low-E double glazed roof 183

Figure 6.36: Simulated East Building atrium energy consumption due to cooling: comparison between a fritted double ETFE and a low-E double glazed roof 184

Figure 6.37: Simulated interior air and radiant temperature differences (°C) between the fritted double ETFE-covered building and low-E double glass-covered building under clear sky L_{\downarrow} (W/m²) 185

Figure 6.38: Simulated interior air and radiant temperature differences (°C) between the fritted double ETFE-covered building and low-E double glass-covered building under overcast sky L_{\downarrow} (W/m²) 186

Figure 6.39: Simulated heating energy consumption difference (kWh) between the fritted double ETFE-covered building and low-E double glass-covered building under clear sky L_{\downarrow} (W/m²) 187

Figure 6.40: Simulated cooling energy consumption difference (kWh) between the fritted double ETFE-covered building and low-E double glass-covered building under clear sky L_{\downarrow} (W/m²) 188

Figure 7.1: Materials classification according to average interior air and radiant temperatures under cold weather conditions	203
Figure 7.2: Materials classification according to average interior air and radiant temperatures under warm weather conditions	203
Figure 7.3: Materials classification according to total energy consumption	204
Figure B.1: Downward long-wave radiation (W/m^2) model	218
Figure C. 1: Interior air temperature ($^{\circ}C$) for both boxes in ten minute intervals.....	220
Figure C. 2: Interior radiant temperature ($^{\circ}C$) for both boxes in 10 minute intervals	220
Figure C. 3: Interior wall surface temperature ($^{\circ}C$) for both boxes in 10 minute intervals	221
Figure C. 4: Interior roof surface temperature ($^{\circ}C$) for both boxes in 10 minute intervals	221
Figure C. 5: Interior relative humidity (%) for both boxes in 10 minute intervals.....	222
Figure C. 6: Energy consumption (kWh) for both boxes in 10 minute intervals	222
Figure E. 1: External air temperature ($^{\circ}C$) for East building modelling	235
Figure E. 2: Shortwave radiation (W/m^2) for East building modelling	235
Figure E. 3: Long-wave radiation (W/m^2) for East building modelling	236

List of Tables

Table 2.1: Calculated U-value, g-value and visible transmission τ for a double ETFE layer panel aged in urban outdoors. Optical and solar properties were evaluated at initial time (T0), after three months (T3) and six months (T6) of exposure, as well as for different tilt angles from the horizontal (0° , 45° and 90°) (Mainini <i>et al.</i> , 2014)	11
Table 2.2: Tensile strength and strain at break in relation to temperature (Zhang <i>et al.</i> , 2012).....	13

Table 2.3: Comparison of U-value of ETFE Cushion and Glass (CWCT, 2010; Robinson-Gayle <i>et al.</i> , 2001).....	22
Table 3.1: Result summary of thermal properties of greenhouse covering materials (Feuilloy <i>et al.</i> , 1996).....	39
Table 3.2: Result summary of a novel Glass-ETFE cladding system (Max <i>et al.</i> , 2012).....	46
Table 3.3: Average transmission values (%) of untreated ETFE foil.....	52
Table 3.4: Peak transmission values of untreated types of ETFE foil.....	52
Table 3.5: Average weighed transmission values (%) of treated ETFE foil.....	54
Table 3.6: Average transmission values (%) of treated ETFE foil.....	56
Table 3.7: Peak transmission values of treated types of ETFE foil.....	56
Table 3.8: Measuring methods for thermal conductivity through plastic materials....	58
Table 3.9: Comparison of methods for the thermal characterisation of multi-foil insulation.....	62
Table 4.1: Categorisation of fully clouded and clear, sunny sky in relation to downward long-wave radiation and air temperature (Kipp & Zonen, 2010).....	77
Table 5.1: Summary of IES capabilities and limitations, and consequent actions taken.....	98
Table 5.2: <i>g</i> and <i>j</i> values according to surface types (Alamdari <i>et al.</i> , 1983).....	101
Table 5.3: Glass covered box 1 st group of simulations: initial stages of modelling .	114
Table 5.4: Mean hourly energy values (kWh) and coefficient of determination for simulated in relation to measured energy consumption for the glass covered box, 1 st group of simulations: initial stages of modelling.....	116
Table 5.5: Glass covered box 2 nd group of simulations: materials refinement.....	117

Table 5.6: Mean hourly energy values (kWh) and coefficient of determination for simulated in relation to measured energy consumption for the glass covered box, 2 nd group of simulations: materials refinement	118
Table 5.7: Glass covered box 3 rd group of simulations: Bespoke heating and ventilation system implementation (1 st attempt).....	120
Table 5.8: Mean hourly energy values (kWh) and coefficient of determination for simulated in relation to measured energy consumption for the glass covered box, 3 rd group of simulations: Bespoke heating and ventilation system implementation (1 st attempt).....	122
Table 5.9: Glass covered box 4 th group of simulations: Bespoke heating and ventilation system implementation (2 nd attempt).....	123
Table 5.10: Mean hourly energy values (kWh) and coefficient of determination for simulated in relation to measured energy consumption for the glass covered box, 4 th group of simulations: Bespoke heating and ventilation system implementation (2 nd attempt).....	124
Table 5.11: Glass covered box 5 th group of simulations: Bespoke heating and ventilation system implementation (3 rd attempt).....	125
Table 5.12: Mean hourly energy values (kWh) and coefficient of determination for simulated in relation to measured energy consumption for the glass covered box, 5 th group of simulations: Bespoke heating and ventilation system implementation (3 rd attempt).....	126
Table 5.13: ETFE covered box 1 st group of simulations: ETFE membrane representation	129
Table 5.14: Mean hourly energy values (kWh) and coefficient of determination for simulated in relation to measured energy consumption for the ETFE covered box, 1 st group of simulations: ETFE membrane representation.....	131
Table 5.15: ETFE covered box 2 nd group of simulations: examining the effect of distance between ETFE membranes.....	133

Table 5.16: Mean hourly energy values (kWh) and coefficient of determination for simulated in relation to measured energy consumption for the ETFE covered box, 2 nd group of simulations: examining the effect of distance between ETFE membranes	134
Table 5.17: ETFE covered box 3 rd group of simulations: air infiltration and heat loss through the ETFE frame (1 st attempt)	135
Table 5.18: Mean hourly energy values (kWh) and coefficient of determination for simulated in relation to measured energy consumption for the ETFE covered box, 3 rd group of simulations: air infiltration and heat loss through the ETFE frame (1 st attempt)	137
Table 5.19: ETFE covered box 4 th group of simulations: heat loss through the ETFE frame (2 nd attempt)	137
Table 5.20: Mean hourly energy values (kWh) and coefficient of determination for simulated in relation to measured energy consumption for the ETFE covered box, 4 th group of simulations: heat loss through the ETFE frame (2 nd attempt)	138
Table 5.21: IES model – description of experimental boxes and ducts	140
Table 5.22: Material surface emissivity values (Fermilab, 2013; InfraredServicesInc, 2013; Scigiene, 2013; University of Missouri, 1993)	141
Table 5.23: IES model – description of cladding	142
Table 5.24: Faceted ETFE covered box with various cushion types	149
Table 5.25: Mean hourly energy values (kWh) and coefficient of determination for simulated in relation to measured energy consumption for various faceted ETFE covered box	150
Table 6.1: East Building IES model description of standard double glazed and clear double ETFE units	159
Table 6.2: East Building IES model description of low-E double glazed and fritted double ETFE units	160
Table 6.3: Materials classification according to average interior air and radiant temperatures under cold and warm weather conditions	189

Table 6.4: Materials classification according to average interior air and radiant temperatures under all weather conditions throughout an entire year.....	190
Table 6.5: Materials classification according to overall energy consumption under cold and warm weather conditions.....	191
Table 6.6: Materials classification according to overall annual energy consumption	192
Table A. 1: Value of overseas trade for the United Kingdom in materials and components for constructional use: Imports (cost, insurance, freight) & Exports (freight on board) in thousand Pounds (Statistics, 2005; Statistics, 2010)	213
Table E. 1 East Building IES model default material properties	233

1 Introduction to research

1.1 Background

The number of innovations regarding material technology that have occurred over the past century allowed for a quick transmission from one architectural trend to another. The 20th century witnessed a withdrawal from typical forms of building and a tendency towards structural novelty that resulted in environmental, financial, aesthetic, comfort and safety benefits. Under these conditions, the floating glass industry, a development first introduced in 1955 that was very popular, was soon outdated and created space in the building materials' market for Ethylene Tetra-Fluoro-Ethylene (ETFE) to develop and establish its presence in the building industry (LeCuyer *et al.*, 2008).

There are certain downsides accompanying the use of glass; such as its fragility, weight and behaviour towards light and heat transmission (Clarke *et al.*, 1998; Robinson-Gayle *et al.*, 2001). If uncoated, glass presents high transmission of near Infra-Red (IR) radiation, which leads to an increase of solar gain and a consequent need for cooling in warm conditions. At the same time, uncoated glass presents a low reflectance of far IR radiation which leads to an increase in heat loss and a related rise in heating requirements during cold weather (Brauer, 1999). The excessive use of glazing also increases the embodied energy and the cost of a structure. Furthermore, the geometry of the building is often an obstacle to the use of glass.

Polymer materials have been examined as an alternative to glass cladding as they are able to offer energy savings without compromising on efficiency and occupant comfort (Clarke *et al.*, 1998; Robinson-Gayle *et al.*, 2001). ETFE stands out among the examined available polymer options, whose benefits can be summarised as its lower weight, the ability to reach larger spans, and freedom of form. Furthermore, ETFE membrane is insensitive to deformations of the primary structure, is Ultra-Violet (UV) resistant, and presents low maintenance costs such as cleaning and low hazard potential in the event of a fire, explosion or windstorm (Schween *et al.*, 2007).

ETFE membrane weighs approximately 1% of the equivalent glass required to cover the same area, therefore reducing the embodied energy of manufacturing and transport significantly than that required by glazing. The lighter weight of the membrane also results in the requirement of a lighter supporting structure than that used in a glass structure, thus further reducing cost and energy demands (LeCuyer *et al.*, 2008;

Robinson, 2005). Reduced frame structures also allow more solar radiation to the building interior, with benefits in the lighting and heating requirements of the space. These benefits have increased the demand for use of ETFE cushions in the building industry.

There is a lack of statistical information on the production and use of ETFE membrane specifically. However, Figure 1.1 presents a summary of National Statistics (NS) data of overseas trade for the United Kingdom concerning plastics used by the construction industry – including ETFE membranes – and flat glass, expressed in thousand pounds (Statistics, 2005; Statistics, 2010). Table A.1 can be found in Appendix A, presenting the detailed information used to create this chart. It is important to point out that this statistical data involves all plastic materials used in the construction process – excluding pipes, appliances, or window and door frames, in which case the chart offers a generic representation of the market tendency.

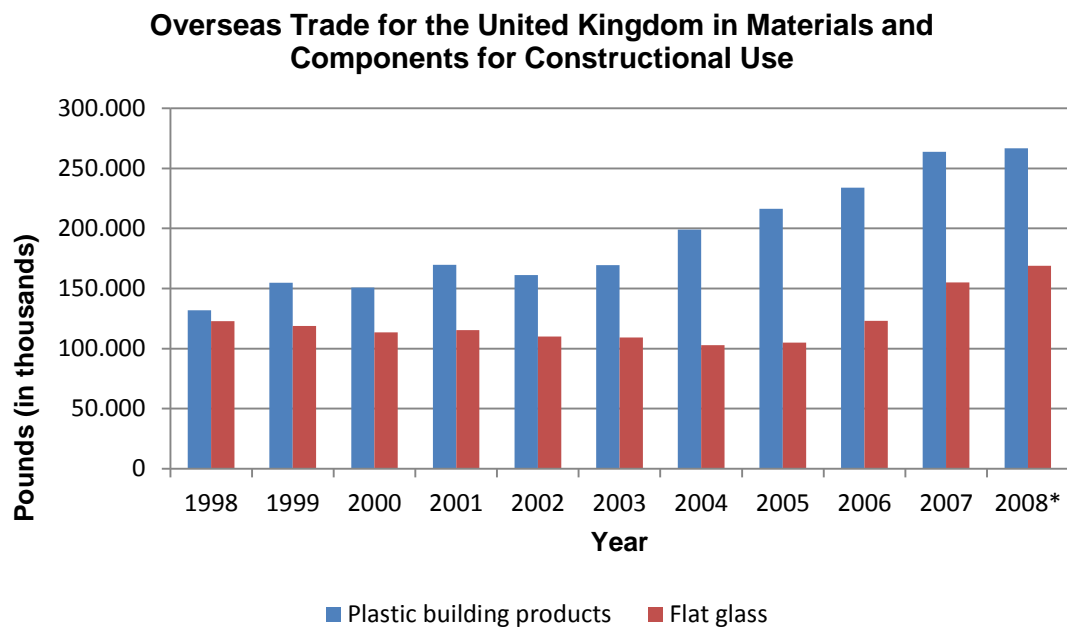


Figure 1.1: Value of Overseas Trade for the United Kingdom in Materials and Components for Constructional Use: Summary of Imports (cost, insurance, freight) & Exports (freight on board) In Thousand Pounds (Statistics, 2005; Statistics, 2010)

*The available data for 2008 covered the first 10 months of the year. In reality, the presented numbers would be expected to be slightly higher for the entire year.

Figure 1.1 demonstrates a constant, significant increase in the total of imports and exports of plastic building products in the UK over the past decade, whereas the

equivalent values for glass present a slower increase rate and at lower scale. The proportion of ETFE membrane imports and exports could not be specifically identified as part of this total, since the National Archives provided figures in summary for “plastic building products” and “flat glass”. Nevertheless, the presented data reveals a rising interest in the building industry towards plastics, which supports the stated increase in the research on, and use of, ETFE membranes.

1.2 Literature supporting the research

As Poirazis *et al.* (2010) point out; ETFE cushions cannot be treated like glass while performing an energy study on its thermal performance. There is a certain amount of ambiguity accompanying the use of the membrane regarding its thermal behaviour, which stands as a barrier for the professionals involved in the building design process from treating ETFE cushions as a more popular option.

ETFE film is transparent to long-wave radiation to a certain extent, in contrast to glass, which is opaque to it. Though several studies have examined ETFE membranes, there is still no measured information for the quantification of the long-wave radiation transmission through ETFE cushions (Poirazis *et al.*, 2010). This study aims to address this issue by performing an experimental and computational study on the thermal response of an ETFE cladding unit, alongside a glass cladding, exposed to the same external conditions and supported by the same internal condition regulating mechanism. Following, is a summary of the literature supporting the need for this work; that researchers have prepared in collaboration to the building industry, having investigated the properties of ETFE. What this work is attempting to amend is the lack of a single holistic approach covering all aspects of ETFE thermal behaviour.

Relevant work has been performed by Poirazis *et al.* (2010), who conducted a study on an ETFE cushion under a summer scenario. Heat transfer through the membrane was measured, the maximum foil temperatures were estimated and a mathematical model was developed to calculate the heat transfer for each foil.

Max *et al.* (2012) examined ETFE membranes as part of a novel greenhouse glazing system. Their work used three hot boxes that were covered alternately with a single glazed unit, in combination with a single ETFE film and the arrangement of ETFE film-glass-ETFE film, an experimental setup similar to the one used for the present work, as will be described later.

Antretter *et al.* (2008) at the Fraunhofer Institut für Bauphysik, Germany, investigated the uneven distribution of heat in the interior of membrane cushions. Their work concerned the use of a full scale model of a structure covered by an ETFE cushion to verify the results that occur when Computational Fluid Dynamics (CFD) is used to predict heat distribution under several inclinations. In synopsis, the work of Antretter *et al.* demonstrated that 30% of heat flux took place through convection and 70% through radiation, identifying the importance of the latter in the study of heat transfer through an ETFE cushion.

1.3 Aims, objectives and research methodology

This aim of this work is to investigate the nature of the plastic ETFE membrane and the potential energy benefits that accompany its use by replacing glass as a cladding material. The thesis attempts to cover the current vagueness regarding the material's thermal behaviour, which prohibits the use of the membrane from becoming a common practice option when evaluating cladding materials as per their environmental performance. The outcome of it is of interest to designers that are focused on building physics, aiming at comfortable interior conditions and low energy consumption. To achieve this goal, a number of objectives and the corresponding research methods have been set.

- Review ETFE foil and cushions as a suitable replacement for glass.

To achieve this, the current practice in ETFE membranes and cushions is examined. Plastics are evaluated as a viable alternative to glass cladding and ETFE is classified with other plastics of the same category. This process is done through literature review of journals, conference proceedings, books and product information material.

- Characterise dynamic thermal response of ETFE.

The existing theoretical and experimental research regarding the thermal behaviour of films, glass and ETFE cushions is outlined. The thermal response of ETFE membrane is analysed, regarding key heat transfer mechanisms – conduction, convection and radiation. Radiation is confirmed as a significant factor in the total heat transfer through an ETFE membrane compared to total heat transfer through glass. This is achieved through literature review of journals, conference proceedings, books, product information material, government and industry documents.

- Review standards on heat transfer measurement.

The methods for the measurement of heat transfer are specified, as established by standards and research bodies, either in a laboratory or an in-situ real life setup. This is achieved through literature review of journals and government documents.

- Quantification of radiative transfer of different types of single ETFE membrane.

This is done via laboratory-based experimentation. A Fourier Transform Infra-Red (FTIR) spectrometer is used to determine the amount of shortwave and long-wave radiation allowed through five types of single ETFE foil – clear, clear fritted, matt, white and white fritted.

- Thermal characterisation of a two-layer ETFE cushion compared to double pane of glass.

A physical experiment is performed using the hot box method, under in-situ real life conditions. The thermal behaviour of each material is expressed as a response to external conditions, using air and radiant temperatures.

- Appraise available models for the classification of sky types, in particular a detailed estimation of long-wave radiation (L) and sky emissivity (ϵ).

The existing research in literature is examined for the division to clear, partly cloudy or overcast skies and numerous other variations in between these stages. This is done through literature review of journals, conference proceedings and books. Available models are evaluated and one is selected as most able to simulate long-wave radiation based on ground measurements and the proposed experimental procedure. Experimental measurements are used to reproduce calculated results and validate the chosen long-wave and emissivity model.

- Analyse thermal behaviour of two-layer fritted ETFE cushion against double pane of glass.

This is achieved through a desk-based study and analysis of experimental results. Data is divided into separate sets regarding clear and overcast sky conditions. The correlation between energy consumption of experimental boxes and air temperature, shortwave and long-wave radiation is determined.

- Devise design template for the optimal deployment of architectural ETFE cushions.

This is performed via computer aided thermal and energy modelling. More specifically, Integrated Environmental Solutions (IES) building simulation program is used to reproduce measured performance of experimental units. The necessary modifications and considerations to achieve agreement between recorded and simulated performance are discussed. Guidance is provided for designers who attempt to estimate thermal and energy performance of an ETFE structure.

- Quantify energy saving potential of different types of ETFE cushions in relation to different types of glass.

This is performed through computer aided thermal and energy modelling. IES is used to model an existing building as a case study on the comfort and energy saving potential of ETFE cushion covers in relation to a glass covers on a typical built setup. Clear and fritted ETFE cushions are examined against standard and low-E glass, and classify them according to their thermal and energy behaviour.

1.4 Contribution to knowledge, impact of work

This work is intended to identify and fill the gaps in knowledge regarding thermal transfer through the ETFE membrane and its space heating energy saving potential. The results of this research are designed to assist architects that are researching, or dealing with, the thermal transfer behaviour of non-typical cladding materials – i.e. not glass – when performing an interdisciplinary role between architectural design and building physics. More specifically, this aims to ease and clarify the material selection process, whether that takes place at an early or later design stage. The stage of the design process is not strictly defined, as computer simulation and energy calculations are performed throughout the entire design process on various occasions, with the designer revisiting them to validate and examine decisions regarding form, orientation, materials and detailing of the structure.

The conclusions and recommendations for further work stemming from the experimental work have been published in conference proceedings. A journal paper is expected to be the outcome of computational modelling, which is anticipated to summarise and cover the knowledge gaps related to the use of ETFE cushions. The information conveyed through these publications is useful for the creation of a profile

for ETFE membranes when using thermal and energy calculation modelling. Furthermore, another outcome of the research concerns the discussion and suggestions regarding the accuracy of the digital representation of the shape of an ETFE cushion using IES or any other similar simulation tool.

Regarding the impact of this work, it involves achieving financial and environmental benefits through the use of ETFE cushions. Space heating is a significant contributor to the energy use recorded for the building sector in the United Kingdom (Government, 2012). ETFE cushions were selected as a promising alternative to glass, offering good insulation properties that could reduce the heating requirements of a building. This work assists in the better understanding and exploitation of this feature associated with ETFE cushions as a response to the UK Governmental effort to lower the energy consumption in the building sector and reach 2020 CO₂ emissions targets.

Another aspiring impact of this work is to increase occupant comfort within an ETFE structure. The air trapped inside ETFE cushions offers good insulating capacity and a comfortable interior environment, characterised by steadier air and radiant temperatures than those recorded behind glass cladding, as this research demonstrates. The present research compares the behaviour of both materials under the same conditions, characterising the thermal response of each and the consequent impact that would have on occupant comfort.

1.5 Boundaries and limitations

This research focuses on a winter heating scenario and the performed outdoors experiments took place in the United Kingdom, which presented suitable conditions for the study of heating requirements associated with an ETFE cushion roof. The case of overheating of the experimental units due to high solar input did take place and the examination of a cooling scenario was taken into consideration, however for practicality purposes the focus of the research was decided to remain around winter heating. A cooling scenario could be the item of focus for another research project in the future.

Another limitation that describes this work is that it does not examine in detail all available plastic materials that have been considered as alternatives to glass. As the number of plastic materials is significantly high, the literature review covers merely a synopsis of the suitable plastics that have been examined, as well as their structural and thermal characteristics in brief mention (Yin-ping *et al.*, 1995). The review also

describes in a compact manner the criteria by which the selection process has been made in order to conclude to ETFE membrane as the optimum choice.

Furthermore, experimentation was limited to either several single membranes of ETFE or a single double layered cushion. As typical practice entails three layered cushions (with the ability to reach a maximum of five layers), it would have been useful to carry on the research with a number of layers higher than two, or a variety of frits and colourings. However, a simplified system of two ETFE layers was selected to examine the thermal behaviour of ETFE cushions.

Finally, this study met a lack of construction industry guidance on how to test thermal transmission through ETFE cushions. To amend this issue the study followed the existing suggestions on how to test multi-foil insulation as the closest alternative (Eames, 2009). In-situ testing conditions were used for this research. The experimental units used for this study are based on the structure of the hot box setup, exposed to natural external weather conditions (Feuilloley *et al.*, 1996; Geoola *et al.*, 2009).

2 Introduction to ETFE

2.1 Background

ETFE was originally invented in 1940 by DuPont, an American chemical company, as the result of their search for an insulation material which could be used for industrial machinery (LeCuyer *et al.*, 2008). It was first used in the construction process to replace the pre-existent cladding of Teflon® Fluorinated Ethylene Propylene (FEP) that was previously installed in the Burger's Zoo, in Arnheim, The Netherlands; but had torn (Figure 2.1). This application took place in 1982 and was used to cover two plant houses; Tropical Hall and Desert Hall (Foiltec, 2011).



Figure 2.1: ETFE roof of the Burger's Zoo Desert Hall, Vector Foiltec, 1982 (VectorFoiltec, 2011)

ETFE cushions are commonly employed as cladding material in large installations that are found in hospitals, shopping malls, atria, exhibition spaces etc. (Robinson-Gayle *et al.*, 2001).

Over the past decade ETFE foils and cushions appeared in internationally renowned architectural projects, such as the 2001 Eden Project, the 2005 Allianz Arena and the 2008 National Aquatics Centre of the Beijing Olympics, otherwise known as the Water Cube (Figure 2.2). It was selected as the optimum solution to the following challenges: the matter of enclosing the maximum volume with a minimum area of material, the need to reduce the weight of the overall structure, and the requirement for plastic deformation in order to respond to seismic activity (LeCuyer *et al.*, 2008; Schween *et al.*, 2007). The material was found to be suitable for the development of unconventional architectural schemes since due to its high flexibility ETFE is able to carry well the deformations of the primary structure without affecting the load capacity or the longevity of the cushion (Schween *et al.*, 2007).



Figure 2.2: (Left to right) Eden Project, Nicholas Grimshaw and Partners, 2001; Allianz Arena, Herzog & de Meuron, 2005; Interior of the National Aquatics Centre, PTW Architects and Arup, 2008 (buildingskins, 2010)

2.2 Information on ETFE foil

ETFE is a melt-processable fluoropolymer, belonging to the sub-category of polymer materials called thermoplastics. This category relates to polymer materials that soften and become easily shaped and bent when heated (Kopeliovich, 2011).

Regarding the production process of ETFE, the primary raw ingredient is fluorite; a natural mineral which is combined with hydrogen sulphate and trichloromethane to produce chlorodifluoromethane. The resulting product undergoes pyrolysis at 700 °C in order to manufacture tetrafluoroethylene, a colourless and odourless gas. When combined to ethylene, the outcome is the ETFE copolymer in the form of powder or compressed into pellets (LeCuyer *et al.*, 2008; Robinson-Gayle *et al.*, 2001). The next step involves the heating up of the resin powder or pellets to 265-285 °C (NOVUM, 2011). Once it has been melted, ETFE is extruded in the form of film. The most frequently used extrusion process involves the use of long extruder barrels with the provision of residence time for the melting of the ETFE resin into film (DuPont, 2011).

The combination of ethylene and Teflon® supplements the foil with the beneficial features of both materials – the ease of moulding and extrusion of polyethylene and the anti-adhesive property of Teflon®. There has been an increasing demand for strength of the material mainly because of the need for large spans, the existence of high wind loads and a requirement for reduced duration of load levels. This was addressed through increasing film thickness and the number of film layers (Schöne, 2007; Schween *et al.*, 2007).

Literature indicates that ETFE is chemically very stable and has a high resistance to chemical and UV radiation, therefore it does not lose its optical properties over time (Robinson-Gayle *et al.*, 2001; Schween *et al.*, 2007). Research by Mainini *et al.* (2014) examined the effect of pollution on the thermal transmission and optical and solar performance of the specimens due to soiling. The examined ETFE panels were exposed for three and six month periods to outdoor urban conditions in the city of Milano, Italy. The ETFE samples were situated towards South orientation at different angles from the horizontal (0, 45° and 90°). A UV/Vis/NIR Spectrophotometer PerkinElmer Lambda 950 was used to measure solar, UV, visible and NIR transmission and reflectance. Light transmission and solar gain reduction through a double layer ETFE ranged on average between 4-8%. The measured reflectance and transmission of single ETFE foils were modelled using Lawrence Berkeley National Laboratory (LBNL) Optics 6.0 and thermal transmission (U-value), solar heat gain coefficient (g-value) and visible transmittance (τ) were computed using LBNL Windows 7.1. The published results of this work can be found in Table 2.1. The maximum visible and solar performance decay was noted for the horizontal specimens, whereas the minimum for the vertical specimens.

Table 2.1: Calculated U-value, g-value and visible transmission τ for a double ETFE layer panel aged in urban outdoors. Optical and solar properties were evaluated at initial time (T0), after three months (T3) and six months (T6) of exposure, as well as for different tilt angles from the horizontal (0°, 45° and 90°) (Mainini *et al.*, 2014)

	U-value of panel (W/m²K)	g-value	Visible transmission τ
2 Layer panel – Tilt 90° from horizontal			
T0	2.916	0.834	0.806
T3	2.916	0.798	0.765
T6	2.916	0.799	0.765
2 Layer panel – Tilt 45° from horizontal			
T0	2.998	0.834	0.806
T3	2.998	0.787	0.748
T6	2.998	0.783	0.742
2 Layer panel – Tilt 0° from horizontal			
T0	3.047	0.834	0.806

T3	3.047	0.790	0.753
T6	3.047	0.775	0.733

The tensile strength of the foil ranges between 35-50 MPa. Research by Wu *et al.* (2011) demonstrates that for a stress below 15 MPa, ETFE acts like a linear elastic material and its strain varies between 2-3%; in other words, it is harder to stretch than a fabric membrane. For a stress of about 22 MPa a second rigid turning point on the stress-strain curve is noticed, whereby strain reaches 15% (Wu *et al.*, 2011). Research by Galliot *et al.* (2011) found those two yielding points to be around below 20 MPa and near 25 MPa respectively, as seen in Figure 2.3. For stresses in the range of 22-45 MPa according to Wu *et al.* (2011) or between 25 and 55 MPa according to Galliot *et al.* (2011) using biaxial loading on a cruciform specimen, the strain increases until it reaches its breaking point of 350-400%, in which case ETFE acts like a bilinear elastic isotropic material.

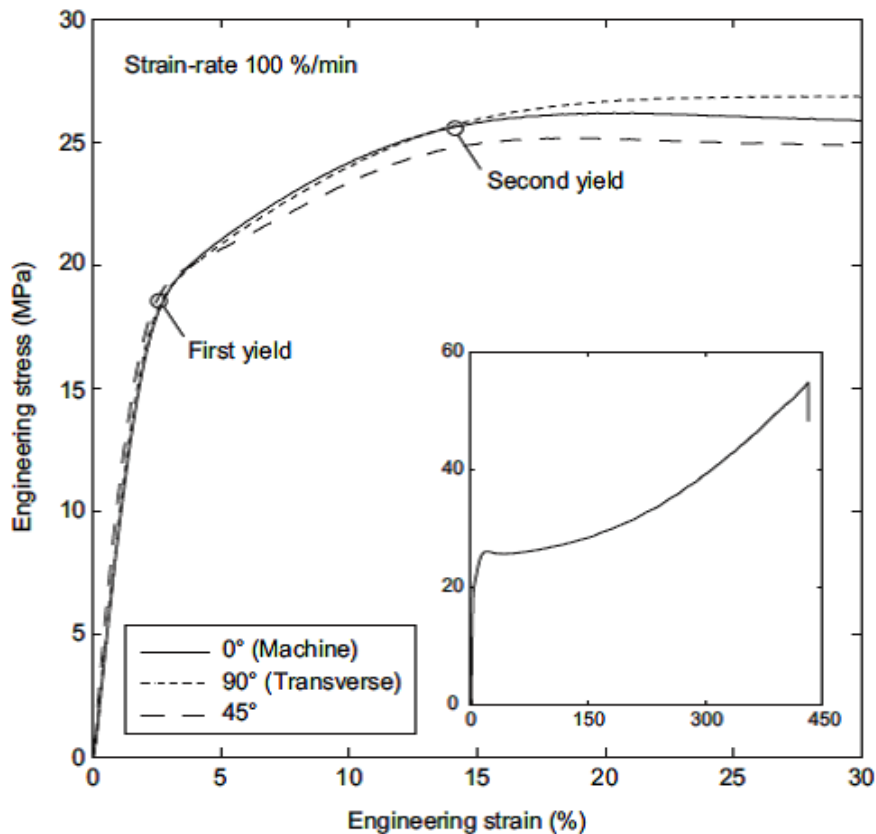


Figure 2.3: Typical uniaxial stress-strain curves at different orientations (Galliot *et al.*, 2011)

Relevant research by Charbonneau *et al.* (2014) performed 24-h uniaxial creep tests, 7-day creep tests and stress-strain tests, resulting to average yield stresses for ETFE film ranging between 24-29 MPa and average failure stresses ranging between 42-70 MPa. This work points out that ETFE film under tensile tests presents higher resistance to yield and failure in the longitudinal (the direction of extrusion) than the transverse direction. Furthermore, ETFE film was found to be more ductile in the transverse direction.

Zhang and Gao (2012) focus on the relationship between tensile strength, the strain at break, and temperature. The summarized data is presented in Table 2.2.

Table 2.2: Tensile strength and strain at break in relation to temperature (Zhang *et al.*, 2012)

Temperature (°C)	Tensile strength (MPa)	Strain at break (%)
10	48	229
15	47	224
20	42	269
40	31	321
50	31	322
60	32	324

ETFE is a very flexible material that can deform significantly before its breaking point (Tanno, 1997). Elongation decreases with an increase of temperature up to 260 °C, a turning point after which elongation rises sharply as the material enters a melting state for temperatures varying between 250 °C and 280 °C (Chen *et al.*, 2012; DuPont, 2011). In parallel, the material's tensile strength decreases with the increase of temperature up to 100 °C, after which it will not be further affected until it reaches its melting point. Finally, crystallisation of the ETFE molecules decreases as irradiation temperatures increase. In particular, the crystallisation temperature presents a rapid decrease at 270 °C, the temperature close to the switch of the elongation properties (Oshima *et al.*, 1997). Degradation occurs above 300 °C (Chen *et al.*, 2012).

Glass reinforcement is commonly used to enhance the wear properties of the material. During the construction process the glass fibres will line parallel to the direction of the flow of filling the mould. Tensile strength will be 70-75% of that parallel to fibre orientation when they are measured perpendicular to fibre orientation (DuPont, 2011).

2.3 Manufacturing and assembly of ETFE foil and cushions

ETFE foil is commonly produced either by blowing the material through a ring die or through the extrusion of the material through long extruder barrels that provide residence time for the melting of the ETFE resin (LeCuyer *et al.*, 2008; NOVUM, 2011). The process of blowing is financially more efficient than that of extrusion; however it produces foil of lower optical properties as it may cause imperfections. For that reason, it is extrusion that is the most preferred process for ETFE foil production. The produced foil can reach up to 5 m width. The thicknesses in which the foil is available vary between 50 and 250 μm (LeCuyer *et al.*, 2008).

The surfaces of ETFE foil may be treated by subjecting it to chemical applications, electrical discharges or intense radiation. More frequently it is printed, a process identified among the ETFE industry as fritting. During this procedure the printed patterns are created for the purposes of reflecting light and heat, reducing translucency; or for visual purposes, such as aesthetics or advertisement. The patterns are created by the use of sprayed-on fluoropolymer inks – usually silver, and may allow for several levels of transparency, depending on the purpose of the fritting application (LeCuyer *et al.*, 2008). Solar protection can be enhanced with the adding of more than one printed layers within the structure (Schöne, 2007). Other typical applications on glasses and plastics involve the coating with anti-abrasive, strength and impact enhancing or low-melting substances (Bugaev *et al.*, 2000; Tsilingiris, 2003).

ETFE is often coloured, however, the colouring process is found to work against its anti-adhesive property. The film can also receive a processing described by Schöne (2007) as “corona” treatment, whereby it is exposed to an electric discharge that severs the molecular bonds on the surface. The severed bonds are then free to attach the particles that exist in the corona discharge environment, causing a strong chemical attraction to inks and coatings. This method allows the creation of an imprint that will last longer on the film surface. This is found useful, as a high print coverage has been found to result to up to 60% reduction of the radiation transmission. Schöne suggested that the imprinting and irradiating are performed on the interior side of the foil to maintain its anti-adhesive nature, which protects from dirt residue remaining on the surface, requiring cleaning.

ETFE foil is typically assembled to cushions of two to five layers and welded around the edges (LeCuyer *et al.*, 2008). Thermoplastic Elastomer (TPE) is placed in the profile between the aluminium and the ETFE pillow preventing the wearing of the

material, especially in cases where the local climate will contain varying temperatures that will cause movement (NOVUM, 2011). ETFE foils are joined on the edges through a combination of heat and pressure over time, without the use of additives. At the edge of the foils, the welding is formed around a reinforcing element (typically known by the commercial name keder rod), which will either be a Polyvinyl Chloride (PVC) rope, an Ethylene Propylene Diene Monomer (EPDM) cord or an aluminium bar (Miskeen, 2009; Robinson-Gayle *et al.*, 2001; Schween *et al.*, 2007). The welding width on the edge of the cushion typically has a size of 10 mm (Schöne, 2007).

To calculate the evolution of ETFE foils under inflation and the consequent deformed geometry curvature, Hinz *et al.* (2007) performed bursting tests, analysing the material properties in the viscoelastic range up to the breaking point. A close-range photogrammetric system was used in collaboration to specific image analysis software to record the deformation in the shape of the foil when put under air pressure. The result of the work was a deformation function describing the calculated geometry curvature.

Further related work was performed by Borgart (2010), who investigated the design of the cushions and the grid of the skeleton structure, based on the optimisation algorithm of Laplace-Young, where internal air pressure is dependent on the membrane stress and radius. Cushions with a square base were found to not present a uniform stress distribution. The maximum stress appeared in the middle of the membrane, where the maximum curvature of radii is met (Borgart, 2010; Lucas *et al.*, 2007).

Another research regarding the shape of ETFE cushions is that of Bartle *et al.* (2010), who developed a numerical model for the prediction of deformation, strain and stress distribution of the cushions. Through finite element analysis, they determined the shape of a cushion as a function of the internal pressure due to air inflation and the elastic properties of the membrane. According to the findings of that research, the shape of the cushion and the stress in the membrane were found to not be co-related since ETFE foil is expected not to yield prior to an internal pressure of 800 Pa, a value that is significantly higher than the air pressure typically applied, as it will be described later on.

One of at least two boundary films forming an air chamber produces a pre-stressed membrane which is suitable for a robust structural system due to equilibrium geometry. Equilibrium geometry requires for a homogenous and isotropic stress state in the corners of areas with opposite directions of curvature (Schöne, 2007). ETFE pillows

exert a tensile load at their perimeter in addition to the external loads like snow or wind (Robertson, 2011).

The edges of the cushions are clamped and attached to the supporting structure by using aluminium profiles which embody thermal breaks and a drainage system in-between the cushions (LeCuyer *et al.*, 2008). Figure 2.4 presents a detail of the profile and an accompanying protective bird wire. On some occasions algae may form around the edges of the cushions, where the cushion camber meets the frame, forming a water puddle which attracts birds. A bird wire is therefore used to prohibit birds from sitting on the cushions' perimeter and damaging the ETFE foil in the attempt to feed on the algae.



Figure 2.4: Detail of the framing and wires that protect the material from birds puncturing the cushions (LeCuyer *et al.*, 2008)

Rainwater is guided between the cushions, on top of the frames. The cushions and frames are inclined to assist the water run-off. A gutter is located at the lowest end of the roof, to gather and drain the rainwater. The cushions and frames are cleaned manually; the person cleaning them walks either directly on the cushions or on the perimeter frames, attached by a safety rope to hooks bolted on the frames.

The work of Arasteh (1989) indicated that the burying of a spacer into a frame will result in lower edge-of-cladding U-values and slightly lower frame U-values. However, a big frame is not necessarily optimal as an increased projected frame area will cause a decrease in the overall visual area and the incoming visible light.

Air valves are fixed on the cushions (Figure 2.5). The valves are connected to an air pump system that will provide the cushion with a constant air pressure of 250-700 Pa (Miskeen, 2009; Robinson-Gayle *et al.*, 2001).

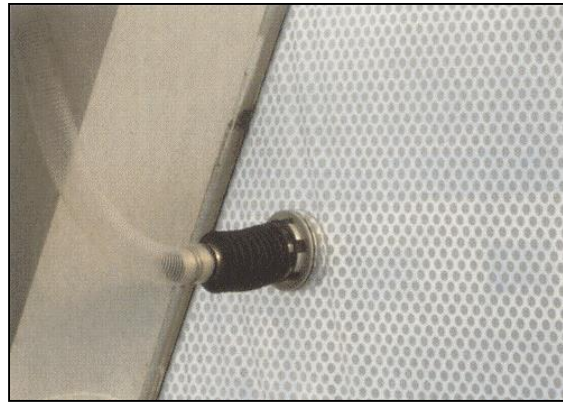


Figure 2.5: Air valve embedded on the ETFE foil (LeCuyer *et al.*, 2008)

The inflation units are linked to pressure sensors used to detect and compensate for the loss of air through imperfections on the material joints (Miskeen, 2009). The fans are connected to an electronic switch that indicates their operation as soon as interior pressure drops below the required levels. A lack of detailed, verified information on the energy consumption of the fans has been identified, an issue which this research intended to cover during the experimentation round. However, the gradual deflation of the cushions occurred at such a low rate that the pumping with air was hardly found necessary throughout the total duration of the experiment, which lasted more than three months. Therefore, this work characterises the energy consumption due to the use of inflation units as insignificant for a small ETFE cushion.

In the literature, a publication attempting to describe energy use of the embedded fans used in a large structure using ETFE cushions is that by Tanno (1997). For a roof structure of 1000 m² Tanno quantified the hourly energy consumption due to fan operation to be 100 Wh, expected to function 50% of the time, resulting to an approximate energy consumption of 438 kWh per year for the support of the cushion system. The figure estimated by Tanno is comparable to the annual electricity consumption of 440 kWh for an electric hob, as has been estimated by Newborough *et al.* (1999), for a household with an average usage pattern. This comparison is meant to demonstrate that for a large structure compiled of ETFE cushions the energy consumed on the inflation of the cushions is not negligible, though very small, as it translates to an average total of 0.44 kWh/m² of cushion area for an entire year.

In the case of failure in the air supply system, non-return valves within the system protect the cushion from deflating rapidly and allow for a leeway of 4-8 hours during which the cushion can maintain its pressure without the provision of air. Past this time a backup air supply unit will be required to operate (LeCuyer *et al.*, 2008; Robinson-Gayle *et al.*, 2001).

Dehumidifiers are required to accompany the function of the air pumps to remove the humidity that may be trapped inside cushions (LeCuyer *et al.*, 2008). Again, there is a lack of recorded energy data in relation to the use of dehumidifiers for a cushion structure. Energy Star (2012) in collaboration with the Association of Home Appliance Manufacturers (AHAM) provide with information to estimate the necessary capacity in pints to select a dehumidifier. For a moderately damp interior of 1000 m² area a dehumidifier of minimum 32 pints or 18 L capacity is estimated to be needed (Star, 2012). A Kenmore 35 pint – or 20 L – dehumidifier is selected as a representative common product from that category, with an hourly energy consumption of 530 Wh (Kenmore, 2013). If this dehumidifier runs approximately 50% of the time, the overall annual energy consumption will be 2321 kWh/yr. Keeping in mind that this is a modest option, the estimated energy requirement would translate to at least 2.3 kWh/m² of cushion area per year, constituting the energy expense on the function of dehumidifiers significantly higher than the function of the air support system.

This value is comparable to the equivalent associated to a typical domestic dehumidifier. The United States Department of Energy (2012) describes the typical hourly energy consumption of a domestic dehumidifier to be 785 Wh. If we assume that a dehumidifier of this capacity were to be employed for the support of an ETFE cladding system operating half the time, the total annual energy consumption would add up to 3438 kWh/yr, or 3.4 kWh/m² of cushion area per year. Therefore, though energy consuming, the dehumidification process of the cushions is not out of ordinary practice.

To overcome the need for inflating the cushions, Wu *et al.* (2011) suggested a spring structure embedded inside the cushion as an alternative to the air system, to avoid the drawbacks of financial and energy expenses. This system involves a combination of elastic and rigid bodies, i.e. the flexible foil, the spring, frame and stiff plates (Figures 2.6 and 2.7). A form finding and a stress analysis were performed using the finite element modelling package ANSYS. The results of the numerical analysis have not yet been published. The research concluded that the cushion maintained its shape and

appearance, with the spring successfully maintained in compression. There was no recorded need for re-tension of the foil, despite the lack of air supply and maintenance. As this is an ongoing work, following results and publications are expected to examine the suitability of this structural system for a variety of applications as an alternative to the conventional pneumatic ETFE cushion system.

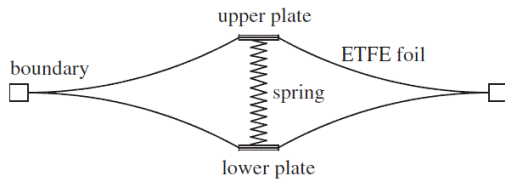


Figure 2.6: Schematic section of spring-cushion structure (Wu *et al.*, 2011)



Figure 2.7: Spring-cushion structure (Wu *et al.*, 2011)

For the reduction of rain noise a net can be applied as a damper for the incident drops, maintaining a separate layer of water in the exterior of the cushion (Schöne, 2007). However, this application will decrease the transmission of visible light. The research of Desmarais *et al.* (1999) has indicated that the smaller the mesh holes of an applied net, the larger the decrease in solar income, therefore affecting the interior temperature of the space.

Toyoda *et al.* (2010, 2013) experimented with six types of ETFE cushions in search for a solution to rainfall noise. The different types of air-cushion-membrane systems included a double and triple-layer cushion, as well as silicone-gel layers of 1 mm thickness and non-woven fabric of 8 mm thickness embedded inside and outside of the ETFE cushion (Figure 2.8).

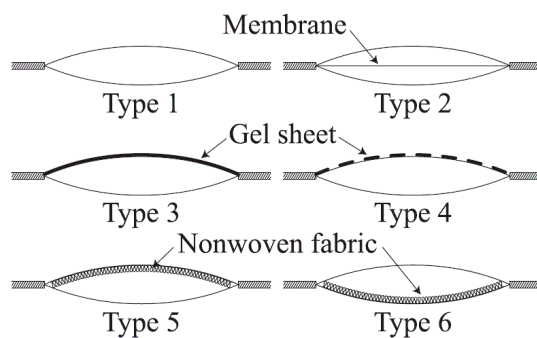


Figure 2.8: Types of air-cushion-membrane structures (Toyoda *et al.*, 2013)

The work concluded that the additional middle membrane did not have a positive effect on the reduction of rain noise. The application of silicone-gel sheet located on the outer

upper side of the cushion was the most effective towards rainfall noise reduction at frequencies between 250 and 2000 Hz, which is the most important range considering noise control. This result is due to the fact that the gel sheet provides with additional mass. The greater benefit was observed in the case when the gel sheet covered the cushion entirely, followed by the gel sheet that covered half the cushion area. Finally, the 8 mm non-woven fabric also had a beneficial effect towards the reduction of rain noise, as it provided with excitation-force deformation to the impact of raindrops on the membrane. The case where the fabric was situated on the outer layer of the cushion was more successful than the case where the fabric was located on the inner layer.

Finally, to conclude with the available alternatives regarding treatments, ways of assembling or combining ETFE foil, amorphous silicon thin-film cells can be laminated in between two ETFE sheets to further exploit solar input. The flexible photovoltaic films have a thickness of about 1 μm and are located within ETFE membranes in order to be protected against loads, stresses, moisture and weathering (Figure 2.9). The solar films have a capacity of producing 45-50 W/m^2 for a typical size of 30 x 300 cm (AGC, 2013; Cremers, 2009; SOLARNEXT, 2013). This is an innovative type of application, expected to become common-practice, in which case more information will be published regarding the behaviour of such a system.



Figure 2.9: Flexible photovoltaic construction integrated in an ETFE cushion (Cremers, 2009)

Further relevant research was undertaken by Hu *et al.* (2014), who experimented with a three-layered ETFE cushion integrating photo-voltaic panels, investigating the system's electrical performance and temperature- and pressure-related viability. The ETFE cushion was placed horizontally and the flexible, curved photo-voltaic panels were situated in the middle layer of the ETFE cushion. The experimental device scheme was named PV-ETFE system and it also comprised of an ETFE cushion support subsystem, a subsystem for solar energy control and a subsystem for pressure

control. Six experiments took place under high and average solar irradiance (ranging between 325 to 595 W/m²), taking into account the effect of ambient temperature and wind velocity upon the PV-ETFE system. The average stored electricity was 61 Wh and the system operation and feasibility were deemed successful. Although increased temperatures inside the ETFE cushion were an initial concern regarding the operation of the photo-voltaic system, eventually they did not obstruct the function of the PV-ETFE system. The authors pointed out that the potential of stored electricity for building use was not examined in that research and yearly system performance remains to be examined through future work.

2.4 Comparison of ETFE foil with glass

Glass as a cladding material presents numerous advantages that can be summarised to its quick manufacturing speed, its stability towards environmental hazards, its resistance towards scratching, its transparency, which offers good visual performance, and its low cost. On the other hand, the downsides of glass involve its fragility, weight and behaviour towards heat transmission, as it will be examined in more detail further on (Brauer, 1999). The excessive use of glazing increases the embodied energy and the cost of a structure. Furthermore, the geometry of the building is often an obstacle to the use of glass due to limitations associated with form, spanning distance and material weight. For these purposes a variety of polymer materials, including ETFE, have been tested in the pursuit of a replacement to glazing (Clarke *et al.*, 1998; Robinson-Gayle *et al.*, 2001).

As mentioned previously, the structural benefits of ETFE in comparison to glass can be summarised to its lower weight, the ability to reach larger spans and freedom of form. Furthermore, ETFE is insensitive to deformations of the primary structure, UV resistant, low maintenance costs such as cleaning and low hazard potential in the event of a fire, explosion or windstorm (Schween *et al.*, 2007).

For a typical thickness of 200 µm ETFE weighs below 0.35 kg/m² (much less than glazing, which typically weighs 10 kg/m² for a thickness of 4 mm), therefore reducing the embodied energy of manufacturing and transport to 1% of that required by glazing. The lighter weight of the membrane also results to the requirement of a lighter supporting structure than that used in a glass structure, thus reducing cost and energy demands (Knippers *et al.*, 2011; LeCuyer *et al.*, 2008; Robinson, 2005).

Regarding light transmission, ETFE allows for transmission values in the band of 280-2000 nm, from ultraviolet, including the visible spectrum which varies between 720 and 400 nm, and reaching long-wave IR radiation (Read, 1985; Schöne, 2007). A single foil transmits 94-97% of visible light, a higher percentage than the equivalent 89% of single glazing. A cushion of two ETFE layers transmits approximately 76% of visible light, which is similar to the amount of visible light transmitted by a typical double glazed unit. Due to the cushion's curvature, the visual features of ETFE will be partially obscured, which makes the material suitable for uses where clear visual contact with the exterior is not a necessity. This is one of the reasons why ETFE is not often used as wall cladding but instead is usually located on roofs (Robinson-Gayle *et al.*, 2001; Robinson, 2005).

The thermal transmission of a building element or non-homogeneous building structures in total is typically measured through the U-value, as described by the standard BS EN ISO 7345 as “the heat flow rate in the steady state divided by area and by the temperature difference between the surroundings on each side of a system” (7345, 1995; NPL, 2012).

In the case of a single ETFE layer the U-value is undesirably high and due to the small thickness of the material it can cause negative effects when calculating the overall thermal performance of a structure, especially in comparison to a glazed unit. However, since ETFE is typically assembled in cushions of at least two layers, its U-value will be lower and therefore is comparable to that of a double glazed unit due to the resistance of the air layer. Table 2.3 demonstrates the comparison of the U-value of ETFE and glass, depending on the number of foils or panes in each case (CWCT, 2010; Robinson-Gayle *et al.*, 2001).

Table 2.3: Comparison of U-value of ETFE Cushion and Glass (CWCT, 2010; Robinson-Gayle *et al.*, 2001)

Number of foils/panes	U-value (W/m ² *K)
ETFE cushion	
Two foils	2.9
Three foils	2.0
Four foils	1.5
Five foils	1.2

Glass	
Single glazing (4 mm)	5.7
Double glazing (4-6-4 mm)	3.3
Triple glazing (4-12-4-12-4 mm)	1.9

The whole-life environmental performance of a material requires evaluation of its embodied energy. Depending on the life cycle calculation, the embodied energy of a material may include the energy related to the mining of raw materials, their purification and processing, transportation, construction and the calculation of the actual energy required during the use of the material. The process goes further on, including the maintenance and disposal or recycling of a material (Capper *et al.*, 2012).

The production process of ETFE foil is much simpler than that of glass and requires less energy (Galliot *et al.*, 2011). The process for ETFE was outlined earlier on in the text, in the chapter regarding information on the foil. On the other hand, the production of glass requires the melting of raw materials to reach the melting point of silica, which is above 1700 °C with the addition of lime and soda to lower the melting point. Limestone and sodium carbonate will release carbon dioxide, in which case fining agents must be added to prevent the formation of bubbles. For the production of float glass, the molten glass is poured on a molten tin bath at the temperature of 1150 °C and cooled down with the use of hydrogen and nitrogen gases (Mangonon, 1999). A strong heat exchange occurs through the contact of the glass and metal surface of the mould, resulting in thermally induced stress. The surface can be treated with gas for the creation of a smoother surface and a strength above 130-150 MPa (Gorokhovskiy *et al.*, 2000; Hessenkemper, 2002). In summary, the manufacturing process for glass calls for excessive raw materials and significantly higher energy inputs to achieve the required melting points. (Robinson-Gayle *et al.*, 2001).

The embodied energy related to the production process of ETFE membrane, as measured per tonne, is estimated to be 26.5 GJ/t, which is comparable to that of a 6 mm pane of float glass, 20 GJ/t (Robinson, 2005). Another source specifies the importance of taking into account the frame when estimating the embodied energy of an ETFE cushion; the Institut Bauen und Umwelt (2011) produced an Environmental Product Declaration (EPD) stating that for a cushion of 1 m², for an embodied energy

of 1036.9 MJ, 31% is contributed by the foil production, 51% by the frame production and 18% by the transport to the site.

It is significant to note that the energy required for the production of a cushion also depends on the required amount of edge rod, the inflation accessories, aluminium profile and seal. Therefore, as the cushion size increases, the perimeter-to-area ratio and the embodied energy decrease (Chilton, 2013).

The light weight of ETFE foil in combination to the fact that ETFE cushions can cover larger areas than glazing creates a lower requirement of supporting panel joints. Additionally, the pillow system, the aluminium connections and the steel frames will have 10-50% of the weight that is required for the support of a typical glass cladding (Miskeen, 2009; Robinson-Gayle *et al.*, 2001; Robinson, 2005). Therefore, when its embodied energy is measured based on its coverage per material quantity it is found to be 27 MJ/m², which is much more beneficial in relation to glass: 300 MJ/m² (Robinson, 2005).

In terms of waste management ETFE foils cause little contamination in the form of gas release, as they do not fall in the riskier category of contaminating plastics which contain chlorine (La Mantia, 1996; Robinson-Gayle *et al.*, 2001). The structure of thermoplastics makes them resistant to degradation due to hydrolysis, which classifies them as non-biodegradable plastics (Zheng *et al.*, 2005). Therefore, since ETFE is a thermoplastic, it will not biodegrade and, as in the case of glass, will continue to exist within the ground for thousands of years. For that reason, recycling is preferred over landfill (Robinson-Gayle *et al.*, 2001).

Glass is widely recyclable, however float glass requires virgin materials as there are severe risks related to possible impurities that may occur from using recycled glass (Robinson-Gayle *et al.*, 2001). Impact, strength, thermal conductivity, and density are some of the properties of glass that have been registered as affected during the recycling process (Energy, 1978). Similarly, ETFE is completely recyclable but since ETFE foil must be produced from virgin materials, the recycled material is typically used in other components, like air valves or hoses (Galliot *et al.*, 2011; LeCuyer *et al.*, 2008). That is due to the fact that recycling damages the macromolecular structure of polymers, which causes changes in the properties of the materials and reduces the durability of the resulting recycled products (La Mantia, 1996).

2.5 Comparison of ETFE foil with other plastics

Polymers occur from a combination of natural elements manipulated in a chemical manner, resulting in an endless number of combinations and possible outcomes (Campo, 2008). The largest number of polymers falls under the category of plastics, which are materials primarily characterised by structural rigidity (Callister *et al.*, 2011).

The distinction between polymers and plastics lies in the fact that a polymer is a pure material occurring as a macromolecular product of polymerisation, whereas plastics or resins occur when additives are used to enhance the properties of the resulting material. As for co-polymerisation, Mangonon (1999) defines it as the result of mixing different types of structural groups within the chain of the polymer, as opposed to adding and repeating the same unit.

A combination of intensification of interest in plastics and technological improvements led to the introduction of fluoropolymers, such as Polytetrafluoroethylene (PTFE) and polyethylene in engineering applications during the 1950s. By that point, developments in research concerning plastics had sufficiently increased their impact strength and thermal stability. Plastic materials are generally divided into three categories based on their production process: thermoplastics, elastomers and thermosets, with ETFE falling into the first category (Campo, 2008).

Thermoplastics (TP) can be divided into two categories, involving the commodities which include polyethylene, polyolefins, styrenes, vinyls and others, and the engineering plastics which involve acetals, fluoroplastics, polyamides, polycarbonates, polyesters, etc. (Mangonon, 1999).

There is a significant variety of polymer materials, each suitable for different application requirements. The number of distinct products and their specifications is vast, significantly complicating the selection process. In order to choose between this variety, the designer needs to take into account the main requirements of the application, which are typically dependent on weld lines, stress concentration, temperature, humidity, fibreglass orientations or creep (Campo, 2008).

An issue that needs to be considered when it comes to choosing amongst polymers is the use of additives that are required to enhance the performance of polymers, much like in the case of the enhancement of glass performance. Such additives include flame retardants and stabilizers which will alter the properties of polymers. Furthermore, some additives, such as those regarding mechanical strength, will increase the

difficulty of processing of the material, thus raising the temperature required for melting or moulding (Campo, 2008).

The most significant properties of transparent films by which a material is selected for cladding purposes are the transmission of solar and of long-wave thermal radiation (Yin-ping *et al.*, 1995). However, stability, strength and endurance are also very important aspects in the selection process. Other properties of plastics that are important in the design development are their density, as well as their water absorption and transmission. Low density is an advantage in engineering design, as the lighter weight of construction materials will require less supporting structure. Polyethylenes are classified as a low density material, which in the case of ETFE is 1.7 g/cm³ (Mangonon, 1999).

The optical parameters regarding the properties of plastic materials concern their transmittance, haze and gloss. The last two refer to the scattering and specular reflection during transmission to the total light transmitted (Burek *et al.*, 1989). Wang *et al.* (2001) focused on the effect of haze on the optical properties of plastic membranes. Haze is defined as the percentage of transmitted light through a polyethylene blown thin film, deviating from the incident beam by more than 2.5°. Regarding the direct transmission of polymer films, when the fraction of incident radiation does not deviate from the incident direction of light exceeds 90%, the film is characterised as transparent. When the same fraction is below 90% the film is considered translucent.

One of the polymers that has been tested and found to be unsuitable in replacing glass is poly (methyl methacrylate) - known as Plexiglas or acrylic - due to its dependence of mechanical characteristics upon temperature changes at a range close to room temperatures. The material is brittle at a temperature of 4 °C, whereas it adopts a significant plastic deformation at 50-60 °C (Callister *et al.*, 2011). Though it has half the weight of glass, it still weighs significantly more than ETFE. Plexiglas has solar energy transmission of up to 85% and light transmission of 92%, which are values that are comparable to ETFE. Finally, like ETFE, it is also resistant to chemical attack, whilst remaining vulnerable to corrosion (Callister *et al.*, 2011; Plexiglas, 2011).

Due to its good optical transparency, another material that has been examined is polystyrene; it presents good thermal and structural stability, though its values are still lower than those of ETFE. General purpose polystyrene cannot be classified as an engineering thermoplastic due to its inefficient structural strength (52 MPa); for that

reason the material is also available in a High Impact form with enhanced mechanical properties. It presents lower tensile elongation and a higher thermal coefficient than ETFE, as well as a lower maximum operating temperature, and therefore classed as an inferior material for building purposes (Boedeker.com, 2012; Callister *et al.*, 2011).

Other melt-processable thermoplastics with properties similar to those of ETFE are fluorocarbons or fluoroplastics, which are characterised by their chemical inertness, high temperature resistance, very low friction coefficients and good dielectric properties (Mangonon, 1999). The main commercial product in that category is Teflon® (PTFE) fluoropolymer resin, mainly used as non-stick coating in several applications. In comparison to this material, ETFE presents a higher tensile strength and creep resistance. Compared to PTFE, ETFE is less dense and stiff and more resistant to gamma radiation. However, ETFE is inferior to fluorocarbons regarding its resistance to chemical attack and friction, even at high temperatures (DuPont, 2011).

In brief, many other polymers are unsuitable as a possible replacement for glazing, as overall they fail to offer good visual performance and energy transmittance, which are two of the main concerns of this comparison. Although some polymers will present durability, strength, chemical stability, a low weight or a combination of the above their properties will in total be inferior to those of ETFE in terms of an engineering performance (Baille *et al.*, 2006; Callister *et al.*, 2011).

The Izod impact test has classified ETFE to be amongst the polymers with the highest impact energy absorption (Miskeen, 2009). However, ETFE cannot be considered to be a “high performance engineering material”, as it would be required for it to maintain its mechanical properties under high temperatures and present high chemical resistance and strength against corrosion, which the material manages to fulfil only to a certain degree. Furthermore, according to Campo (2008), for a material to be characterized as an engineering thermoplastic, it takes a maximum of 48 MPa of tensile strength, when Tefzel® ETFE presents 40 MPa. at a temperature of 23 °C (Tefzel®210, 2012). The behaviour of ETFE against corrosion and abrasion can be improved with the application of anti-adhesive and abrasion resistant coating.

To summarise, in relation to other plastics ETFE is classified as a material with a broad consumption spectrum, common in application and low in cost. Additionally, it is found not to react with acids or alkalis. ETFE has an overall relatively high mechanical, thermal, chemical and electrical resistance in relation to a large number of its alternatives (Minamisawa *et al.*, 2007).

Over recent years a notable development of ETFE has appeared, called Ethylene-Fluorinated Ethylene Propylene (EFEP Neoflon®). Its main advantages are that it presents glass-related optical transmission of 87% at 100 µm, a lower melting temperature of 160 °C, tensile elongation of 500% and an improved fire resistance. However, its main disadvantage is the material's slightly lower tensile strength at 45 MPa and therefore has not been broadly commercialised yet (Daikin, 2013; IDES, 2013; Schöne, 2007).

This chapter provided introductory information on the composition, manufacturing and use of the ETFE membrane. The introduction of ETFE membrane in the building industry has been discussed and a summary of internationally renowned architectural projects was provided describing how the foil came to become a recognisable alternative among engineering materials. Following this, the production process of ETFE foil has been outlined, accompanied by a description of its structural, mechanical and chemical properties of the material. Furthermore, the assembly and employment of ETFE cushions as defined, in combination with the employment of air valves and an inflation system. The chapter also contained a brief reference of alternative solutions in combination with ETFE cushions that have been examined by several researchers, such as a spring structure inside the cushion or the application of a net to reduce rain noise, covering all necessary information regarding practical concerns related to the use of ETFE foil in construction.

In addition, the chapter contained a review of the literature comparing ETFE foil to glass, aiming to establish the membrane as a suitable replacement when used as cladding material in facades or roofs. The benefits and negatives of this replacement are discussed, in order to assist designers in the selection process. The comparison concerns manufacturing speed and use of materials, embodied energy, stability towards environmental hazards, weight, transparency and behaviour towards light and heat transmission. Prior to the selection of ETFE as a suitable replacement for glass, numerous polymers have been examined as alternatives. ETFE membrane was compared and classified with other plastics of the same category to distinguish it as the optimal option in the pursuit for a replacement to glass cladding. The criteria for this selection include the use of additives involved in the production process of plastics, their transmission of solar and of long-wave thermal radiation, stability, strength and endurance, density, optical parameters and response to heat and environmental hazards.

The following chapter will examine the behaviour of ETFE in relation to heat transfer as it has been investigated so far by conducted research and set the tone for further understanding and estimation of the behaviour through computational tools.

3 Heat transfer

Heat transfer is generically defined as the energy in transit due to a temperature difference (Incopera *et al.*, 1985). The three basic modes of heat transfer are conduction, convection and radiation. This chapter will examine the behaviour of ETFE in relation to heat transfer as it has been known so far by conducted research and define the ground for further understanding and estimation of the behaviour through computational tools. This will later on lead to the calculation of the energy consumption of a building due to the employment of ETFE and allow for comparisons to the equivalent energy when typical glass is used.

3.1 Background

The three basic modes of heat transfer are hereby introduced in brief, to set the ground for the necessary literature background. Conduction involves the transfer of energy through a medium by molecular motion, with the heat moving from an area of high temperature towards one of low temperature. The rate equation for conduction is Fourier's law (Equation 3.1) (Holman, 1963).

$$q = k * A \frac{\partial T}{\partial x} \quad \text{Equation 3.1}$$

q : The rate of heat flow in x direction (W)

k : Thermal conductivity (W/m °C)

A : Area normal to x direction through which heat flows (m²)

T : Temperature (°C)

x : Length (m)

Convection describes the transfer of energy between a solid and a fluid flowing past it, which essentially is another form of conduction, taking place through the fluid. The equivalent rate equation for convection is Newton's law (Equation 3.2) (Holman, 1963).

$$q_c = h * A(T_s - T_\infty) \quad \text{Equation 3.2}$$

q_c : The rate of heat flow by convection (W)

h : Heat transfer coefficient (W/m² °C)

A : Area through which heat flows (m²)

$T_s - T_\infty$: Temperature potential difference for heat flow away from surface (°C)

Radiation takes place when heat is transmitted in the form of electromagnetic waves (Incopera *et al.*, 1985). More specifically, electromagnetic radiation is the energy form that involves what we perceive of as heat and light and the bounding media through which radiation occurs can be a vacuum, a gas or a transparent material (Ghoshdastidar, 2004; Poirazis *et al.*, 2010). Radiative flux is proportional to the fourth power of the temperature of a body, as originally established by Stefan and Boltzmann and the radiative heat transfer between two surfaces is expressed in Equation 3.3 (Holman, 1963).

$$q_r = \sigma \varepsilon A (T_1^4 - T_2^4) \quad \text{Equation 3.3}$$

q_r : Rate of heat flow by radiation (W)

σ : Stefan-Boltzmann constant ($5.669 \cdot 10^{-8} \text{ W/m}^2 \text{ K}^4$)

ε : Emissivity ($\varepsilon < 1$ for a non-black body)

A : Heat transfer surface area (m^2)

T_1 : Absolute surface temperature, surface 1 ($^{\circ}\text{K}$)

T_2 : Absolute ambient surface temperature, surface 2 ($^{\circ}\text{K}$)

The result of this rate equation can be seen in Figure 3.1, which depicts the relationship between heat flow and temperature difference in the case of the heat emitted by a black surface, when its surroundings have a temperature of absolute zero (Toolbox, 2013).

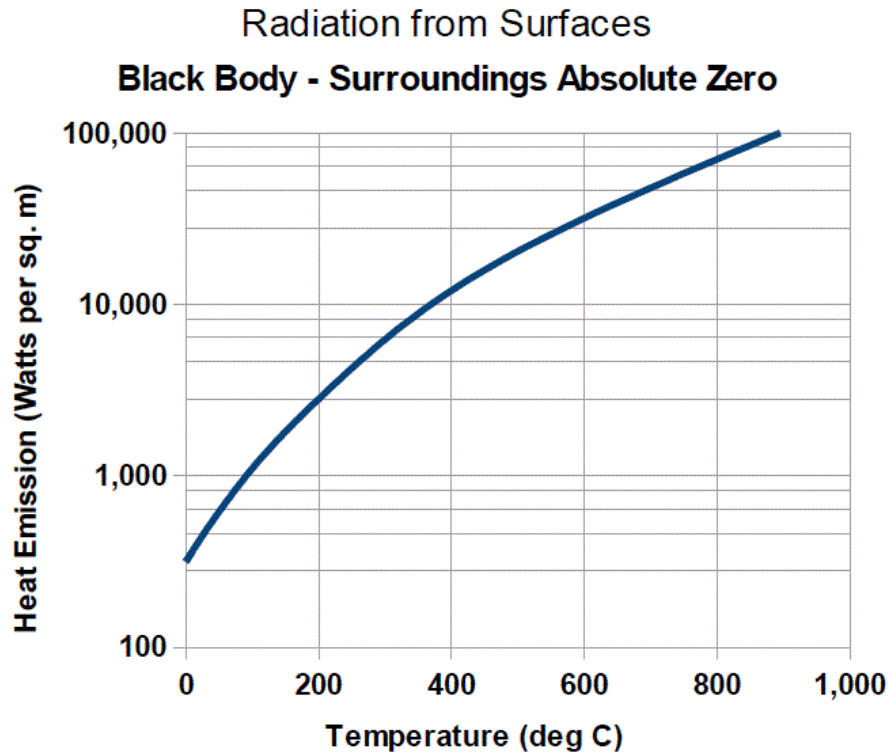


Figure 3.1: Heat radiation from black body - external surroundings at absolute zero temperature (Toolbox, 2013)

Examining radiation in more detail, the fundamental properties of radiative transfer are reflectance (ρ), absorbance (α) and transmission (τ). According to the law of conservation of energy, all radiation must either be reflected, absorbed or transmitted; therefore, the resulting relation between the three properties is: $\rho + \alpha + \tau = 1$. If the medium is thick enough or opaque, then: $\tau = 0$ (Modest, 2003).

Another important radiative property is emissivity ε ($0 < \varepsilon < 1$), which represents the energy emitted from the medium surface divided by the energy that would be emitted from a black surface at the same temperature, in which case $\varepsilon = 1$ for a perfect emitter (Holman, 1963).

In comparison to conduction and convection, radiative properties are directly dependent on direction (related to the view factor, which will be discussed further on), wavelength λ (m) and temperature ($^{\circ}\text{C}$) (Modest, 2003). The wavelengths covered by thermal radiation are in the range of 100-1,000,000 nm; including a part of Ultraviolet (UV) radiation between 100 and 380 nm, all of visible radiation between 380 and 780 nm and Infrared (IR) radiation at 780-1,000,000 nm. The largest part of the IR spectrum

is commonly divided to Near Infra-Red (NIR) radiation between 780 and 1,400 nm, Shortwave Infra-Red (SWIR) radiation between 1,400 and 3,000 nm, Mid-wave Infra-Red (MWIR) radiation at 3,000-8,000 nm, Long-wave Infra-Red (LWIR) radiation at 8,000-15,000 nm and Far Infra-Red (FIR) radiation between 15,000 and 1,000,000 nm (Jones, 2000; Standards, 2007).

To set the basis for the description of the radiative properties of a material, the black body emissive spectrum is regarded, whereby, according to Wien's displacement law (Equation 3.4), the maximum wavelength λ_{max} with the maximum energy is reversely proportional to the absolute temperature of the black body (Robert *et al.*, 1981).

$$\lambda_{max} * T = b \quad \text{Equation 3.4}$$

λ_{max} : Maximum intensity wavelength (m)

T : Black body temperature (°K)

b : Wien's displacement constant ($2.89 \cdot 10^{-3}$ m*K)

The spectral distribution for the emissive temperature of a black body is expressed by Planck's law in Equation 3.5.

$$E_{\lambda,b} = \frac{\beta_1}{\lambda^5 [\exp\left(\frac{\beta_2}{\lambda_{max} * T}\right) - 1]} \quad \text{Equation 3.5}$$

$E_{\lambda,b}$: Spectral black body emissive power

β_1 : $3742 \cdot 108$ (Wnm⁴/m²)

λ : Wavelength (nm)

β_2 : $1439 \cdot 104$ (nmK)

$$\text{Where } \beta_1 = \frac{h_p * c_0^2}{2 * \pi}$$

$$\beta_2 = \frac{h_p * c_0}{\sigma}$$

h_p : Planck's constant ($6.62 * 10^{-34}$ Js)

σ : Boltzmann constant ($5.67 * 10^{-8}$ W/m²K⁴)

c_0 : Speed of light in vacuum ($2.99 * 10^8$ m/s)

In a vacuum and in most gases at normal temperatures, electromagnetic radiation takes place at the speed of light (Jones, 2000).

Another radiation parameter to take into account is the view factor, otherwise known as configuration or shape factor. It is denoted as dF_{di-dj} and represents the fraction of energy that leaves a black body element dA_i and arrives at a black body element dA_j (Siegel *et al.*, 1972). View factors express the radiative heat transfer between surfaces through mathematical relations describing how the two surfaces are facing each other. Equation 3.6 presents that geometrical positioning and Figure 3.2 shows a diagram of that relationship (Incopera *et al.*, 1985).

$$dF_{di-dj} = \frac{\cos\theta_i * \cos\theta_j}{\pi * R^2} dA_j \quad \text{Equation 3.6}$$

θ_i : The angle normal to the surface dA_i and the length R between the two elements dA_i and dA_j

θ_j : The angle normal to the surface dA_j and the length R between the two elements dA_i and dA_j

R : Length of line joining the two elements dA_i and dA_j

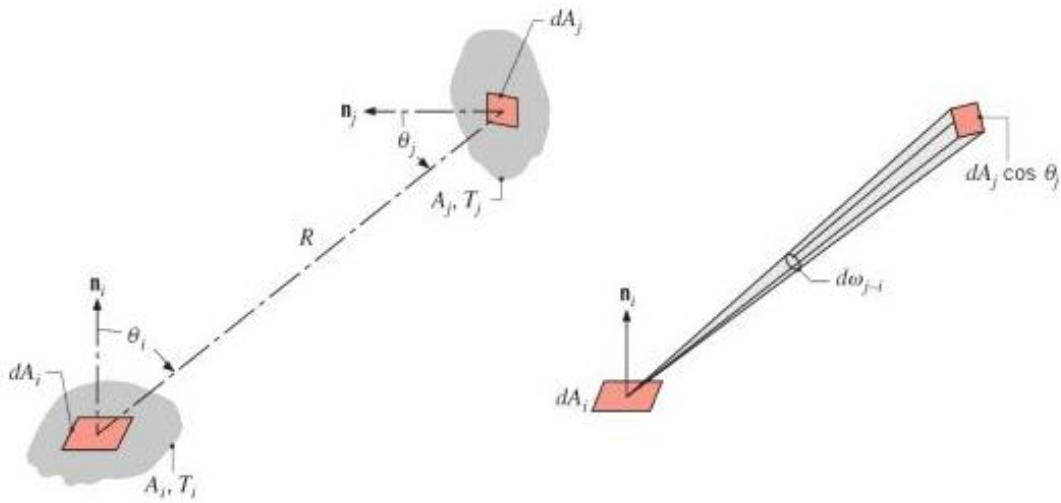


Figure 3.2: View factor associated with radiation exchange between surfaces of area dA_i and dA_j (Incopera *et al.*, 1985)

The view factor depends on the size of the element dA_j and its orientation in relation to dA_i (Siegel *et al.*, 1972). Given this relation, the curved surface of an ETFE cushion will complicate the estimation of the view factor, since each point of the cushion surface

is at a different orientation relatively to the radiative source. In the case where the convex surface dA_i of the cushion cover does not have an easily calculated geometry, it will then have to be subdivided into a number of isothermal surfaces which will be considered individually in regards to the radiative surface dA_j (Modest, 2003). This process was considered in relation to computational means and is discussed in detail further on in the chapter discussing the thermal modelling of a cushion using IES.

The two main areas of radiation that concern this research are shortwave and long-wave radiation, otherwise known as solar and terrestrial radiation respectively. The two are emitted at distinct wavelengths. Solar radiation is emitted from the sun and passes through the atmosphere. It is detected only during daytime. It is reflected by the Earth's surface and atmosphere; the solar radiation that reaches the Earth's surface involves wavelengths between UV to IR waves; 0.2 μm to 3 μm . Terrestrial radiation is the energy emitted from the Earth and atmosphere. It is detected during both day- and night-time. It is energy radiated at invisible thermal IR wavelengths between 4-40 μm (Incopera et al., 1985). The wavelengths that each radiative area covers are shown in Figure 3.3. The two areas will be examined in further detail in the experimental Chapter 4. (UDEL, 2014)

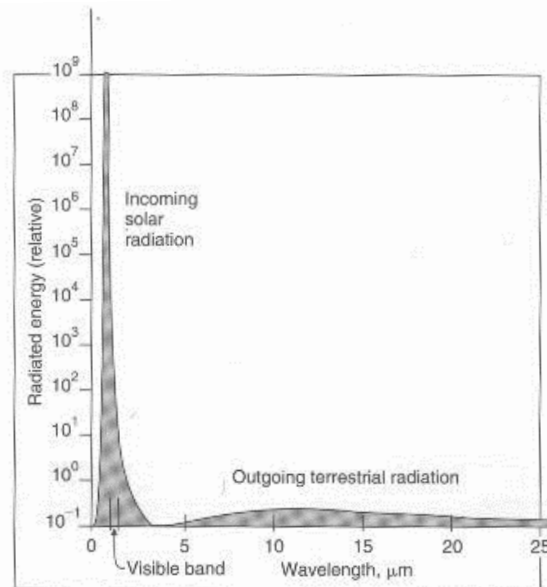


Figure 3.3: Solar and terrestrial radiation (UDEL, 2014).

3.2 The thermal behaviour of greenhouses

Most of the initial research performed on ETFE and its energy loss or gain in comparison to glazing has concerned greenhouses, as this was initially the most common structural environment where the material was applied.

A greenhouse maintains a warm environment mainly because of the heated air that remains trapped inside its space. FIR radiation with a wavelength in the range of 15 to 1000 μm will escape a greenhouse if glass is employed as cladding material (Johnson, 1991). For that reason, thermal greenhouse covers are typically films that block IR

radiation varying between 700 nm and 1,400 nm to reduce the risk of frost in the absence of heating, or to reduce the heating requirements in the presence of a heating system (Espí, 2006). Films and in particular ETFE have been broadly employed in greenhouses since although double glazing on greenhouse cladding reduced heat losses; it also reduced light transmission, therefore cutting down crop growth rate. Additionally, glazing increased initial costs, due to its material worth and its weight that called for a sturdy supporting structure (Critten *et al.*, 2002).

On the other hand, in polyethylene covered greenhouses the heat loss due to radiation has been found to be so high that on a cold, calm, clear sky night the cover temperature is lower than the temperature of the external air. Due to their thickness, film covers have a small thermal capacity and a poor insulation performance. (Papadakis *et al.*, 2000).

The research of Michalsky *et al.* (1999) highlighted the need to measure the sum of both the direct irradiance and the diffuse horizontal irradiance. A research by Baille *et al.* in 2006 focused on the night energy balance of a heated plastic greenhouse, which is close to the focus of the present research. The analysis of the energy balance inside the greenhouse focused around the calculation of the soil surface and air volume energy balance, the determination of leakage losses and the convective heat transfer, as well as the estimation of the energy balance of the greenhouse cover.

The analysis of the greenhouse energy balance concerned periods with steady microclimatic conditions. The air volume energy balance was estimated as follows (Equation 3.7) (Baille *et al.*, 2006):

$$Q_h + H_S + H_{c,i} + H_{f,s} = 0 \quad \text{Equation 3.7}$$

Q_h : Heat supplied by the heating system of the greenhouse (W/m²)

H_S : Convective heat transfer from the soil inside the greenhouse

$H_{c,i}$: Convective heat transfer from the inside of the cover

$H_{f,s}$: Exchange of heat due to air leakage

The greenhouse cover energy balance was estimated in absence of condensation and neglecting thermal mass, as described in the following Equation 3.8 (Baille *et al.*, 2006).

$$R_{n,e} + R_{n,i} + H_{c,e} + H_{c,i} = 0 \quad \text{Equation 3.8}$$

$R_{n,e}$: Net radiation outside the greenhouse ($R_{n,e} = R_a - R_{c,e}$)

Where R_a : Atmospheric radiation

$R_{c,e}$: Radiation emitted by the outer cover surface

$R_{n,i}$: Net radiation inside the greenhouse ($R_{n,i} = R_{c,i} - R_s$)

Where $R_{c,i}$: Radiation emitted by the inner cover surface

R_s : Radiation emitted by the soil

$H_{c,e}$: Convective heat transfer from the outer cover surface

$H_{c,i}$: Convective heat transfer from the inner cover surface

The research resulted that heat loss due to leakage appears to be dependent on wind speed. The main reason for that is the convective exchange between the air inside the greenhouse and the inner cover surface. An increase in wind speed caused an increase in the heat loss due to leakage and a decrease in the convective heat flux on either the outer or the inner cover surfaces. The convective losses also appeared to increase with the increase of heating.

The research further concluded that radiation losses played a major role in the heat loss through the cover of a polyethylene enclosed greenhouse. To resolve the aforementioned issues, the paper suggested an increase in air-tightness and the use of low emissivity covers in the long-wave band (Baille *et al.*, 2006).

Another study by Berroug *et al.* (2011) developed a mathematical model for the numerical estimation of greenhouse nocturnal heat losses. The assumptions that were made for that work concern the present research. Relative humidity and temperature of inside air were considered to be uniform, the heat capacity of inside air and cover were neglected, the climate was considered to be hourly invariable, the heat and humidity exchanged between ground and inside air were neglected and no condensation was taken into account.

The work of Berroug *et al.* (2011) also discussed in detail the sensible and latent heat loss due to air leakage, as in the following Equation 3.9 and Equation 3.10.

$$Q_{ai} = h_{ai} * (T_o - T_i) \quad \text{Equation 3.9}$$

Q_{ai} : Sensible heat loss due to leakage (W/m²)

h_{ai} : Sensible heat transfer coefficient ($h_{ai} = \frac{\rho * c_a * N * V}{3600 * A_g}$)

Where ρ_{air} : Air density (kg/m³)

c_a : Specific heat of air (J/kgC)

N : Leakage rate per hour

V : Greenhouse air volume (m³)

A_g : Ground area (m²)

T_o : External air temperature of greenhouse (°C)

T_i : Internal air temperature of greenhouse (°C)

$$Q_l = \frac{h_{ai}}{\gamma} * (e_i - e_o) \quad \text{Equation 3.10}$$

Q_l : Latent heat loss due to leakage (W/m²)

h_{ai} : Sensible heat transfer coefficient

γ : Psychrometric constant (0,0667 kPa/K)

e_i : Inside water vapour pressure (kPa)

e_o : Outside water vapor pressure (kPa)

The research concluded that for that given set of experiments, 12% of the total heat input was lost due to sensible and latent leakage and 66% due to convective exchange through the air and inner cover of the greenhouse. This energy is then further dissipated at the outer cover as 66% due to radiation and 34% due to convection. These results of the research conducted by Berroug *et al.* (2011) influenced the development of the present research by highlighting the significance of heat loss due to radiation in comparison to that due to convection. The present research later continues by investigating the relationship of heat loss through an ETFE cover to external radiative conditions. Special focus will be placed on the effect of a clear or overcast sky on the thermal and energy behaviour of an ETFE cover.

Another study by Geoola *et al.* (2009) focused on the experimental examination of greenhouse dry and wet covers using a hot box enclosing two chambers, one chamber including a cooling system and the other a heating system, divided by the cladding under examination. The cold chamber had a set temperature to -1 °C whereas in the hot chamber the power was adjusted between 10 and 60 °C. Air velocities up to 5.1 m/s were achieved with the use of two fans. The research indicated that the heat transfer coefficient increased as did the temperature difference between the two chambers. Furthermore, for a steady temperature difference, the U-value increased as did the wind speed. Finally, a conclusion of the research is that presence of condensation lowered the U-value of plastic UV Polyethylene films, as water drops reduced the transmission of IR radiation.

Furthermore, research based on literature by Longo *et al.* (2012) has indicated that condensation plays an important role in maintaining low energy needs due to heating of the greenhouse, especially in the case of cover materials with a large long-wave radiation transmission.

Another experimentation performed by Feuilloy *et al.* (1996) used the hot box method, with one heated enclosed chamber underneath the cladding material. The pre-set conditions of the model involve an outside air temperature steadily set to 0 °C, the sky temperature at -20 °C and the internal air temperature varying between 0 and 50 °C. Wind velocity was set to 4 m/s. The results of this research support the above statements, as in the case of plastic covers condensation will decrease the transmission of thermal radiation. The research indicated that in the case of glass, condensation does not improve the transparency to long-wave radiation, as glass already has an emissivity close to one, much higher than the emissivity of plastic covers.

The summary of the measured results of this work is presented in Table 3.1, demonstrating that condensation reduces the U-value of plastic covering materials, in contrast to the case of glass, whereby condensation increases the material's U-value. The research of Feuilloy *et al.* as described here helps demonstrate the effect of condensation on the U-value of various plastic covering materials, other than ETFE.

Table 3.1: Result summary of thermal properties of greenhouse covering materials (Feuilloy *et al.*, 1996)

Specimen	U-value (W/m²K) without condensation	U-value (W/m²K) with condensation
Plastic films (200 µm)		
Low Density Polyethylene (LDPE) + single layer Ethyl Vinyl Acetate (EVA) finish	12.1	10.2
LDPE + 3 layer EVA	10.0 – 11.6	8.7 – 10.4
LDPE + 3 layer anti-drop EVA	10.2 – 11.4	9.2 – 9.8
LDPE + mineral finish	10.1 – 10.4	8.5 – 9.2
Glass (4mm)		
Single pane of glass	6.1 – 6.9	6.7 – 7.6

The work of Feuilloy *et al.* demonstrated that calculating the exact degree to which condensation affected the thermal properties of the cladding material was a challenging task, as it depended on numerous factors, such as the type of cover, its slope as well as the droplet size and form. Further experimentation by Zhang *et al.* (1996) indicated that polyethylene covered spaces collected less humidity on their interior surface in relation to glazed spaces.

3.3 The thermal behaviour of films, glass and ETFE foils and cushions

Figure 3.4 is the result of the research performed by Tsilingiris (2003) on the comparative evaluation of the IR transmission of polymer films. Wu *et al.* (2008) also investigated this area by using Fourier Transform InfraRed spectroscopy (FTIR) to measure the radiative thermal properties of thin polymer films and in specific polyethylene (PE), aluminium foil (AF) and polyamide (WB). FTIR is the method used to define the IR spectrum of absorbance, emissivity, light conductivity or Raman scattering of a solid, liquid or gas through the gathering of spectral data in a wide wavelength range (Griffiths, 1983). FTIR was also used by the current research to examine in detail the material properties of different types of ETFE foil. The results of this analysis will be presented in section 3.4 of this chapter.

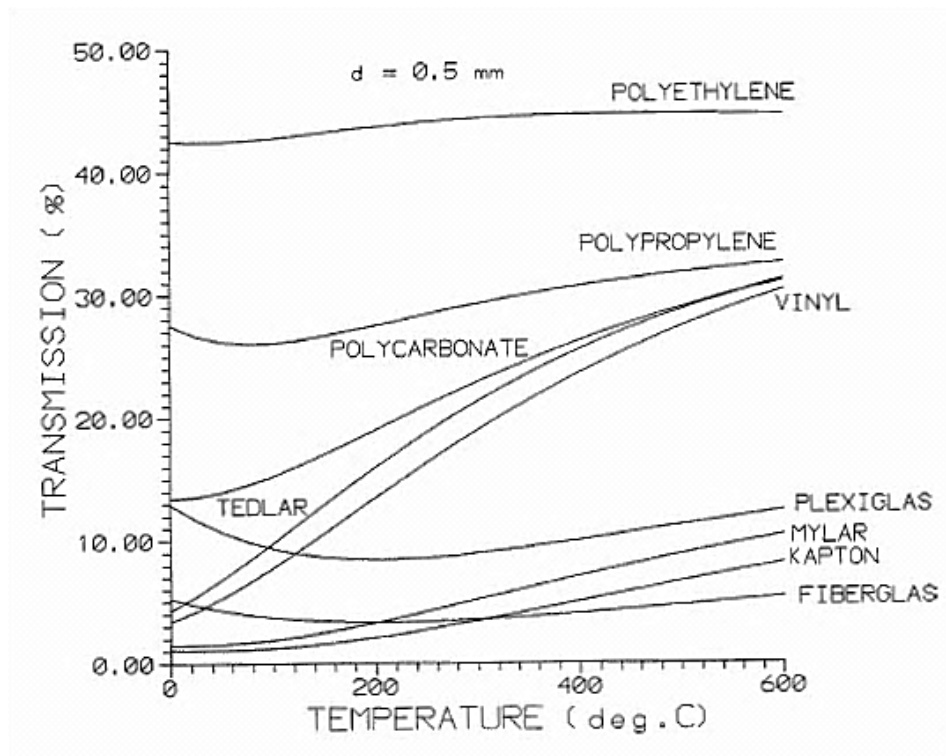


Figure 3.4: Calculated comparative total transmission of polymer films for a 0.5 mm thickness (Wu et al., 2008)

As demonstrated in Figure 3.4, polyethylene surpasses in the amount of IR it transmits for a variety of temperatures the next closest option of polypropylene by approximately 12% and the most common alternative of Plexiglas by about 30%. Such high thermal transfer percentage might be undesirable due to causing excessive heat gain or loss, in which case the control of incoming or escaping radiation is required.

Fritting is the most common means to reduce incoming or outgoing radiation. Fritting falls into a category of treatments that can be referred to as “heat mirrors”. A heat mirror is a wavelength selective coating demonstrating reflectance or transmission of radiation in three fields of the electromagnetic area: High-Energy Solar (HES), which also includes mainly the visible spectrum and a part of IR radiation varying between 300 and 100,000 nm (Lampert, 1981). Fritting is typically located among two membranes forming a cushion, usually on the interior of the cladding unit, in the same way that Low-E coating is often placed in the interior of two panes of a double glazed unit (Brauer, 1999).

According to Poirazis *et al.* (2010), in the case of a cold night the use of a frit lowers long-wave heat loss and in the case of a warm day it decreases the shortwave heat gain through reflection and absorption. It has been mentioned that fritting is the

equivalent treatment to Low Emissivity coating that is typically applied to glazing to increase the overall reflection of IR radiation through the application of a thin silver film (Brauer, 1999). However, as the present research later demonstrates, fritting is not comparable to low-E coating and it does not perform in a similar manner. Via experiments and simulations, the present research verifies the statement that fritting reflects a large part of shortwave radiation, and, therefore reduces solar heat gain. However, the research also rejects that a frit reflects long-wave radiation, which means that it does not reduce radiative heat loss as Low-E coating does. This will be further investigated in the secondary simulations chapter. The most common materials used for film deposition are silver and aluminium. Their thicknesses vary between 50,000 nm and 200,000 nm (Smith *et al.*, 1998). Research by Mohelnikova (2009) focused on the study of materials for reflective coatings of window glass. The result was that the optimum function of a coating film depends on a combination of a high visible transmission with wavelength $\lambda \in [380 - 780 \text{ nm}]$ and a high reflectance of a wavelength in the range of $\lambda \in [500 - 80,000 \text{ nm}]$. Although these results have been estimated for fenestration glazing, they are also found applicable in the case of ETFE foil, as they will be further examined in the following chapter regarding the results of the FTIR analysis.

A research that discussed heat transfer through various greenhouse cladding materials was that of Papadakis *et al.* (2000). The thermal transmission U-values present large variations, whether they be measured in-situ or calculated. Especially thin covers made of single films present small thermal capacity, which results to poor insulation material performance and even greater variation to their thermal transmission (Figure 3.5).

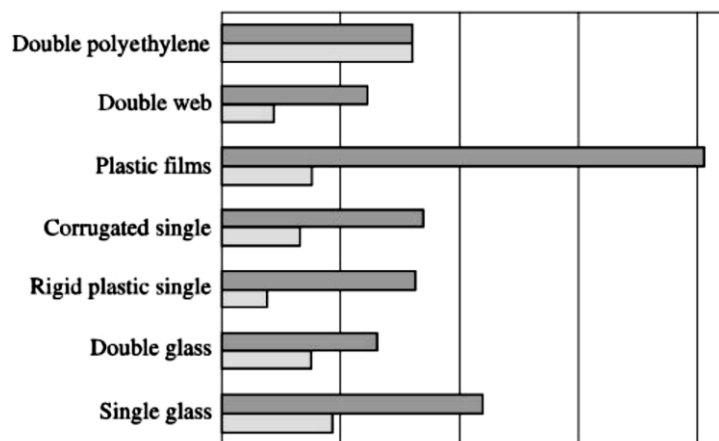


Figure 3.5: Minimum and maximum values of the coefficient of heat transfer (W/m^2K) for several types of greenhouse covering materials (Papadakis *et al.*, 2000)

Furthermore, U-values are suited for non-homogenous specimens, such as entire building structures. Despite of the great variation in their recorded U-values, Papadakis

et al. (2000) advocate the benefits of the use of films as thermal covers. As the research indicates, the significant heat loss related to the poor insulating properties of films can be balanced in comparison to a glass structure by heat loss related to air leakage from the necessary supporting structure.

Poirazis *et al.* (2010) performed a study on a summer scenario, where heat transfer through the ETFE membrane was measured, the maximum foil temperatures were estimated and a mathematical model was developed to calculate the heat transfer for each foil. The research concluded that there was an estimated 12% increase of heat flux due to night-time long-wave radiation, in comparison to glazing. The increase in heat gain during the day was found to be less significant in terms of energy performance than the heat loss occurring at night. This study by Poirazis *et al.* did not investigate a heating scenario and, therefore, did not debate the potential impact of the noted elevated night-time heat loss to an entire building energy use. The present research later tries to estimate such an impact via experiments and a whole building simulation.

Membrane cushions present an uneven distribution of heat in their interior. Antretter *et al.* (2011) at the Fraunhofer Institut für Bauphysik, Germany, performed a full scale model of a structure covered by an ETFE cushion (Figure 3.6) to verify the results that occur when CFD is used to predict heat distribution under several inclinations.



Figure 3.6: Experimental structure with ETFE roof built by the Fraunhofer Institut für Bauphysik (Antretter *et al.*, 2011)

The simulations that were performed involving the model setup intended to reproduce living conditions, therefore for the interior of the space they were set at 20 °C, whereas outside the model they varied between -10 to +30 °C.

The cushion under assessment was modelled as round, with a diameter of 4.75 m and a maximum height in the centre of 1 m. The gap between the two films creating the cushion encouraged an increase in heat transfer via convection due to the temperature difference between the two surfaces.

The cushion was inclined in simulations at angles of 0, 45 and 90 degrees from the horizontal; while measurements of temperature, wind velocity and heat flux density were taken at several points within the cushion interior to examine the heat flow distribution (Figure 3.7).

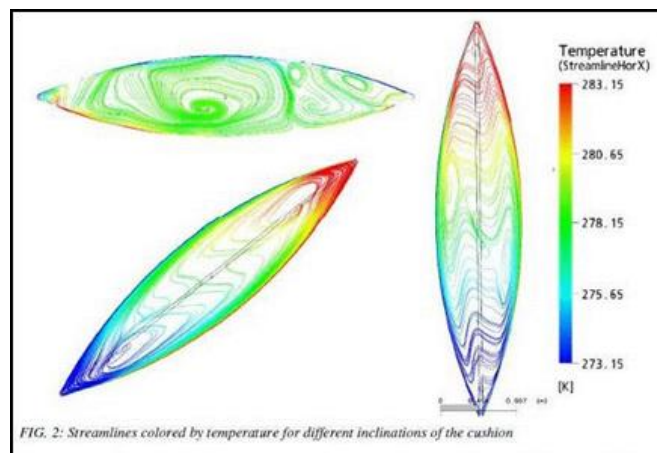


Figure 3.7: Heat flow distribution within cushion as occurring from the use of CFD (Antretter et al., 2011)

For a temperature difference of 30 °C it was discovered that 30% of the total heat flux took place through convection, whereas 70% took place through radiation, supporting the significance of radiation in the study of heat transfer through an ETFE cushion.

The measured results regarding convection demonstrated certain movement of heat in an attempt to achieve balance within the cushion; where the heat flow occurred in an unpredictable manner, related to time, with rising and falling heat plumes. The temperature of the cushion appeared to be uniform in the middle of the cushion, while warmer areas are noticed on the borders, located in the upwards directions (Antretter et al., 2011).

Max et al. (2012) experimented with a novel greenhouse glazing system whereby three hot boxes were covered alternately with a single glazed unit, a single glazed unit in combination with a single ETFE film and the arrangement of ETFE film-glass-ETFE film, as seen in Figure 3.8.

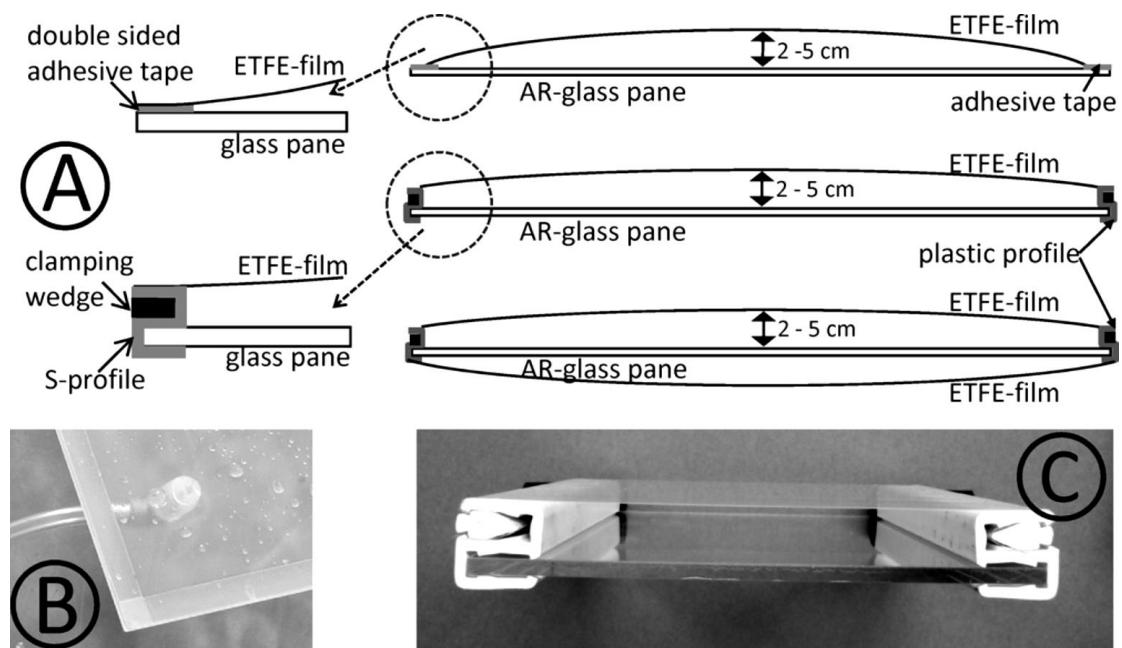


Figure 3.8: Experimental Glass and ETFE composite cladding system (Max et al., 2012)

The hot box setup was located on the campus of the Institute of Biological Production Systems, in the Leibniz University of Hannover, Germany, at a latitude of 52.23 N, altitude of 9.42 E and 52.3 m above sea level. The boxes were comprised of 200 mm thick insulation sheets and the overall box structure had a 2400 by 1900 mm base and a height of 1200 mm (Figure 3.9). The surface of the hot boxes had an inclination of 26 degrees, which is typical for greenhouse roofs at high geographical latitudes, of central and Northern Europe. Each box enclosed two electric heaters of 800 W capacity and two of 2000 W capacity.



Figure 3.9: Hot box setup with open lids (Max *et al.*, 2012)

Internal conditions of the boxes as well as external weather conditions were measured on the site and the U-values of each cladding system were calculated according to the DIN EN 673. Measurements were taken with and without condensation, which simulated crop transpiration. The thermal flux through the glazing units were measured at an average external temperature of 10 °C and a temperature difference between interior and exterior environments of 20±2 °C. Table 3.2 presents a summary of the results.

Table 3.2: Result summary of a novel Glass-ETFE cladding system (Max *et al.*, 2012)

Specimen	U-value (W/m²K) without condensation	U-value (W/m²K) with condensation
Single pane safety glass (3 mm)	6.2	6.6
Glass (3 mm) - ETFE Film (100 µm) (adhesive tape mounted)	3.7	4.1
Glass (3 mm) -ETFE Film (100 µm) (profile mounted)	3.3	3.6
ETFE Film (100 µm) - Glass (3 mm) - ETFE Film (100 µm) (profile mounted)	2.4	2.5

Finally, a study resulting in a mathematical model was that of Jian (2010), regarding the simulation of energy performance of ETFE membranes in building applications. Jian stated that the existing methodology for energy simulation is non-applicable on ETFE due to its chemical structure, shape, dimensions and physical properties.

Jian summarised the assumptions that are commonly adopted to facilitate calculations for the development of existing mathematical models. These assumptions primarily concern material properties, beginning with the fact that ETFE foils are treated as an isothermal surface, when that is not correct. Furthermore, heat storage in the foil is usually neglected in simulations, as well as the edge effect – whereby heat flow is considered to be one-dimensional and vertical to the foil. Additionally, the absorbed solar radiation is assumed to be evenly distributed, a fact also unrealistic; and the air within the cushions is considered to be still and independent from any heat gain or loss due to infiltration. It is necessary to incorporate air movement in the calculations, whether that is due to gravitational natural processes or the function of a pressurising fan or a dehumidifier. Finally, as Jian points out, the air gap within the foils is typically considered to be in dry condition, which causes errors in the estimation of heat transfer. According to Jian, to respond to this discrepancy between real-life and estimated thermal behaviour, CFD is required to accurately represent the conditions inside the cushion. This observation comes into agreement with the work of Antretter *et al.* mentioned earlier, who used computational modelling to examine and simulate the distribution of heat transfer within an ETFE cushion.

3.4 Material properties – lab based spectral data

This section examines the material radiative properties of distinct types of ETFE foil in a laboratory environment. Five different types of ETFE foil were tested at the University of Bath at the Chemistry Department laboratory using a Fourier Transform Infra-Red (FTIR) Perkin Elmer Spectrum™ 100 spectrophotometer (Figure 3.10). The tested samples were provided by Vector Foiltec.



Figure 3.10: FTIR Perkin Elmer Spectrum 100 spectrophotometer

The ETFE samples were examined under a range of IR wavelengths, from 2,500 nm and 16,667 nm, corresponding to the wavenumbers $4,000$ and 600 cm^{-1} . The range measured here does not cover the entire thermal radiation spread of 100 nm to 1,000,000 nm; however it does cover the radiation range typically blocked by most thermal greenhouse covers of 7,000 nm to 14,000 nm, as mentioned previously in this chapter (Espi, 2006). For that reason, these measurements will be used to describe the radiative behaviour of the material and compare different types of ETFE membrane. Since ETFE membrane is not typically employed in a single layer form, these measurements will also be further supplemented by the main experiment that takes into account the effects of conduction and convection and which remains to be described in the following chapter.

Figure 3.11 shows the bands of the electromagnetic radiation spectrum and the red arrow defines the area examined by the FTIR equipment.

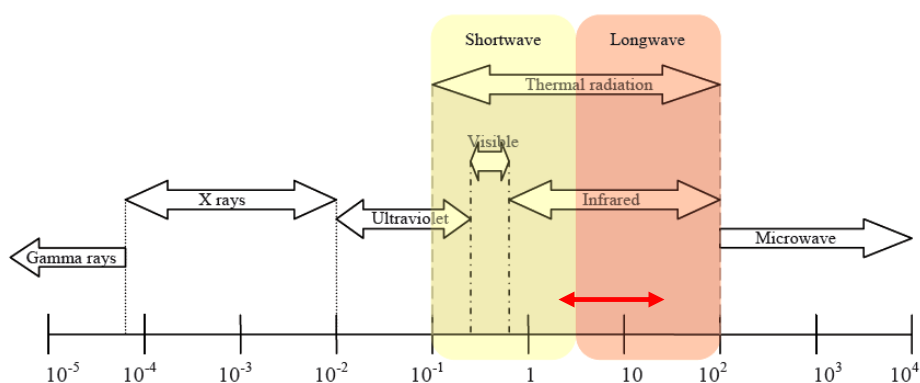


Figure 3.11: Electromagnetic radiation spectrum (μm) (Poirazis et al., 2010).

The five types of ETFE foil that were tested varied in thickness and material properties (Figure 3.12):

- 100 μm thick clear foil
- 120 μm thick clear fritted foil with the silver treatment covering 65% of the specimen
- 100 μm thick white foil
- 150 μm thick matt foil
- 170 μm thick white foil with silver dotted frit covering 80% of the foil surface

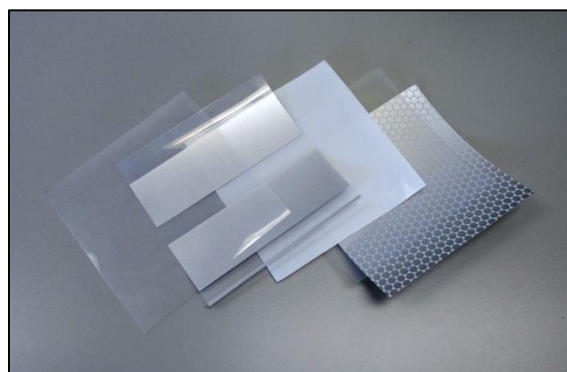


Figure 3.12: Tested ETFE samples (Starting from the left: clear, clear fritted, white, matt, white fritted foil)

In the cases of the fritted clear and white foils, measurements were taken on both the silver print and the non-print areas. A weighted average is used to represent the overall transmission of the membrane, depending on the percentage of the surface covered by the silver treatment, such as in the present case of the dotted white foil. The measurements were taken on the non-print side of the foil, since the fritting is typically located on the inside of the ETFE cushion for protective purposes, resulting to the untreated side being exposed to the external radiation.

The equipment used is a model of 2005 and achieves an optical system resolution of up to 0.5 cm^{-1} (PerkinElmer, 2005). Newer versions of the machine, such as the

PerkinElmer Spectrum 100 Optica, manage to reach an accuracy of 0.01 cm^{-1} at a wavelength of $2,000\text{ cm}^{-1}$ and a slightly reduced accuracy of 0.008 cm^{-1} at peak measurements (PerkinElmer, 2008). The tendency of the accuracy to decrease at the measurement of peaks was also noted while using the present equipment. For that reason, measurements were repeated multiple times at different areas of the same sample, compared and averaged to ensure that the figures were accurate. The repeated measurements for the untreated materials consistently presented nearly identical figures of less than 1% deflection, with the exception of the matt foil, whose repeated measurements presented an approximate variation of 3% in the peaks. This high level of accuracy in the measurements points towards the fact that this lack of consistency in the results cannot be explained through the precision of the measurements.

The preparation process for the use of the spectrometer involves the thorough cleaning of the plate that will receive the sample, the aperture and the samples themselves, as the presence of particles would compromise the accuracy of the measurements. The next step is to position the sample so as to cover the aperture and tighten the force gauge arm on top of it at approximately 100 N to ensure that direct contact is achieved between the aperture and the sample. Past that point the equipment is ready to take measurements of transmission and absorbance. The examined membranes were divided into two sets – one of untreated and one of treated with a silver print, with the untreated foils to be the first under examination.

In the case of untreated types of ETFE foil, the recorded transmission occasionally reached above 100%, an issue that can be related to the measurement accuracy of the equipment or the precision of the data analysis software. Figure 3.13 presents a summary of the measured transmission of the three untreated examined five types of ETFE foil; clear, matt and white.

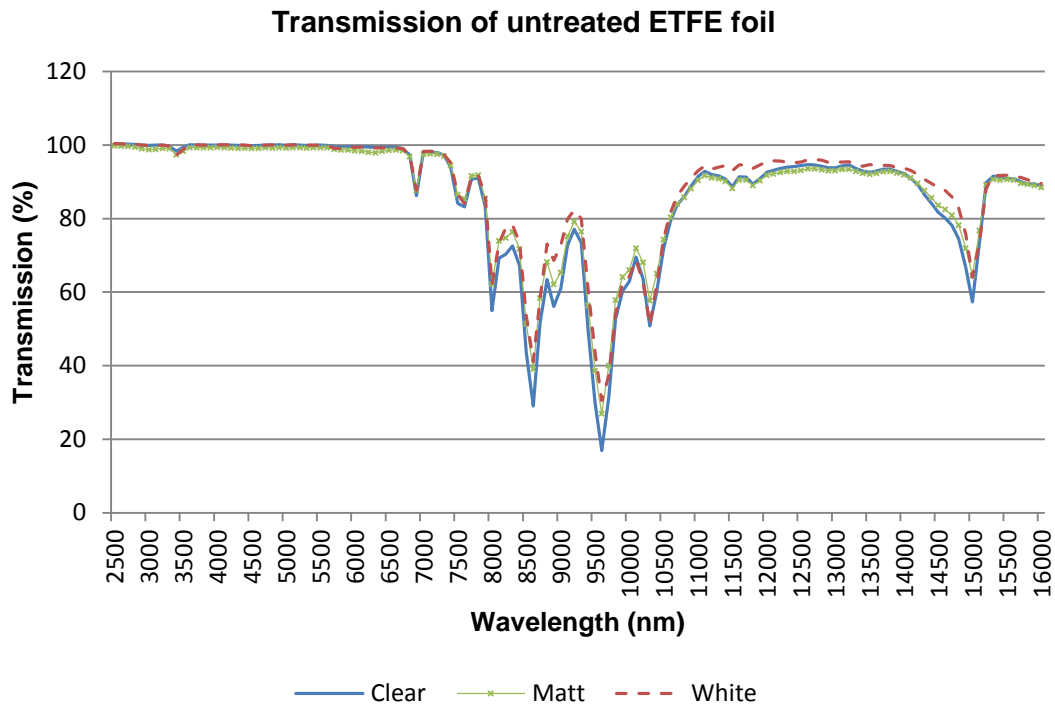


Figure 3.13: Transmission of clear, matt and white ETFE foil

The untreated foils, clear, matt and white ETFE, presented identical curves of nearly 100% of transmission throughout the most part of the mid-IR range; between 2,500 and 8,000 nm. Past that point the recorded transmission of the three specimens presented a significant variation of lower values between 17% and 93%, particularly throughout an extended part of the “thermal” LW-IR area between 8,000 and 12,000 nm. For the rest of LW-IR wavelengths the transmission values increase to a minimum of 90% until they reach a wavelength of approximately 15,000 nm. Beyond that wavelength a small part of the far IR zone of 15,000 to 1,000,000 nm is represented. To cover the IR zones that are not included in these measurements, different equipment would be required, such as an FT-NIR spectrometer to cover the “visible” NIR and “solar” SW radiation between 780 and 2,500 nm and a Raman spectrometer for the measurement of the FIR radiation between 15,000 and 1,000,000 nm.

Table 3.3 presents the average transmission of the three types of untreated ETFE foil as a result of these measurements. The very small difference in the transmission values for the entire FTIR measurement range and also for the LW measurements in particular suggests that the material’s transmission is not dependent in an obvious way on the thickness or the colouration of the material.

Table 3.3: Average transmission values (%) of untreated ETFE foil

	Clear ETFE (100 µm)	Matt ETFE (150 µm)	White ETFE (100 µm)
Average transmission (%)			
Throughout the entire range of the FTIR measurements: 2,500 – 16,000 nm	86	87	89
Throughout the specific range of LW-IR measurements: 8,000 – 15,000 nm	77	79	81

At a closer examination of the results, the differences noted in the peak measurements for the three types of the material do not present a clear correlation that would allow the radiative response of each material to be traced back to the nature of the material. The peak transmission values for the three types of untreated ETFE foil and their corresponding wavelengths can be found in Table 3.4. The differences in transmission values between the untreated types of ETFE foil varied between 0% at a wavelength of 10,300 nm to a maximum of 14% at a wavelength of 9,600 nm. Both the matt and the white foil presented a steadily higher transmission than the clear ETFE foil throughout the entire range of the measurements.

Table 3.4: Peak transmission values of untreated types of ETFE foil

	Clear ETFE foil (100 µm)	Matt ETFE foil (120 µm)	White ETFE foil (100 µm)
Wavelength (nm)	Transmission (%)		
6,900	86	88	88
7,100	98	98	98
7,600	83	85	84
7,700	91	92	91
8,000	55	62	62
8,300	73	76	78
8,600	29	39	41
8,800	63	68	73
8,900	56	62	69

9,200	77	79	82
9,600	17	27	31
10,100	70	72	69
10,300	51	58	51
11,100	93	92	94
11,400	91	90	94
13,200	95	93	95
15,000	57	65	64
15,300	92	91	92

Regarding the treated ETFE foil samples, the silver print covers 65% of the clear foil area and 80% of the white foil area, as seen in Figure 3.14 (the clear, less fritted foil is shown on the left and the white, more fritted foil on the right). Measurements were taken on both the frit and the untreated areas of the foil. These measurements were weighted by multiplying them by the corresponding coverage percentage and adding the results to get the overall performance of each examined foil. The overall results are presented below in Figure 3.15.

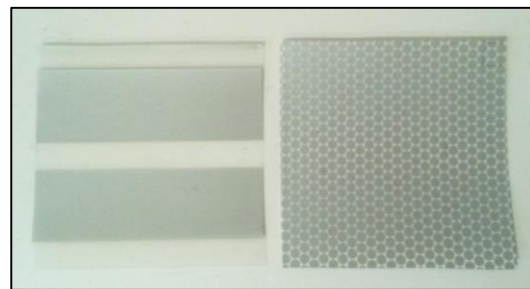


Figure 3.14: Treated ETFE samples

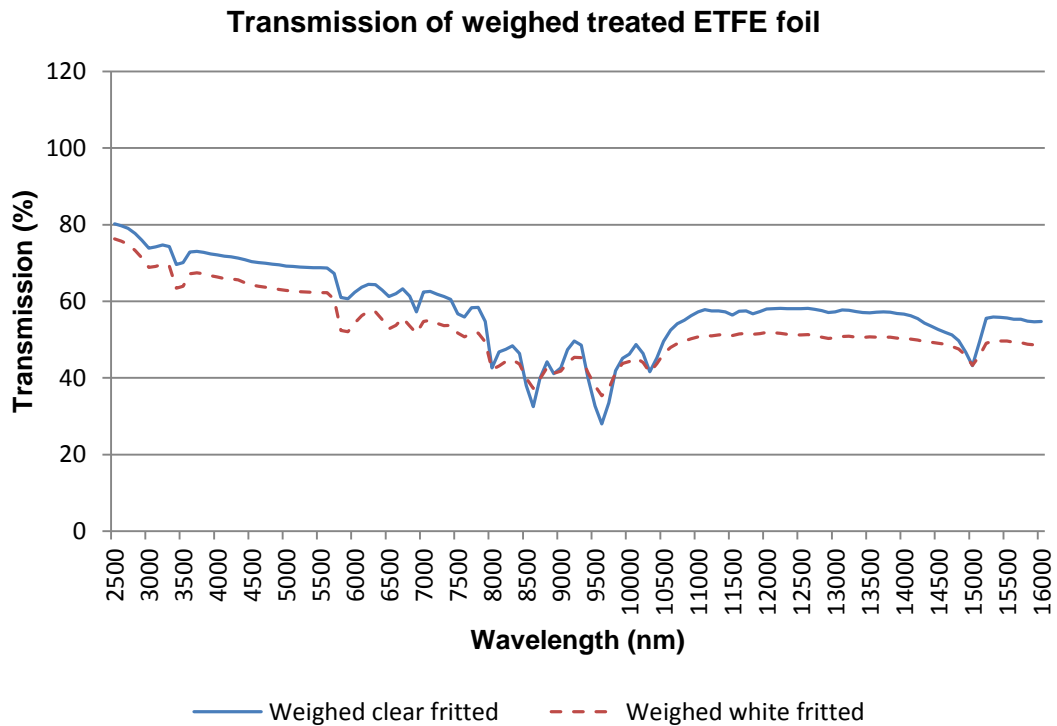


Figure 3.15: Transmission of weighed clear and white fritted ETFE foil

This conversion is useful in identifying the significant effect of the frit on the thermal transmission of an ETFE foil. The white fritted foil, having higher print area coverage by 15% more than the clear fritted foil, presents lower transmission for the most part of the wavelength range under examination. As Table 3.5 demonstrates; this difference in the amount of covered area results to a 4-5% difference in the weighed transmittance.

Table 3.5: Average weighed transmission values (%) of treated ETFE foil

	Clear fritted ETFE (120 μm)	White fritted ETFE (170 μm)
Average transmission (%)		
Throughout the entire range of the FTIR measurements: 2,500 – 16,000 nm	58	53
Throughout the specific range of LW-IR measurements: 8,000 – 15,000 nm	51	47

However, as the area coverage of the frit is not the same, it is not efficient to compare the overall transmission of the two treated types of ETFE foil. Therefore, further analysis will concern the measurements that were taken directly on the fritted area, without any weighing of the results.

The clear and white foils that carried a silver print presented very close curves. Figure 3.16 presents a summary of the transmission of the two silver-print types of ETFE foil; clear and white, as it was measured directly on the silver print of the membrane.

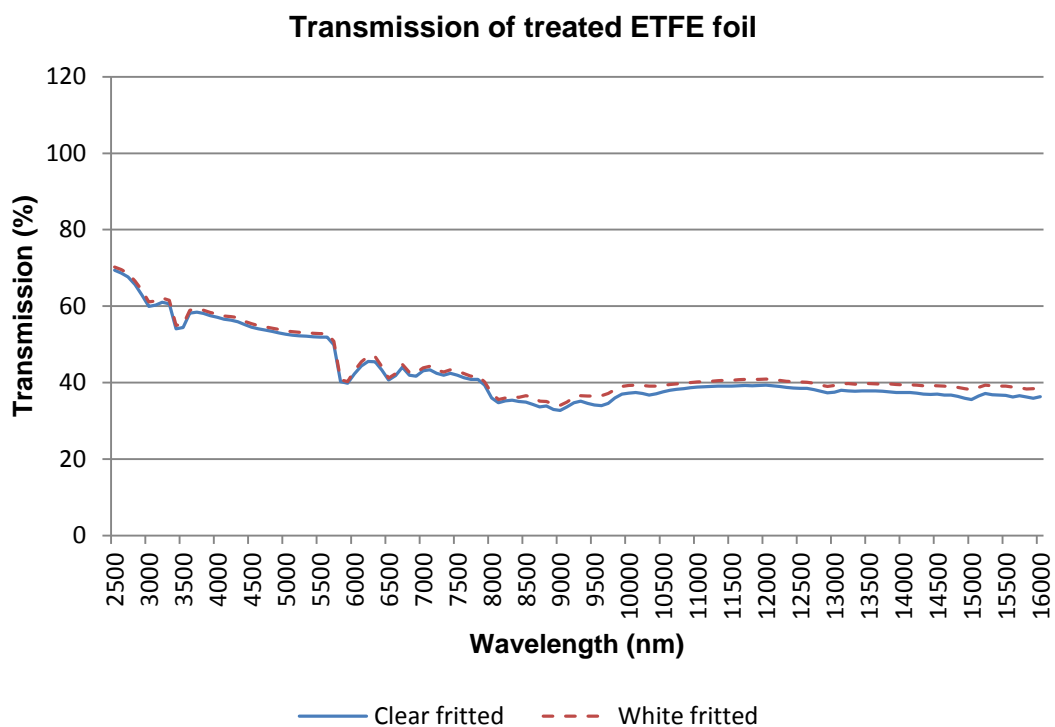


Figure 3.16: Transmission of clear and white fritted ETFE foil

The clear and white treated ETFE foils present much lower transmission values throughout the whole range. Their curves are nearly identical throughout the MIR range, until 8,000 nm and through a part of the LW-IR, up to a wavelength of approximately 9,200 nm. Past this point, for the rest of the LW area and part of FIR wavelengths, the white foil presents slightly higher transmission values, but they consistently fall under a difference of 3% so that does not really allow to draw any significant conclusions as per the distinct behaviour of the two materials.

Table 3.6 presents the average transmission of the two types of untreated ETFE foil as a result of these measurements. As previously, the difference in the transmission values between the clear and white fritted foils is so small that can be rendered insignificant for both the entire FTIR measurement range and the LW measurements. As before, there is a lack of correlation between the measured transmission and material thickness.

Table 3.6: Average transmission values (%) of treated ETFE foil

	Clear fritted ETFE (120 µm)	White fritted ETFE (170 µm)
Average transmission (%)		
Throughout the entire range of the FTIR measurements: 2,500 – 16,000 nm	43	44
Throughout the specific range of LW-IR measurements: 8,000 – 15,000 nm	37	39

At a detailed examination of the results, the differences noted in the peak measurements for the two types of the material do not present a clear correlation between the radiative response of each material and its thickness or colouration. The peak transmission values for the three types of untreated ETFE foil and their corresponding wavelengths can be found in Table 3.7. The differences in transmission values between the treated types of ETFE foil varied between 0% at a wavelength of 6,500 nm to a maximum of merely 2% at wavelengths of 6,300, 8,500, 9,500 and 10,000 nm.

Table 3.7: Peak transmission values of treated types of ETFE foil

	Clear fritted ETFE foil (120 µm)	White fritted ETFE foil (170 µm)
Wavelength (nm)	Transmission (%)	
5,600	52	53
5,800	40	41
6,300	45	47
6,500	41	41

6,700	44	45
6,800	42	43
7,000	43	44
8,100	35	36
8,500	35	37
9,000	33	34
9,400	35	36
9,500	34	36
10,000	37	39

3.5 Methods for the measurement of heat transfer through ETFE foils and cushions

Apart from single material measurements, thermal transmission measurement is also suitable to be applied to non-homogenous structures, comprised by separate construction elements. In addition to transmittance, there is also the option of using thermal conductivity if we are interested in the characterisation of heat transfer through a single homogenous material. The International Standard BS EN ISO 22007 (2012) outlines the methods through which these values can be measured for plastics in the controlled environment of a laboratory.

- Hot Wire
- Line Source / Needle Probe
- Transient Plane Source
- Temperature Wave Analysis
- Laser Flash
- Guarded Hot Plate
- Guarded Heat Flow Meter

The National Physical Laboratory (NPL) (2012) and the analysing and testing company NETZSCH (2013) suggest further measurement methods, such as:

- Low-temperature Guarded Hot Plate
- High-temperature Guarded Hot Plate

- Vacuum Guarded Hot Plate
- Axial Heat Flow Meter

However, only the methods for the measurement of thermal transmission and conductivity for plastic materials as suggested by the British Standards are selected to be evaluated as suitable for the examination of ETFE foil. The second list of methods suggested by the NPL and NETZSCH have so far been standardised for use only on other materials, such as metals, insulation, ceramics and refractories, which is why they will not be further studied in detail.

A summary of the attributes and applications of the methods specifically suitable for plastics is presented in Table 3.8. The information provided by the ISO 22007 Standard was supplemented by the details obtained from the Standard linked to each method (ApacheSim, 2013; Charbonneau *et al.*, 2014; Hu *et al.*, 2014; Knippers *et al.*, 2011; Mainini *et al.*, 2014). Where the equivalent Standard was not accessible or information was missing, further specifications were retrieved from equipment description found in the site of NPL (2012) and the commercial site of Hukseflux Thermal Sensors (2013) (Hottel, 1954; University of Missouri, 1993).

Table 3.8: Measuring methods for thermal conductivity through plastic materials

Testing methods	Hot Wire	Line Source / Needle Probe	Transient Plane Source	Temperature Wave Analysis
Specifications				
Type of plastic materials	Isotropic materials (mainly solid polymers).	Isotropic materials (both solid and molten polymers).	Isotropic or anisotropic materials. Suitable for sheets of materials or thin films.	Thin polymer films (both solid and molten polymers).
Description	Transient method. A wire heater is located inside a sample or between two samples. Heat is emitted and temperature is measured either by the wire heater itself or through a thermocouple.	Transient method. A line-source probe in the form of a needle inside sample. Heat is emitted by the probe and temperature is measured by a thermocouple.	Transient method. An electrically insulated resistive-element sensor comes in contact with two halves of the material. Electrical power is provided and heat is emitted and recorded by	Two electrical resistors are in contact to each side of the specimen. A temperature wave is propagated by one of the resistors, while the other measures the heat flux.

			the resistive-element itself.	
Conformation	ISO 8894-1 ISO 8894-2	ASTM D 5930	ISO 22007-2	ISO 22007-3

Range

Measuring range	Thermal conductivity: Up to 15 W/mK Thermal diffusivity: Up to $5 \cdot 10^{-6} \text{ m}^2/\text{s}$	Thermal conductivity: 0.1 W/mK to 6 W/mK (Hottel, 1954)	Thermal conductivity: 0,01 W/mK to 500 W/mK Thermal diffusivity: $5 \cdot 10^{-8} \text{ m}^2/\text{s}$ to $10^{-4} \text{ m}^2/\text{s}$	Thermal diffusivity: $1,0 \cdot 10^{-8} \text{ m}^2/\text{s}$ to $1,0 \cdot 10^{-4} \text{ m}^2/\text{s}$
Temperature range	Up to 1250 °C	-55 °C to 180 °C (Hottel, 1954)	-225 °C to 725 °C	Electric current: 1 µA to 10 mA

Sample configuration

Thickness	Minimum 50 mm	Minimum volume 80 ml (Hottel, 1954)	Slab specimens: 1 mm to 10 mm Thin film specimens: 0,01 mm to 1,0 mm	10 µm to 500 µm
Diameter	Minimum 200 mm * 100 mm	Minimum 40 mm (Hottel, 1954)	Minimum 20 mm thickness	10 mm * 10 mm

Notes

	Molten polymers are a risk for the temperature-measuring element.	Capable of very fast measurements.	Method can be applied only in solid state materials. Also applicable in cases with orientation effects.	Measurements can be made in ambient air or in reduced pressures.
--	---	------------------------------------	---	--

Testing methods	Laser Flash	Guarded Hot Plate	Guarded Heat Flow Meter
------------------------	--------------------	--------------------------	--------------------------------

Specifications

Type of plastic materials	Homogeneous, isotropic and opaque materials.	Large, flat specimens (commonly insulators)	Large, flat specimens
----------------------------------	--	---	-----------------------

Description	A short energy pulse is emitted in front of the specimen. The temperature rise is measured at the back of the specimen.	Steady-state method. Either one or two specimens situated in contact to one or both sides of a heating plate. Temperature is measured by sensor located on or in the specimen surface. Heat flow is specified from electrical power provided to heater.	Quasi-steady-state method. Either one or two specimens situated in contact to one or both sides of a heating plate. Temperature is measured by sensor located on or in the specimen surface. Heat flow is measured by heat flux transducer (typically thermopile).
Conformation	ISO 22007-4	ISO 8302	ASTM E 1530
Range			
Thermal resistance range	Thermal diffusivity: $1 * 10^{-7} \text{ m}^2/\text{s}$ to $1 * 10^{-4} \text{ m}^2/\text{s}$	Thermal conductivity: 0 to 0.1 W/mK (University of Missouri, 1993)	Thermal conductivity: 0,1 W/mK to 10 W/mK
Temperature range	-100 °C to 400 °C	5 °C to 40 °C (University of Missouri, 1993)	-173 °C to above 200 °C
Sample configuration			
Thickness	0.5 mm to 3 mm	25 mm to 250 mm (University of Missouri, 1993)	1 mm to 20 mm
Diameter	5 mm to 20 mm	Minimum 200 mm Up to 610 mm × 610 mm (University of Missouri, 1993)	50 mm
Notes			
	Contactless measurement of temperature rise with IR detector.	Commonly used and broadly acknowledged method for the measurement of thermal	Consideration of specimen endurance to higher temperatures. Material might

		conductivity of materials (Ward <i>et al.</i> , 2005). Measurements can be performed in gas environment or in vacuum.	need pre-conditioning at highest temperatures.
--	--	--	--

Some of these laboratory-based methods are complex and expensive to perform. Furthermore, some of them are fit to measure plastics above a certain thickness, which exceeds the thickness of ETFE foil, such as the Hot Wire, the Line Source, the Guarded Hot Plate and the Guarded Heat Flow Meter methods. The remaining Transient Plane Source, the Temperature Wave Analysis and the Laser Flash methods are suitable for the measurement of a single ETFE membrane.

However, to fully examine the thermal behaviour of an ETFE membrane as it is commonly used in the building industry we would have to test it in the form of a cushion. In search for an alternative method to measure transmission and conductivity for an ETFE cushion, the available methods for the thermal characterisation of multi-foil insulation were examined as a close alternative. The available methods involve the following, as outlined by Eames (2009) on behalf of the UK Department for Communities and Local Government.

- Guarded Hot Plate
- Guarded Hot Box
- In-situ testing
- Hot box

Table 3.9 highlights the features of each method for the purpose of comparing and selecting the most suitable option for this research (Eames, 2009; Papadakis *et al.*, 2000; Ward *et al.*, 2005). The Guarded Hot Plate has already been examined; however the method will be considered again in this comparison as the most representative selection of the laboratory-based methods described previously and as a similar method to the Guarded Hot Box.

Table 3.9: Comparison of methods for the thermal characterisation of multi-foil insulation

Testing methods	Guarded Hot Plate	Guarded Hot Box	In-situ testing	Hot box
Attributes	Measures the thermal conductivity of flat surfaced materials of uniform thickness.	Measures the thermal conductivity of inhomogeneous materials and façade structures.	Measures the thermal conductivity of the entire experimental unit or part of it instead of a single material.	Measures the thermal conductivity of large inhomogeneous specimens and façade structures.
Process	Use electronic equipment to provide a unidirectional constant and uniform density of heat flow rate when placed against a specimen.		Determines the performance of a real structure by exposing it to real conditions and recording data for a long time period.	Uses a device comprising of two air spaces separated by the material under examination; i.e. one metering and one climatic chamber on either side of the specimen.
Advantages	Robust, reliable, steady-state measurements on small specimens.		Realistic results, as test structure is exposed to real weather conditions.	Offers flexibility through control over testing environment.
Disadvantages	Increased complexity to build and high cost.		Decreased accuracy and increased complexity regarding data measurement and analysis.	

The in-situ testing method was selected for the purposes of this research. Primarily, the guarded hot plate and the guarded hot box were found unsuitable for the testing of ETFE foil due to increased complexity to build and high cost; the in-situ testing would be much simpler to build and conduct in contrast to the two lab-based measurement methods. Furthermore, as the in-situ testing can examine an entire experimental unit including a façade structure, it is found suitable for the study of an ETFE cushion, in contrast to the lab-based options that could only test the ETFE membrane itself, without taking into consideration the insulating effect of the air trapped inside. Finally, the in-situ method was selected over the unguarded hot box method as it provides with a variety of measured responses of the material to diverse circumstances because of

the exposure of the testing unit to real-life conditions. This will allow the investigation of a broad spectrum of the membrane's thermal behaviour.

A related research is that of Ward *et al.* (2005) on behalf of the Building Research Establishment (BRE), using the in-situ testing method to examine multi-foil insulation. Two experiments took place using multi-foil insulation to improve the performance of existing buildings in separate UK locations. In the first experiment the insulation was used to enhance the walls of the building and in the second experiment the roof and floor. The in-situ measurements were performed as defined by the ISO 9869 standard. The U-value was calculated in accordance to the BS EN ISO 6946 standard and an average thermal transmission value was extracted for the materials under examination. The research compared the averaged results of the in-situ measurements to those obtained by an NPL guarded hot box, concluding that the on-site experiment is able to provide data that is in good agreement to the data recorded in a more controlled environment. This work supports the validity of in-situ testing and backs the decision to follow this method for the conduction of the present research.

To summarise, this chapter initially provided a brief introduction to the basic notions of heat transfer; conduction convection and radiation. Other concepts that were also discussed shortly are the radiative properties reflectance, absorbance and transmission, wavelength and view factor.

This introduction to heat transfer is put into context through the following part of the chapter presenting a summary of the existing literature on the primary employment of ETFE foil in greenhouses in regards to its thermal behaviour. The reason for that is that most of the initial research performed on ETFE foil and the energy loss or gain associated with it in comparison to glazing has concerned greenhouses, as this was initially the most common structural environment where the material was applied. A description of heat transfer in greenhouses has been discussed alongside the comparison of use of either glass or plastic as a cladding. Heat loss and condensation were debated.

Following this investigation was an overview of the thermal behaviour of films, glass and ETFE membrane under the prism of thermal transmission. What is more, a set of measurements was performed using an FTIR spectrometer, allowing for a description of the radiative properties and the comparison of different types of ETFE foil. As these measurements described only a part of the thermal behaviour of the material, it was established that further experimentation was required.

For this reason, this chapter also focused on summarising the available methods for the measurement of heat transfer as they have been established by standards and research bodies, either in a laboratory or a real life setup. This constituted the basis for the conducted in-situ experiment, as it will be described in Chapter 4.

4 In-situ experiment

The physical experimentation compared the thermal performance of a two-layered inflated cushion against a double glazed unit with a 6 mm gap, in absence of gas fillings and low-E coatings.

4.1 Planning of experiment

A set of boxes were used for the experiment, which were cubes of 900 mm height, width and length, with walls and floor made of a single layer of 100 mm PIR foam insulation. The assembly was held in place externally by a wooden frame which enclosed a rubber strip in its perimeter to minimise air loss. The box and frame edges were sealed with polyurethane spray foam. The box was coated with white matt waterproof paint on the inside and outside. The structure was located on the roof of the Department of Architecture and Civil Engineering building at the University of Bath (51.38°N, 2.36°W), in Southwest England. Figures 4.1 to 4.3 illustrate the experimental apparatus.



Figure 4.1: Experimental set-up on the roof of the Department of Architecture and Civil Engineering building



Figure 4.2: Experimental set-up



Figure 4.3: The ETFE cushion alongside the double glazed unit

In order to minimise the risk of condensation the boxes were fitted with a ventilation and dehumidification system. A 100 mm Vent-Axia Silhouette Fan (Figure 4.4) and an exhaust vent outlet with shutters (Figure 4.5) were used in each box to assist the controlled ventilation of the experimental unit and eliminate condensation issues, while functioning by default at a maximum extraction rate of 26 L/sec. The fans in both boxes were running continuously and maintained good interior relative humidity levels, which will be explored in more detail in the following section. (Fantronix, 2013; Masters, 2013)



Figure 4.4: Wall-mounted fan (Fantronix, 2013)



Figure 4.5: Wall-mounted exhaust vent (Masters, 2013)

The extracted air went through a plastic ventilation tube of 100 mm diameter, enveloped in a 25 mm thick layer of sheep's wool insulation and surrounded by an external reflective flexible tube of 150 mm diameter. The tube system was connected in an air-tight manner to a separate external box constructed from 100 mm PIR rigid foam insulation holding 285 g of loose desiccant silica gel in each box. The silica gel was dried out prior to weighing and instalment in the boxes. After being introduced to the desiccant boxes the same air was then returned to the experimental boxes to avoid heat loss through a fitted outlet with shutters. Figures 4.6 and 4.7 depict a schematic plan and section, and a diagram of the whole experimental setup.

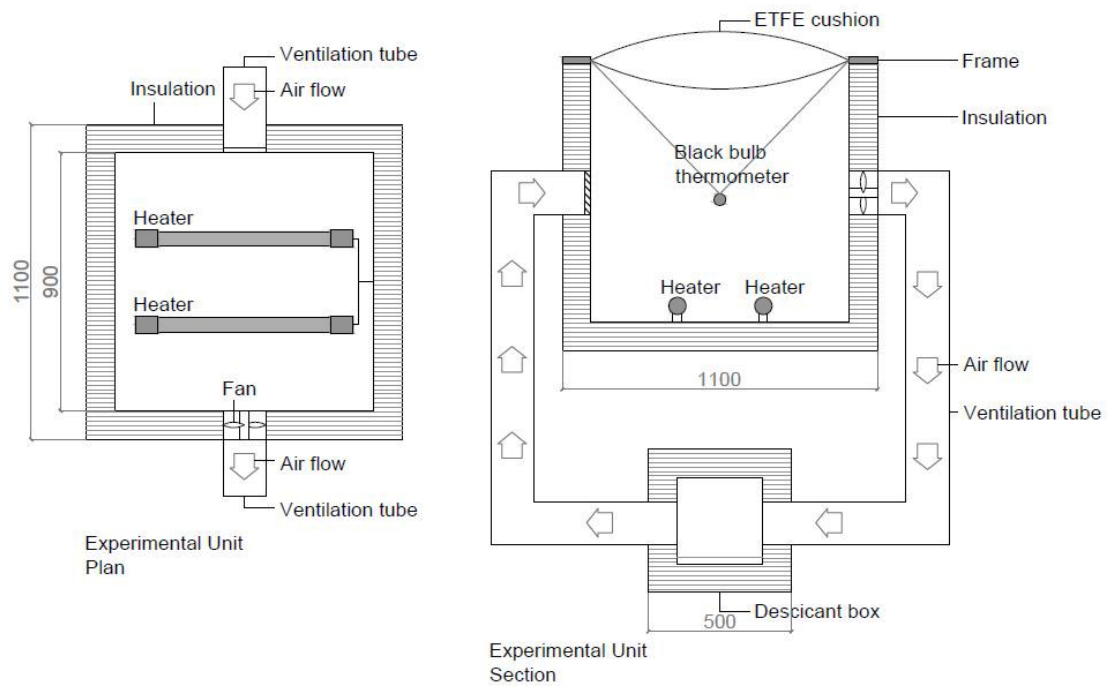


Figure 4.6: Schematic plan and section of experimental setup

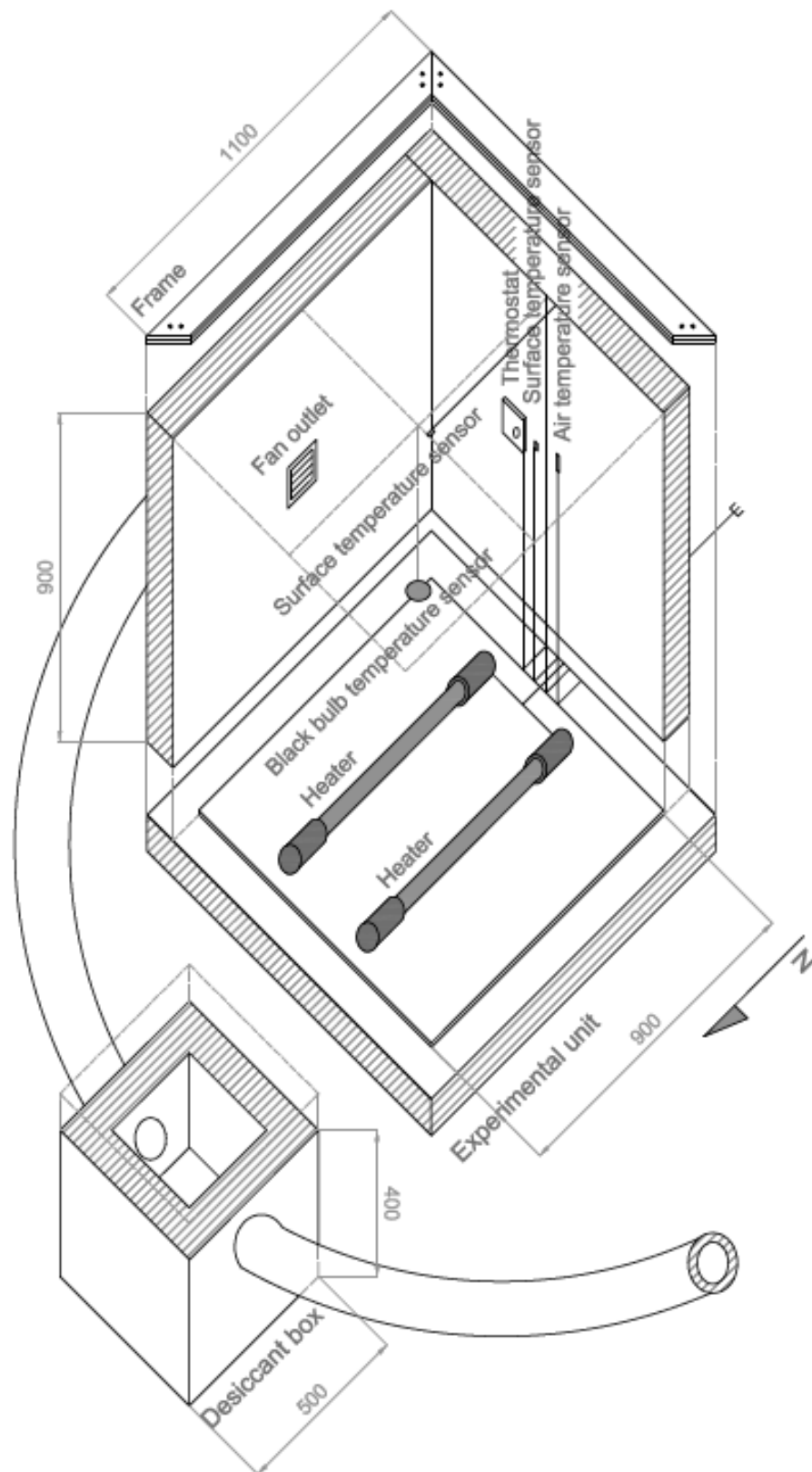


Figure 4.7: Schematic diagram of experimental setup

The ETFE unit was comprised of a two-layer cushion with dimensions of 900 mm x 900 mm. The cushion membrane had a thickness of 200 μm and the internal side of the cushion is covered by a reflective dotted silver frit, which is representative of typical ETFE applications, as described previously in Chapter 2 on the introduction to the material. The ETFE unit was prefabricated and supplied by Vector Foiltec and was inflated to 220 Pa using a Michelin 12250 12 v Digital Tyre Inflator Air Compressor. The selected pressure of 220 Pa was recommended by the manufacturing company of the cushion and was in agreement with the available literature, as described in Chapter 2. The edge of the ETFE cushion incorporated a rod which was used for the secure support and anchoring of the cushion within the frame constructed in the laboratories at the University of Bath. A schematic detail of the frame is presented in Figure 4.8.

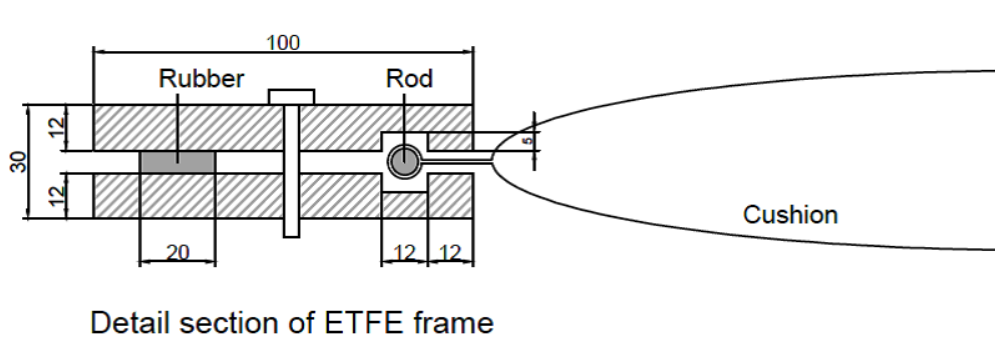


Figure 4.8: Schematic frame detail

The glass unit was comprised of a double glazed panel of 900 mm X 900 mm and a common composition of 4 mm glass – 6 mm air gap – 4 mm glass. The thickness of the glass was selected to ensure the weight of the cover was manageable.

Each box enclosed two Dimplex model T tubular heaters of 655 mm length and 80 mm diameter, with a heating capacity of 120 W each. Such electric heaters are typically made of non-corrosive aluminium. The heaters had a direct view of the film and glass covers. The energy consumed by the heaters was measured using Elster A100c electricity meters. Their pulsed output was recorded using Grant SQ2010 Data Loggers. The number of pulses was recorded at 5 minute intervals.

Two K-type thermocouples were located centrally on the inside of the South-facing wall and the cover of each box to record surface temperatures, with a standard accuracy of ± 2.2 $^{\circ}\text{C}$ (ReoTEMP, 2014; Thermometrics, 2014). The experimental units were

elevated on a metal platform on the roof of the University building, unobstructed by any natural or built surroundings. For that reason the thermocouple recordings remained uninfluenced by extraneous radiative effects from the local albedo. The surface temperatures were measured with the use of a Grant SQ800 Data Logger. Each box also housed air temperature, black bulb radiant temperature and humidity sensors to monitor interior conditions.

Black bulb radiant temperature is defined as the temperature of a sphere at the point in question which would exchange no net radiation with the environment (CIBSE, 2006). Black bulb thermometers were constructed, securing a thermocouple in a lightweight black sphere (Figure 4.9). The thermometers were located in the centre of each box.



Figure 4.9: Black bulb thermometers

The internal box air temperature and black bulb radiant temperature were recorded using a Grant SQ2010 Data Logger, whereas humidity was measured with the use of a Tinytag Data Logger. Several data loggers were used for the recording of each attributing internal condition as they had different capabilities. More specifically, the SQ800 is a device dedicated to logging results recorded solely by thermocouples, whereas the SQ2010 Data Logger is able to record current, voltage, resistance and temperature.

A calibration process was performed to overcome differences between the recorded data for the two boxes and to provide a modifying factor that could be applied to correct the measured results and ensure that issues like heat loss due to infiltration were taken into account. The calibration process will be described in the following section of this chapter. Finally, the Tinytag Data Loggers were capable of recording both humidity and air temperature. However, the Tinytag devices were selected to record only humidity, as the calibration process revealed that they performed less accurately in documenting air temperature than the system involving the thermocouples and Grant Data Loggers.

Figure 4.10 presents a schematic diagram of the experimental setup and the location of electrical and electronic devices for each box.

Schematic of electrical and electronic equipment within experimental box

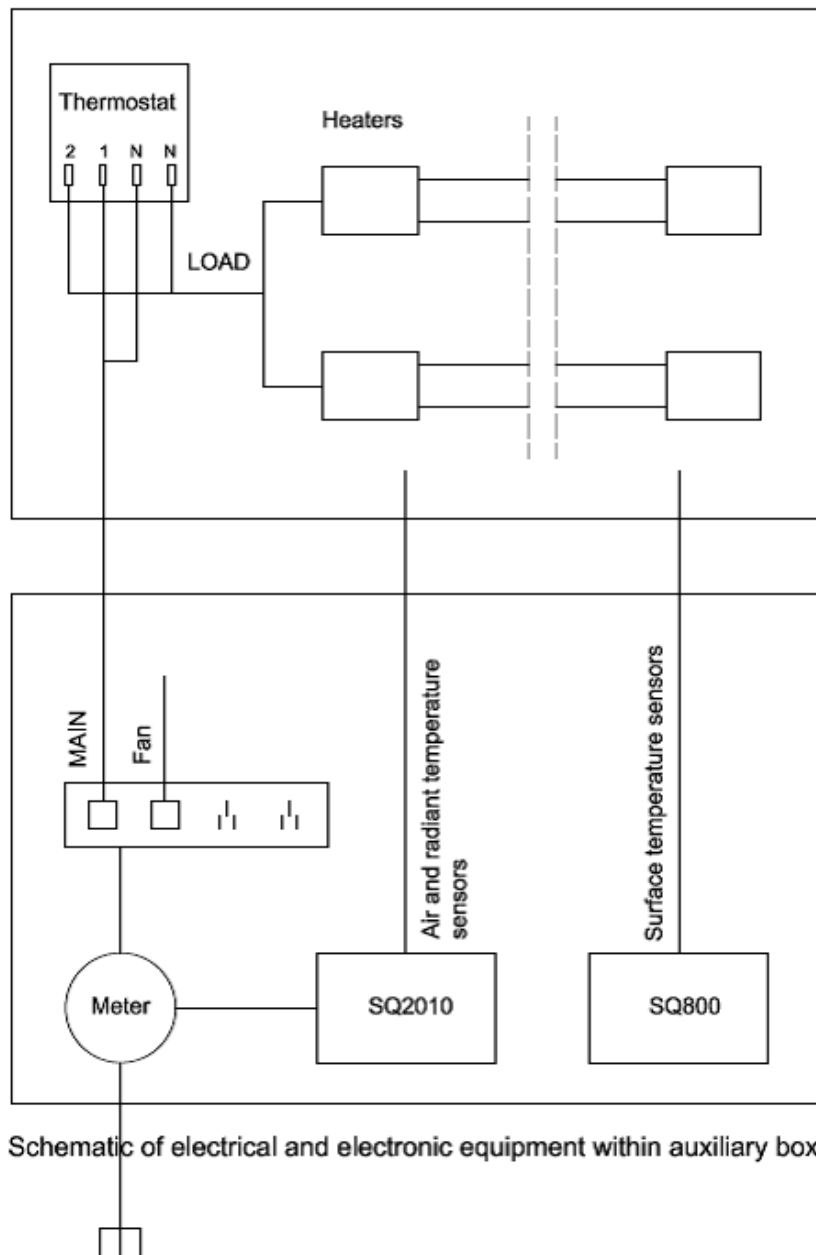


Figure 4.10: Schematic diagram of electrical and electronic devices set-up

External air temperature was monitored in the same location of the experiment, using equipment that was shielded from the elements. Additionally, a Kipp & Zonen CMP3 pyranometer and a CGR3 pyrgeometer were used for the measurement of the corresponding incident shortwave and long-wave radiation (Figures 4.11 and 4.12).



Figure 4.11: CMP3 Pyranometer by Kipp & Zonen (Kipp&Zonen, 2012)



Figure 4.12: CGR3 Pyrgeometer by Kipp & Zonen (Kipp&Zonen, 2012)

One pyranometer was shaded by a band that was adjusted to the geographic location of the 6 East building on the University of Bath campus. The shading band was manually adjusted to avoid the effect of direct solar radiation. A second CMP3 pyranometer was used to measure direct solar radiation.

4.2 Box calibration

Prior to conducting the experiment, each box was calibrated by covering them with a 12 mm plywood sheet, protected by a layer of white, waterproof, non-reflective paint. The boxes were calibrated continuously between the 10th of January and the 18th of February 2013. Both boxes were exposed to the same shortwave and long-wave radiation and external air temperature conditions with the same heating, ventilation and recording equipment, placed in the same locations.

The box that would later be covered with the ETFE cushion was situated on the South of the box that would later be covered with glass and was therefore more exposed to the prevailing winds of the area. This resulted in a greater heat loss and required the use of adjustment coefficients on the measured data to match the trend describing the interior thermal conditions and the co-responding energy performance of the glass box.

To obtain the regulating coefficients the average value of each measured parameter for the ETFE-receiving box were deducted from the equivalent average value for the double glazing covered box. These coefficients were then added to the measured

results to equalise the behaviour of the ETFE covered box to that of the double glazing covered box. Equations 4.1 to 4.6 describe the relationships that were later applied to the measured interior conditions and energy consumption when the box covers were replaced with the intended cladding.

$$T_{a\ ETFE} = T_{a\ glass} + 0.7 \quad \text{Equation 4.1}$$

$T_{a\ ETFE}$: Interior air temperature of the ETFE-receiving box (°C)

$T_{a\ glass}$: Interior air temperature of the glass- receiving box (°C)

$$T_{bb\ ETFE} = T_{bb\ glass} - 0.4 \quad \text{Equation 4.2}$$

$T_{bb\ ETFE}$: Interior black-bulb temperature of the ETFE- receiving box (°C)

$T_{bb\ glass}$: Interior black-bulb temperature of the glass- receiving box (°C)

$$T_{w\ ETFE} = T_{w\ glass} - 0.3 \quad \text{Equation 4.3}$$

$T_{w\ ETFE}$: Interior wall temperature of the ETFE- receiving box (°C)

$T_{w\ glass}$: Interior wall temperature of the glass- receiving box (°C)

$$T_{r\ ETFE} = T_{r\ glass} - 0.5 \quad \text{Equation 4.4}$$

$T_{r\ ETFE}$: Interior roof surface temperature of the ETFE- receiving box (°C)

$T_{r\ glass}$: Interior roof surface temperature of the glass- receiving box (°C)

$$RH_{ETFE} = RH_{glass} + 5.3 \quad \text{Equation 4.5}$$

RH_{ETFE} : Interior relative humidity of the ETFE- receiving box (%)

RH_{glass} : Interior relative humidity of the glass- receiving box (%)

$$P_{ETFE} = P_{glass} - 0.53 \quad \text{Equation 4.6}$$

P_{ETFE} : Recorded pulses for the ETFE- receiving box

P_{glass} : Recorded pulses for the glass- receiving box

The relative error between experimental and computational data was estimated to indicate the precision of the estimated calibrated values in relation to measured values, using Equation 4.7.

$$\% e_{rel} = \frac{R_{meas} - R_{pred}}{R_{meas}} * 100 \quad \text{Equation 4.7}$$

e_{rel} : Relative error

R_{meas} : Measured value

R_{pred} : Predicted value

The error between the estimated and measured interior air and radiant temperatures of the ETFE box resulted to 3.5% (or 0.04 °C) and 1.9% (or 0.02 °C) respectively. The error between the estimated and measured wall temperature for the ETFE box was found to be 1.6% (or 0.02 °C) and for the roof temperature 3.3% (or 0.03 °C). Finally, the error between the estimated and measured relative humidity was calculated to be 24.4% (or 0.24%), while the error for the pulses was 2.4% (or 0.02). As the estimated error for all monitored values was smaller than the adjustment coefficients used in the box calibration, it is considered negligible.

After the calibration of the measured results, the two boxes covered by wood presented identical thermal behaviour and energy consumption, which allowed the following recordings under the ETFE cushion and the glass unit to be evaluated on a comparable basis. The result of this process on internal conditions and energy consumption will be further analysed in section 4.4.

4.3 Results – Exterior conditions

The external condition measurements presented were recorded between 00:00 on the 30th of March 2013 and 23:00 on the 5th of April 2013. Following a two-month recording period the data was processed and a seven day period with a suitably broad variation in weather conditions was selected for further analysis. The values are presented at a sampling rate of one recording per 10 minutes.

Shortwave measurements describe the recorded incoming solar radiation presented in Figure 4.13 in time intervals of ten minutes. The higher the indicated shortwave value, the more solar input was recorded on site. Shortwave values above 50 W/m² and below 120 W/m² demonstrate an overcast sky, whereas above 500 W/m² and up to 1000 W/m² indicate a clear sky; the intermediate values signify partly cloudy conditions (Kipp

& Zonen, 2012). The solar conditions varied between completely overcast and clear sky. The blue (bottom) band in Figure 4.13 shows the overcast sky radiation range and the orange (top) band shows the clear sky radiation range.

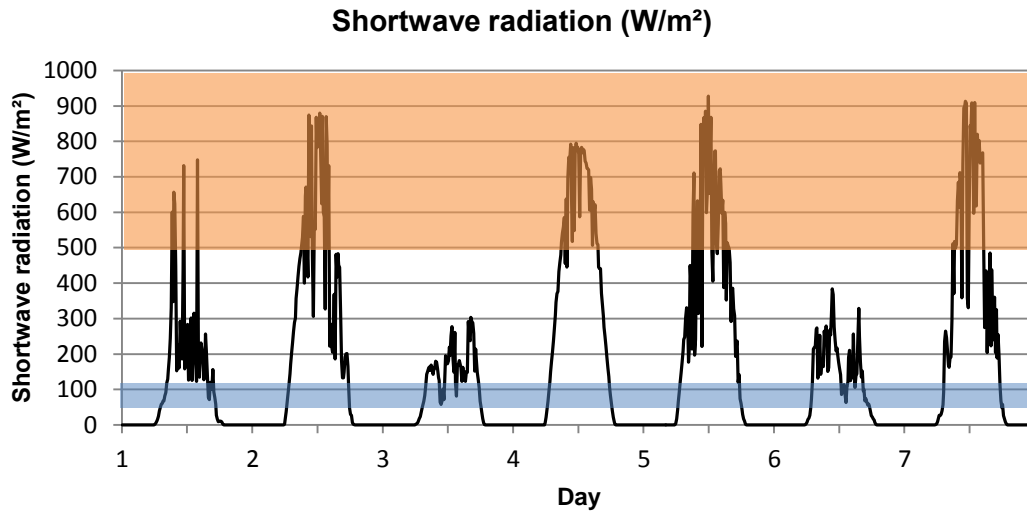


Figure 4.13: Shortwave radiation (W/m²)

A variety of external air temperatures were evident throughout the monitoring period, as it can be seen in Figure 4.14, demonstrating that external air temperatures measured on site between -2.7 °C and 6.8 °C. The range of external environment temperature was constantly below the desired 19 °C, therefore causing the system to initiate its heating function most of the time.

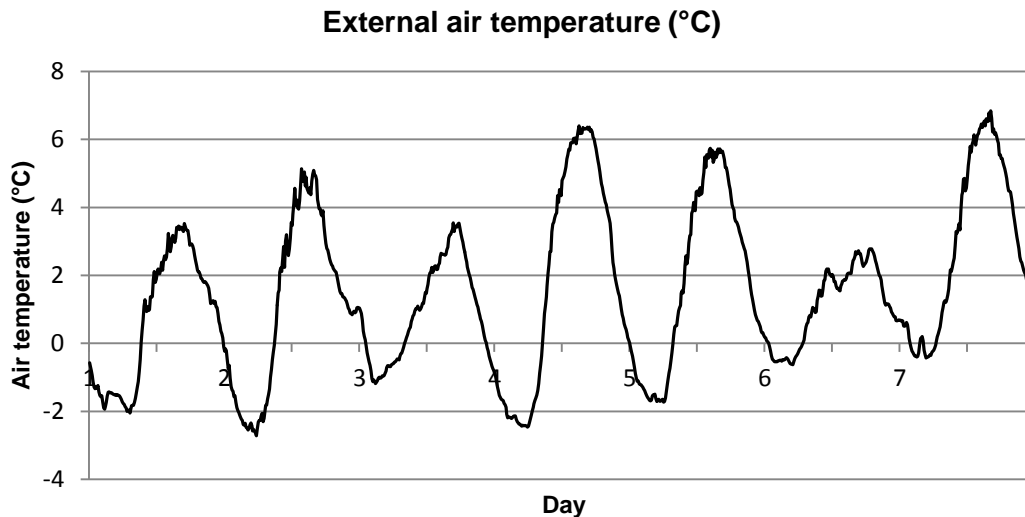


Figure 4.14: External air temperature (°C)

To complete the profile of external conditions it was necessary to provide information on long-wave radiation. The long-wave measurements represent net long-wave radiation as measured by the pyrgeometer device. All surfaces receive shortwave radiation during the day and continuously exchange long-wave radiation during day and night (Papadakis *et al.*, 2000). Lower net long-wave values $\approx -150 \text{ W/m}^2$ indicate a clear sky, whilst values $\approx 0 \text{ W/m}^2$ indicate a fully overcast sky (Kipp&Zonen, 2010).

Long-wave radiation is significant, as it will indicate the existence or lack of clouds above the cladding material and the environmental measurement equipment. Heat loss through the material will be greater under a clear sky, rather than under a cloudy one (Zhang *et al.*, 1996).

The importance of clouds on sky radiation increases with the drop of temperature (Berdahl *et al.*, 1982). This fact is significant in the case of this experiment as it took place under partly cloudy conditions, when the solar influence on the passive design aspect of the boxes was at its lowest.

Regarding the estimation of the thermal radiance of the sky, the effect of a cloud on the spectrum of atmospheric radiation can be perceived of and simulated as a black body emitter. It is easier to detect an overhead cloud at an angle of $\theta=0^\circ$, in comparison to an angle that would locate the cloud near to the horizon. Furthermore, it is interesting to take into account that lower clouds are more emissive, therefore have a greater

impact on sky radiation and their existence is easier to detect by measurement instrumentation, in contrast to clouds located at higher levels (Berdahl *et al.*, 1982).

However, it is not typically the net long-wave radiation that is used to describe external conditions; but the converted downward long-wave derived from the negative measured values of incoming radiation. L_{\downarrow} symbolises downward long-wave radiation and it is dependent on air temperature, as seen below in the conversion from the measured net long-wave radiation L_{net} (Equation 4.8) (Alados, 2012; Kipp&Zonen, 2010):

$$L_{\downarrow} = L_{net} + \sigma * T_b^4 \quad \text{Equation 4.8}$$

L_{\downarrow} : Downward long-wave radiation (W/m²)

L_{net} : Measured net long-wave radiation (W/m²)

σ : Stefan-Boltzmann constant (5.67 * 10⁻⁸ W/m²K⁴)

T_b^4 : Body temperature of CGR3 device (K) (where K=°C + 273.15)

The instruction sheet for the CGR3 equipment categorises downward long-wave radiation according to two main sky types; clear and fully overcast, and in relation to ambient air temperature, as presented in Table 4.1 (Kipp&Zonen, 2010).

Table 4.1: Categorisation of fully clouded and clear, sunny sky in relation to downward long-wave radiation and air temperature (Kipp & Zonen, 2010)

Ambient temperature (°C)	Clear & sunny sky L_{\downarrow} (W/m ²) (When $L_{net} \approx -150$ W/m ²)	Fully clouded sky L_{\downarrow} (W/m ²) (When $L_{net} \approx 0$ W/m ²)
-20	80	230
0	165	315
30	330	480

Figure 4.15 presents the converted downward long-wave radiation for the dates under examination.

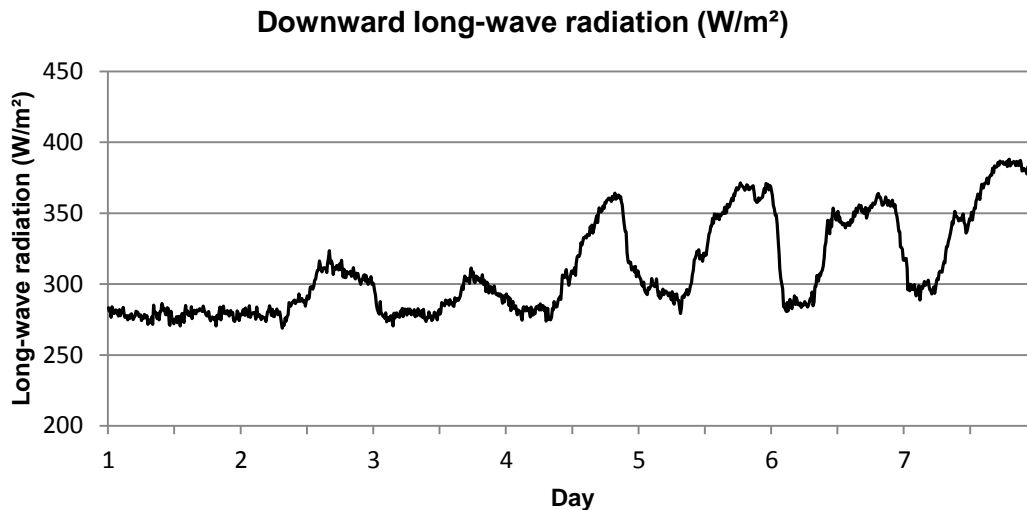


Figure 4.15: Downward long-wave radiation (W/m²)

A review of long-wave models was conducted to further examine the literature on the background and relationship of downward long-wave radiation L_{\downarrow} and emissivity ϵ , as it is developed in more detail in section 4.4. A model was developed based on the existing literature for the estimation of long-wave radiation on ground-based measurements and real-life measurements were used to examine the model's validity.

4.4 Long-wave radiation and emissivity

There has been extensive research on the classification of sky types in a more detailed relation to L_{\downarrow} . Several models have been developed concerning the distinction between clear, partly cloudy or overcast skies and numerous other variations in between them. Ander (2003) defines a clear sky as one in which no more than 30% of its dome is obscured by clouds. A partly cloudy sky is a sky where 30% to 80% is covered by clouds and an overcast sky is defined as a sky with at least 80% of its dome covered by clouds. The estimation of L_{\downarrow} for all three sky types is typically performed through all-sky models that are capable of representing the entire range, as opposed to a clear sky model or an overcast sky model (Perez *et al.*, 1993; Standards, 1997; Standards, 2004).

The main models found in the literature for the estimation of L_{\downarrow} under clear, partly cloudy or overcast sky are those of Brunt (1932), Idso and Jackson (1969), Brutsaert (1975), Berdahl and Martin (1984) and Prata (1996), as summarised and examined by Alados (2012) and Iziomon (2003), that depend significantly upon experimentally

defined coefficients based on the geographical site location. Their parameterisations offer an alternative for the calculation of L_{\downarrow} under all-sky conditions in cases where cloud information is not available; however, as they are based on a number of assumptions and simplifications they cannot offer guaranteed accurate results for all weather conditions and for all geographical sites.

There has been research that estimated emissivity independently from geographically specific sites. Such work is that of Sedlar *et al.* (2009), who determined emissivity to have a value of approximately 0.7 for clear skies and 1 for completely overcast skies, in agreement to prior research such as that of Konzelmann *et al.* (1994) and Marty and Philipona (2000).

Herrero *et al.* (2012) investigated the parameterisation of L_{\downarrow} in a mountainous site for all-sky conditions. Lower ϵ values indicated a clear sky; on very clear days with low temperatures and relative humidity emissivity was found to vary between 0.5 and 0.6, values that are in agreement with the work of Brutsaer (1975). For that particular set of measurements, Herrero *et al.* (2012) defined 0.77 to be the emissivity specifying the limit between clear sky and partly covered sky. They describe a partly covered sky as a transition zone between the two main situations of clear sky and completely overcast. This region extends up to an ϵ value of 0.9, above which point emissivity is that of a completely overcast sky, up until the limit of 1.

The expression of downward long-wave radiation in relation to effective emissivity has been used by various researchers as in the following Equation 4.9 (Alados, 2012; Chen *et al.*, 2013):

$$L_{\downarrow} = \epsilon * \sigma * T_b^4 \quad \text{Equation 4.9}$$

L_{\downarrow} : Downward long-wave radiation (W/m²)

ϵ : Emissivity ($0 < \epsilon < 1$)

σ : Stefan-Boltzmann constant ($5.67 * 10^{-8} \text{ W/m}^2\text{K}^4$)

T_b^4 : Meter body temperature (K)

Regarding the approximation of clear sky emissivity, another experimentally derived approach is that of Monteith (1961), as seen in Equation 4.10 (Stensrud, 2007).

$$\varepsilon_o = 0.725 + 0.17 * \log_{10} e_w \quad \text{Equation 4.10}$$

e_w : Vapour pressure related to wet-bulb temperature

$$e_w = 6.112 * \exp\left(\frac{17.67 * T_{dp}}{T_{dp} + 243.5}\right)$$

T_{dp} : Dew point temperature (°C)

This relationship was tested against the weather data under examination. Results ranged between 0.81 and 0.85 and the provided an average value for clear sky emissivity of 0.83; much higher than the previously suggested values, however, a good fit for the current data set.

A more extensive literature summary was performed, to conclude that the existing popular methods for estimating sky emissivity are primarily based on experimentally derived parameters and therefore are not able to provide accurate results that suit all weather data sets, even using the clear sky category which allows for the most precise estimates. Various models were tested against the weather data gathered during this research and were found unsuitable to provide with accurate results. As these models are not used in this study, this summary can be found in Appendix B.

Equation 4.9 was used to estimate emissivity ε from the available downward long-wave data, as shown in Figure 4.16. This allowed the categorisation of the sky conditions for clear and overcast in the absence of shortwave radiation.

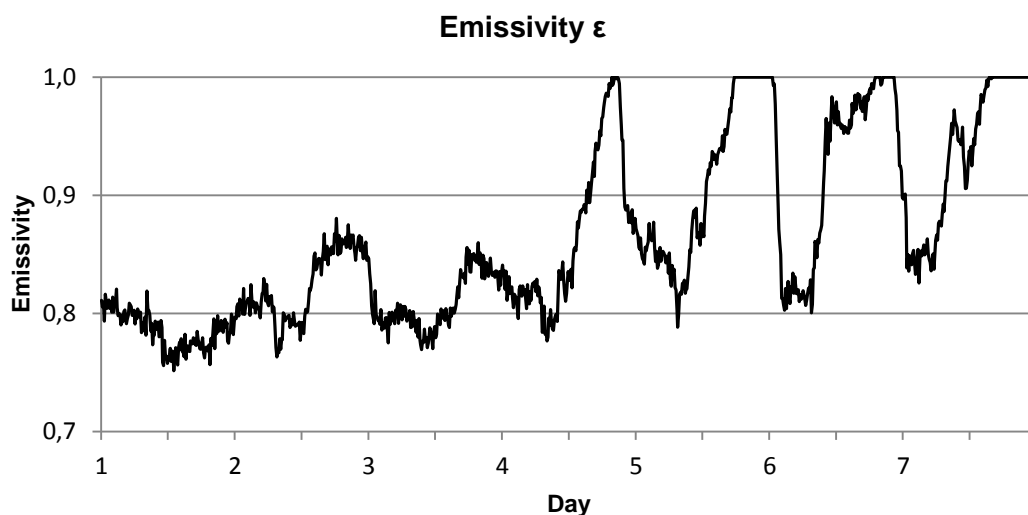


Figure 4.16: Emissivity ε

The calculated emissivity values will be used in the following section, allowing the interpretation of weather conditions and sky classification to be implemented in relation to the thermal and energy response of each box to external environmental conditions. A subjective assumption was made, selecting clear and overcast sky emissivity value thresholds as the best fit for this data set in agreement to sky classification via personal observation and with the help of shortwave radiation measurements. Two of the examined methodologies were combined, selecting the adapted equation of Monteith (1961) resulting in 0.83 as the upper limit for a clear sky emissivity value and the classification suggested by Herrero *et al.* (2012), using 0.9 as the lower limit of an overcast sky emissivity value.

4.5 Results and analysis – Interior conditions and energy consumption

The result of the overall behaviour of each material as a response to external conditions will be demonstrated through internal conditions; i.e. internal air, radiant, wall and roof temperatures and humidity levels. Thereafter, part of these results will be used to express the energy consumption of each box in relation to the interior-exterior environment relationship.

- The range of air temperatures recorded in the ETFE covered box varied between approximately 17 and 48 °C and the range of radiant temperatures varied between 16 and 53 °C. At the same time, the range of measured air temperatures inside the glass box spread between 17 and 50 °C, whereas the measured radiant temperatures ranged between nearly 16 and 58 °C. The graphs depicting these ranges in detail, in 10 minute intervals, can be found in Appendix C (Figures C.1 and C.2). The high measured internal temperature values were recorded under clear sky conditions, whereas both materials absorbed and transmitted shortwave solar radiation, which caused peak rises in the recorded results. During the rest of the time and when the heating system was operating, (during the night-time and under cloudy skies), both boxes steadily maintained interior conditions close to the desired set point of 19 °C, as an average value suggested by CIBSE for heating requirements of a number of spaces (CIBSE, 2006).

The lower recorded upper threshold of overheating air temperatures of the ETFE box could be associated to the better U-value of the cushion. The reflective properties of the silver dotted print on the interior surface of the upper membrane comprising the ETFE cushion also assisted the effect of the insulating properties of the cushion on the

maintenance of internal conditions. The lower measured radiant temperatures within the ETFE box under a clear sky could be justified through the transparent nature of the material towards long-wave radiation and the consequent radiative heat loss.

This is consistent with the fact that glass is opaque to long-wave radiation and therefore retains more heat, whereas ETFE allows some of this heat to escape. As the focus of this thesis concerns the energy requirements in relation to heating, a different approach was required, ignoring the effects of shortwave radiation. In the absence of solar input both materials maintained a radiant temperature that was settled around the set goal of 19 °C, demonstrating that both materials were able to maintain comfortable conditions.

The recorded data was divided into two datasets; one for a clear sky and one for overcast sky conditions. To avoid the effect of incoming solar radiation and the consequent overheating of the boxes, the data analysis concerns only night-time recordings, between 19:00 pm and 06:00 am. For the purpose of visual clarity, the data on interior measurements and energy consumption that are presented here is in the form of hourly average values. Scatter diagrams were used to demonstrate the correlation between the different variables under examination. Trend lines were added to clarify the development of the data relationship. The standard deviation of data was estimated to express computational error and describe the spread of the measured values from the mean values, according to Equation 4.11.

$$\sigma = \sqrt{\frac{1}{M} \sum_{1}^M (R_{meas} - R_{mean})^2} \quad \text{Equation 4.11}$$

M : Total number of measurements

R_{meas} : Measured value

R_{mean} : Mean estimated value

The following results allow the analysis of internal air and radiant temperature in relation to long-wave values. Figures 4.17 and 4.18 present the recorded air temperatures in both boxes under a clear and an overcast sky respectively. The standard deviation for the plotted air temperature inside the ETFE box in relation to a clear sky was 0.09 °C and in relation to an overcast sky it was 0.16 °C. The standard

deviation for the plotted air temperature inside the glass box under a clear sky was 0.09 °C and under an overcast sky it was 0.12 °C.

The ETFE box consistently recorded higher air temperatures than the glazed box – closer to the desired 19 °C – under both climatic conditions – though by a very small difference (below 1 °C), which falls within the margin of error. Additionally, the ETFE box showed a slight tendency for the air temperature to drop as long-wave radiation increased, i.e. as the sky became cloudier, a trend that was not noticed for the glass box.

The mean air temperature difference between the ETFE and the glass box was 0.29 °C under a clear sky and 0.38 °C under an overcast sky. Under clear sky conditions, the trend for the ETFE-related temperature to decrease with the increase of clouds was of the order of 0.03 °C and the equivalent trend for the glass-related temperature was 0.02 °C and, therefore, could not be considered a significant indicator of behaviour. Under overcast sky conditions, the trend for the ETFE-related temperature to decrease with the increase of clouds increased to 0.26 °C the equivalent trend for the glass-related temperature became 0.11 °C.

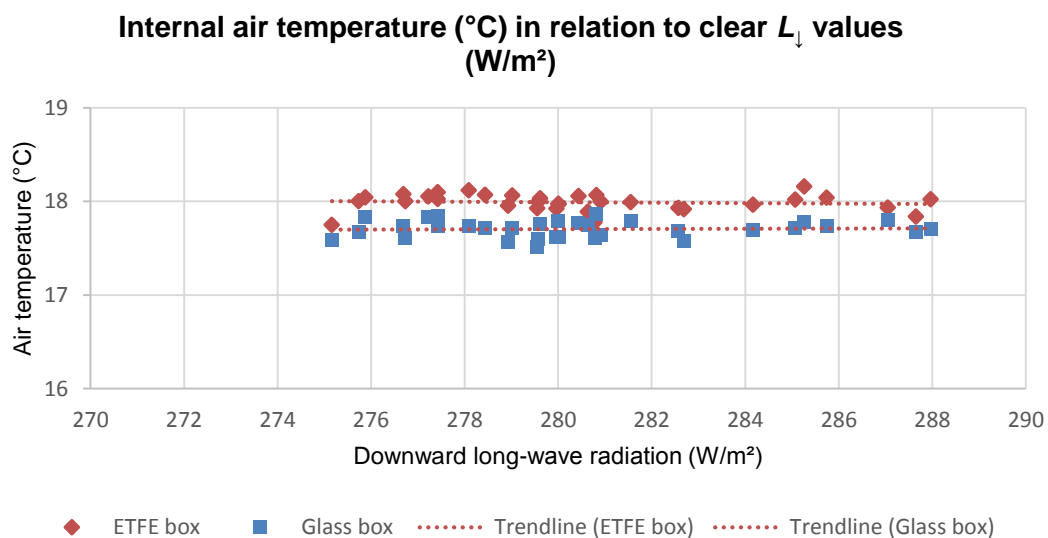


Figure 4.17: Internal air temperatures (°C) in relation to clear sky long-wave radiation (W/m²)

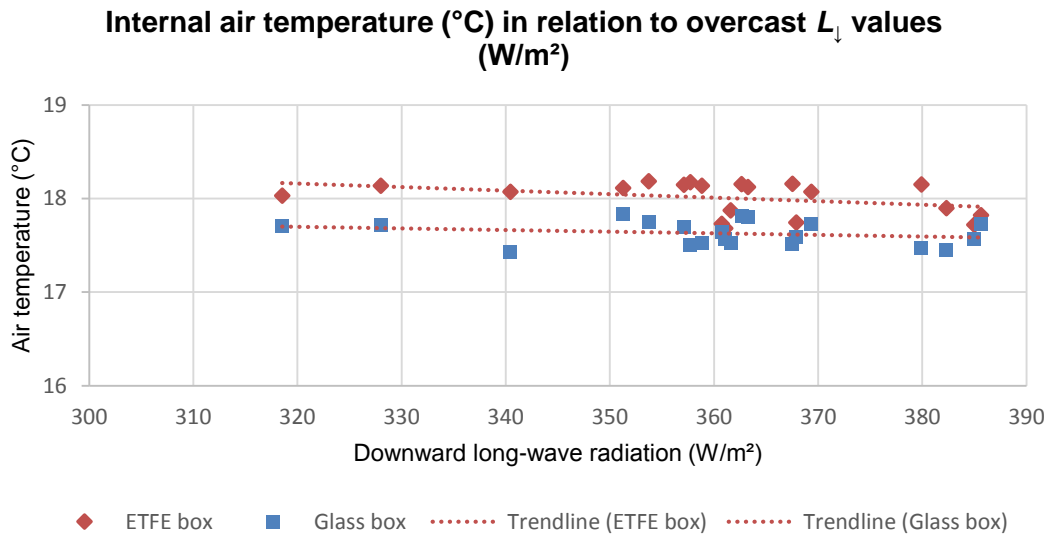


Figure 4.18: Internal air temperatures (°C) in relation to overcast sky long-wave radiation (W/m²)

The following results concerning the black bulb radiation measurements presented a similar behaviour whereby under both a clear and an overcast sky the ETFE box recorded higher black bulb radiant temperatures than the glass-covered box. Figures 4.20 and 4.21 demonstrate that relationship between recorded interior and exterior radiant conditions under low and high L_{\downarrow} values respectively. The standard deviation for the plotted radiant temperature inside the ETFE box in relation to a clear sky was 0.08 °C and in relation to an overcast sky it was 0.12 °C. The standard deviation for the plotted radiant temperature recorded in the glass box under a clear sky was 0.10 °C and under an overcast sky it was 0.11 °C.

The mean radiant temperature difference between the ETFE and the glass box was 0.51 °C under a clear sky and 0.59 °C under an overcast sky. Under clear sky conditions, the trend for the ETFE-related temperature to decrease with the increase of clouds was of the order of 0.05 °C and the equivalent trend for the glass-related temperature was 0.01 °C and, therefore, could not be considered a significant indicator of behaviour. Under overcast sky conditions, the trend for the ETFE-related temperature to decrease with the increase of clouds increased to 0.18 °C and the equivalent trend for the glass-related temperature became 0.05 °C. Again, any noticeable shift in the trend of radiant temperature decreasing with cloud increase is considered negligible.

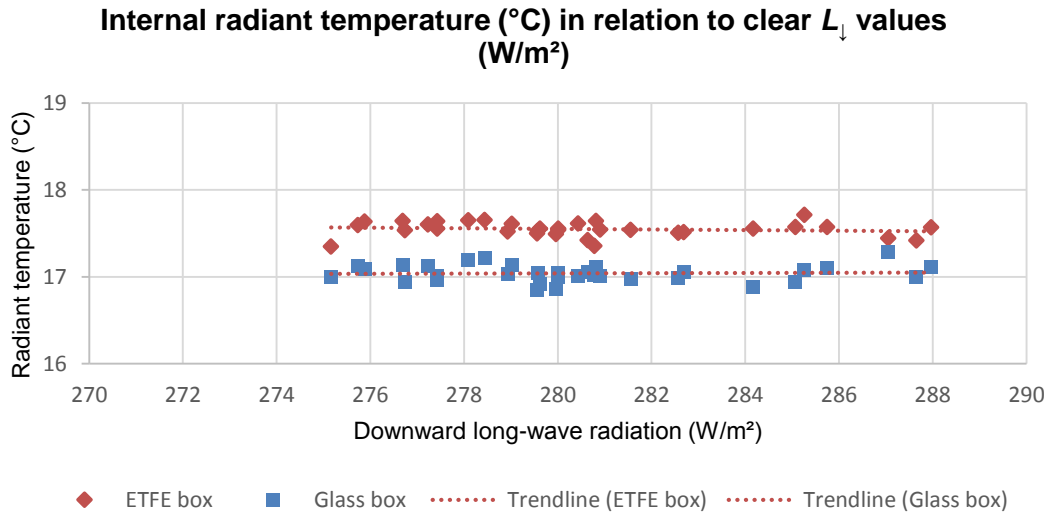


Figure 4.19: Internal radiant temperatures (°C) in relation to clear sky long-wave radiation (W/m²)

The prevailing trends allow a comparison between the two materials. The pattern of behaviour was the same for both air and radiant temperatures and under both types of sky; this indicates that the ETFE-covered box was more successful than the glass-covered box in maintaining interior conditions closer to the desired set temperature and therefore achieving a more comfortable environment; even by a minimum average deviation in the case of air temperature under a clear sky.

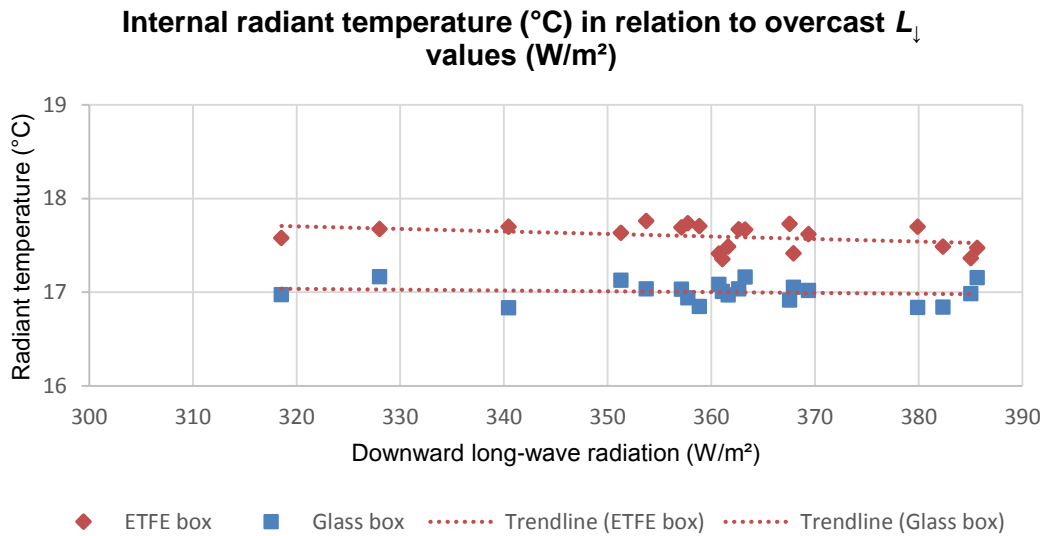


Figure 4.20: Internal radiant temperatures (°C) in relation to overcast sky long-wave radiation (W/m^2)

Other interior conditions under observation were the South-facing wall and the roof surface temperatures of each box. The interior side of the South-facing wall was selected to avoid exposing the thermocouple to solar input and, therefore, overheating. The measurement probe was situated at the centre of the wall. The wall temperatures recorded inside the ETFE-covered box ranged between 15 and 42 °C and inside the glass-covered box between 15 and 44 °C. This range was in agreement with the previously presented overall air and radiant temperature ranges, which demonstrated that the ETFE box overheated less than the glass box. A detailed graph presenting overall wall surface measurements can be found in Appendix C (Figure C.3). As previously, two separate graphs are used to depict wall surface temperature under clear and overcast sky (Figures 4.22 and 4.23).

The standard deviation for the plotted wall temperature inside the ETFE box in relation to a clear sky was 0.11 °C and in relation to an overcast sky it was 0.13 °C. The standard deviation for the plotted wall temperature recorded in the glass box under a clear sky was 0.13 °C and under an overcast sky it was 0.12 °C.

The mean wall temperature difference between the ETFE and the glass box was 0.10 °C under a clear sky and 0.19 °C under an overcast sky. Under clear sky conditions, the trend for the ETFE-related temperature to decrease with the increase of clouds was of the order of 0.03 °C and the equivalent trend for the glass-related temperature was 0.01 °C and, therefore, could not be considered a significant indicator of behaviour.

Under overcast sky conditions, the trend for the ETFE-related temperature to decrease with the increase of clouds was 0.05 °C, while the equivalent trend for the glass-related temperature became 0.20 °C. The shift in the trend of wall temperature decreasing with cloud increase is considered negligible.

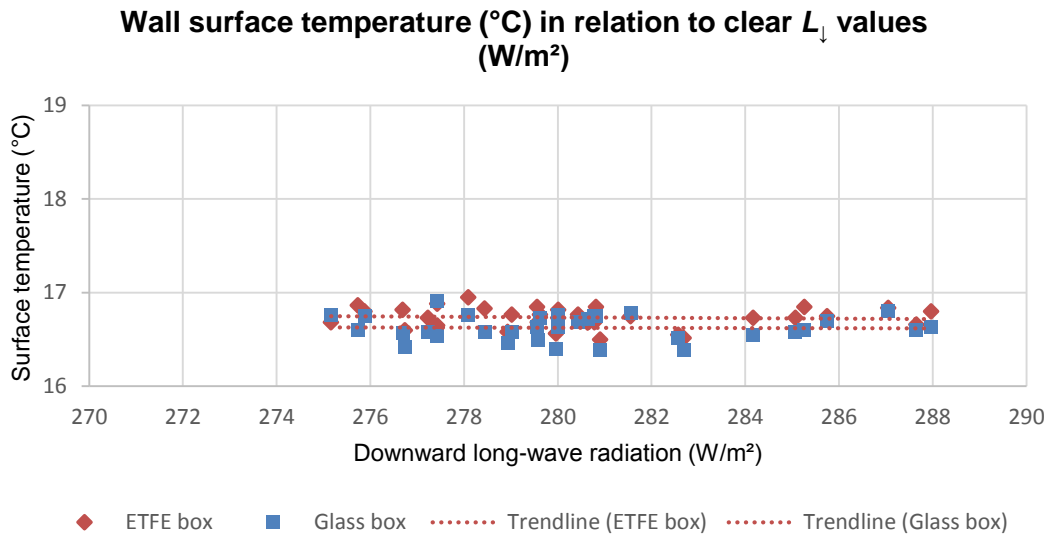


Figure 4.21: Wall surface temperature (°C) in relation to clear sky long-wave radiation (W/m²)

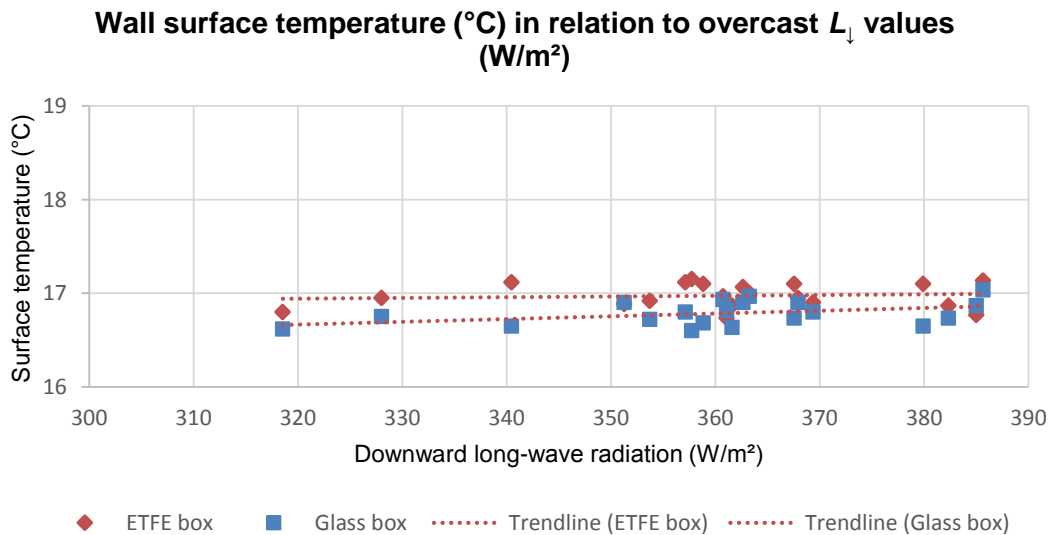


Figure 4.22: Wall surface temperature (°C) in relation to overcast sky long-wave radiation (W/m²)

The wall temperatures for both boxes were similar under clear and overcast sky conditions. Wall temperatures were lower than both air and radiant temperatures. This can be partly explained by the fact that the measurement probe was situated away from the centre of the box, where the heating devices were located, and partly due to the convective heat loss through the box walls. Furthermore, the recorded interior radiant temperature was in essence the sum of the heat produced by the radiant heaters and re-emission from the walls. This confirms that the wall surface temperatures are lower compared to the black bulb temperature measurements; but it also explains the proximity between wall surface to the radiant temperature, rather than to air temperature.

Regarding the interior roof surface temperatures, the measurements in the ETFE-covered box varied between 9 and 58 °C and in the glass-covered box between 8 and 55 °C (Appendix C, Figure C.4). Figures 4.24 and 4.25 present the recordings ignoring overheating solar effects. Due to the exposure of both cladding materials, their poorer insulating ability – in comparison to the box walls and floor – and the consequent heat loss through them, the range of interior surface measurements is significantly lower than the previously presented interior temperature data.

The standard deviation for the roof temperature of the ETFE box in relation to a clear sky was 0.65 °C and in relation to an overcast sky it was 0.43 °C. The standard deviation for the roof temperature of the glass box under a clear sky was 0.70 °C and under an overcast sky it was 0.50 °C. The increased margin of error between measured and mean estimated value can be explained by the fact that those measurements were taken at a location more exposed to external conditions, such as external air temperatures and wind, and therefore were prone to larger fluctuations.

The mean roof temperature difference between the ETFE and the glass box was 0.98 °C under a clear sky and 0.87 °C under an overcast sky. Under clear sky conditions, the trend for the ETFE-related temperature to decrease with the increase of clouds was of the order of 0.28 °C and the equivalent trend for the glass-related temperature was 0.17 °C, which fall within the margin of error and are considered negligible. Under overcast sky conditions, the trend for the ETFE-related temperature to decrease with the increase of clouds increased to 0.81 °C the equivalent trend for the glass-related temperature became 1.15 °C. This can be explained by the decreasing heat loss that is associated with an increase in cloud presence.

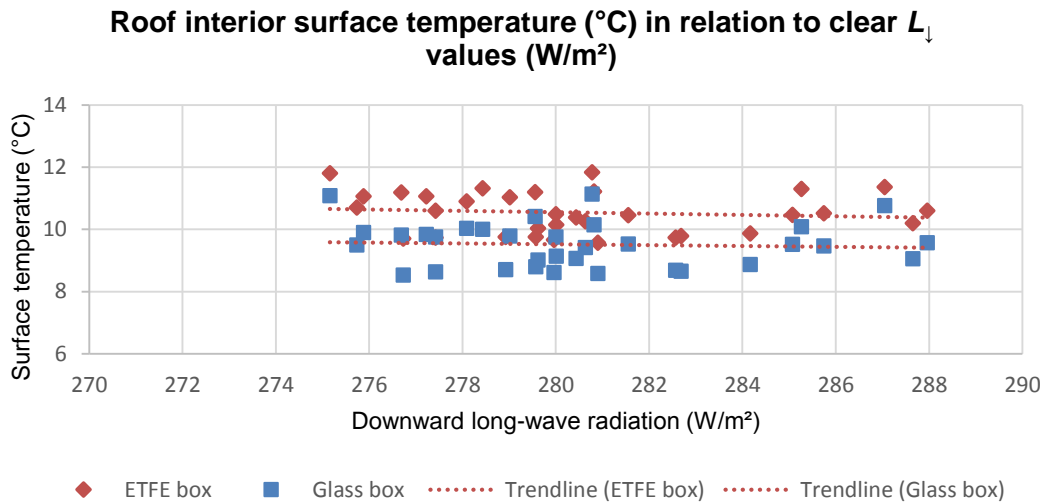


Figure 4.23: Roof interior surface temperature (°C) in relation to clear sky long-wave radiation (W/m²)

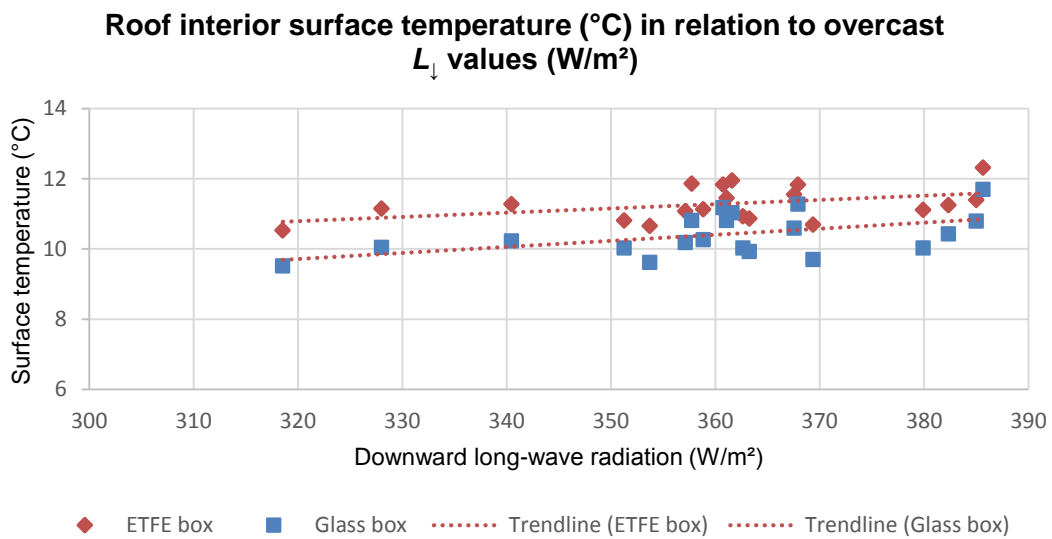


Figure 4.24: Roof interior surface temperature (°C) in relation to overcast sky long-wave radiation (W/m²)

The fact that the temperature was higher in the interior surface of the ETFE cushion in relation to that of glass can be explained by the higher radiant temperature values that were recorded in the centre of the ETFE box, right underneath the location of the probe used for the surface measurements. Furthermore, the higher insulating value of the ETFE cushion contributed in the overall higher interior surface temperatures.

- Finally, one more interior measured parameter was relative humidity. The dehumidifying system functioned successfully, keeping humidity levels consistently under 40%. The humidity levels recorded in the ETFE-covered box ranged between 18 and 38% and in the glass-covered box between 11 and 34% (Appendix C, Figure C.5). Condensation was avoided even when external temperatures were low. Figures 4.26 and 4.27 demonstrate the relationship between interior and exterior relative humidity levels under a clear and overcast sky respectively.

The standard deviation for the relative humidity of the ETFE box in relation to a clear sky was 3.44% and in relation to an overcast sky it was 1.03%. The standard deviation for the relative humidity of the glass box under a clear sky was 3.68% and under an overcast sky it was 1.26%.

The mean relative humidity difference between the ETFE and the glass box was 5.35% under a clear sky and 5.83% under an overcast sky. Under clear sky conditions, the trend for the ETFE-related relative humidity to decrease with the increase of clouds was of the order of 3.39% and the equivalent trend for the glass-related relative humidity was 4.49%. Under overcast sky conditions, the trend for the ETFE-related temperature to decrease with the increase of clouds resulted to 2.66%, while the equivalent trend for the glass-related temperature became 2.11%.

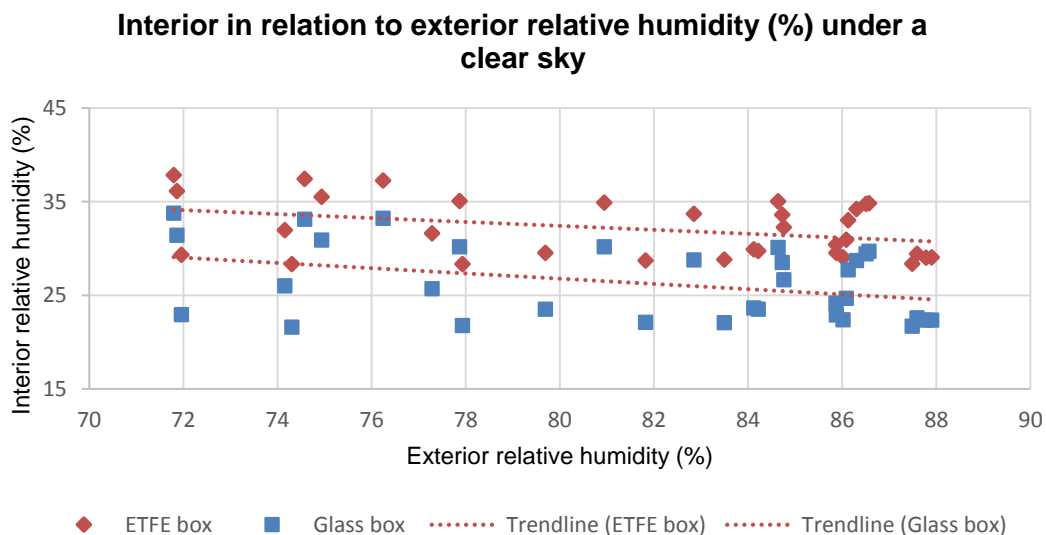


Figure 4.25: Interior in relation to exterior relative humidity (%) under a clear sky

Interior in relation to exterior relative humidity (%) under an overcast sky

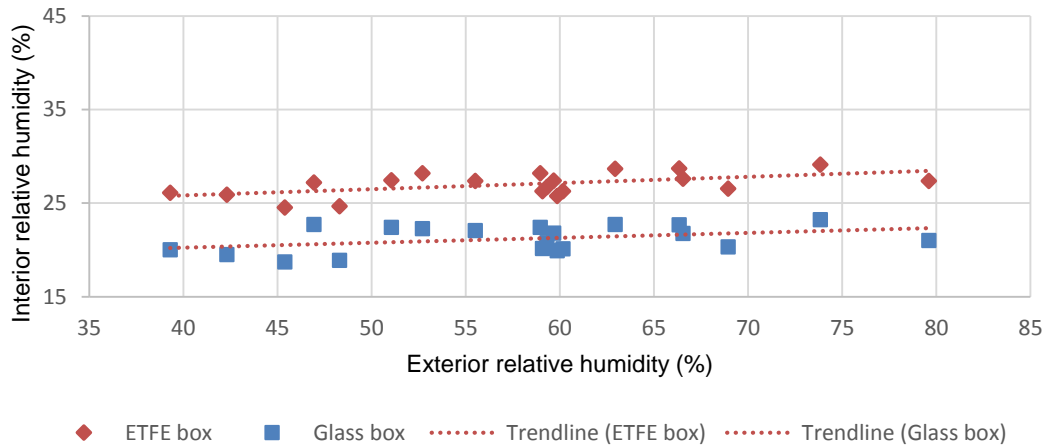


Figure 4.26: Interior in relation to exterior relative humidity (%) under an overcast sky

The ETFE box consistently demonstrated higher relative humidity levels. This relative humidity discrepancy can be explained through the recorded air temperature difference inside the two boxes. As relative humidity is the ratio of water vapour pressure to saturated vapour pressure at a specific temperature, it is dependent on temperature.

To summarise so far, both materials responded in a similar manner, with the ETFE-covered box often presenting results closer to the desired values in comparison to the glass-covered box. This demonstrates that the ETFE cushion was as successful in creating an insulated, comfortable environment, as the double glazed unit.

- These results lead to the other main focus behind this study, which is the amount of energy consumed by each box in the attempt to maintain the desired interior temperature. Figure C.6 found in Appendix C depicts the energy consumption of each box in kWh. To measure energy consumption, a pulse was recorded every time the heaters were operating; each recorded pulse represented 1 Wh. The measured pulses were initially sampled every five minutes; however, the measurements were summarised to ten minute intervals to reduce visual noise in the graph. The measured pulses were then converted to energy by multiplying by six (the number of ten-minute intervals in an hour) and dividing by 1,000 (to convert to kWh). The energy expended for the operation of the ventilation system was removed, so the consumption that is discussed here refers to the power used for heating only.

The heaters enclosed in each box were set to maintain the internal air temperature at 19 °C. The total measured energy consumption required to heat the ETFE box throughout the entire period under examination was 11.07 kWh, almost equal to the equivalent 11.13 kWh recorded for the glass box. The total energy consumption for the ETFE-covered box came after the calibration process to ensure that additional heat loss was taken into account. The comparable heating requirement demonstrates that the ETFE cushion can, in fact, be a considerable alternative to glass with the potential for energy savings under the right weather conditions. The amount of energy saving potential will be further examined in the later chapter on simulations.

Regarding the interior conditions, the results will be examined in two groups corresponding to clear and overcast sky environments (Figures 4.28 and 4.29). To objectively compare the energy consumption of the ETFE box under clear and overcast skies, the difference between internal and external air temperature would have to be the same in both cases and with solar input absent, so as not to influence the thermal performance of the box. As this was not the case in the present experiment, energy consumption is hereby examined in relation to interior-external temperature difference as an expression of the distinct thermal response of each box. The interior temperature used here to subtract the difference to exterior temperature is the averaged value between the interior measurements for both boxes.

The standard deviation for the energy consumption of both boxes in relation to both a clear and an overcast sky was 0.01 kWh. The mean energy consumption difference between the ETFE and the glass box was practically negligible under a clear and an overcast sky. Under all sky conditions, the trend for both the ETFE- and glass-related energy consumption to decrease with the increase of internal-external temperature difference was of the order of 0.03 kWh.

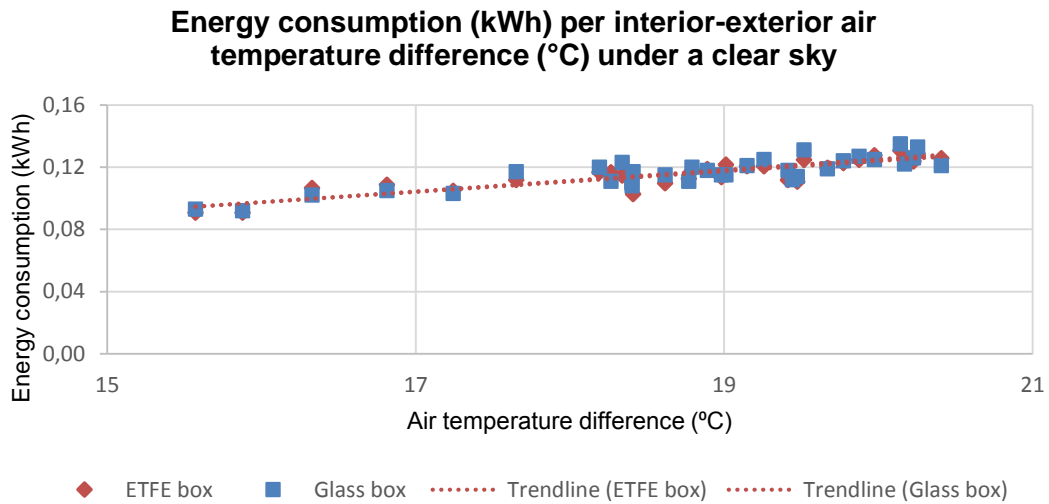


Figure 4.27: Energy consumption (kWh) per interior-exterior air temperature difference (°C) under a clear sky

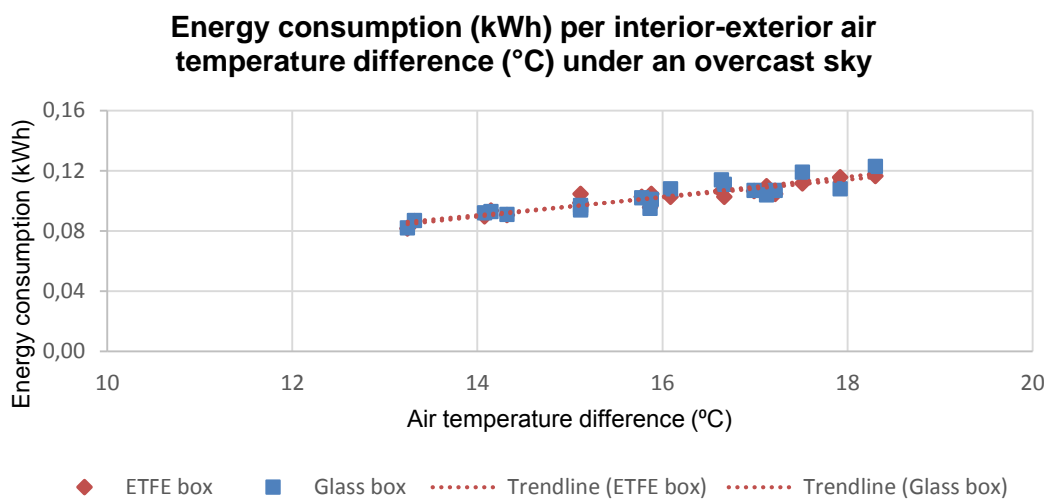


Figure 4.28: Energy consumption (kWh) per interior-exterior air temperature difference (°C) under an overcast sky

The heating operation of both boxes is nearly identical when examined in detail. As expected, both boxes present increased energy consumption under a clear sky, in which case radiative energy losses were greater than under an overcast sky. Furthermore, energy consumption followed the rising trend of temperature difference. The difference between the energy consumption of each box is very small in this case

to trace back to the nature of each material. Given that the size of the boxes was accompanied by small heating requirements, a real-life building will be used in Chapter 6 to estimate realistic larger-scale energy savings and determine the viability potential of ETFE cushions for certain building types and sizes.

4.6 Summary and conclusions

This chapter concerned the experimental procedure conducted using a double layered ETFE cushion alongside a double glazed unit. The chapter described the experimental boxes and the apparatus used for the regulation of interior conditions. Fans were used to ventilate the experimental boxes and avoid the onset of condensation. The chapter described the equipment required for the measurement of external conditions – air temperature, shortwave and long-wave radiation, relative humidity, wind direction and velocity and barometric pressure.

Prior to the undertaking of the experiment, the calibration of the boxes took place. Both boxes were exposed to the same shortwave and long-wave radiation and external air temperature conditions and bared the same heating, ventilation and recording equipment, placed in the same locations.

This relationship of long-wave radiation (L_{\downarrow}) and emissivity (ϵ) was examined through a literature review. A model was developed based on existing literature for the estimation of long-wave radiation on ground-based measurements which was then tested against locally measured conditions.

External conditions varied during the recording of data for this set of testing. This allowed a correlation between external condition fluxes and the responding thermal behaviour dictated by each material to be derived. The result of the overall behaviour of each material in response to external conditions was primarily demonstrated through internal air and radiant temperatures, wall and roof temperatures and internal relative humidity levels. The energy consumption of each box was then examined as a key factor determining the viability of the material in comparison to glass.

The recorded data was divided into two datasets; one for clear sky and one for overcast sky conditions. The ETFE cushion performed similarly to glass under high shortwave inputs, causing the experimental box to overheat. To avoid the effects of incoming solar radiation the data under examination included only night-time recordings. Scatter diagrams were used for the demonstration of the results to show the correlation

between the two variables under examination. Trend lines were added to clarify the development of the relationship between different parameters.

When configured in the form of a cushion, ETFE membrane was found to perform in a manner that was comparable to that of glass. The ETFE cushion was suitable for providing comfortable interior conditions under cold weather conditions in the absence of solar input and frequently more successful than the double glass used in comparison.

Regarding the energy performance of the ETFE and glass boxes, they both responded to external conditions following similar trends, with the glass box consuming more energy than the ETFE box in total numbers. To conclude, this study indicates that ETFE can be successfully implemented to replace glass in buildings exposed to cold weather conditions, while offering a comfortable interior environment at a comparatively low energy cost. The gain in the energy consumption is small but not negligible, and in combination to the benefits that accompany the use of ETFE cushions it establishes the material as an efficient alternative to double glazing.

The following Chapter 5 describes the process of modelling the thermal and energy response of an ETFE cushion using the computer simulation program Integrated Environmental Solutions (IES). The measurements and findings presented in the present chapter will be used to calibrate the simulated model and examine the accuracy of the program. The necessary assumptions and adjustments will be discussed to offer guidance to designers wishing to include ETFE cushions in their preliminary energy saving calculations.

5 Primary modelling using IES

5.1 Computational modelling of the energy and thermal behaviour of an ETFE cushion

A dynamic computational modelling environment was used to predict the energy consumption and thermal conditions of a building covered with ETFE cushions. This began with the characterization of the necessary performance parameters required to successfully model an ETFE cushion using the IES simulation tool; more specifically, the thermal application tool of the computational package. IES Virtual Environment was selected as a powerful, in-depth tool for building performance analysis. It allows the user extended input implementation and offers complex and detailed output regarding the building's thermal and energy performance. Other tools that could have alternatively been used were EnergyPlus, Design Builder, TAS, TRNSYS, EcoTect and ESP-r.

EnergyPlus is a dynamic building energy model that also allows to build the geometry of a structure or use a Google SketchUp plug-in to import geometry (EnergyPlus, 2014). It is a tool similar to IES in many aspects. Energy Plus was used in the thesis to alter and convert a weather file, as IES did not offer that option, which will be described in the following section.

Design Builder can be used together with EnergyPlus to create building geometry. It is made for creating and assessing building designs, at all stages of the design process (DesignBuilder, 2014). However, it is a less complex program in comparison to IES, providing the user with less accurate input and output regarding building modelling and performance simulation.

Environmental Design Solutions Limited (EDSL) Tas allows dynamic thermal simulation of buildings through automated procedures (Tas, 2014). Like IES, Tas does not offer great flexibility in importing geometry, which would probably cause the same issues that occurred while using IES –as described at a later section of this Chapter, IES presented obstacles and complications in the modelling the ETFE cushion.

TRNSYS is a modular dynamic energy and systems modelling tool that uses individual engineering components, defined by a set of parameters and functions that direct their operation, combined to create complex engineering systems (TRNSYS, 2014).

TRNSYS is a complete and complex program regarding the design of thermal systems, which makes it a strong candidate in comparison to IES.

Autodesk EcoTect is a simplified tool in comparison to IES that provides a less in-depth influence over input and understanding of output regarding the thermal and energy processes that take place throughout building simulation (EcoTect, 2014).

ESP-r is a tool used to support the construction process regarding the energy and environmental performance of a building. It is a mathematical software that assists the coordination of thermal and energy simulation, CAD applications, performance evaluations etc. It can be used together with EnergyPlus to create a building geometry and it is useful to simulate innovative technologies (ESP-r, 2014). Like Tas and TRNSYS, ESP-r was a considerable alternative in comparison to IES.

As Tas, TRNSYS and ESP-r were not used, it remains unknown whether these programs would be able to solve the geometry-related issues that occurred through the use of IES in relation to the modelling of the ETFE cushion.

5.1.1 Primary modelling using IES

This section of the thesis intends to devise a design template for the optimal architectural deployment of ETFE cushions. To achieve this, the building energy simulation program IES was used to reproduce the measured performance of the experimental units as it was described in the earlier chapter. This chapter describes the simulation process, as well the necessary considerations and modifications that had to be made to achieve agreement between monitored and simulated performance. The anticipated outcome of this process is to provide guidance for designers when seeking to evaluate the thermal and energy performance of an ETFE structure.

IES was selected as a tool commonly used by the building industry to achieve economic and environmental savings. It is a tool suitable for this thesis as it can accurately provide a detailed representation of interior thermal conditions and energy use due to heating. The equations embedded in IES and, more specifically by ApacheSim, the dynamic thermal simulation program, are examined in this chapter and are supplementary to the contents of Chapter 3 on heat transfer. Furthermore, the simplifications which are made by the program are discussed as they are expected to affect the simulated results.

Table 5.1 provides a synopsis of the capabilities and limitations of IES, mapped to the key parameters that were simulated and the steps that were taken to resolve any issues encountered. The next section describes in detail the calculations, abilities and limitations of the program that are expected to influence the accuracy of the presented simulated results.

Table 5.1: Summary of IES capabilities and limitations, and consequent actions taken

IES capabilities	IES limitations	Actions taken
Allows the import of weather file for accurate simulation results.	Does not provide a tool to alter or generate the weather file.	Used Energy Plus to elaborate and convert weather file into format accepted by IES.
Takes into account a large amount of detailed weather data.	Weather files are based on hourly time-steps – frequent simulations are run based on interpolations of the hourly weather data.	Accordingly used hourly simulations to analyse thermal and energy behaviour of materials under examination.
Offers a template to directly model basic 3D geometry or to import same through SketchUp.	IES is not a user-friendly tool for highly accurate 3D modelling. Does not allow the modelling of complex geometries and curves.	Simplified model geometry and represented curved surfaces as a series of flat surfaces or facets.
Provides an extensive list of building products and materials. Allows alterations to be made to the materials profiles, and new materials to be introduced to the system.	IES requires users to have a thorough understanding of materials science to accurately operate its Building Template Manager.	Described ETFE cushions based on information from manufacturers, bibliography and knowledge obtained from experimental rounds. Performed numerous calibration simulations before reaching a representative model.
Performs complex thermal and energy calculations in a timely manner.	Some simplifications in the thermal calculations are made during the simulation process. Examples of such simplifications are: heat transfer is assumed as one dimensional or the fact that radiative simulations do not take into account view factors.	Used hourly simulations to analyse thermal and energy behaviour of materials under examination to eliminate noise in data and lower the effect of simplifications.
Allows user to choose from, or manipulate, a small number of heating and ventilation systems.	Provides limited options of systems. Offers limited scope for the alteration of room plant and	Used MacroFlo (bulk airflow analysis tool) to model fan operation, using an original alternative solution to

	control systems, which are operated based on on/off cycles and time limitations using absolute profiles.	simulate the ventilation system. Used ApacheHVAC for heating, cooling and humidity control through modulating formulas.
--	--	--

5.1.2 IES background calculations

- Regarding heat conduction and storage, ApacheSim assumes that the conductive heat transfer through each building element is one-dimensional and that the thermo-physical properties of each layer composing any building element are uniform, (IES-VE, 2013). This expresses the basic Equation 3.1 describing conduction in the form of Equation 5.1, as follows (ApacheSim, 2013).

$$\frac{\partial^2 T}{\partial x^2} = \frac{\rho * c_s}{k} \frac{\partial T}{\partial x} \quad \text{Equation 5.1}$$

T : Temperature (°C)

x : Length (m)

ρ : Density of solid (kg/m³)

c_s : Specific heat capacity of solid (J/kg K)

k : Thermal conductivity (W/m² K)

Furthermore, ApacheSim can only represent building elements with a finite number of nodes, calculating heat transfer and storage for each node at set simulation time-steps. This is done by applying Equation 5.1 at each node to achieve an accurate model that is discretised in space and time. Finally, considering heat flow and heat storage in air masses contained within the building, air gaps are modelled as pure resistances so as to simplify calculations.

- In relation to forced (mechanical) and natural (buoyancy) convection, ApacheSim performs its calculations using the heat transfer coefficient, as it was previously described in Equation 3.2. In the case of natural convection, ApacheSim introduces a potential simplification regarding the heat transfer coefficient, providing the user with two options; the first is to include the use of an approximate constant value of the heat transfer coefficient, thus obtaining a linear relationship between convective heat transfer and temperature difference. The alternative option is to allow the heat transfer coefficient to be re-calculated as a function of temperature difference,

therefore introducing non-linearity and complicating the process but increasing the accuracy of the findings.

What is more, ApacheSim calculates exterior convection in relation to wind velocity, as it is introduced through the weather file, using McAdams' empirical equations (Equations 5.2 and 5.3) (ApacheSim, 2013).

$$\text{For } v < 4.88, \quad h = 5.6 + 4.0 * v \quad \text{Equation 5.2}$$

$$\text{For } v \geq 4.88, \quad h = 7.2 * v^{0.78} \quad \text{Equation 5.3}$$

v : Wind speed (m/s), read from the simulation weather file

However, as the information contained in the simulation weather file is in hourly intervals, linear interpolation is required between time-steps to allow for further calculations at more frequent time steps. The user is given the option to override this process through the specification of an approximate fixed value for an external convective heat transfer coefficient. However, this would compromise the accuracy of the results, which is why such an override was avoided while performing this study (ApacheSim, 2013).

Regarding interior convection, the user is similarly given several options for the modelling of air masses inside a building, based on either, i) fixed or variable convection coefficients as specified by CIBSE, or ii) variable convection coefficients as specified by Alamdari and Hammond (1983). Alternatively, the user is once again allowed to override this process by inserting a fixed value for an internal convection coefficient. The present set of simulations used variable convection coefficients for the underlying calculations for increased accuracy; therefore, variable convection coefficients was the only option examined in detail. Equation 3.2 is in this case transformed to Equation 5.4 (ApacheSim, 2013; Alamdari *et al.*, 1983).

$$h = f * g * (T_s - T_\infty)^{j-1} \quad \text{Equation 5.4}$$

f : Coefficient depending on mean air speed

$$\text{Where: } f = 1.0 + 0.7 * v$$

g : Coefficient depending on surface orientation (see values in Table 5.2)

$T_s - T_\infty$: Temperature potential difference for heat flow away from surface (°C)

j : Exponent (see values in Table 5.2)

Table 5.2: g and j values according to surface types (Alamdari *et al.*, 1983)

Surface type	g	j
Vertical surfaces	1.4	1.33
Horizontal surfaces (upward heat flow)	1.7	1.33
Horizontal surfaces (downward heat flow)	0.64	1.25

Finally, another simplified specification is that applied to the air supply rate in terms of volume flow (l/s), which is done using a default reference air density of 1.2 kg/m³ (ApacheSim, 2013).

- Regarding radiation, ApacheSim takes into account the angle of incidence, therefore evolving Equation 3.3 to the following form of Equation 5.5, which expresses the radiation flux for a small surface element (ApacheSim, 2013).

$$dq_r = \frac{1}{\pi} \sigma \varepsilon T_a^4 \cos \theta d\omega dA \quad \text{Equation 5.5}$$

dq_r : Radiation flux (W/m²)

σ : Stefan-Boltzmann constant (5.669 *10⁻⁸ W/m² K⁴)

ε : Emissivity ($\varepsilon < 1$ for a non-black body)

T_a : Absolute temperature of the surface (K)

θ : Direction angle measured from the surface normal

$d\omega$: Element of solid angle

dA : Element of surface area (m²)

More specifically, for the accurate representation of interior long-wave radiation, Equation 3.3 would normally be expected to be taken into account in combination with the view factor, as it has been previously explained through Equation 3.6 in the chapter describing heat transfer phenomena. The view factor, otherwise known as the configuration or shape factor, represents the fraction of energy that leaves a black body element dA_1 that arrives at a second black body element dA_2 (Siegel *et al.*, 1972). The view factor expresses the radiative heat transfer between surfaces through mathematical relationships describing how the two surfaces are facing each other. The

view factor depends on the size of the element dA_2 and its orientation in relation to dA_1 . Given this relation, the curved surface of an ETFE cushion would be theoretically expected to complicate the estimation of the view factor, since each point of the cushion surface is at a different orientation relative to the radiative source.

However, ApacheSim does not take into account the view or shape factor when estimating radiant exchanges for the means of simplification. Instead, ApacheSim modelling uses the mean radiant temperature of an enclosure to reduce complexity of the underlying computational processing, as described by CIBSE (CIBSE, 2006). This reduces the net radiant exchange between a surface and its enclosure to the form of Equation 5.6. It is assumed that the emissivity values of the surfaces that compose the enclosure are all almost identical. The linearisation of fourth-power terms in Equation 5.6 is part of the mean radiant temperature methodology (ApacheSim, 2013).

$$q_r = h_r(T_s - T_{MRT}) \quad \text{Equation 5.6}$$

q_r : Net radiative loss from the surface (W)

h_r : Heat transfer coefficient for exchange with a mean radiant temperature (MRT) node

T_s : Surface temperature (K)

T_{MRT} : Mean radiant temperature of enclosure (K)

To verify that this simplification did not have a significant impact on the accuracy of the present model, the curved surface area of an ETFE cushion was primarily represented by a flat ETFE membrane. Consequently with this assumption, further modelling was performed representing the cushion in IES through a series of different models with a distinct number of flat surfaces as facets in each case. These models were then used to run simulations and the results were compared, proving to be nearly identical. The accuracy of the energy consumption and interior conditions in relation to the ETFE cushion shape will be examined in section 5.2 of this chapter.

The effect of air to interior radiation is taken into consideration in the ApacheSim calculations by including the water vapour influence but not the CO_2 contribution to air emissivity. As humidity rises, the surfaces of an enclosure exchanges more radiation with the air than with each other, introducing a latent heat effect whereby the radiant fraction of a heat source appears reduced (ApacheSim, 2013). Air radiant exchanges are calculated using a model developed by Hottel, (1954) estimating the extent of area of radiant influence.

Hottel's model goes into more detail estimating air emissivity as a function of partial vapour pressure. However, the ventilation ducts in combination with the auxiliary box performed successfully in the conducted physical experiment, maintaining low internal humidity levels, as it was described in the previous chapter. Therefore, the effect of humidity on the radiative interior environment was not further examined.

Regarding exterior long-wave radiation, ApacheSim uses a calculation process provided in CIBSE Guide A. The ApacheSim calculations are based on a model for the estimation of net long-wave gain of an external surface taking into account its inclination, the measured long-wave radiation received from the sky and the ground, as well as the absolute temperature of the external surface (ApacheSim, 2013). The external surface of interest allowing the entry of long-wave radiation is the exterior layer of the ETFE cushion, which is in the horizontal plane, elevated on a metal platform away from the ground or any other obstructions and situated next to a CGR3 pyrgeometer. Therefore, the long-wave values were used as recorded.

Regarding solar shortwave radiation, ApacheSim and SunCast (the shading and solar tracking calculation tool) perform a discretisation of the incident solar flux that reaches an external building surface. To calculate the solar flux, shortwave radiation is separated to distinct meteorological elements, the direct (beam) radiation originating directly from the sun, the diffuse radiation coming from the sky vault and scattered radiation, as it is reflected by the ground (ApacheSim, 2013). As in the case of the measurement of long-wave radiation, shortwave radiation was recorded in the absence of obstructions and reflections in the physical experiment. This allowed for the recorded values to be used directly in the calculations that are described in the following section on weather file preparation.

SunCast records the amount of irradiation that is received by external surfaces and in the case of glazing, the extent of solar radiation that reaches internal surfaces and then redirected on to other surfaces and so on; a process referred to as solar tracking. In the case of transparent surfaces, ApacheSim estimates the transmission, absorption and reflection of the radiation according to the element's physical properties. Opaque elements are also estimated to partially absorb and reflect solar radiation with an absorbance of 0.55. The tracked radiation beam will then either re-direct to opaque surfaces or escape the building through glazing. Once the beam has escaped the building, ApacheSim does not track its path any further, even if it was reflected back by the surface of an adjacent building. However, once again, this limitation does not

affect present simulations as the physical model was free from surrounding reflecting surfaces.

As in the case of exterior convection and wind speed velocity, interpolation is once again performed to estimate the tracking process with accuracy. For that purpose, the tracking process is performed twice during each time step, increasing the complexity of the calculations. The user is not given the option to override this interpolation in contrast to the case of exterior convection. Finally, solar transmission, absorbance and reflectance is calculated for 10 different angles of incidence at 10° intervals for purposes of simplification. No interpolation is used for this process (ApacheSim, 2013).

- Regarding room environmental control, ApacheSim offers limited options over the room plant and control system. Calculations are performed considering the idealised control of room temperature and humidity based on an on/off cycle. This function mode allows only a certain amount of flexibility based on the use of regulating heating or cooling set-points or saturation thresholds. An additional allowance for room condition fluctuation is based on setting time limitations using absolute profiles.

ApacheSim treats air temperature and humidity in an enclosure as uniform, a calculation process characterised as the stirred tank model. MacroFlo is a program for the simulation of bulk air flow through openings in the building envelope. ApacheHVAC, which is used in conjunction to MacroFlo allowing the detailed simulation of heating, cooling and humidity control systems, also comes with certain simplifications. These tools are used at the modelling calibration stage, described in section 5.1.5.

5.1.3 Weather file preparation

In summary, thermal modelling primarily needs to take into consideration the heating or cooling requirements of a space, the external and internal conditions, the surface and air temperatures and humidity. Additionally, apart from the internal gains due to occupancy, equipment and lighting, infiltration also needs to be considered (CIBSE, 2004). A weather file was composed in preparation for the simulation of the experimental units, to ensure that the simulation was undertaken assuming the same external conditions as those experienced in reality. The contents of this section describe the process that was required to convert and supplement the recorded data obtained from the weather station (shortwave, long-wave radiation, wind speed and direction) into a weather file format suitable for IES, which is FWT.

An original weather file for the location was initially acquired from EnergyPlus, the energy simulation tool freely available by the U.S. Department of Energy (EnergyPlus, 2013). The selected file that was altered was originally created for London, Gatwick and carried the code 037760 (IWEC). The weather file was altered using the following calculations described in this section, which can be found at the EnergyPlus Engineering Reference to Calculations (EnergyPlus, 2012). EnergyPlus was selected for this task as IES did not offer a weather file alteration option and since it is a freely available, commonly used and reliable energy calculation software.

As the engineering reference information from EnergyPlus was considered vague on certain occasions, an additional source was selected to supplement the guidance to alter the contents of the weather file, which is Wärme und Feuchte instationär (WUFI) (translating from German to “heat and moisture transient”), a program that allows the calculation of heat and moisture transfer through building components exposed to natural weather conditions. The online database of WUFI offers an explicitly analytical manual of the calculations and physical background that are used for the composure of a weather file.

To calculate energy consumption in relation to heating and cooling loads it was necessary to determine the external conditions that affect these calculations, which include the solar position, the dry bulb and dew point temperatures, the amount of incident direct normal and diffuse horizontal radiation on the building site, relative humidity, barometric pressure, sky cover, as well as wind direction and speed, expressed in hourly intervals (EnergyPlus, 2012). Of these conditions, the solar position (altitude and azimuth) and the direct normal and diffuse horizontal radiation required calculating; whereas the rest were used as directly measured by the weather station.

Initially, the equation of time (in minutes) was estimated, as seen in Equation 5.7 (WUFI, 2013).

$$z = -7.66 * \sin y - 9.87 * \sin(2y + 24.99^\circ) + 3.83^\circ * \sin y$$

Equation 5.7

z: Variable difference in time between the actual point when the sun is at zenith and noon

Equation 5.7 required an auxiliary quantity; the position of the sun, which was estimated following Equation 5.8 (WUFI, 2013).

$$y = 0.9856^\circ * J - 2.72^\circ \quad \text{Equation 5.8}$$

y : Auxiliary quantity used in the equations

J : Number of day of the year

The local apparent solar time (in hours) was estimated, representing the actually observed sun, as in Equation 5.9 (WUFI, 2013). Figure 5.1 shows a graph for the “equation of time”, the difference between the local apparent solar time and the local mean solar time – in this case, the central European time (Stine *et al.*, 1985).

$$LAT = \frac{CET - (15^\circ - \Lambda)}{15^\circ/h} + \frac{z}{60 \text{ min}/h} \quad \text{Equation 5.9}$$

LAT : Local Apparent solar Time (h)

CET : Central European Time (15° East, with 4 min for 1° difference in geographical longitude Λ)

Λ : Geographical longitude

z : LAT-LMT (Local Mean Time)

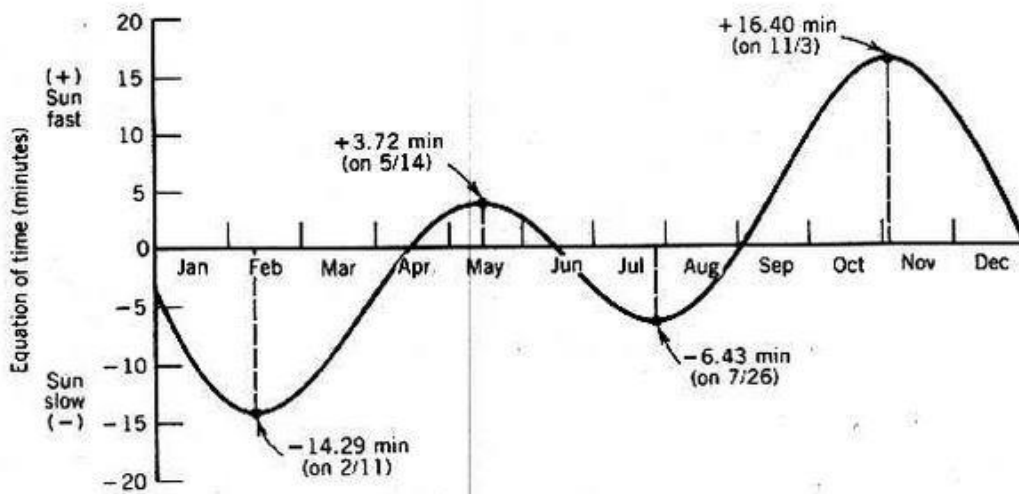


Figure 5.1: Equation of time (Stine *et al.*, 1985)

The LAT was then used to carry on with the description of the exact solar position; in which case the coordinates w and ψ were calculated using Equations 5.10 and 5.11 (WUFI, 2013).

$$w = (LAT - 12h) * \frac{15^\circ}{h} \quad \text{Equation 5.10}$$

w: Distance between the sun and the meridian, also known as the hour angle. It increases steadily by 15°/hour. It is perpendicular to the meridian, therefore zero at noon and it holds a negative value before noon and a positive value after noon. Figure 5.2 shows a diagram of the hour angle w (Stine *et al.*, 1985).

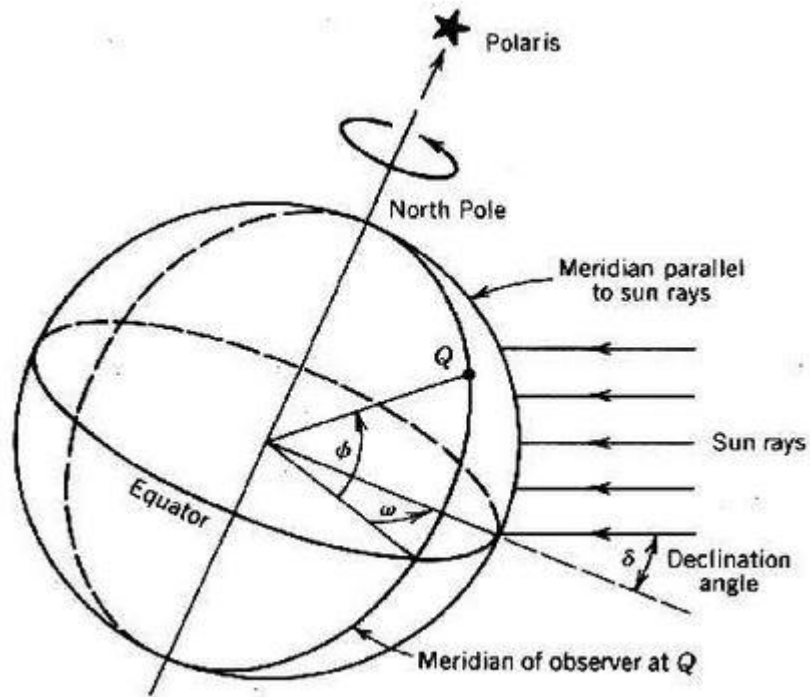


Figure 5.2: Hour angle (Stine *et al.*, 1985)

$$\sin\psi = 0.3978 * \sin(y - 77.51^\circ + 1.92^\circ * \sin y) \quad \text{Equation 5.11}$$

ψ: Declination. Expresses the distance of the sun from the celestial equator. Figure 5.3 shows the solar declination, marked in the diagram as δ (Stine *et al.*, 1985).

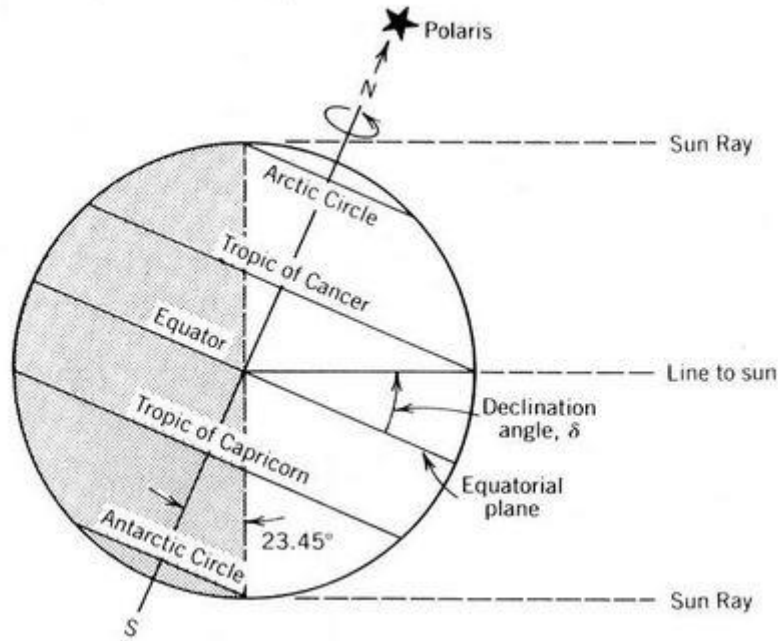


Figure 5.3: Solar declination (Stine et al., 1985)

Following, was the transformation from the coordinate system of w and ψ to altitude ξ and azimuth η as seen in Equations 5.12, 5.13 and 5.14 (WUFI, 2013).

$$\sin\xi = \cos\psi * \cos w * \cos\varphi + \sin\psi * \sin\varphi \quad \text{Equation 5.12}$$

φ : Geographical latitude

$$\sin\eta = \frac{\cos\psi * \sin w}{\cos\xi} \quad \text{Equation 5.13}$$

$$\cos\eta = \frac{\cos\psi * \cos w * \sin\varphi - \sin\psi * \cos\varphi}{\cos\xi} \quad \text{Equation 5.14}$$

Once the solar position was established, the next step concerns the conversion of solar radiation data to direct normal radiation and diffuse horizontal radiation, a process described using the measured shortwave radiation throughout Equations 5.15 to 5.18 (WUFI, 2013).

$$I_{dir} = \sin\xi * I_{dir_normal} \quad \text{Equation 5.15}$$

Where I_{dir} : Direct radiation vertically incident on a surface facing the sun

ξ : Solar altitude

$$I_{dir_normal} = \frac{I_{global} - I_{diffuse}}{\sin\xi} \quad \text{Equation 5.16}$$

$$I_{diffuse_in} = I_{diffuse} * \left(\cos\frac{P}{2}\right)^2 \quad \text{Equation 5.17}$$

$I_{diffuse_in}$: Diffuse component scattered by the air and the clouds which comes from all directions and can be considered isotropic.

P : Tilt of surface to the horizontal.

The tilt of surface P from the horizontal was estimated using Equation 5.18 (WUFI, 2013).

$$\cos\theta_i = \sin\gamma * \cos P + \cos\xi * \sin P * \cos(\eta - \eta_s) \quad \text{Equation 5.18}$$

θ_i : Angle of incidence. The angle of the direct normal radiation with the normal to the component surface

η : Azimuth to the surface

η_s : Solar azimuth

Finally, another condition that was calculated was the extra-terrestrial horizontal radiation (in $W \cdot h/m^2$). As the formula to estimate this value was not found in either the EnergyPlus or the WUFI reference, Equation 5.19 was used as it was published by Wong et al. (in MJ/m^2) (Wong *et al.*, 2001):

$$G_o = \frac{24}{\pi} * I_{sc} * E_o * \cos\varphi * \cos\psi [\sin\omega_s - \left(\frac{\pi}{180}\right) * \omega_s * \cos\omega_s]$$

Equation 5.19

G_o : Hourly extra-terrestrial radiation (MJ/m^2) (1 $MJ=277.78$ Wh)

I_{sc} : Solar constant (1367*3.6 kJ/m^2h)

E_o : Eccentricity correction – factor of the Earth's orbit, where:

$$E_o = 1.00011 + 0.034221 * \cos\Gamma + 0.00128 * \sin\Gamma + 0.000719 * \cos 2\Gamma + 0.000077 * 2\Gamma$$

Equation 5.20

Where: $\Gamma = 2\pi\left(\frac{J-1}{365}\right)$

Γ : Day angle

J : Day number of the year

φ : Latitude

ψ : Solar declination

ω_s : Sunset-hour angle for a horizontal surface

Once the above calculations were completed, the file was converted in .FWT form using the EnergyPlus weather file converter and then implemented within the Weather folder content of the IES Shared Content section. IES was then ready to perform a thermal and energy simulation reproducing the realistic conditions of the physical experiment.

5.1.4 Representing the physical model in IES

This section describes the process followed to represent the physical model in a form suitable for simulation in IES. Several simplifications and assumptions had to be made to recreate the real-life model within the computational tool.

Regarding the design of the experimental units using IES, the ventilation ducts linking the main box to the auxiliary dehumidifying box had to be represented in rectangular form, as IES converts curved shapes into a series of flat plane surfaces. For the same reason the camber of the ETFE cushion could not be accurately represented. To resolve this inefficiency, repeated simulations were performed using several flat surfaces to represent the curved surface of an ETFE cushion, as it will be described in detail further along.

Another necessary adjustment was that the function of the fans was not implemented in the IES model. Although useful for energy applications, the simulation of indoor air movement through a software such as IES is limited, due to the fact that IES is non-specific for the purpose. To resolve this issue, the holes linking the main box, the auxiliary ventilation box and the ducts were modelled as windows, set to continuously open, and the air circulation caused by the fans was modelled as air flowing through those windows. This simplified representation of reality allowed simulations to consider all of the boxes and ducts as a uniform space. The real-life recorded energy consumption used for comparison with the simulated energy results concerned only the heating requirements of the space, excluding the energy consumed for the operation of the fans.

Regarding the representation of the ducts, the thickness of the sheep wool insulation contained in the composite tubing system was an average value of 25 mm. In reality, the sheep wool insulation presented a variation in thickness and density when it was installed among the ventilation tubes due to the nature of the material and the flexible tubes. Therefore, a sensitivity analysis was performed altering the thickness of the sheep wool to check the effect of conductivity with variable material thickness. A series of simulations were performed for a variety of thicknesses to verify that the realistic width of 25 mm would, in fact, reproduce simulated results close to the measured real-life results. These simulations will not be presented as they merely proved what was expected of the material behaviour and are, therefore, of no investigative interest.

Finally, regarding heating control, a modulating formula was set in the thermal template of IES, that instructed the controller to operate if the room air temperature dropped below 19 °C ($t_a < 19$).

Taking all the above into consideration, a series of sensitivity tests were conducted in order to refine the model. The following section of this chapter describes this process.

5.1.5 Calibration

As in the real-life experiments, two identical boxes were designed in IES, one covered with glass and one with an ETFE cushion. The box covered with glass was designed and tested first, as the properties of the covering material were known with greater certainty. A series of sensitivity tests took place, changing various parameters until an agreement was achieved between the simulated and the measured interior thermal conditions and energy consumption. This established an accurate simulated “reference” box on which the covering glass would then be ready to be replaced by a modelled ETFE cushion.

Figure 5.4 demonstrates the primary model as it was designed in the IES environment, used for the sensitivity tests performed with a glass cover.

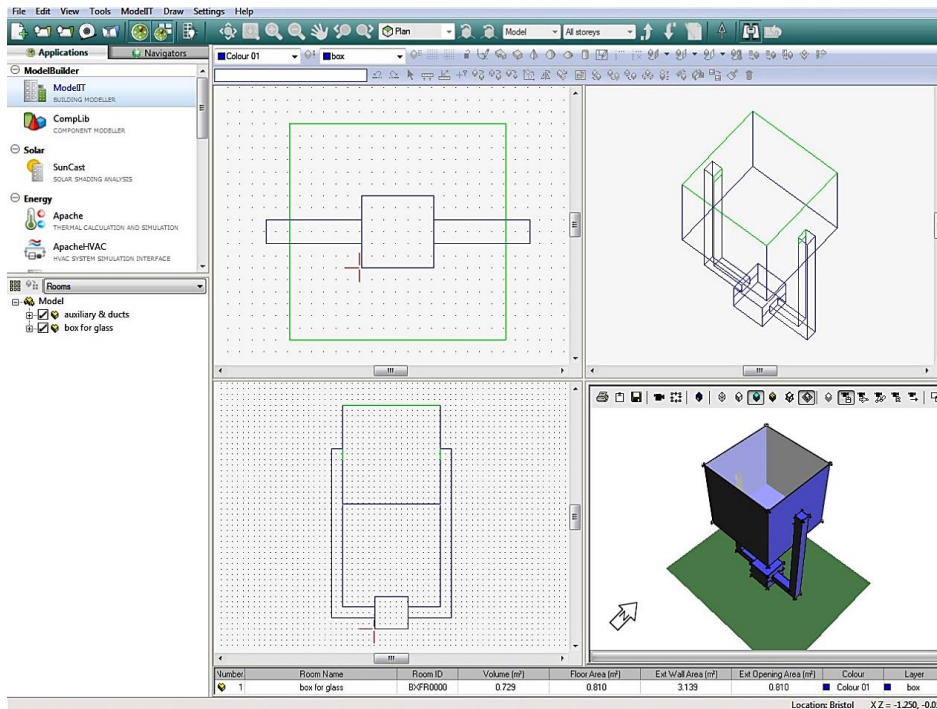


Figure 5.4: Primary model built in the IES ModelIT environment

Figure 5.5 depicts a snapshot of the Edit Construction materials palette of the IES Building Template Manager. The snapshot was taken while editing a double glazed unit.

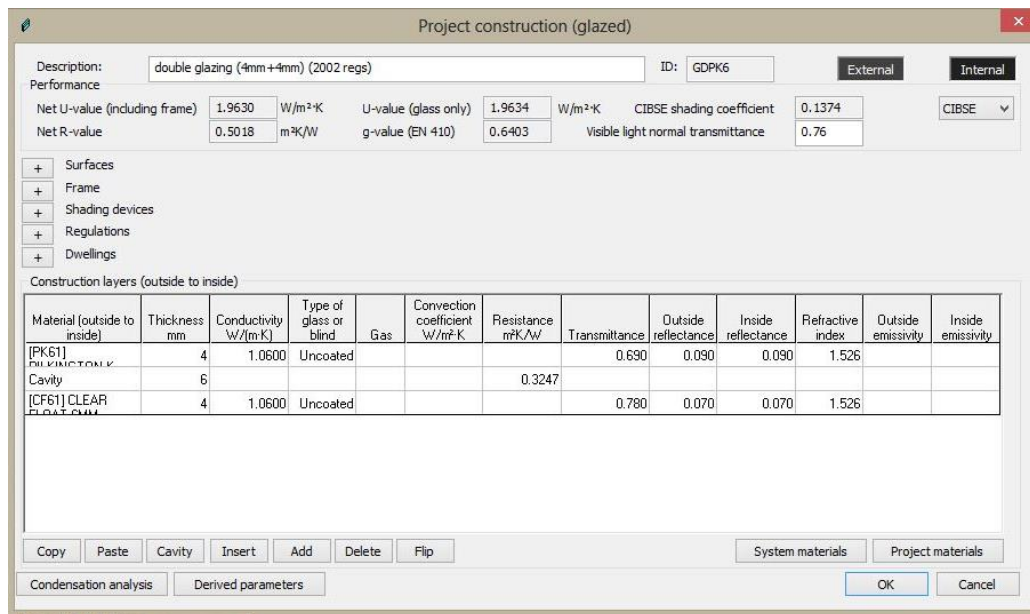


Figure 5.5: IES Edit Construction materials palette of the Building Template Manager

The opening profiles for the glass and later on for the ETFE unit, as well as the holes connecting the ducts to the auxiliary and main box were set using MacroFlo, the IES multizone air movement interface. Figure 5.6 shows a screen-shot taken while editing the ETFE box in MacroFlo; however, both the glass and ETFE units were treated in the same way in the interface. The glass unit was input as an opening with a 0% openable area that was set to OFF continuously, whereas the holes were portrayed as openings with a 100% openable area, set to ON continuously. The crack flow coefficient used to represent air leakage through the duct was set to 6 (l/s*m*Pa^{0.6}), as this was the maximum value that the programme allowed.

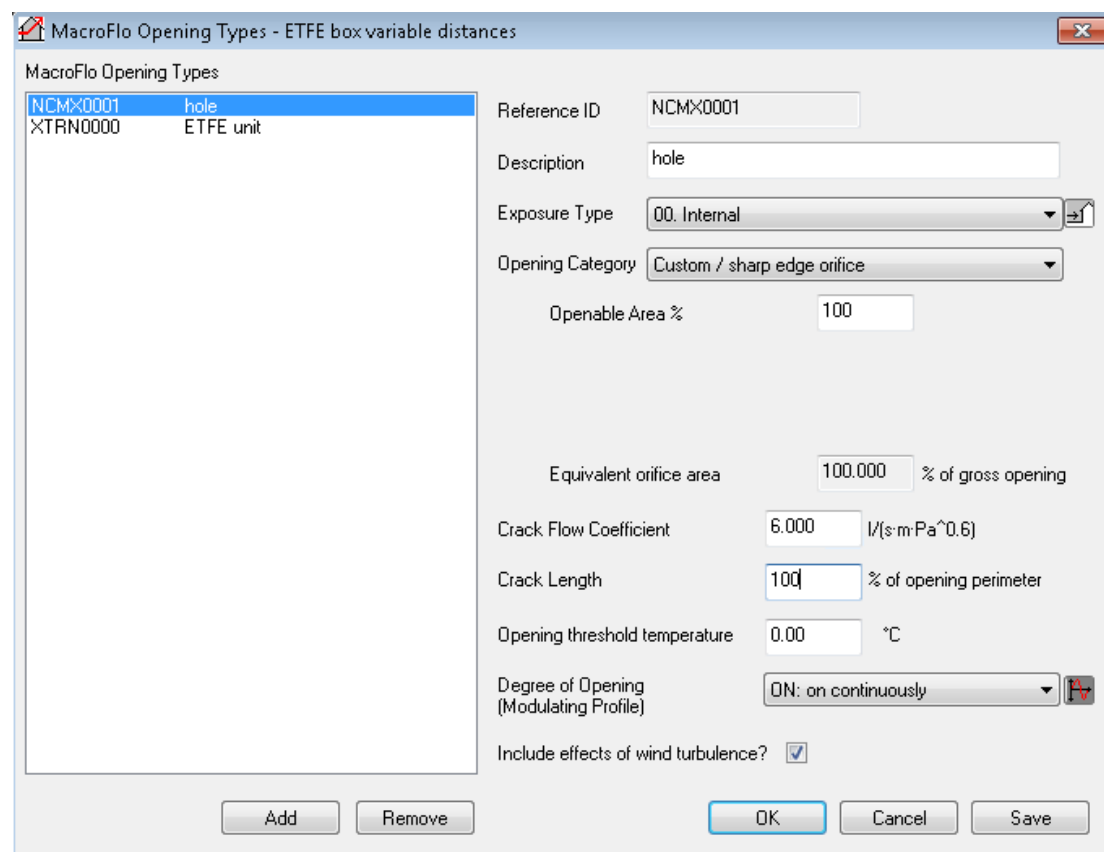


Figure 5.6: MacroFlo tool of the IES multizone air movement interface

- This part of the calibration process describes the sensitivity testing that was undertaken for the glass box, discussing how each parameter, when selectively altered, affected the overall accuracy of the modelled energy and thermal behaviour. Initially,

the description of the calibration process only revolves around energy consumption and will not be repeated for air and radiant temperatures for the purposes of brevity.

The simulations that have been selected for presentation in the following tables were the most representative among a total of simulations. On a number of occasions, when the difference between simulated results was practically negligible, that simulation was not recorded.

Consequently, a statistical analysis was performed and the simulated energy results were compared to the measured through the relationship of energy consumption (kWh) per interior to exterior air temperature difference ($^{\circ}\text{C}$). This process will be discussed for both boxes in sections 5.1.7 for the IES simulations and accuracy and in section 5.1.8 for the analysis of results.

Simulations were grouped for the purposes of clarity of presentation and organisation of context. The first group of simulations is presented in Table 5.3 and concerns the initial stages of modelling the glass covered box. To examine the accuracy of each simulation, the data sets of the simulations and the measured results of energy consumption (in kWh) are presented for comparison using their mean values (columns) as seen in Figure 5.7.

Table 5.3: Glass covered box 1st group of simulations: initial stages of modelling

Simulation	Description
Simulation 01	<p>As a starting point, the material selected for the experimental boxes walls and floors was polyurethane board of 100 mm thickness and the covering glass was a standard double-pane unit of 4 mm glass thickness and a 6 mm cavity thickness.</p> <p>The box was initially designed without the ventilation ducts and auxiliary box. Furthermore, infiltration was not considered at initial modelling stages; but consisted of a default permeability-based air exchange rate of 0.25 ach with external air.</p> <p>As a result, the simulated energy was significantly underestimated in comparison to the measured results. Additionally, the simulated values varied significantly from the measured, not following the trend of the recorded values.</p>
Simulation 02	<p>The ventilation ducts and auxiliary box were added. The material used for the modelling of the auxiliary boxes was polyurethane board of 100 mm.</p> <p>Regarding the modelling of the ducts, they were actually a composite of interior flexible plastic tubing, sheep's wool insulation and exterior uninsulated flexible aluminium tubing covered for secure placement by silver reflective duct tape. These materials did not exist in the IES library. For that reason the material thermal properties would have to be inserted</p>

	<p>manually; however, at such an initial stage alternative materials already found in the IES library were used for the purpose of model simplification.</p> <p>The selected materials were rigid aluminium plate of 2 mm for the two types of duct tube and glass fibre quilt of a thickness of 25 mm representing the sheep's wool insulation. The exaggerated thickness of 2 mm was selected for the aluminium as the Edit Construction palette of the Building Template Manager did not allow for a smaller value for this particular material.</p> <p>The simulated energy consumption resulted to even lower values than the first simulation, whereas the variation away from the measured results increased significantly.</p>
Simulation 03	<p>An additional infiltration of 0.25 l/s was added to the modelled system.</p> <p>However, the infiltration inserted value proved very low, as the mean simulated value increased but still remained lower than the mean measured, while the variation in relation to the measured results still remained significant.</p>
Simulation 04	<p>The additional infiltration was raised to 0.5 l/s.</p> <p>As a result, the average simulated energy consumption increased and the deviation from measured values decreased.</p>
Simulation 05	<p>Infiltration was raised to 0.8 l/s.</p> <p>The average simulated energy consumption increased accordingly, whereas the deviation from the measured values further decreased.</p>
Simulation 06	<p>Infiltration was raised to 1.0 l/s.</p> <p>The average simulated energy consumption increased, while the deviation from the measured values further decreased.</p>
Simulation 07	<p>Infiltration was raised to 1.5 l/s.</p> <p>The average simulated energy consumption increased, reaching the same value as the mean measured energy consumption. Still, although the deviation from the measured values further decreased, it remained considerable indicating that further changes needed to be made.</p>

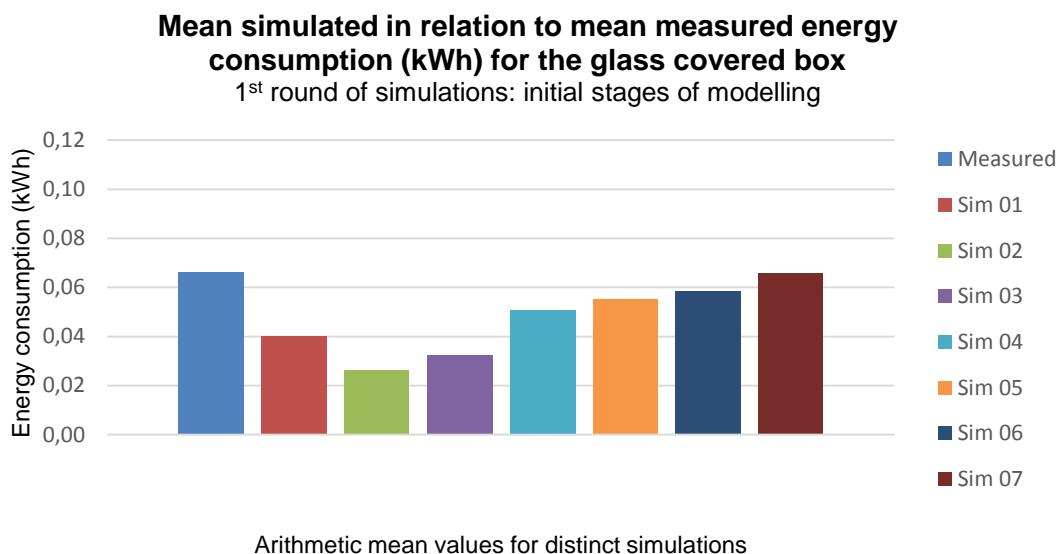


Figure 5.7: Mean values of simulated in relation to measured energy consumption (kWh) for the glass covered box, 1st group of simulations: initial stages of modelling

Table 5.4 presents the mean values of simulated energy consumption, as well as the R^2 coefficient of determination for each simulation, to demonstrate how close the simulated data was to the fitted regression for the measured data.

Table 5.4: Mean hourly energy values (kWh) and coefficient of determination for simulated in relation to measured energy consumption for the glass covered box, 1st group of simulations: initial stages of modelling

	Measured energy	Sim 01	Sim 02	Sim 03	Sim 04	Sim 05	Sim 06	Sim 07
Mean energy (kWh)	0.066	0.040	0.027	0.032	0.051	0.055	0.059	0.066
R^2 coefficient of determination		0.920	0.905	0.908	0.898	0.889	0.897	0.892

The noted disagreement between simulated and measured results, as expressed through the mean difference values between each simulation and measured results, demonstrated the need for more radical changes to the reference model. The following Table 5.5 involves the second group of simulations where the materials properties

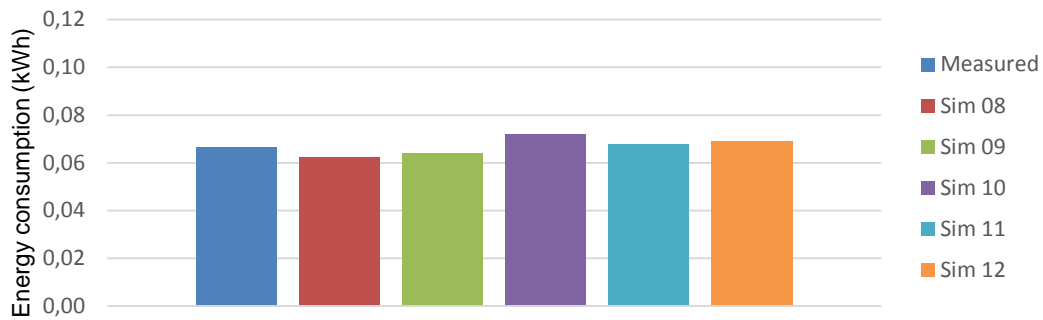
were refined. The related Figure 5.8 shows the mean values representing the simulation process.

Table 5.5: Glass covered box 2nd group of simulations: materials refinement

Simulation	Description
Simulation 08	<p>Infiltration was returned to the default value of 0.25 ach to investigate the effect of the new changes taking place through this simulation.</p> <p>As described in Simulation 02, the ducts were modelled using materials that already existed in the IES library. In this turn, to achieve a smaller material thickness the flexible aluminium tubing material properties were replaced by the properties of paperboard-laminated sheets with a thickness of 1 mm. The glass fibre quilt material properties were replaced by those of batt insulation with a thickness of 25 mm (IES did not specify whether the batt insulation was made of fiberglass, rock or slag wool or a cotton variety).</p> <p>As a result, the simulated energy dropped below the real life measured results. The deviation of simulated from measured energy consumption, however, remained the same.</p>
Simulation 09	<p>Additional infiltration was increased to a value of 1.6 l/s. A number of lower infiltration values was previously considered and found inadequate. They will not be analysed here as the magnitude of the effect of increasing infiltration was examined previously, in the 1st group of simulations.</p> <p>The simulated energy increased closer to the average measured energy consumption and the deviation dropped slightly.</p>
Simulation 10	<p>The interior material properties of the ducts were changed to those of PVC of 1 mm thickness, while added infiltration remained at 1.6 l/s.</p> <p>Simulated energy consumption raised above measured and deviation increased accordingly.</p>
Simulation 11	<p>Internal and external emissivity values of the box and ducts were reduced to 0.8 from the default 0.9 provided by IES. Material properties and infiltration value remained the same.</p> <p>As a result, simulated energy dropped closer to the measured and deviation reduced.</p>
Simulation 12	<p>To further examine the effect of emissivity, internal and external emissivity values of the box and ducts were reduced to 0.7, with all other properties, materials and infiltration remaining the same.</p> <p>Simulated energy and deviation both increased, moving away from the desired measured values.</p>

Mean simulated in relation to mean measured energy consumption (kWh) for the glass covered box

2nd round of simulations: materials refinement



Arithmetic mean values for distinct simulations

Figure 5.8: Mean values of simulated in relation to measured energy consumption (kWh) for the glass covered box, 2nd group of simulations: materials refinement

Table 5.6 presents the mean energy values presented in Figure 5.8 and the estimated R^2 coefficient of determination, to demonstrate how close the simulated data was to the fitted regression for the measured data.

Table 5.6: Mean hourly energy values (kWh) and coefficient of determination for simulated in relation to measured energy consumption for the glass covered box, 2nd group of simulations: materials refinement

	Measured energy	Sim 08	Sim 09	Sim 10	Sim 11	Sim 12
Mean energy (kWh)	0.066	0.062	0.064	0.072	0.068	0.069
R² coefficient of determination		0.907	0.917	0.899	0.917	0.915

The next stage of the calibration process concerns the attempt to simulate the heating system using the IES ApacheHVAC tool (Figure 5.9) and the Thermal tool of the Building Template Manager (Figure 5.10).

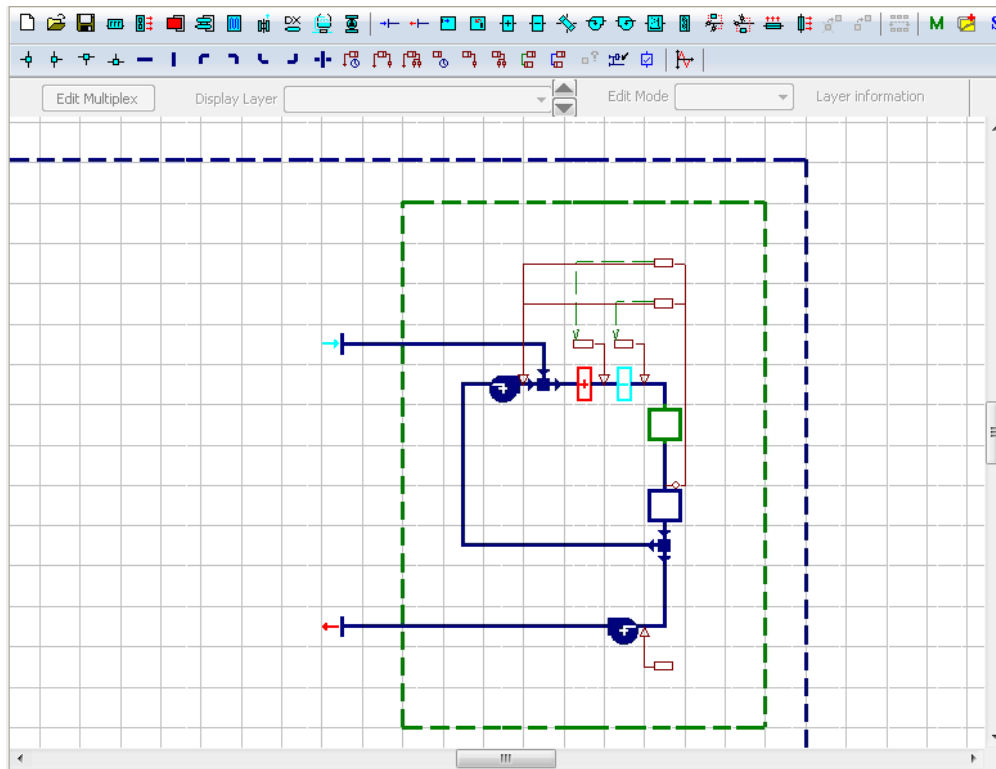


Figure 5.9: ApacheHVAC tool of the IES HVAC system simulation interface

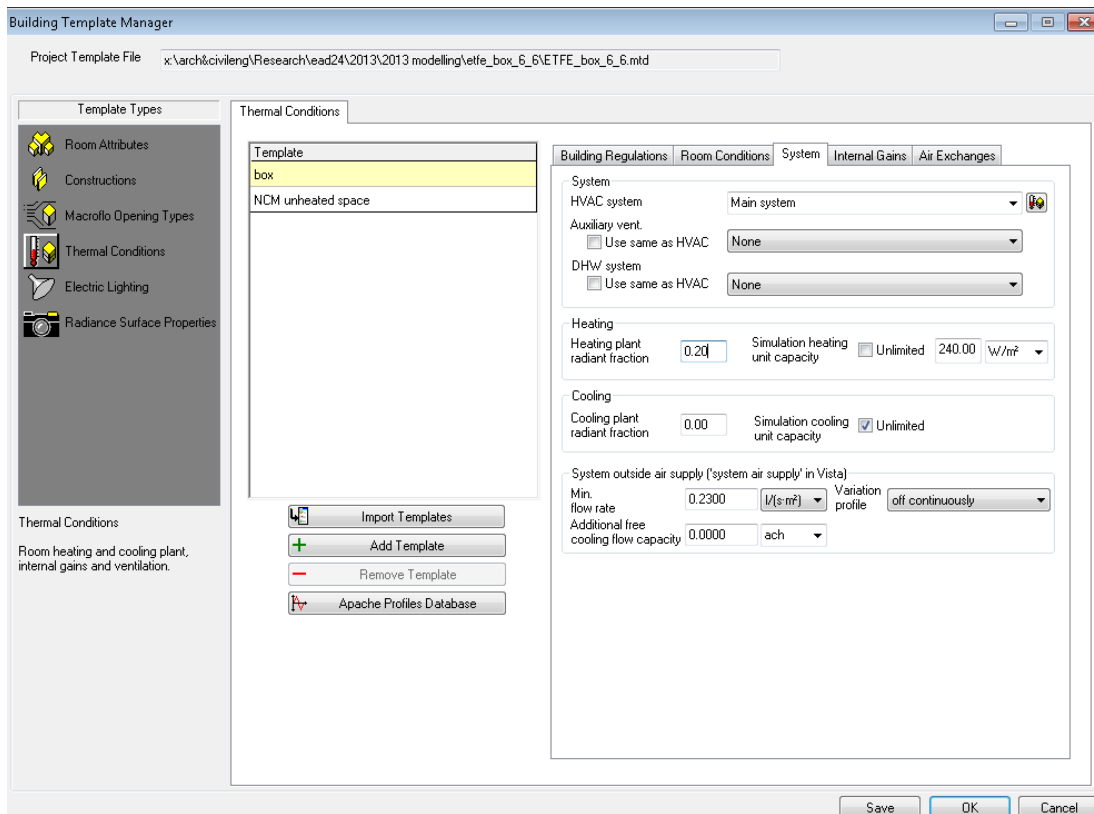


Figure 5.10: Edit Thermal tool of the IES Building Template Manager

So far, the heating system was controlled through the IES thermal template, with the controller regulated to function at a 19 °C set point. Table 5.7 describes the attempts for a different approach to the simulation of room conditioning. Results of the simulations using the revised heating system are shown in Figure 5.11.

Table 5.7: Glass covered box 3rd group of simulations: Bespoke heating and ventilation system implementation (1st attempt)

Simulation	Description
Simulation 13	<p>Infiltration was returned to the default value of 0.25 ach to investigate the effect of the new changes taking place through this simulation.</p> <p>The IES ApacheHVAC tool was used to create a prototype HVAC system, using a self-contained PTAC (packaged terminal air conditioner system) (Figure 5.9). A fan was implemented in probation, set to run continuously, circulating 26 l/s between the interconnected areas of the experimentation box, the ducts and the auxiliary box.</p> <p>The mean simulated energy consumption was significantly lower than the mean measured energy and the variation of the results increased in comparison to previous simulations.</p>

Simulation 14	<p>Added infiltration with external air was increased to 2.0 l/s. A number of lower infiltration values was previously considered and found inadequate. They will not be analysed here as the effect of increasing infiltration was examined previously, in the 1st group of simulations.</p> <p>Simulated energy consumption raised above the measured, whereas variation remained at the same levels.</p>
Simulation 15	<p>The heater dead band (part of the HVAC PTAC system) was raised to 4 K (which is normally the default value) from a previous value of 0. Infiltration remained at 2.0 l/s.</p> <p>As a result, the mean simulated energy and variation both increased.</p>
Simulation 16	<p>The heater dead band was raised to 5 K. Infiltration remained at 2.0 l/s.</p> <p>The mean simulated energy and the variation both decreased.</p>
Simulation 17	<p>The heater dead band was raised to 10 K. Infiltration remained at 2.0 l/s.</p> <p>The mean simulated energy and the variation both decreased.</p>
Simulation 18	<p>The heater radiant fraction was left at 0.2 (which is normally the default value) using the IES Thermal tool of the Building Template Manager (Figure 5.10). The simulation heating unit capacity was changed to 0.24 kW from the default setting of unlimited. Infiltration remained at 2.0 l/s.</p> <p>As a result, the mean simulated energy and the variation both increased.</p>
Simulation 19	<p>The heater radiant fraction was raised to 0.5. Heating unit capacity was left as 0.24 kW and infiltration remained at 2.0 l/s.</p> <p>No change was noticed in the mean simulated energy, yet variation decreased slightly.</p>

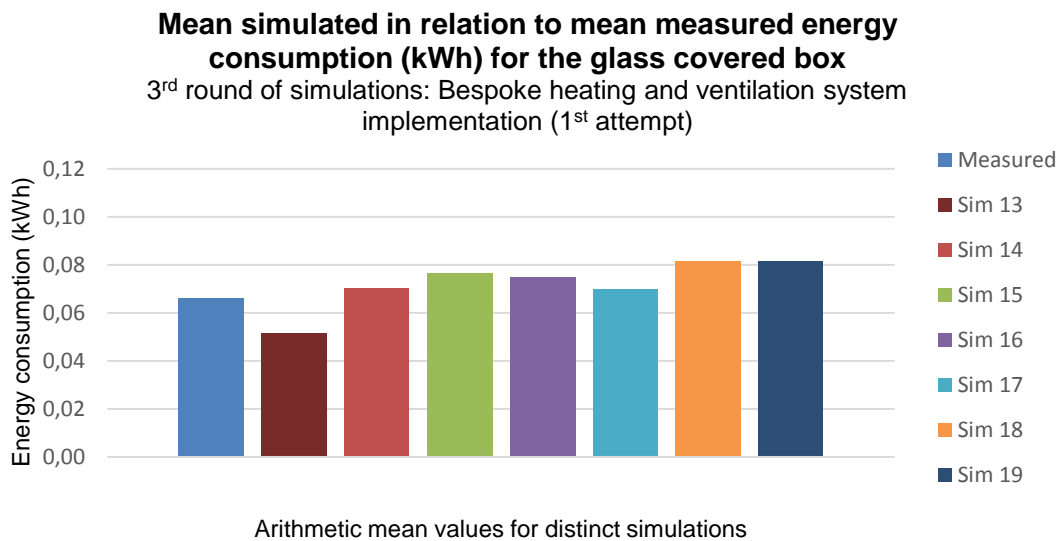


Figure 5.11: Mean values of simulated in relation to measured energy consumption (kWh) for the glass covered box, 3rd group of simulations: Bespoke heating and ventilation system implementation (1st attempt)

Table 5.8 presents the mean energy values and the R^2 coefficient of determination, to demonstrate how close the simulated data was to the fitted regression for the measured data.

Table 5.8: Mean hourly energy values (kWh) and coefficient of determination for simulated in relation to measured energy consumption for the glass covered box, 3rd group of simulations: Bespoke heating and ventilation system implementation (1st attempt)

	Measured energy	Sim 13	Sim 14	Sim 15	Sim 16	Sim 17	Sim 18	Sim 19
Mean energy (kWh)	0.066	0.051	0.070	0.076	0.075	0.070	0.081	0.081
R² coefficient of determination		0.598	0.766	0.873	0.888	0.910	0.813	0.822

Since this type of bespoke heating system was leading to erroneous results, other types of heating systems were explored from the IES ApacheHVAC tool by trial and error. Table 5.9 describes these attempts and Figure 5.12 summarises the results.

Table 5.9: Glass covered box 4th group of simulations: Bespoke heating and ventilation system implementation (2nd attempt)

Simulation	Description
Simulation 20	<p>After a few intermittent simulations, infiltration was reduced back to 0.15 l/s. Additionally, the HVAC link of the bespoke heating and ventilation system was switched off. A direct heater was selected to operate the system.</p> <p>As a result, the mean simulated energy value dropped – though still at higher levels than the measured. Variation also dropped from the levels of the last recorded simulation group.</p>
Simulation 21	<p>A fin tube radiator was implemented in the system, replacing the previously used direct heater. Infiltration remained at the same level.</p> <p>The mean simulated energy and variation increased.</p>
Simulation 22	<p>A radiant ceiling heater was introduced to the system, replacing the fin tube radiator. Infiltration remained at the same level.</p> <p>The mean simulated energy and variation decreased.</p>
Simulation 23	<p>The direct heater used in Simulation 20 was re-introduced to the system. The HVAC link remained switched off. Through ApacheSim, the heater radiant fraction was switched to 0.2 from a previously used value of 0.5. Infiltration remained at the same level.</p> <p>The mean simulated energy and variation decreased.</p>

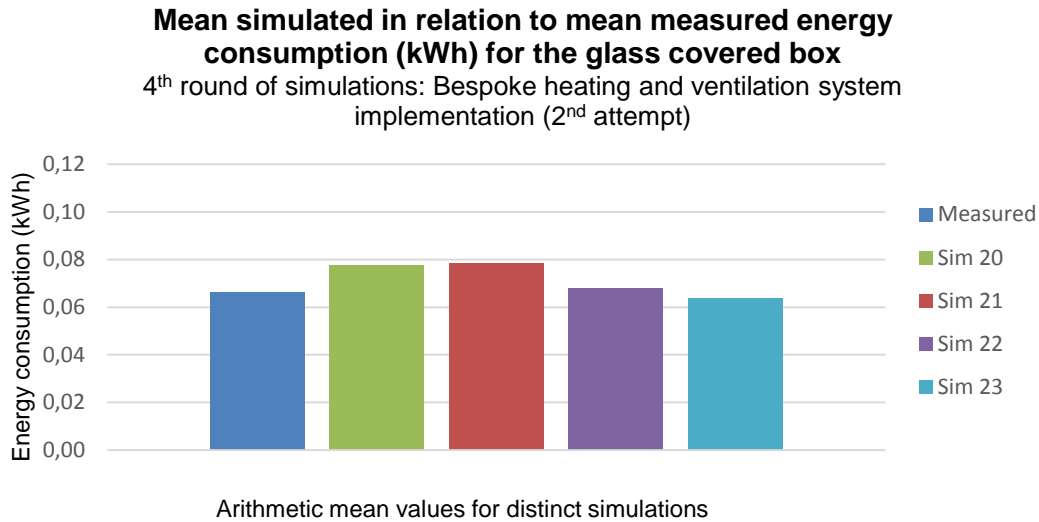


Figure 5.12: Mean values of simulated in relation to measured energy consumption (kWh) for the glass covered box, 4th group of simulations: Bespoke heating and ventilation system implementation (2nd attempt)

Table 5.10 presents the estimated mean energy values and the R^2 coefficient of determination, to demonstrate how close the simulated data was to the fitted regression for the measured data.

Table 5.10: Mean hourly energy values (kWh) and coefficient of determination for simulated in relation to measured energy consumption for the glass covered box, 4th group of simulations: Bespoke heating and ventilation system implementation (2nd attempt)

	Measured energy	Sim 20	Sim 21	Sim 22	Sim 23
Mean energy (kWh)	0.066	0.078	0.079	0.068	0.064
R² coefficient of determination		0.858	0.806	0.797	0.925

Seeing as the implementation of a bespoke heating system through IES ApacheHVAC was not successful and that the switching off of the HVAC link in the ApacheSim template appeared to improve results, a return was made to previous steps using the observations made on the last group of simulations. Table 5.11 describes the final

adjustments to the heating system that led to a more accurate simulation of the energy performance, summarized in Figure 5.13.

Table 5.11: Glass covered box 5th group of simulations: Bespoke heating and ventilation system implementation (3rd attempt)

Simulation	Description
Simulation 24	<p>Infiltration remained to the default value of 0.25 ach. The HVAC link was switched off. Through ApacheSim, the heater radiant fraction was switched back to 0.5.</p> <p>The mean simulated energy increased, while variation remained the same.</p>
Simulation 25	<p>All settings remained as in Simulation 24. The infiltration for the ducts and auxiliary box was set to 26 l/s and the setting “from adjacent room” was selected to simulate the fan operation.</p> <p>The mean simulated energy decreased, while variation remained the same.</p>
Simulation 26	<p>All settings remained as in Simulation 25, including the increased infiltration in the ducts and auxiliary box. Extra infiltration of 0.25 ach was added to the ducts and auxiliary box towards the exterior environment.</p> <p>The mean simulated energy and variation of results remained the same.</p>
Simulation 27	<p>As the added infiltration to the ducts and auxiliary box appeared to be too low to have an effect, it was increased to 2 ach.</p> <p>As a result, the mean simulated energy increased, while variation of results remained the same.</p> <p>Although in some occasions this simulation overestimated energy, it was selected as the optimum, as it served to also provide very accurate values for the air and radiant internal temperatures. This process is described in more detail further along.</p>

Mean simulated in relation to mean measured energy consumption (kWh) for the glass covered box
 5th round of simulations: Bespoke heating and ventilation system implementation (3rd attempt)

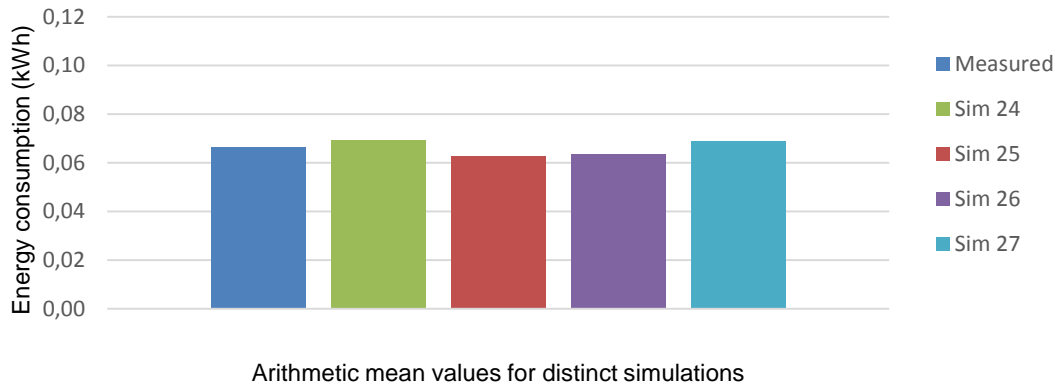


Figure 5.13: Mean values of simulated in relation to measured energy consumption (kWh) for the glass covered box, 5th group of simulations: Bespoke heating and ventilation system implementation (3rd attempt)

Table 5.12 presents the mean energy values and the R² coefficient of determination, to demonstrate how close the simulated data was to the fitted regression for the measured data.

Table 5.12: Mean hourly energy values (kWh) and coefficient of determination for simulated in relation to measured energy consumption for the glass covered box, 5th group of simulations: Bespoke heating and ventilation system implementation (3rd attempt)

	Measured energy	Sim 24	Sim 25	Sim 26	Sim 27
Mean energy (kWh)	0.066	0.069	0.063	0.063	0.069
R² coefficient of determination		0.917	0.921	0.921	0.911

The result of the final energy consumption, as well as the air and radiant temperature simulations can be seen alongside the corresponding measured values in Figures 5.14,

5.15 and 5.16. These results and the accuracy of the model will be further analysed in section 5.1.7 dedicated to the IES model results and accuracy. For the time being, the reference model of the glass-box will be used as a benchmark to describe the calibration of the reference model of the ETFE-covered box.

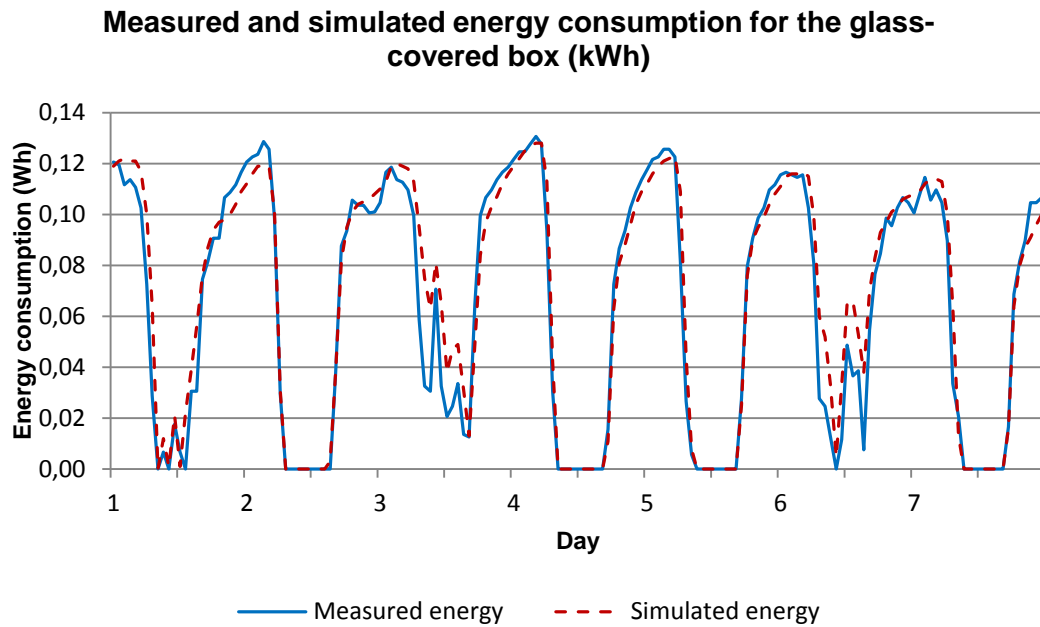


Figure 5.14: Measured and simulated energy consumption for the glass-covered box (kWh)

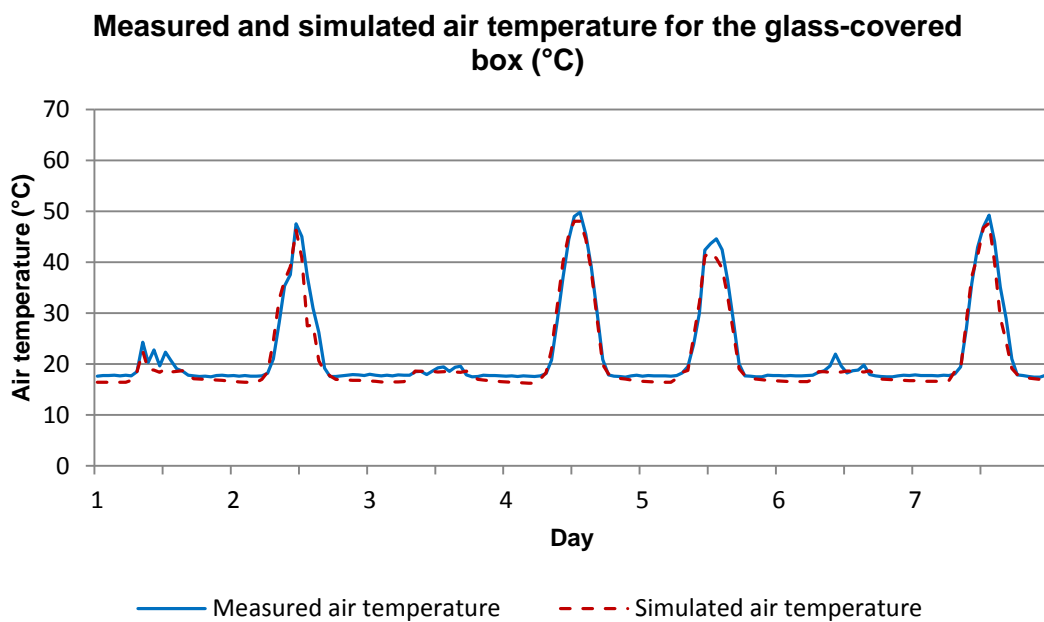


Figure 5.15: Measured and simulated air temperature for the glass-covered box (°C)

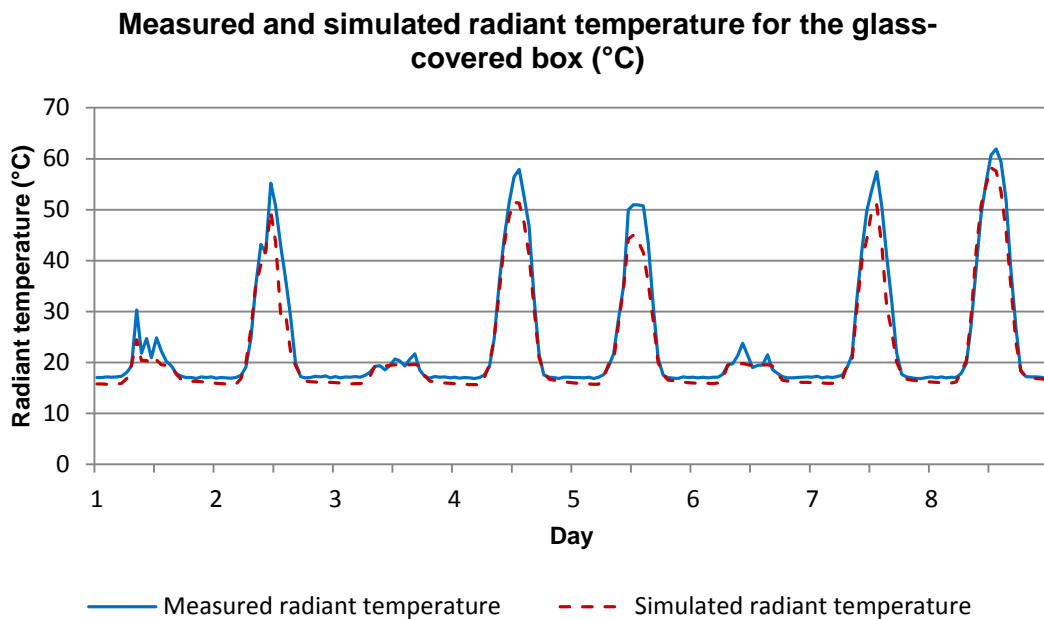


Figure 5.16: Measured and simulated radiant temperature for the glass-covered box (°C)

- This section describes the calibration process for the IES simulation of the ETFE covered box. The glass box reference model was used as a basis, and the double glazed cover was replaced by two flat parallel layers of ETFE membrane placed at a distance of 200 mm from each other (the maximum distance at the top of the cushion camber). The sensitivity testing process was repeated, examining the effects of each parameter changed in each simulation. As before, the results will be presented in groups, using the mean simulated and measured values, as well as the mean difference between them to describe the accuracy of each simulation.

To assist the calibration description, Figure 5.17 shows a schematic diagram of the modelled ETFE layers.

A: Clear surface of the upper ETFE membrane, exposed to the elements.

B: Clear surface of the upper ETFE membrane, located in the interior of the cushion.

C: Fritted surface of the lower ETFE membrane, located in the interior of the cushion.

D: Clear surface of the lower ETFE membrane, located towards the box interior.

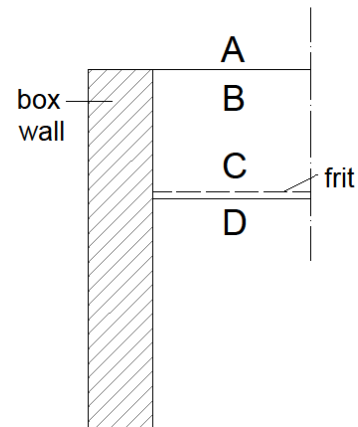


Figure 5.17: Schematic annotation of the modelled ETFE layers

The physical properties of the ETFE foil were taken from the Vector Foiltec material properties sheet for Texlon®, the DuPont material properties sheet for Teflon® and further personal communication with Vector Foiltec (DuPont, 2012; Vector, 2012; Vector, 2013).

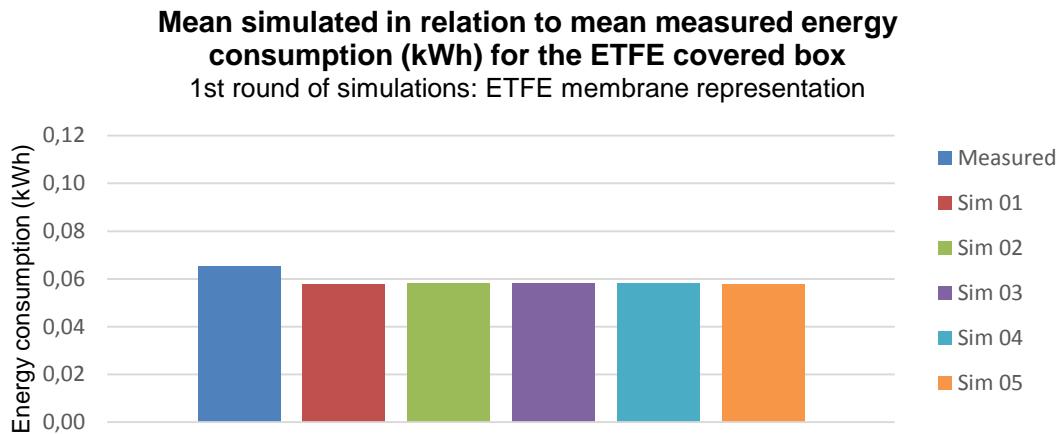
The first group of initial simulations of ETFE membranes is presented in Table 5.13. Figure 5.18 summarises the contents of Table 5.13.

Table 5.13: ETFE covered box 1st group of simulations: ETFE membrane representation

Simulation	Description
Simulation 01	<p>The structure and the material properties of the main and auxiliary boxes, as well as the ducts, were the same as in the simulations performed for the glass covered box. Infiltration was set at the default value of 0.25 ach for the main and auxiliary boxes.</p> <p>Regarding the heating system, the HVAC link was switched off, as in the case of the glass covered box. The heater radiant fraction was set to 0.5.</p> <p>Regarding the ETFE membranes, the following features were set manually using values from the Vector Foiltec Texlon DM 65 product sheet into the IES Building Template Manager palette (Vector 2013):</p> <ul style="list-style-type: none"> - Emissivity for layer A: 0.81 and for layers B, C and D: 0.57 - Conductivity for all layers: 0.23 (W/mK) - Convection coefficient for all layers: 5.6 (W/m²K)

	<ul style="list-style-type: none"> - Solar transmission for layer A. B: 0.911 and for layers C, D: 0.54 - Solar reflectance for layer A: 0.33, for layers B, C and D: 0.34 - Refractive index was left as the default value 1.0, as the Vector Foiltec Texlon product information sheet did not provide with a refractive index value. <p>As a result, the mean simulated energy consumption was significantly lower than the mean measured energy. Also, the variation of the results was higher than the respective value that occurred from the final glass box simulations.</p>
Simulation 02	<p>Infiltration and heating system remained the same.</p> <p>Regarding the ETFE membranes:</p> <ul style="list-style-type: none"> - Emissivity, conductivity, convection coefficient, solar transmission and solar reflectance remained the same. - Refractive index was increased to 1.38 for all layers, using Teflon values (1.35 – 1.38) (DuPont 2012). <p>Although there were differences between the two data sets when examined in detail, the mean simulated energy consumption and the variation of the results remained the same as in Simulation 01.</p>
Simulation 03	<p>Infiltration and heating system remained the same.</p> <p>Regarding the ETFE membranes:</p> <ul style="list-style-type: none"> - Emissivity, conductivity, convection coefficient, solar transmission and solar reflectance remained the same. - Refractive index was increased to 1.49 for all layers, using acrylic glass values (1.490 – 1.492). <p>Although there were differences between the two data sets when examined in detail, the mean simulated energy consumption and the variation of the results remained the same as in Simulation 01.</p>
Simulation 04	<p>Infiltration and heating system remained the same.</p> <p>Regarding the ETFE membranes:</p> <ul style="list-style-type: none"> - Emissivity, conductivity, convection coefficient, solar transmission and solar reflectance remained the same. - Refractive index was increased to 1.59 for all layers, approaching polycarbonate values (1.584 – 1.586). <p>Although there were differences between the two data sets when examined in detail, the mean simulated energy consumption and the variation of the results remained the same as in Simulation 01.</p>
Simulation 05	<p>Air infiltration was set to the default 0.25 ach, plus the additional 2 ach that had been used for the glass box.</p> <p>To simulate air movement inside the experimental unit, air ventilation of 26 l/s was added to the ducts and auxiliary box from the adjacent room (in this case the main box), as it was previously done for the glass covered box.</p> <p>Regarding the ETFE membranes:</p> <ul style="list-style-type: none"> - Emissivity, conductivity, convection coefficient, solar transmission and solar reflectance remained the same.

	<p>- Refractive index was returned to the Teflon value of 1.38, as in Simulation 02.</p> <p>As a result, the mean simulated value and the variation of simulated values away from measured remained the same.</p>
--	---



Arithmetic mean values for distinct simulations

Figure 5.18: Mean values of simulated in relation to measured energy consumption (kWh) for the ETFE covered box, 1st group of simulations: ETFE membrane representation

Table 5.14 presents the estimated mean energy values and the R^2 coefficient of determination, to demonstrate how close the simulated data was to the fitted regression for the measured data.

Table 5.14: Mean hourly energy values (kWh) and coefficient of determination for simulated in relation to measured energy consumption for the ETFE covered box, 1st group of simulations:

ETFE membrane representation						
	Measured energy	Sim 01	Sim 02	Sim 03	Sim 04	Sim 05
Mean energy (kWh)	0.065	0.058	0.058	0.058	0.058	0.058
R² coefficient of determination		0.976	0.976	0.976	0.976	0.975

Changing the refractive index coefficient to values that typically characterise materials with similar properties with ETFE did not have a significant effect on the accuracy of the IES energy simulations. However, for the purpose of consistency, it was decided that the refractive index value 1.38 for Teflon would be used, as the closest material to Texlon, offering the available necessary technical information.

Up to this point, the ETFE cushion was modelled as two flat membranes mounted at a distance of 200 mm from each other. The method used for the U-value calculations was the CIBSE method, which resulted in a U-value of 2.61 W/m²K.

The second group of simulations was performed to ensure that this distance was indeed suitable as an accurate representation of the ETFE cushion. The distance of 200 mm was gradually altered by 10 mm steps, using the IES Edit Constructions tool of the Building Template Manager aiming to reach a U-value of 2.94 W/m²K, which is the value for a two layer clear cushion provided by the technical note of Vector Foiltec, the company that supplied the cushion used in the experiments. The U-value of the cushion was also calculated using BS EN 6946, resulting to a value of 3.2 W/m²K with a margin of error of 0.16 W/m²K, as described in Appendix D. The estimated thermal transmittance for the ETFE cushion of 3.2 m²K/W is close, yet not identical to the suggested thermal transmittance of 2.94 m²K/W provided by Vector Foiltec, even when taking into account the margin of error.

A certain number of simplifications was made in the calculations due to unknown variables, such as the mean absolute temperature of the air inside the cushion and the temperature difference between the ETFE surfaces bounding the air space – which were needed to estimate the bulk thermal transmittance with more accuracy. Instead, values provided by the BS were used, which are expected to have affected the resulting U-value.

Furthermore, in the absence of the temperature of the exterior foil surface and its surroundings T_m , the average internal surface temperature was used to estimate the mean thermodynamic value for the radiative heat transfer coefficient h_{re} of the external ETFE foil. The internal surface temperature that was used would be higher than the external surface temperature under cold weather conditions, in which case it is expected to have slightly raised the overall estimated thermal transmittance of the cushion.

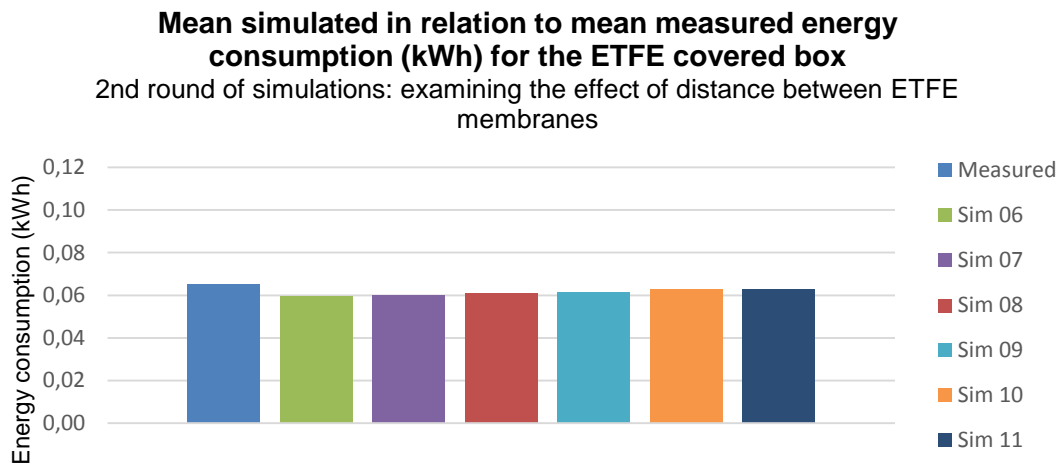
Due to the above mentioned uncertainties that are expected to affect the resulting thermal transmittance, it was decided to base the simulations of Chapters 5 and 6 on the U-value of the ETFE cushion provided by Vector Foiltec. It was later realised that the used value of 2.94 W/m²K was not accurately representative of the ETFE cushion used, which caused this cushion to have a better simulated energy performance than that measured in reality. However, at that point in time the information by Vector Foiltec was the only official information available regarding the U-value of the cushion, and was therefore used. A more focused study on the U-value of a fritted ETFE cushion will be undertaken in Chapter 6, on the secondary modelling using IES.

Table 5.15 describes the second group of simulations, examining the effect of changes to the distance between the two membranes forming the ETFE unit. Figure 5.19 summarises the contents of Table 5.15.

Table 5.15: ETFE covered box 2nd group of simulations: examining the effect of distance between ETFE membranes

Simulation	Description
Simulation 06	Distance between membranes was decreased to 150 mm, increasing the cushion U-value to 2.64 W/m ² K using the CIBSE method. The mean simulated energy consumption increased, yet still remained lower than the mean measured energy. Variation slightly increased in comparison to Simulation 05.
Simulation 07	Distance between membranes was decreased to 100 mm, increasing the cushion U-value to 2.68 W/m ² K using the CIBSE method. The mean simulated energy consumption increased, yet still remained lower than the mean measured energy. Variation remained the same.
Simulation 08	Distance between membranes was decreased to 50 mm, increasing the cushion U-value to 2.76 W/m ² K using the CIBSE method. The mean simulated energy consumption increased, yet still remained lower than the mean measured energy. Variation remained the same.
Simulation 09	Distance between membranes was decreased to 30 mm, increasing the cushion U-value to 2.82 W/m ² K using the CIBSE method. The mean simulated energy consumption increased, yet still remained lower than the mean measured energy. Variation decreased.
Simulation 10	Distance between membranes was decreased to 15 mm, increasing the cushion U-value to 2.91 W/m ² K using the CIBSE method. The mean simulated energy consumption increased, yet still remained lower than the mean measured energy. Variation remained the same.
Simulation 11	Distance between membranes was decreased to 12 mm, increasing the cushion U-value to 2.94 W/m ² K using the CIBSE method.

The mean simulated energy consumption increased, yet still remained lower than the mean measured energy. Variation remained the same.



Arithmetic mean values for distinct simulations

Figure 5.19: Mean values of simulated in relation to measured energy consumption (kWh) for the ETFE covered box, 2nd group of simulations: examining the effect of distance between ETFE membranes

Table 5.16 presents the estimated mean energy values and R^2 , the coefficient of determination, to demonstrate how close the simulated data was to the fitted regression for the measured data.

Table 5.16: Mean hourly energy values (kWh) and coefficient of determination for simulated in relation to measured energy consumption for the ETFE covered box, 2nd group of simulations: examining the effect of distance between ETFE membranes

	Measured energy	Sim 06	Sim 07	Sim 08	Sim 09	Sim 10	Sim 11
Mean energy (kWh)	0.065	0.059	0.060	0.061	0.062	0.063	0.063
R² coefficient of determination		0.968	0.968	0.966	0.966	0.964	0.965

The ETFE box was situated on the South of the glass box, as described in Chapter 4. That means that it was more exposed to the prevailing winds, which would indicate that air infiltration may have been higher than that estimated for the glass box. Furthermore, as the wooden frame around the ETFE was constructed by hand, inconsistencies in build quality are expected. Due to the very light weight of the ETFE cushion there might have been more air leakage in the ETFE-covered box than that estimated for the glass box, as the high weight of the double glazed unit helped secure the box lid firmly into place.

Taking this into account, a 3rd group of simulations was performed, involving the simulation of air leakage and infiltration, which would increase heat loss and energy consumption. Table 5.17 concerns the 3rd group of simulations, first describing the result of adding infiltration to the boxes and afterwards describing the result of alterations to the ETFE frame heat transfer properties. Figure 5.20 summarises the contents of Table 5.17.

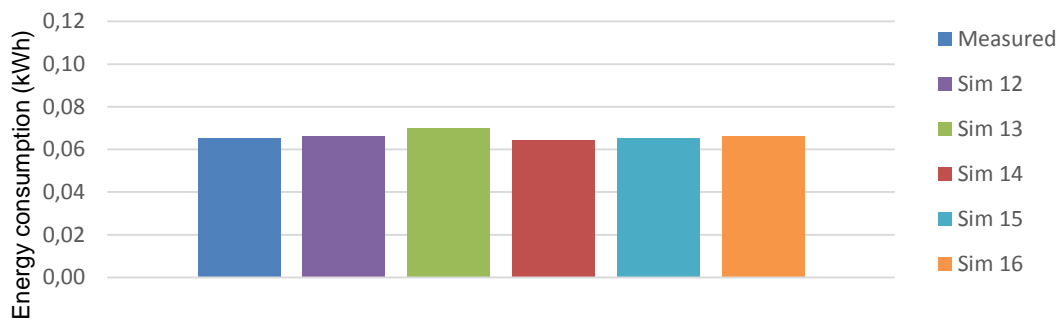
Table 5.17: ETFE covered box 3rd group of simulations: air infiltration and heat loss through the ETFE frame (1st attempt)

Simulation	Description
Simulation 12	<p>Infiltration was increased from 2 ach to 3 ach for the main box, the auxiliary box and the ducts.</p> <p>Default infiltration of 0.25 ach and additional ventilation of 26 l/s between main box, ducts and auxiliary box remained the same.</p> <p>The mean simulated energy consumption increased above the mean measured energy. Variation decreased from the 2nd group of simulations.</p>
Simulation 13	<p>Infiltration was increased to 4 ach for the main box, the auxiliary box and the ducts.</p> <p>Default infiltration of 0.25 ach and additional ventilation of 26 l/s between main box, ducts and auxiliary box remained the same.</p> <p>The mean simulated energy consumption increased. Variation remained the same. As the mean energy consumption was stirring away from measured values, it appeared that this was not the right approach. For that reason focus was placed on further heat loss through the ETFE frame.</p>
Simulation 14	<p>Default infiltration of 0.25 ach and additional ventilation of 26 l/s between main box, ducts and auxiliary box remained the same. Additional infiltration was returned to 2 ach for the main box, ducts and auxiliary box.</p> <p>The ETFE frame resistance was altered in Building Template Manager from 0.1 to 0.05 m²K/W, changing the frame U-value from 4.17 W/m²*K to 5.26 W/m²K.</p>

	The mean simulated energy decreased to a value lower, yet very close to the mean measured energy. Variation remained the same.
Simulation 15	<p>Default infiltration of 0.25 ach, additional infiltration of 2 ach and additional ventilation of 26 l/s between main box, ducts and auxiliary box remained the same.</p> <p>The ETFE frame resistance was altered in Building Template Manager to 0.03 m²K/W, changing the frame U-value to 5.88 W/m²K.</p> <p>As a result, the mean simulated energy increased to reach the same value as the mean measured energy, while variation remained the same.</p>
Simulation 16	<p>Default infiltration of 0.25 ach, additional infiltration of 2 ach and additional ventilation of 26 l/s between main box, ducts and auxiliary box remained the same.</p> <p>The ETFE frame resistance was altered in Building Template Manager to 0.01 m²K/W, changing the frame U-value to 6.67 W/m²K.</p> <p>The mean simulated energy increased, while variation remained the same.</p>

Mean simulated in relation to mean measured energy consumption (kWh) for the ETFE covered box

3rd round of simulations: air infiltration and heat loss through the ETFE frame (1st attempt)



Arithmetic mean values for distinct simulations

Figure 5.20: Mean values of simulated in relation to measured energy consumption (kWh) for the ETFE covered box, 3rd group of simulations: air infiltration and heat loss through the ETFE frame (1st attempt)

Table 5.18 presents the estimated mean energy values and the R² coefficient of determination, to demonstrate how close the simulated data was to the fitted regression for the measured data.

Table 5.18: Mean hourly energy values (kWh) and coefficient of determination for simulated in relation to measured energy consumption for the ETFE covered box, 3rd group of simulations: air infiltration and heat loss through the ETFE frame (1st attempt)

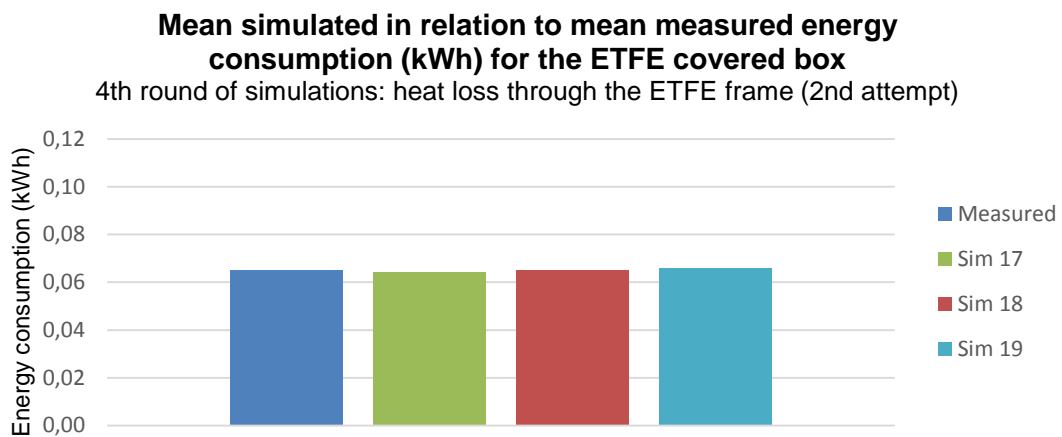
	Measured energy	Sim 12	Sim 13	Sim 14	Sim 15	Sim 16
Mean values (kWh)	0.065	0.066	0.070	0.064	0.065	0.066
R² coefficient of determination		0.961	0.956	0.964	0.964	0.962

As a result of this group of simulations, the estimated energy consumption was very close to the measured energy consumption. However, the simulated air and radiant temperatures diverged away from the measured interior conditions, which meant that although the general approach was successful, further fine-tuning of the IES model was still necessary. The 4th and final group of simulations focused solely on heat loss through the ETFE frame, as it is presented in Table 5.19. Figure 5.21 shows a summary of the information from Table 5.19.

Table 5.19: ETFE covered box 4th group of simulations: heat loss through the ETFE frame (2nd attempt)

Simulation	Description
Simulation 17	<p>Default infiltration of 0.25 ach, additional infiltration of 2 ach and additional ventilation of 26 l/s between main box, ducts and auxiliary box remained the same.</p> <p>The ETFE frame resistance was returned to 0.1 m²K/W.</p> <p>The outside and inside area surface ratio of the frame were increased from 1.00 to 2.00, increasing the frame U-value from 4.17 W/m²K to 5.88 W/m²K.</p> <p>The mean simulated energy consumption decreased, while variation remained the same.</p>
Simulation 18	<p>Default infiltration of 0.25 ach, additional infiltration of 2 ach and additional ventilation of 26 l/s between main box, ducts and auxiliary box remained the same.</p> <p>The outside and inside area surface ratio of the frame were increased to 3.00, increasing the frame U-value to 6.82 W/m²K.</p> <p>The mean simulated energy consumption increased, while variation remained the same.</p>
Simulation 19	<p>Default infiltration of 0.25 ach, additional infiltration of 2 ach and additional ventilation of 26 l/s between main box, ducts and auxiliary box remained the same.</p>

	<p>The outside and inside area surface ratio of the frame were increased to 4.00, increasing the frame U-value to 7.04 W/m²K.</p> <p>The mean simulated energy consumption increased slightly, while variation remained the same. This simulation was selected as the optimum, as it served to also provide very accurate values for the air and radiant internal temperatures.</p>
--	--



Arithmetic mean values for distinct simulations

Figure 5.21: Mean values of simulated in relation to measured energy consumption (kWh) for the ETFE covered box, 4th group of simulations: heat loss through the ETFE frame (2nd attempt)

Table 5.20 presents the mean energy values and the R² coefficient of determination, to demonstrate how close the simulated data was to the fitted regression for the measured data.

Table 5.20: Mean hourly energy values (kWh) and coefficient of determination for simulated in relation to measured energy consumption for the ETFE covered box, 4th group of simulations: heat loss through the ETFE frame (2nd attempt)

	Measured energy	Sim 17	Sim 18	Sim 19
Mean energy (kWh)	0.065	0.064	0.065	0.066
R² coefficient of determination		0.964	0.963	0.962

The result of the final energy consumption, as well as the air and radiant temperature simulations can be seen alongside the corresponding measured values in Figures 5.22, 5.23 and 5.24. These results and the accuracy of the model will be further analysed in the following section dedicated to the IES model results and accuracy, which describes in detail both digital models in their final form, as a result of the calibration process.

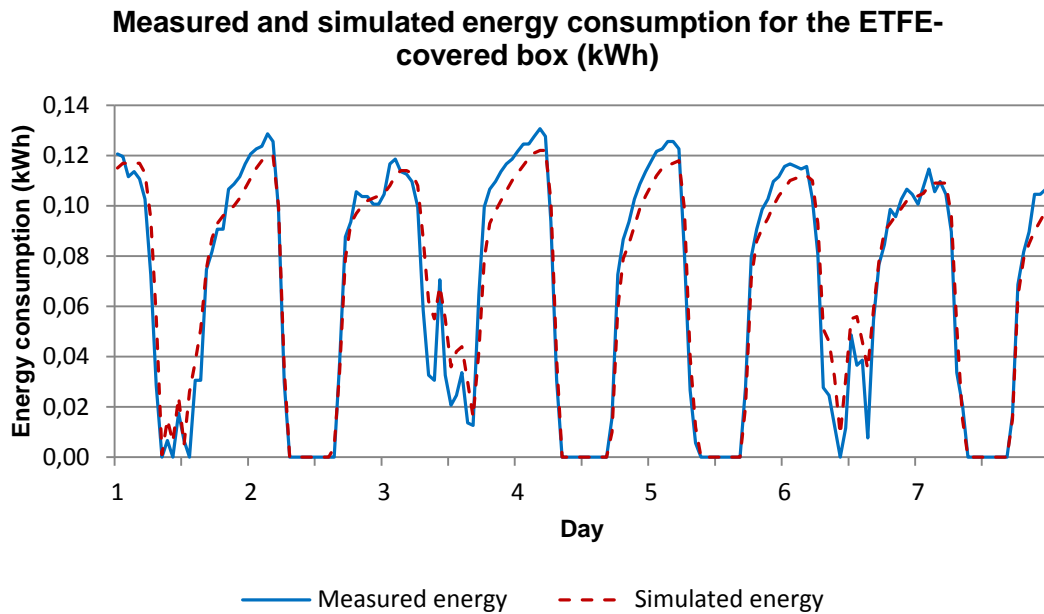


Figure 5.22: Measured and simulated energy consumption for the ETFE-covered box (kWh)

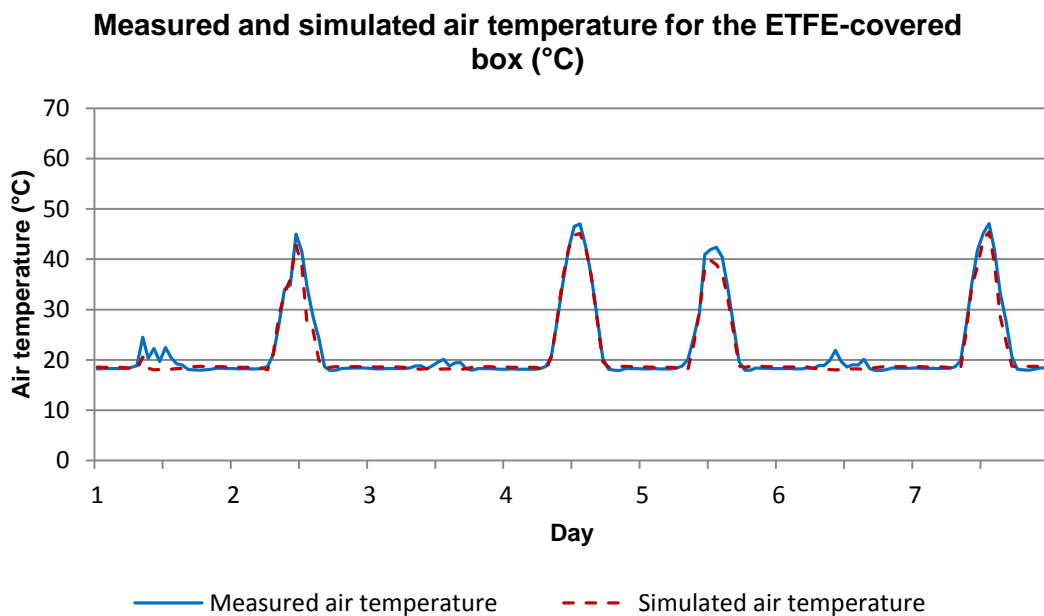


Figure 5.23: Measured and simulated air temperature for the ETFE-covered box (°C)

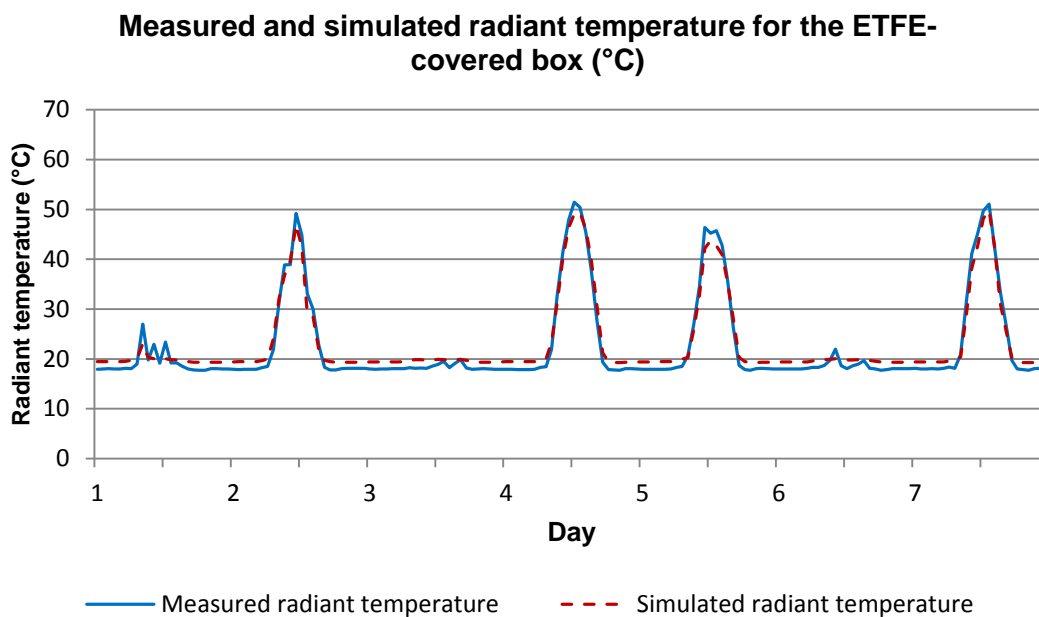


Figure 5.24: Measured and simulated radiant temperature for the ETFE-covered box (°C)

5.1.6 Digital model construction

The material properties used for the box walls and ducts were taken from the IES material library. Table 5.21 provides detailed information on the materials that were used in the IES model to represent the realistic models.

Table 5.21: IES model – description of experimental boxes and ducts

	Thickness (mm)	Conductivity (W/m*K)	Density (kg/m³)	Specific heat capacity (J/kg*K)	U-value (W/m²*K)
Main / auxiliary box					
Polyurethane foam	100	0.025	30	1400	0.24
Duct					
P.V.C.	1	0.160	1379	1004	0.31
Sheep wool insulation	25	0.039	19	1700	
P.V.C.	1	0.160	1379	1004	

The material surface emissivity values were not the default values that IES contains corresponding to the materials used but were inserted manually, as the walls of the boxes were painted for protection. Table 5.22 presents the material surface emissivity values that were used for the model. The values used to compose this table were mean values obtained from a variety of sources, ranging from commercial sites to the U.S. Department of Energy, since there were no officially published values by an international standard.

Table 5.22: Material surface emissivity values (Fermilab, 2013; InfraredServicesInc, 2013; Scigiene, 2013; University of Missouri, 1993)

Material	Emissivity
P.V.C.	0.92
Paint, aluminium (in absence of value for electrical, insulating silver tape used on duct pipes)	0.45
Paint, white plastic	0.84
Lacquer, white	0.92

Furthermore, the box covers were also modelled using the IES Building Template Manager palette. The selected frame for both covering units was hardwood, the frame to opening ratio was measured and set at 10% with a resistance of 0.10 m²*K/W and the selected percentage of sky blocked was “very little (<20%)”. The glass unit was described in the model as: 0.004 m clear float glass – 0.006 m air – 0.004 m clear float glass, with a surface area of 0.18 m². The default values for glass as found in the IES materials library were compared to those provided by the Lawrence Berkeley National Laboratory. It was decided to keep all default values the same, with the exception of the surface emissivity which was supplemented using the online database on glass properties provided by the LBNL (2013).

ETFE membrane was essentially treated by IES as a double glazed unit with different properties. As mentioned earlier, the values used to describe the ETFE cushion were taken from the Vector Foiltec material properties sheet for Texlon®, the DuPont material properties sheet for Teflon®, further personal communication with Vector Foiltec and a report prepared by an external testing centre (the Bavarian Center for

Applied Energy Research) on the “Measurement and Calculation of the Solar and Thermal Properties of ETFE layers” (DuPont, 2012; Korner, 2011; Vector, 2012; Vector, 2013). Detailed values used to describe the properties of the covering units can be found in Table 5.23. Using the CIBSE method in the IES Building Template Manager, the U-value for the glass unit was 2.49 W/m²K alone and 2.63 W/m²K with the frame. Using the CIBSE method, the U-value for the ETFE cushion was 2.94 W/m²K alone and 3.36 W/m²K with the frame.

Table 5.23: IES model – description of cladding

	Glass unit			ETFE cushion		
	Clear float glass	Gas (air)	Clear float glass	ETFE membrane (outside layer, clear)	Gas (air)	ETFE membrane (inside layer, dot matrix 65%)
Thickness (mm)	4	6	4	0.2	12	0.2
Conductivity (W/mK)	1.06		1.06	0.23		0.23
Convection coefficient (W/m²K)		4.16			3.168	
Resistance (m²K/W)		0.127			0.173	
Solar transmittance	0.82		0.82	0.911		0.54
Outside reflectance	0.07		0.07	0.08		0.33
Inside reflectance	0.07		0.07	0.08		0.34
Refractive index	1.526		1.526	1.38		1.38
Outside emissivity	0.92		0.92	0.82		0.81
Inside emissivity	0.92		0.92	0.82		0.57

Once the final form of the IES models was resolved, a detailed verification process was required to verify that the model was not only successful in terms of reproducing the energy consumption of the heating system, but also the internal conditions of the enclosure. The subsequent sections of this chapter describe the process followed to

examine and validate the accuracy of the IES model, in terms of energy consumption, as well as air and radiant temperatures.

5.1.7 IES model results and accuracy

A linear regression analysis was performed using the statistical analysis tool PASW Statistics 18 (formerly SPSS Statistics). The linear regression involved the measured and simulated energy data for the glass model, resulting to a bivariate correlation coefficient R of 0.98, indicating a strong relation of the dependent variable simulated energy consumption to the independent variable measured energy consumption. An error of 0.001 kWh resulted for the estimated energy consumption model. A linear regression was also performed to examine the accuracy of the calculated air and radiant temperatures, in which case the correlation coefficients were 0.98 and 0.99 correspondingly, with an estimated error of 0.32 °C for the simulated air temperature and 0.27 °C for the simulated radiant temperature. These figures suggest that IES was successful in providing an accurate model for the prediction of energy consumption and internal air and radiant temperature of the glass-covered box.

A linear regression analysis was also performed comparing the measured and simulated energy consumption of the ETFE-covered box, resulting in a bivariate correlation coefficient of 0.98 and an error of 0.001 kWh. The correlation coefficients for air and radiant temperature for the ETFE box were 0.99 and 0.99 and the estimated errors were 0.28 °C and 0.20 °C respectively. IES simulated the energy and thermal performance of the ETFE-covered box with more accuracy than the glass-covered box.

The points where there was a noted significant deviation between measured and simulated energy per air temperature difference coincided with lower recorded radiant temperatures and the related lower sky emissivity, as well as lower relative humidity levels, which are features associated with a very clear sky. This suggests that the IES model failed to take into consideration the low clear night sky temperature; which would affect the estimation of the amount of heat escaping the box in the absence of clouds and solar input. This fact could be related to the uncertainty accompanying a weather data file, since it only takes into account a certain number of aspects of the sky nature over hourly time intervals.

5.1.8 Analysis

The measured and simulated results for both boxes were divided into two groups corresponding to clear sky and overcast sky weather data. The analysis regards only night-time data to avoid the effect of shortwave radiation and the consequent overheating of the boxes. A linear regression was performed to determine the relationship of the measured and the estimated energy consumption for each of these categories. Under a clear sky the correlation coefficient for the ETFE box measured and simulated results was 0.83, whereas for the glass box measured and simulated results was 0.86. Under an overcast sky the corresponding correlation coefficients for ETFE and glass were 0.93 and 0.91 respectively. This indicated the ability of the design tool to calculate energy response more accurately under a cloudy sky rather than under a clear sky.

The accuracy of the energy consumption simulations could be considered equal for both materials. As this chapter revolves around the modelling of an ETFE cushion, the analysis will focus further on this material. Figure 5.25 presents the measured and simulated energy consumption of the ETFE-covered box as expressed relative to the difference between internal and external air temperature in regards to the interpretation of the simulation inaccuracy under a clear sky.

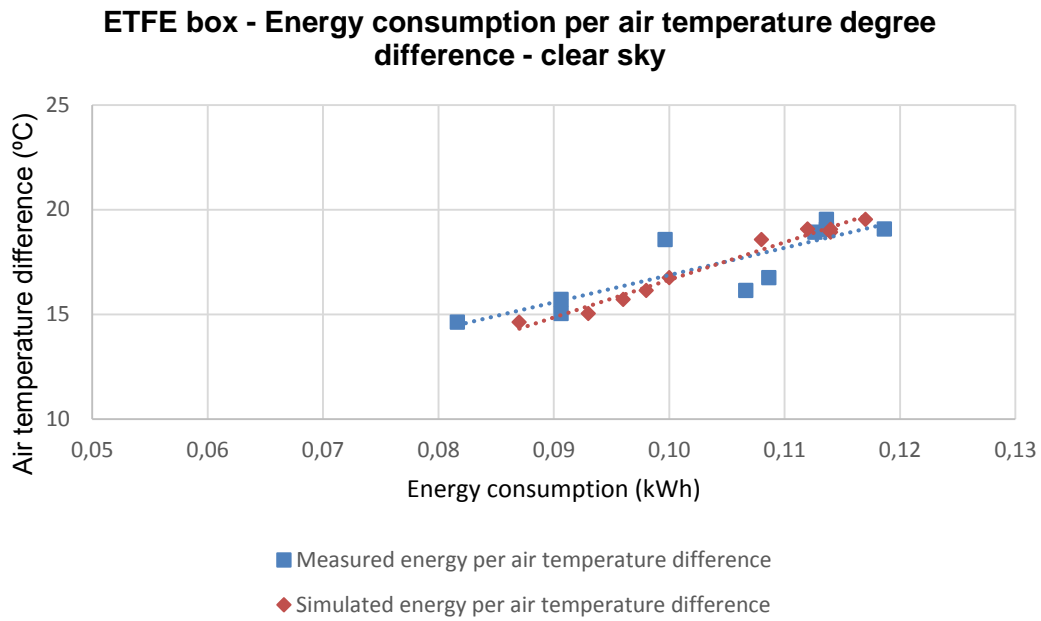


Figure 5.25: Energy consumption of the ETFE box per air temperature degree difference under clear sky conditions

Figure 5.26 presents the measured and simulated energy consumption of the ETFE-covered box as expressed relatively to the difference between internal and external air temperature, in relation to the interpretation of the simulation inaccuracy under an overcast sky.

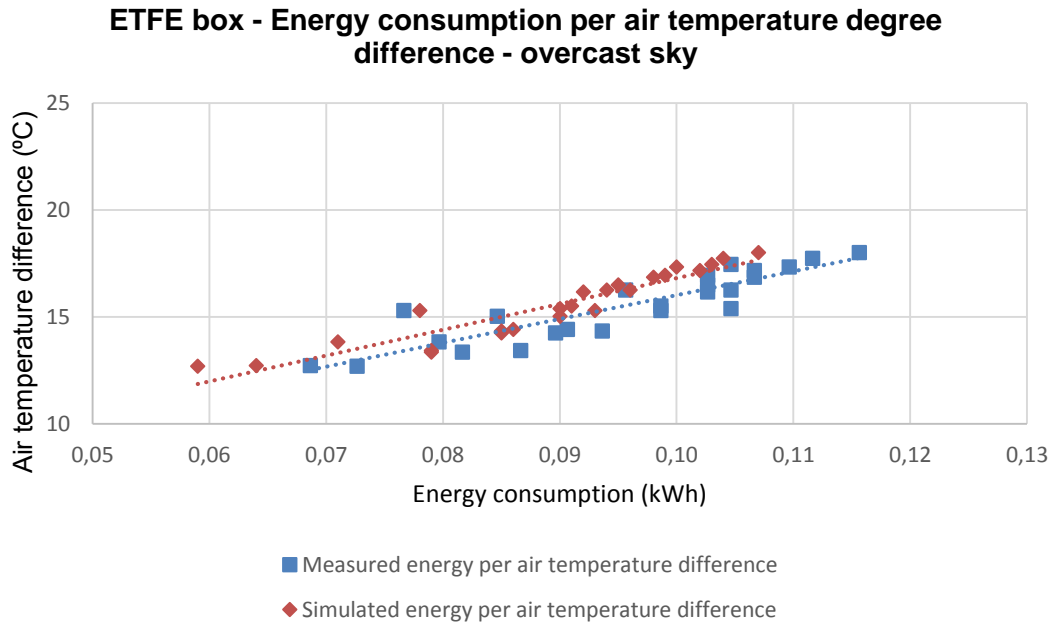


Figure 5.26: Energy consumption of the ETFE box per air temperature degree difference under overcast sky conditions

The points where the deviation between measured and simulated energy was highest coincided with lower recorded radiant temperatures and the related lower sky emissivity, as well as lower relative humidity levels, which were features associated with a very clear sky. This suggested that the IES model failed to take into consideration the low clear night sky temperature; which would affect the estimation of heat loss from the box in the absence of clouds and solar input. This could be related to the uncertainty accompanying a weather data file, since it only considered a certain number of aspects of the sky nature over hourly time intervals.

5.2 Computational modelling of the shape of an ETFE cushion

The ETFE cushion could not be described in IES as a curved surface and was therefore initially represented by two parallel flat surfaces. Furthermore, the distance between the two ETFE layers was finally set to 12 mm, the adjusted distance in order to reach the desired U-value for an ETFE cushion as it was specified by the Vector Texlon[®] material properties sheet (Vector, 2013).

This section discusses the effect of the shape of the modelled cushion on the accuracy of the simulated results. To examine whether the representation of the ETFE cushion as two flat surfaces was a satisfactory option, other alternative ways for modelling the cushion were examined and excluded. This was achieved by dividing the continuous curved ETFE surface into a number of flat trapezoid sub-surfaces (or facets) (Figure 5.27). The following section describes this process.

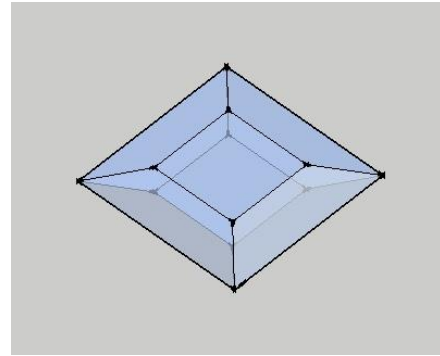


Figure 5.27: Representation of ETFE cushion in SketchUp through faceted surfaces

5.2.1 Digital model construction

The faceted flat surfaces forming the cushions were designed and imported using SketchUp since the program offers a plug-in extension for IES, making it easier to create and transfer geometry compared to programs such as AutoCAD or Microstation. Notably, IES also offers a plug-in extension for Revit, another popular 3d modelling tool.

Each cushion was divided into two parts, a top and a bottom part, both described in IES as unventilated and unheated rooms. The complex faceted cushion geometry could not remain intact, as it was originally designed in SketchUp, since problems with adjacencies in the model geometry (described as slithers) occurred that would not allow the model to run. This was due to the fact that the IES Building Template Manager would not facilitate the design of a complex geometry with a number of inclined surfaces as a single entity. Furthermore, the two separate spaces could not be later connected using the IES Building Template Manager to comprise one single volume, as inconsistencies occurred with the geometry, which restricted the IES Apache thermal tool from running.

A significant problem related to this process is that IES recognises the cushion as a room, and therefore does not provide the user with a U-value for the ETFE unit as it would do if the cushion was represented as a glazed unit. This makes it harder to accurately adjust the shape of the cushion to ensure it has the desired U-value. To resolve this issue, the design of the notional cushion in IES would have to follow the shape and therefore have the same volume as an ideal, calculated cushion. This way

the amount of trapped air inside the cushion should produce a cushion with an overall U-value corresponding to the realistic value. To achieve that, an ideal cushion was designed in SketchUp and the shape was followed closely using the flat surfaces. In reality the cushion would not necessarily be inflated to assume the ideal notional shape but for the purpose of this comparison an assumption was made that this was the case. This model was then imported into IES. The process of achieving the correct volume for each cushion was not perfectly accurate and also very time consuming due to the inflexibility of IES in designing unconventional geometries.

In IES, windows were added to each flat surface comprising the cushions and given the equivalent properties of a clear or fritted ETFE membrane. The windows were set as a 100% permanently closed area using MacroFlo. The top surface of the experimental box standing between the two notional cushion “rooms” was also described in IES as a window, set to having a 100% permanently open area in MacroFlo to represent a hole.

Figure 5.27 showed a single cushion, representing the camber of the ETFE cushion using five flat surfaces. Adding cushions to the IES box, ducts and auxiliary box models, seven notional models were built in total, as they are shown in Figure 5.28. The rest of the models that are shown represented the ETFE cushion using 9, 13, 17, 21, 29 and 33 surfaces respectively.

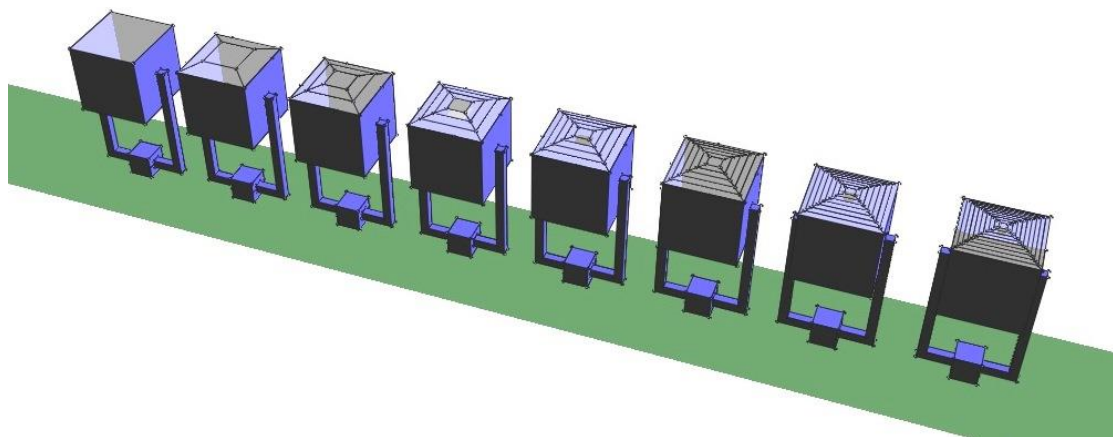


Figure 5.28: IES models used for different representation of the ETFE cushion through a number of flat surfaces

Regarding the models, the main experimental boxes, ducts and auxiliary boxes were the same as described in section 5.1. The heating systems and ventilation rates, as well as the material properties were identical to the equivalent used for the original model representing the ETFE cushion as two parallel surfaces. The only difference was that the outside and inside area surface ratio of the ETFE frames was returned from 4.0 to the initial value 1.0 to lower the amount of estimated heat loss throughout the simulation. This was done to offset the fact that the ETFE cushion system already was expected to present a higher U-value because of the increased amount of frame assumed by the program accompanying each added “window” covering the faceted surfaces. A simulation was run for each of the IES models. The results of the simulated energy underwent a statistical analysis to examine which model presented the best fit. Table 5.24 describes the simulation process of the various cushion types. Figure 5.29 visually summarises the process. Results will be analysed in section 5.1.3 on summary and conclusions.

Table 5.24: Faceted ETFE covered box with various cushion types

Simulation	Description
Simulation 01	The camber of the ETFE cushion was represented by five flat surfaces. The mean simulated energy consumption was lower but close to the mean measured energy. Variation between the simulated and measured results was very low.
Simulation 02	The camber of the ETFE cushion was represented by nine flat surfaces. The mean simulated energy consumption and variation increased significantly.
Simulation 03	The camber of the ETFE cushion was represented by 13 flat surfaces. The mean simulated energy consumption decreased significantly, while variation between results increased.
Simulation 04	The camber of the ETFE cushion was represented by 17 flat surfaces. The mean simulated energy consumption remained the same, while variation between results increased.
Simulation 05	The camber of the ETFE cushion was represented by 21 flat surfaces. The mean simulated energy consumption and variation increased.
Simulation 06	The camber of the ETFE cushion was represented by 29 flat surfaces. The mean simulated energy consumption and variation increased.
Simulation 07	The camber of the ETFE cushion was represented by 33 flat surfaces. The mean simulated energy consumption increased, while variation decreased.

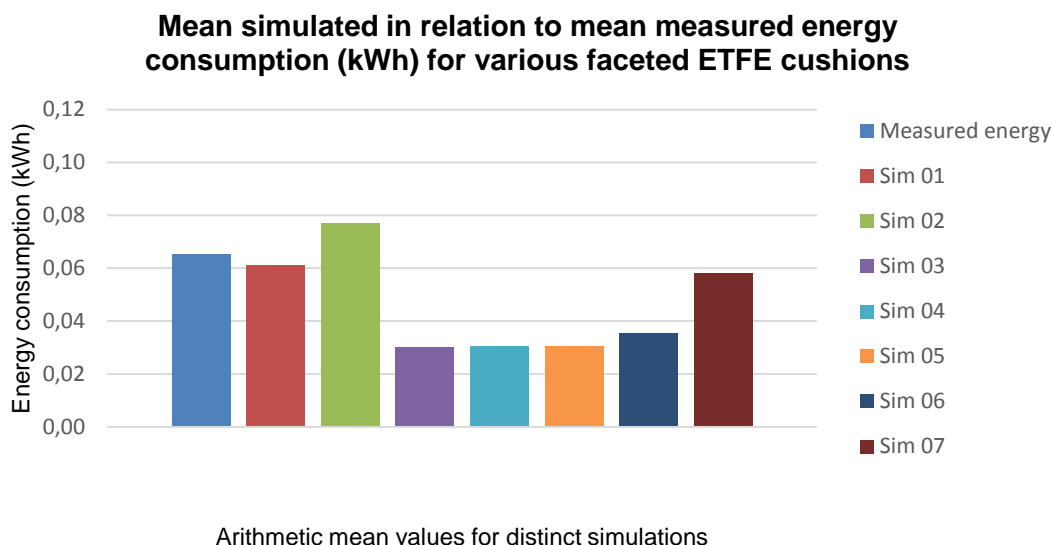


Figure 5.29: Mean values of simulated in relation to measured energy consumption (kWh) for various faceted ETFE covered box

Table 5.25 presents the estimated mean energy values and the R^2 coefficient of determination, to demonstrate how close the simulated data was to the fitted regression for the measured data.

Table 5.25: Mean hourly energy values (kWh) and coefficient of determination for simulated in relation to measured energy consumption for various faceted ETFE covered box

	Measured energy	Sim 01	Sim 02	Sim 03	Sim 04	Sim 05	Sim 06	Sim 07
Mean energy (kWh)	0.065	0.061	0.077	0.030	0.030	0.031	0.035	0.058
R^2 coefficient of determination		0.970	0.763	0.762	0.715	0.688	0.533	0.534

5.2.2 IES model results and accuracy

A linear regression analysis was performed using the statistical analysis tool PASW Statistics 18. The statistical analysis to be described concerned the model that produced the first simulation, as that was the only successful attempt of the group. The

model presenting the ETFE camber as a summary of five surfaces produced results with a bivariate correlation coefficient R of 0.99 between the simulated and measured energy consumption. In parallel, the statistical analysis for the same model produced a bivariate correlation coefficient R of 0.99 between simulated and measured air temperatures and a correlation coefficient R of 0.98 between simulated and measured radiant temperatures. This high statistical correlation demonstrated that this model was a successful attempt to model the ETFE cushion close to its realistic shape.

Figures 5.30 to 5.32 show the measured and simulated results for energy consumption, air and radiant temperatures for the faceted ETFE-covered box.

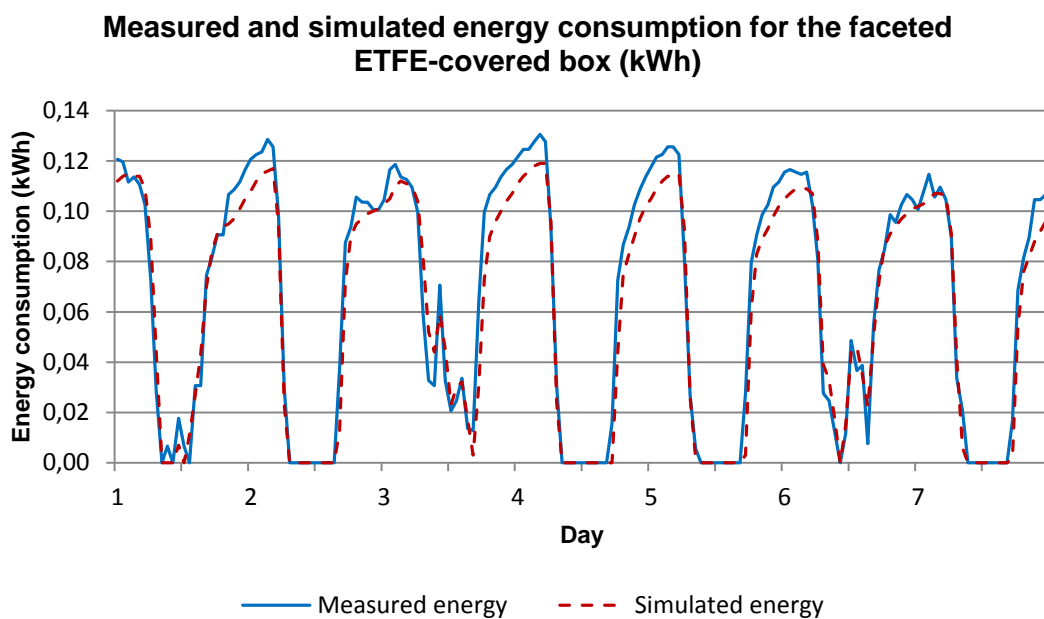


Figure 5.30: Measured and simulated energy consumption for the faceted ETFE-covered box (kWh)

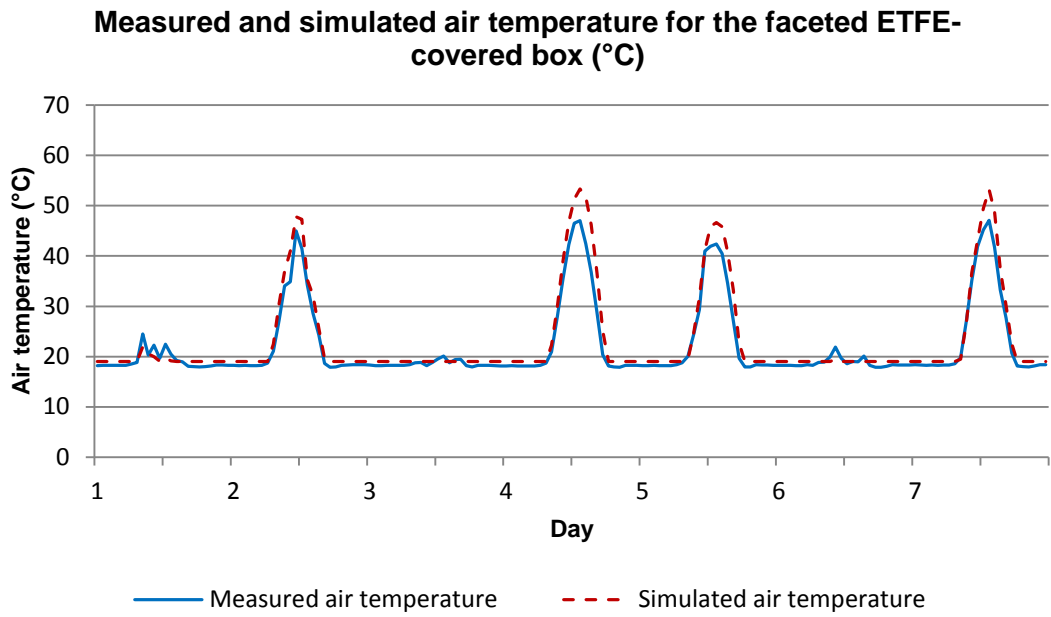


Figure 5.31: Measured and simulated air temperature for the faceted ETFE-covered box (°C)

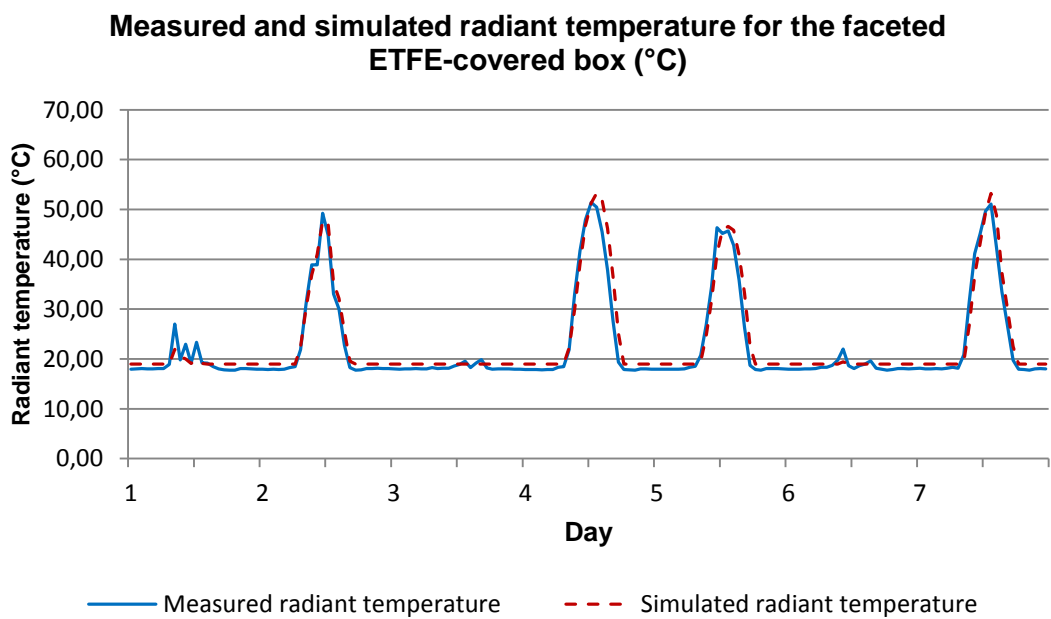


Figure 5.32: Measured and simulated radiant temperature for the faceted ETFE-covered box (°C)

5.2.3 Summary and conclusions

The modelling of an ETFE camber using five flat surfaces finally presented satisfactory results, however, the process of modelling the ETFE cushion using a number of faceted surfaces was attempted repeatedly before it was rejected as time consuming and impractical. The following section attempts to explain the reasons why this method of modelling an ETFE cushion was not successful in producing the desired energy and thermal simulated values especially as the number of flat surfaces increased.

The significant complexity in designing the notional cushion in IES was primarily due to the fact that IES treated each half of a cushion as a room, which meant that the program recognized each modelled ETFE membrane as an inclined wall, roof or floor covered with a window. This was accompanied by issues that made this simulating method redundant; error signals and obstructions to carry on by the program were encountered frequently throughout the process, either due to slithers (small slices where objects did not meet) or due to missing windows as part of the model. Furthermore, each time the ETFE membrane was represented by a number of separate flat surfaces, it was accompanied by an added notional frame, which would add to the estimated overall heat loss and corresponding energy for heating. The complexity of creating a model that represented reality increased with the number of flat surfaces that were modelled.

For these reasons it has been decided that an ETFE cushion is best modelled in IES as two flat parallel surfaces, using the material properties provided in section 6.1.6 and adjusting the distance between the two surfaces to match the expected U-value in accordance to the relevant energy calculation method. It has been determined that the accuracy of this simulation method is satisfactory in describing the energy consumption and the thermal performance of a structure covered by an ETFE cushion. The attempt at finding an alternative way of modelling the energy and thermal behaviour of an ETFE cushion while closely imitating its shape has been decided to be unsuitable and inaccurate.

To summarise, throughout Chapter 4 this thesis compared the energy and thermal performance of two experimental units covered by an ETFE cushion and a glass unit. Chapter 5 made use of the results and knowledge gained from the experimental groups to simulate and predict the energy and thermal performance of the fritted ETFE cushion and the glass unit using IES.

The following Chapter 6 makes use of the obtained knowledge on how to best digitally replicate the performance of ETFE cushions, executing a secondary round of IES modelling. Chapter 6 attempts to specify the amount of energy that can be saved when using different types of ETFE cushions to replace different types of glazing in buildings. An existing built example of an educational building with an ETFE-covered atrium roof will be described and modelled for four scenarios; a clear and a fritted ETFE cushion roof, as well as a standard and a low-E glass roof. The results of these simulations will be used to quantify the energy savings that were achieved by using different types of ETFE cushions in comparison to different types of glazing.

6 Secondary modelling using IES

6.1 The energy saving potential of ETFE cushions when used to replace glass as a roofing material

The existing East Building completed in 2011 on the University of Bath campus has been selected as a case study for this purpose. It is a medium sized three-storey educational building with a clear ETFE-covered atrium at its core, which makes it an excellent representation of the type of non-domestic buildings that commonly employ ETFE units, as it has been previously described through the literature review in Chapter 2.

This chapter will first provide more information on the East Building and then proceed to describe the modelling of the building and perform simulations to predict its thermal conditions and energy consumption for heating and cooling. The East Building was selected to perform simulations due to its geometry and size. The building was used as a base to develop a highly detailed 3D model that could be used for future work comparing simulated with real measured interior conditions and energy consumption. The simulations will be run using different materials to cover part of the roof each time; more specifically using standard and low-Emissivity double glazing, as well as clear and fritted double-layered ETFE cushions. The results of the four simulations will be compared to quantify the overall benefits of using different types of ETFE covers compared to different types of glazing.

6.2 Preparation of secondary modelling using IES

The East Building is comprised of three storeys with a net internal floor area of 4,325 m². The building is part of the recent expansion programme by the University of Bath and it hosts a 350 seat lecture theatre, one floor of teaching rooms and two floors of office space. A central atrium was designed as a circulation space, providing natural lighting to the building core and a return path for the air from the Termodeck hollow precast floor heating and ventilation system. The building was designed to achieve a BREEAM “Excellent” rating due to low energy consumption. So far the awards the building has won have been granted by the LABC Building Excellence Awards in 2011 for “Best Sustainable Project” and “Best Technical Innovation”. It is built of a pre-cast concrete frame, clad-in an IGU glazed curtain wall, timber and render (Bath, 2014).

The central atrium is covered by six double-layered ETFE cushions tilted at 7° from the horizontal plane. The cushions cover a total area of 200 m² – including their frames and support system. Two different sizes of cushions were used: four cushions at 3.4 m x 9.8 m and two cushions at 2.8 m x 9.8 m. Figures 6.1 to 6.4 show the building's North, East and West façades, as well as its interior. The South façade has no openings and it is attached to the adjacent Sports Hall. The building plans, sections and elevations provided by the University of Bath Estates Department are shown in Appendix E.



Figure 6.1: North façade of the East Building, main entrance to the building



Figure 6.2: ETFE cushions covering the central atrium as viewed from the building interior



Figure 6.3: West façade of the East Building



Figure 6.4: South façade of the East Building

The building was modelled using IES. The energy and thermal simulations spanned throughout a typical year. The weather file used contained data for London Gatwick, as provided by IES. This weather file was selected as the geographically closest among the available files. Figures 6.5 to 6.8 show various views of the notional model built in IES, in “format” mode and in “model viewer” mode.

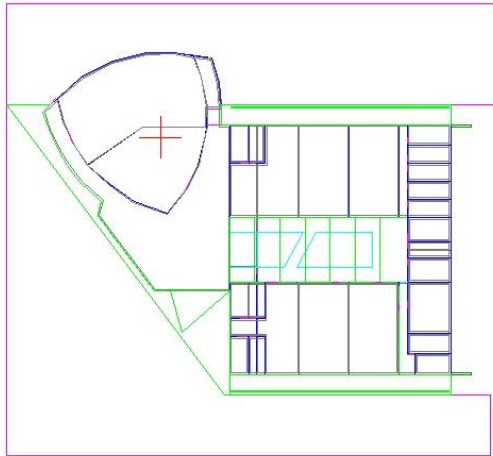


Figure 6.5: East Building modelled in IES:
format plan view

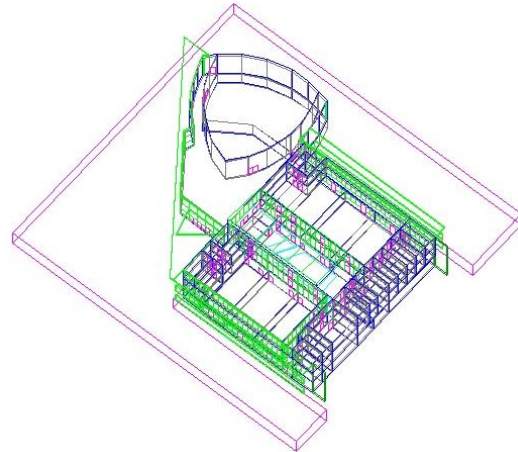


Figure 6.6: East Building modelled in IES:
format axonometric view

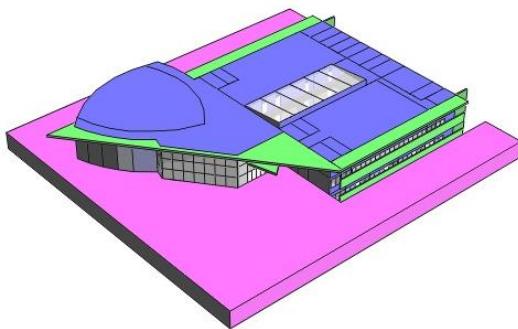


Figure 6.7: East Building modelled in IES:
model viewer South-West 3d view

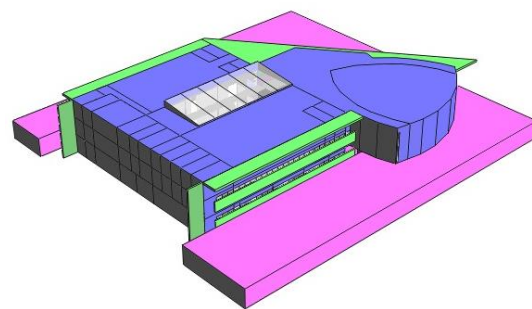


Figure 6.8: East Building modelled in IES:
model viewer North-East 3d view

- Space modelled by IES as a Room
- Shading building element modelled by IES as a Topographical Shade
- Ground modelled by IES as an Adjacent Building

The wall construction and thickness was known but the thermal properties of the East Building materials used were unknown. For that reason, the material thermal properties of the modelled external and internal walls, roof, floors, windows and doors were set at default values, as found in the Building Template Manager, which were assumed to be representative of these conventional building materials. The used default values can be found in detail in Table E.1, Appendix E. Furthermore, the default values were considered to be sufficiently accurate as the purpose of this exercise was not to simulate the actual energy consumption and thermal behaviour of the East Building but to use its geometry as a benchmark to compare its performance under various scenarios: when the atrium roof was covered by different types of glass and when covered by different types of ETFE cushions.

The IES NCM Building Type regarding building regulations was selected to be “Office or Workshop”. Using the Thermal Conditions tab of the Building Template Manager, teaching and working spaces were set to be thermally treated between 08:00 am and 06:00 pm, on office working days (Monday – Friday), whereas circulation areas, such as the entrance foyer, the corridors and the central atrium were set to be continuously untreated. Heating was set to operate when interior temperature dropped below 19° C and cooling to operate when temperature raised above 23° C. External and internal windows and doors were all set to be continuously 100% closed. No occupational heat gains were considered.

The IES default frame for a double glazed unit has a coverage of 10%, made of metal and with a resistance of 0.3373 m²K/W. Although the East Building roof-light frame was aluminium, the frame description and properties were left as default, since this was the followed method for all the other building components. Its absorbance was set to 0.7, the outside and inside surface area ratio were both 1.00 and its overall U-value was 2.02 W/m²K.

In order to achieve the set 2.94 W/m²K U-value suggested by Vector Foiltec for a clear two-layer ETFE cushion, different cavity sizes were tried out in the Building Template Manager using the CIBSE method. A distance of 0.175 m between the two ETFE membranes forming the cushion was selected to provide the desired U-value.

The ETFE cushions covering the East Building did not have a reflective frit. For that reason the double glazed unit selected first for comparison is a standard roof light, without any low-E properties or any form of additional coating and a U-value of 3.12

W/m²K (regarding only the glazed unit). The properties of the two covering materials can be found in detail in Table 6.1.

Table 6.1: East Building IES model description of standard double glazed and clear double ETFE units

	Standard double glass unit			Clear double ETFE cushion		
	Clear float glass	Gas (air)	Clear float glass	ETFE membrane (outside layer, clear)	Gas (air)	ETFE membrane (inside layer, clear)
Thickness (mm)	6	12	6	0.2	175	0.2
Conductivity (W/mK)	1.06		1.06	0.23		0.23
Convection coefficient (W/m²K)		3.17			2.064	
Resistance (m²K/W)		0.146			0.174	
Solar transmittance	0.82		0.82	0.911		0.911
Outside reflectance	0.07		0.07	0.08		0.08
Inside reflectance	0.07		0.07	0.07		0.07
Refractive index	1.526		1.526	1.38		1.38
Outside emissivity	0.837		0.837	0.82		0.82
Inside emissivity	0.837		0.837	0.82		0.82

Due to the fact that ETFE cushions proved to be a high-performance cover material, a second comparison was conducted, this time with a low-E double glazed unit of U-value 2.00 W/m²K to examine the performance of the ETFE roof alongside a high specification roofing system. Furthermore, a third simulation compared the low-E double glazed unit with a fritted ETFE roof to represent advanced properties for both materials. Given that the cushion remained the same, other than the frit properties, the distance between the membranes was left at 0.175 m, which provided a U-value of 2.68 W/m²K, using the CIBSE method. The frit was placed on layer two, i.e. the inside

surface of the upper layer of the cushion. The properties of the low-E double glazed unit and the fritted double ETFE cushion are described in Table 6.2.

Table 6.2: East Building IES model description of low-E double glazed and fritted double ETFE units

	Low-E double glass unit			Fritted double ETFE cushion		
	Clear float glass	Gas (air)	Pilkington (low-E) glass	ETFE membrane (outside layer, clear)	Gas (air)	ETFE membrane (inside layer, dot matrix 65%)
Thickness (mm)	6	12	6	0.2	175	0.2
Conductivity (W/mK)	1.06		1.06	0.23		0.23
Convection coefficient (W/m²K)		3.00			2.064	
Resistance (m²K/W)		0.324			0.174	
Solar transmittance	0.78		0.69	0.911		0.54
Outside reflectance	0.07		0.09	0.08		0.33
Inside reflectance	0.07		0.09	0.08		0.34
Refractive index	1.526		1.526	1.38		1.38
Outside emissivity	0.837		0.837	0.82		0.81
Inside emissivity	0.837		0.05	0.82		0.57

6.3 Secondary modelling results

This section describes the results of the secondary modelling of double-layered ETFE cushions using the notional model of the East Building, first comparing a clear double ETFE cushion in relation to a standard double glazed unit, then to a low-E double glazed unit and later on comparing a fritted double ETFE cushion to a standard double glazed unit and consequently to a low-E double glazed unit. These results will enable

the quantification of the energy saving potential of double ETFE cushions, compared to double glass as a roofing material.

The simulations covered a typical year; however, the comparison and analysis using graphs focus on the results of one week to maintain visual clarity. The week selected for this study lasted between 8-14 October; that period of time was chosen as it presented a demand for both heating and cooling of the East building on different days. The graphs demonstrating external weather data for that period (air temperature, shortwave and long-wave radiation) can be found in Appendix E (Figures E.1 to E.3).

6.3.1 Performance comparison of clear double ETFE-covered notional building to standard double glass-covered notional building

The atrium area was represented in IES as a separate room on each floor, equipped with holes that covered the entire floor and ceiling areas, allowing IES to treat the separate rooms as a unified space. The atrium air and radiant temperatures shown in Figures 6.9 and 6.10 are the average values between the simulated temperatures for each floor. Average values were used to represent the overall atrium temperatures, in order to avoid the effect of stratification noted between different levels. Due to stratification, simulated air and radiant temperatures on the top floor under the roof were lower in comparison to the first two floors because of heat loss in the absence of solar input and higher in the presence of solar input under a clear sky. Dividing data based on different floors would have unnecessarily complicated the interpretation of results and was therefore avoided.

In both graphs, the clear ETFE-covered notional building consistently exhibited higher air and radiant temperatures than the standard glass-covered notional building.

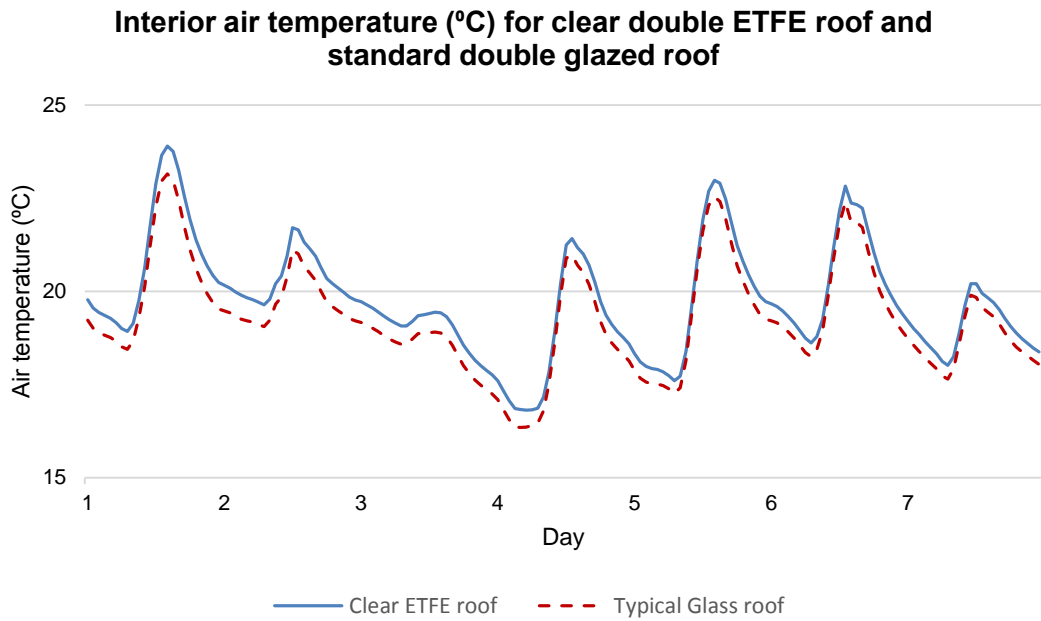


Figure 6.9: Simulated East Building atrium air temperature: comparison between a clear double ETFE and a standard double glazed roof

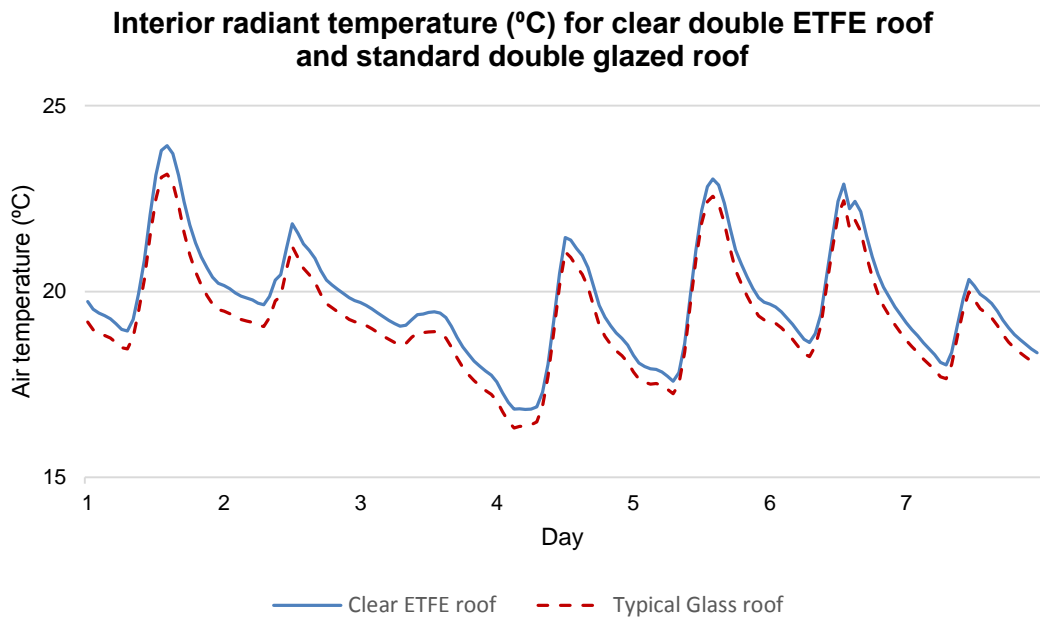


Figure 6.10: Simulated East Building atrium radiant temperature: comparison between a clear double ETFE and a standard double glazed roof

Figure 6.11 shows a summary of the simulated energy consumption of all heated spaces in the East Building, including classrooms, office areas and the amphitheatre, but excluding the entrance reception, circulation areas, and the space hosting electrical and mechanical equipment, such as electrical boards and the boiler. Figure 6.12 shows a summary of the simulated energy consumption of all cooled spaces in the East Building. Although the atrium was not a thermally treated space it affected the overall energy response of the entire building, depending on the heat loss through the two examined covering materials.

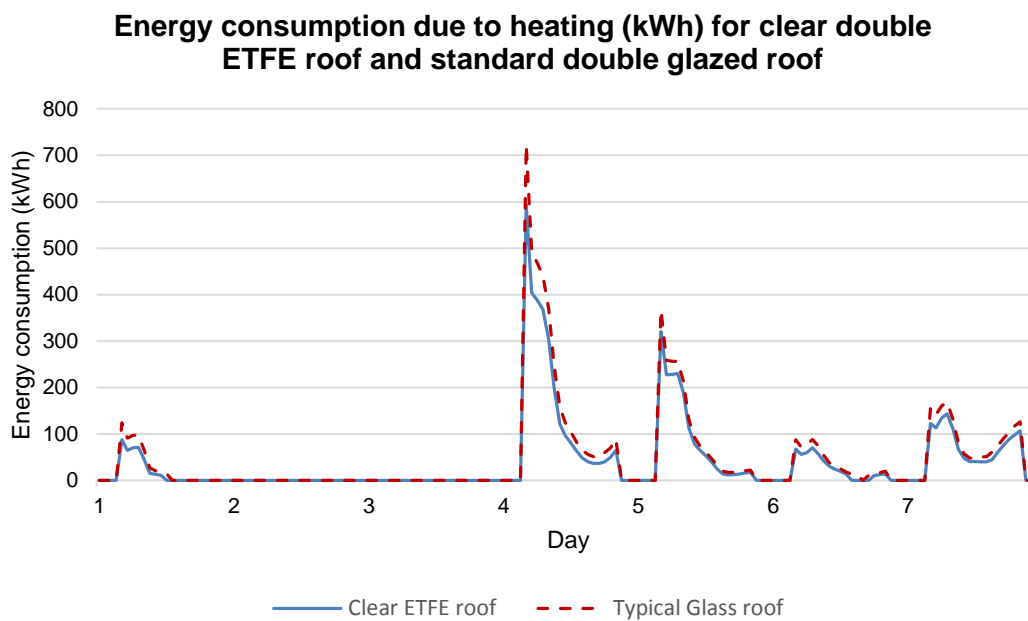


Figure 6.11: Simulated East Building atrium energy consumption due to heating: comparison between a clear double ETFE and a standard double glazed roof

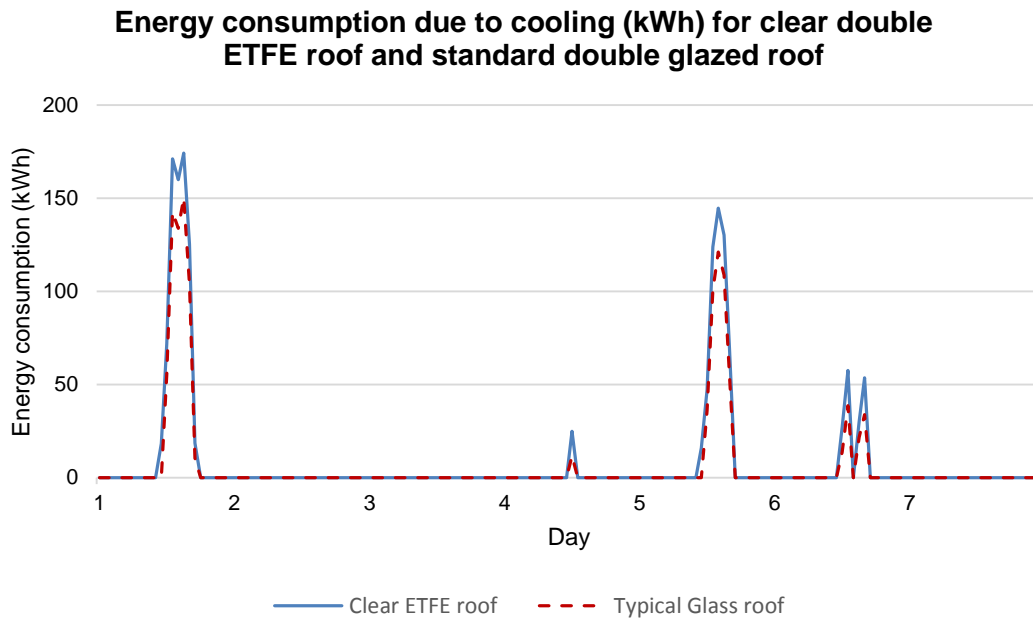


Figure 6.12: Simulated East Building atrium energy consumption due to cooling: comparison between a clear double ETFE and a standard double glazed roof

As Figure 6.11 demonstrates, the standard double glass-covered modelled building presented a higher energy consumption due to heating than the clear double ETFE-covered notional building. In total, the standard double glass-covered notional building was estimated to consume 1001752 kWh due to heating throughout the entire typical year, whereas the clear double ETFE-covered notional building was estimated to consume 974007 kWh due to space heating. In summary, the standard double glass-covered building consumed 2.8% more energy for space heating than the clear double ETFE-covered building.

At the same time, Figure 6.12 shows that the standard double glass-covered building presented a higher energy consumption due to cooling than the clear double ETFE-covered building. In total, the standard double glass-covered building was predicted to consume 570133 kWh due to cooling for an entire typical year, while the clear double ETFE-covered building was predicted to consume 652815 kWh. As a result, the building with the clear double ETFE roof was associated with 14.5% more energy required for space cooling in comparison to the building with the standard double glass roof.

6.3.2 Results analysis

The comparison of the results of the two notional buildings showed that both the air and radiant temperatures associated with the clear double ETFE roof were consistently higher than those related with the standard double glazed roof.

A closer analysis was performed on the air and radiant temperatures predicted for the two models during night-time periods, in the absence of shortwave radiation to avoid the effect of overheating. This analysis was done in the absence of any space heating. Figure 6.13 presents the relationship between air and radiant temperature differences between the clear double ETFE-covered building and standard glass-covered building to downward long-wave radiation values under clear sky conditions.

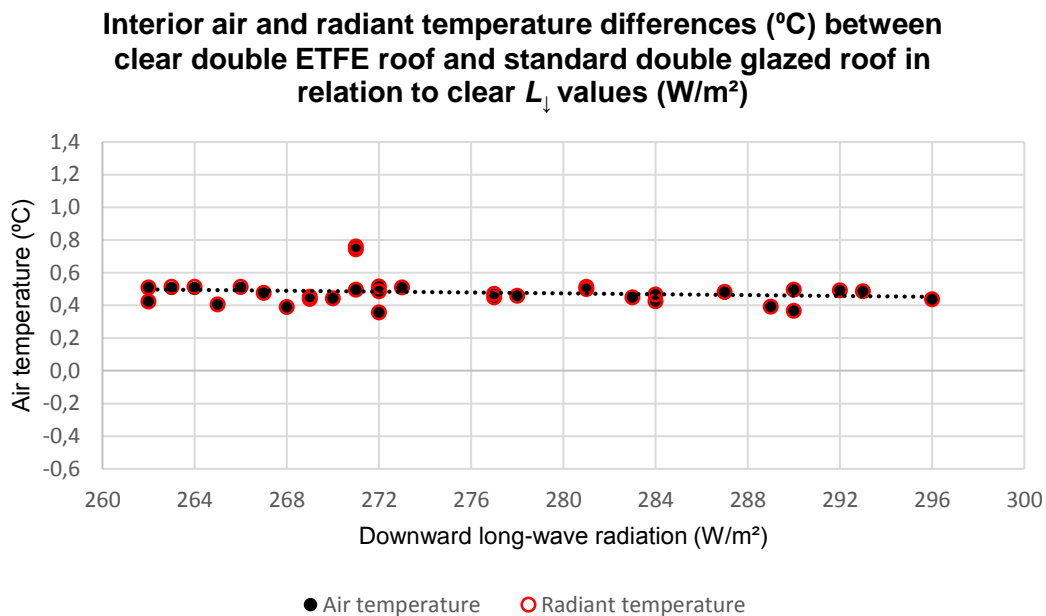


Figure 6.13: Simulated interior air and radiant temperature differences (°C) between the clear double ETFE-covered building and standard double glass-covered building under clear sky L_{\downarrow} (W/m^2)

Figure 6.14 presents the relationship between air and radiant temperature differences to downward long-wave radiation between the clear double ETFE-covered building and standard double glass-covered building under overcast sky conditions.

Interior air and radiant temperature differences (°C) between clear double ETFE roof and standard double glazed roof in relation to overcast L_{\downarrow} values (W/m^2)

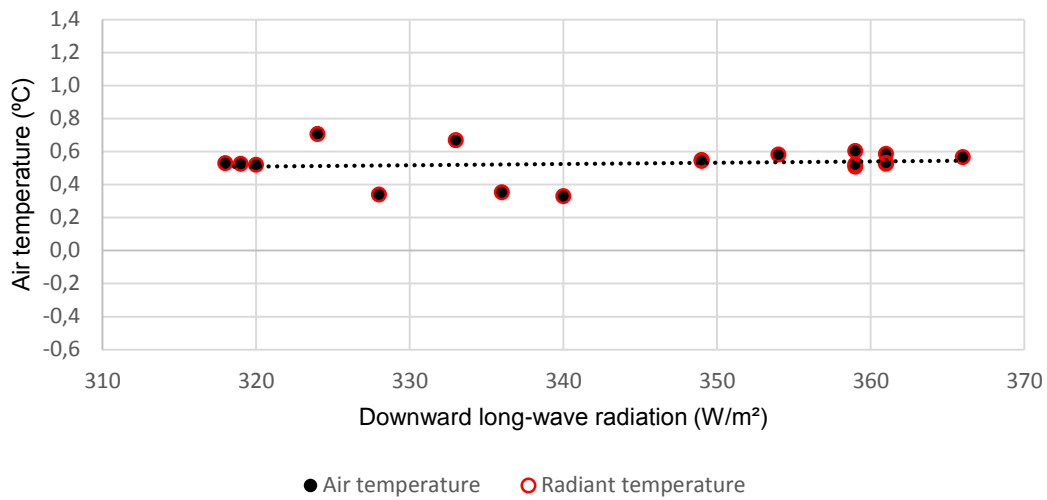


Figure 6.14: Simulated interior air and radiant temperature differences (°C) between the clear double ETFE-covered building and standard double glass-covered building under overcast sky L_{\downarrow} (W/m^2)

The positive temperature differences result from the clear double ETFE cover being consistently associated with higher values than the standard double glass cover. The difference between the predicted interior conditions for the two materials remained constant regardless of changes in long-wave radiation.

Regarding the notional buildings' energy consumption due to space treatment, Figures 6.15 and 6.16 demonstrate the difference in simulated energy consumption for heating and cooling respectively between the clear double ETFE-covered building and the standard double glass-covered building. The analysis focuses on clear sky data only, as no energy consumption was recorded under overcast sky conditions for the period of time under examination.

Heating energy consumption difference (kWh) between clear ETFE roof and standard double glazed roof in relation to clear L_{\downarrow} values (W/m^2)

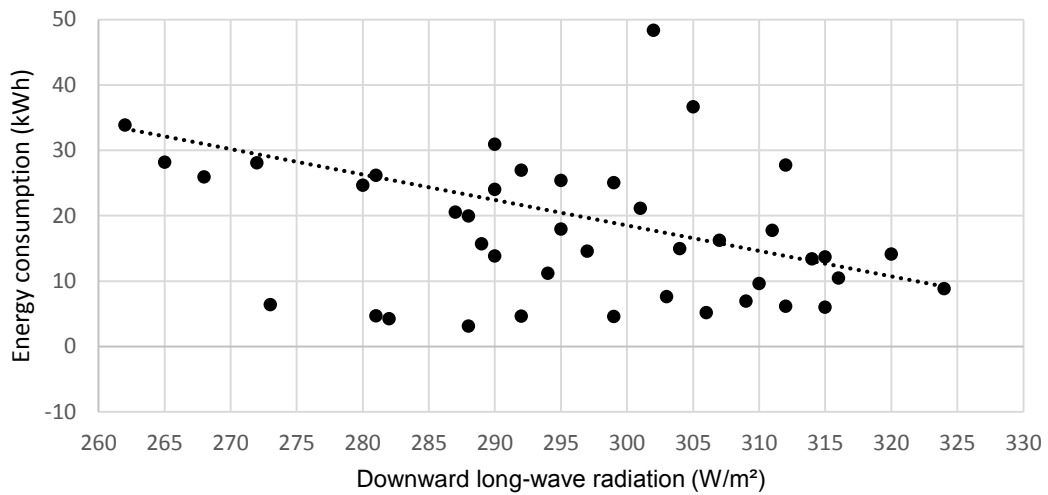


Figure 6.15: Simulated heating energy consumption difference (kWh) between the clear double ETFE-covered building and standard double glass-covered building under clear sky L_{\downarrow} (W/m^2)

Cooling energy consumption difference (kWh) between clear ETFE roof and standard double glazed roof in relation to clear L_{\downarrow} values (W/m^2)

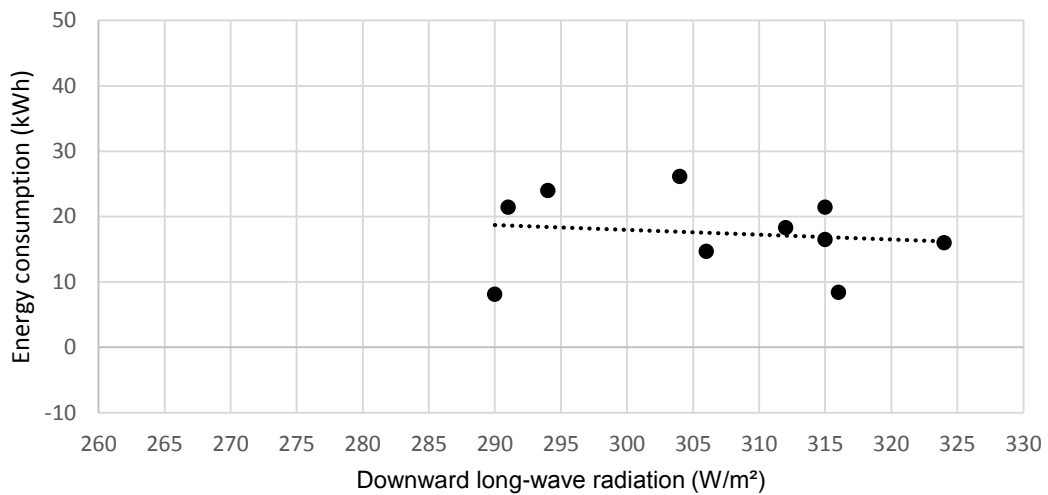


Figure 6.16: Simulated cooling energy consumption difference (kWh) between the clear double ETFE-covered building and standard double glass-covered building under clear sky L_{\downarrow} (W/m^2)

The positive values of the simulated heating energy consumption demonstrate that the building with the standard double glass roof was predicted to consume more energy than the building with the clear double ETFE cushion roof, whereas in the case of simulated cooling energy consumption this relationship was reversed. The difference between the predicted energy consumption for the two buildings due to heating had a tendency to decrease with cloud presence by 24.2 kWh, which is above the margin of error of 20.3 kWh. The difference between the predicted energy consumption due to cooling did not present a correlation to long-wave radiation, as any noted association between the two values fell within the margin of error.

6.3.3 Performance comparison of clear double ETFE-covered notional building to low-E double glass-covered notional building

Figures 6.17 and 6.18 compare the simulated thermal performance of the same clear double layered ETFE-covered notional building with a low-E double-glazed covered notional building. The resulting interior air and radiant temperatures predicted for the two buildings were very close, with higher temperatures predicted for each notional building on separate occasions.

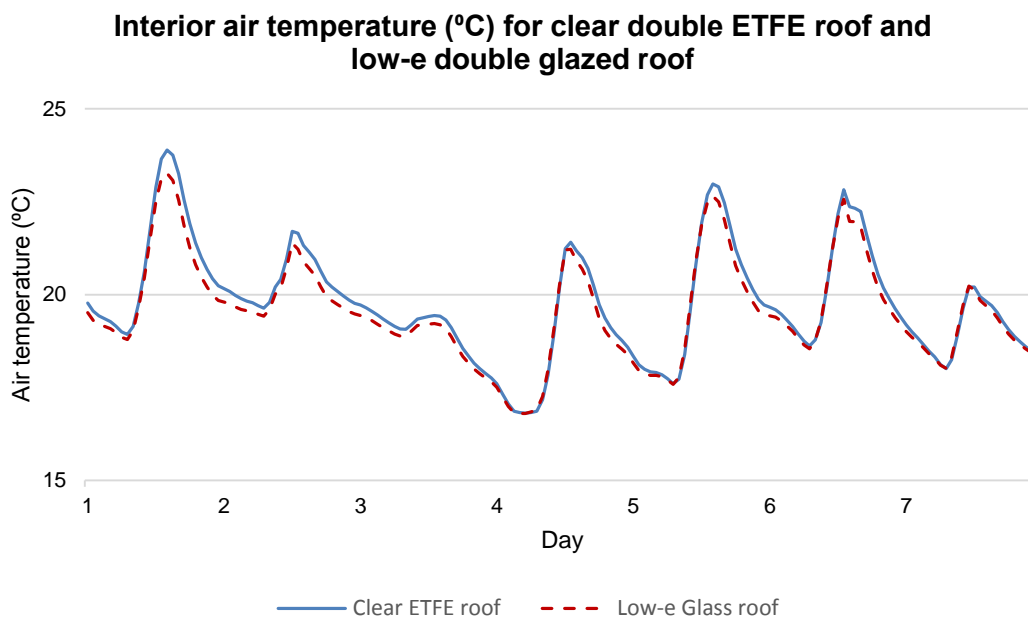


Figure 6.17: Simulated East Building atrium air temperature: comparison between a clear double ETFE and a low-E double glazed roof

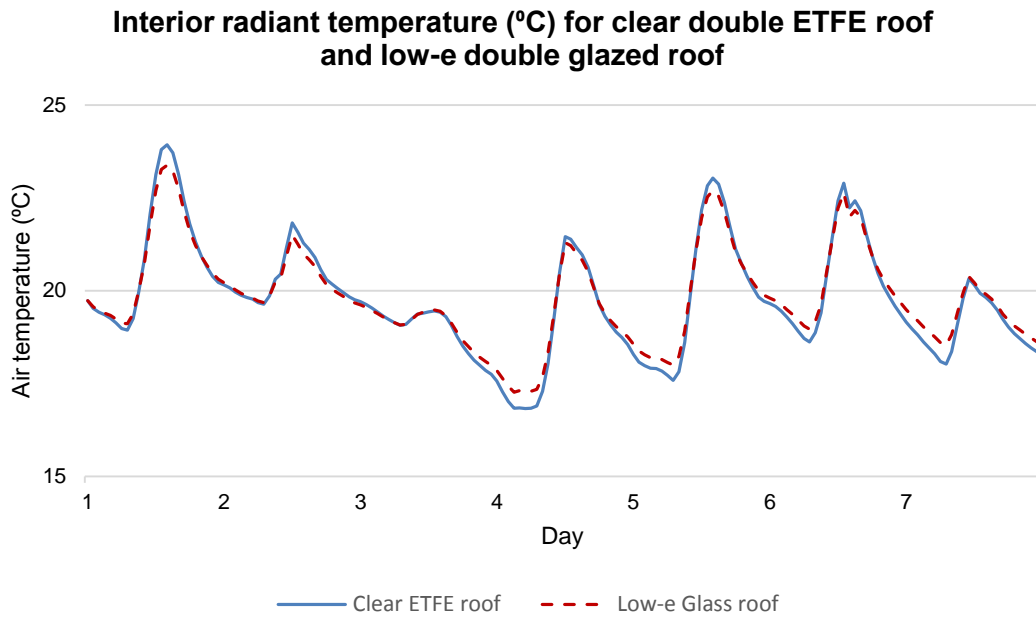


Figure 6.18: Simulated East Building atrium radiant temperature: comparison between a clear double ETFE and a low-E double glazed roof

Figure 6.19 shows the simulated heating energy consumption and Figure 6.20 the simulated cooling energy consumption for the two notional buildings. The low-E double glass-covered notional building was predicted to consume similar energy as the clear double ETFE-covered notional building. In total, the low-E double glass-covered notional building was shown to consume 955443 kWh for space heating throughout a typical year. In comparison to the predicted heating energy consumption of 974007 kWh of the clear double ETFE-covered notional building, the low-E double glass-covered building was predicted to consume 1.9% less energy for heating for an entire typical year.

At the same time, the low-e double glass-covered building was estimated to require less energy for cooling than the clear double ETFE-covered building. In summary, the building with the low-E glass roof was estimated to consume 537657 kWh for space cooling over the period of one year. In comparison to the amount of 652815 kWh predicted for the building covered with the clear ETFE cushion roof, the low-E roof was associated with a lower annual energy consumption due to cooling by 21.4%.

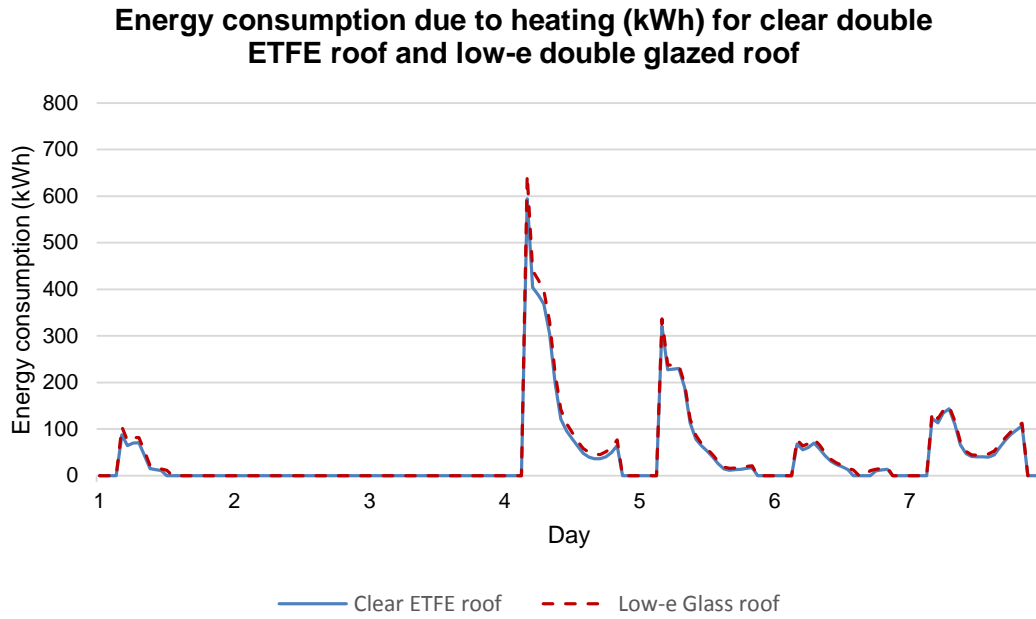


Figure 6.19: Simulated East Building atrium energy consumption due to heating: comparison between a clear double ETFE and a low-E double glazed roof

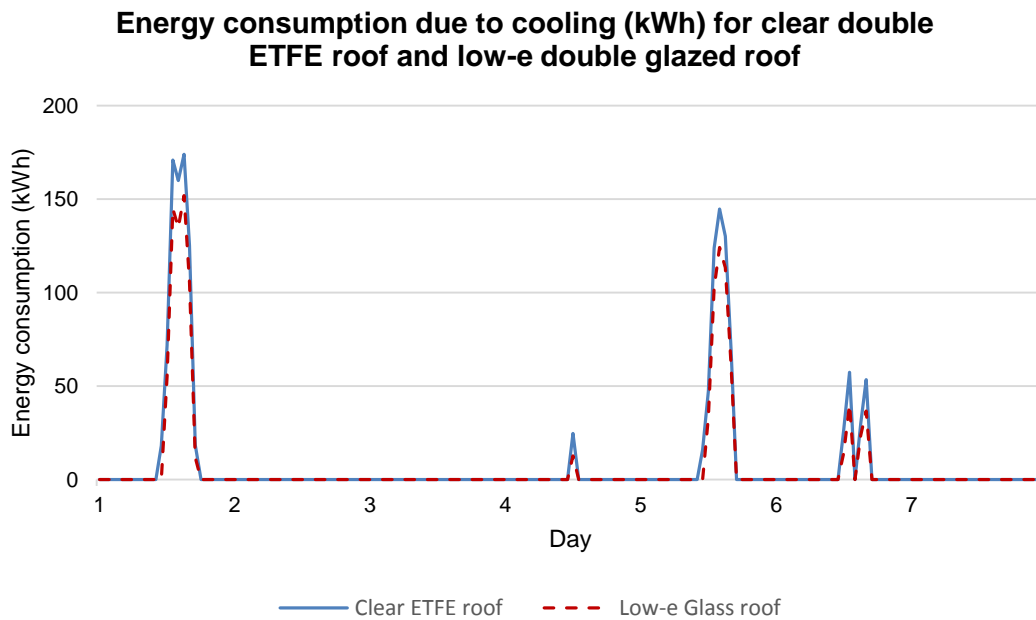


Figure 6.20: Simulated East Building atrium energy consumption due to cooling: comparison between a clear double ETFE and a low-E double glazed roof

6.3.4 Results analysis

The predicted air and radiant temperatures for the two notional buildings presented very close values, with the low-E double glass-covered building exhibiting a range of temperatures closer to the set internal temperature target of 19-23 °C compared to the clear double ETFE-covered building.

A detailed analysis of the air and radiant temperatures predicted for the two models during night-time hours avoided the effects of solar overheating. Figure 6.21 presents the relationship of air and radiant temperature differences to downward long-wave radiation respectively, regarding the clear double ETFE-covered building and low-E double glass-covered building under clear sky conditions.

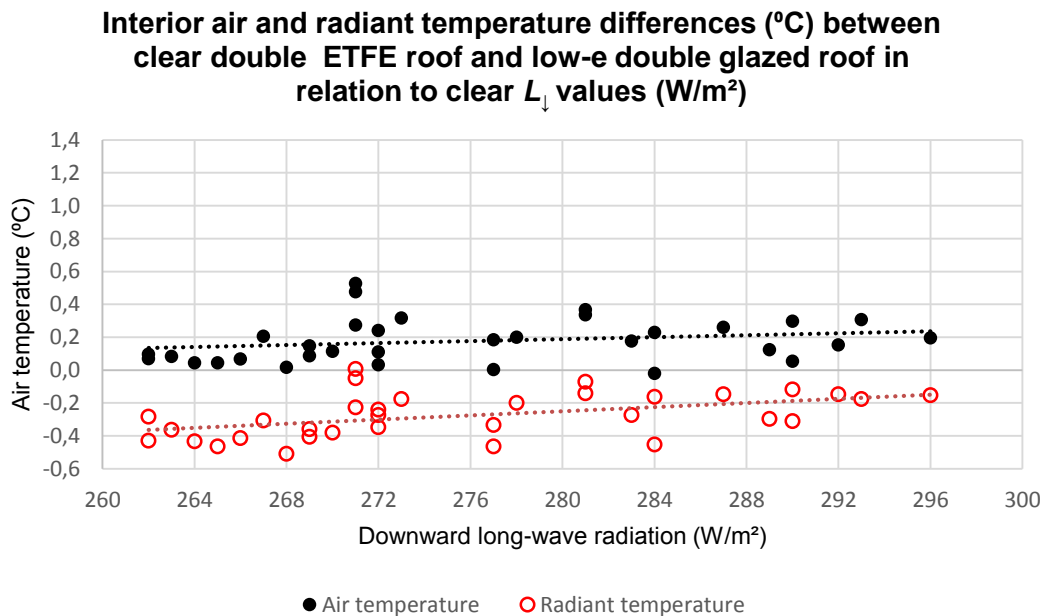


Figure 6.21: Simulated interior air and radiant temperature differences (°C) between the clear double ETFE-covered building and low-E double glass-covered building under clear sky L_{\downarrow} (W/m^2)

Figure 6.22 presents the relationship of air and radiant temperature differences to downward long-wave radiation between the clear double ETFE-covered building and low-E double glass-covered building under overcast sky conditions.

Interior air and radiant temperature differences (°C) between clear double ETFE roof and low-e double glazed roof in relation to overcast L_{\downarrow} values (W/m^2)

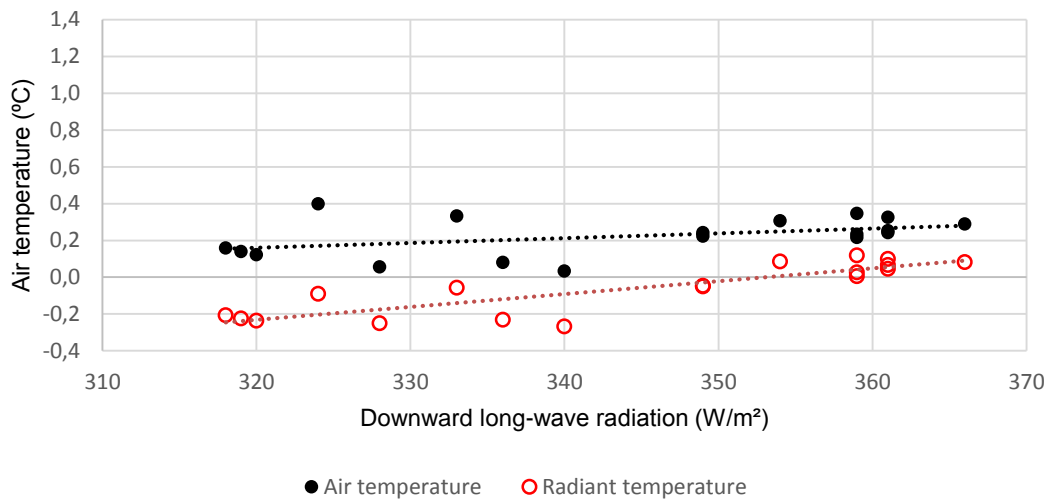


Figure 6.22: Simulated interior air and radiant temperature differences (°C) between the clear double ETFE-covered building and low-E double glass-covered building under overcast sky L_{\downarrow} (W/m^2)

The positive temperature differences represent the occasions when higher air and radiant temperatures were predicted for the clear double ETFE-covered building, whereas the negative temperature differences indicate the cases when higher air and radiant temperatures were predicted for the low-E double glass-covered building. The difference between air and radiant temperatures can be explained through the radiative nature of low-E glass, which works by reflecting long-wave radiation back into the building interior and, therefore, raising interior radiant temperature higher than the equivalent temperature under the clear ETFE cover.

The difference between the thermal performances associated with the two covering materials presented a tendency to increase with cloud presence by $0.14^{\circ} C$ for air temperatures, which, however, fell within the margin of error $0.19^{\circ} C$ and cannot be taken as a valid correlation between thermal behaviour and long-wave radiation. The difference between the thermal performances presented a tendency to increase with cloud presence by $0.28^{\circ} C$ for radiant temperatures under a clear sky. This values is just above the estimated margin of error, which was $0.27^{\circ} C$.

The difference between the thermal performances presented the same tendency to increase with cloud presence by 0.12°C for air temperatures, with a margin of error of 0.21°C ; and 0.34°C for radiant temperatures under an overcast sky, with a margin of error of 0.06°C .

Regarding the notional buildings' energy consumption due to space treatment, Figures 6.23 and 6.24 demonstrate the difference in simulated energy consumption for heating and cooling respectively between the clear double ETFE-covered building and the low-E double glass-covered building. The analysis focuses on clear sky data only, as no energy consumption was recorded under overcast sky conditions for the period of time under examination.

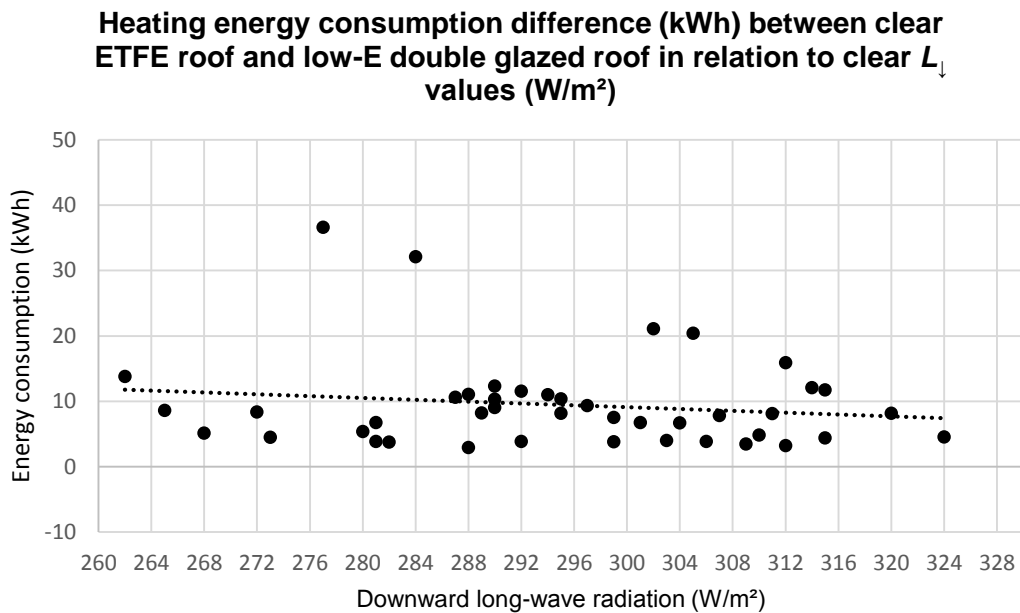


Figure 6.23: Simulated heating energy consumption difference (kWh) between the clear double ETFE-covered building and low-E double glass-covered building under clear sky L_{\downarrow} (W/m^2)

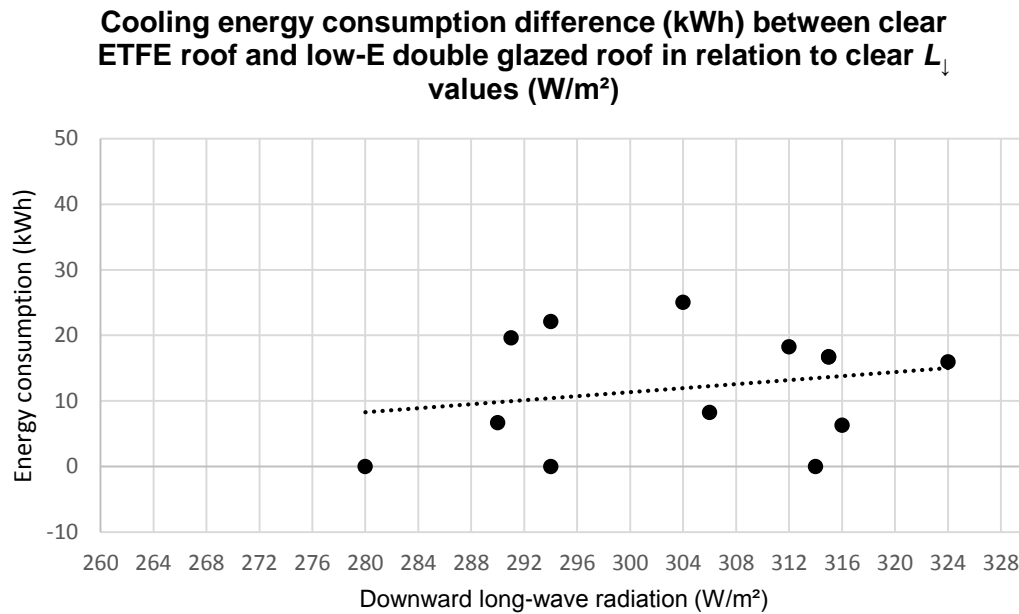


Figure 6.24: Simulated cooling energy consumption difference (kWh) between the clear double ETFE-covered building and low-E double glass-covered building under clear sky L_{\downarrow} (W/m^2)

The positive values of the simulated heating energy consumption demonstrate that the building with the low-E double glass roof was predicted to consume more energy than the building with the clear double ETFE cushion roof, whereas in the case of simulated cooling energy consumption this relationship was reversed. The difference between the predicted energy consumption for the two buildings did not present a correlation to long-wave radiation, as any noted association between the two values fell within the margin of error. The difference in the predicted energy consumption for space treatment for clear ETFE and low-E glass is smaller than the difference between the clear double ETFE roof and the standard double glass roof.

6.3.5 Performance comparison of fritted double ETFE-covered notional building to standard double glass-covered notional building

The next analysis concerned the thermal and energy behaviour of the fritted double ETFE-covered building and the standard double glass-covered building. Figures 6.25 and 6.26 show that the fritted double ETFE-covered building was predicted to give similar interior conditions to the standard double glass-covered building.

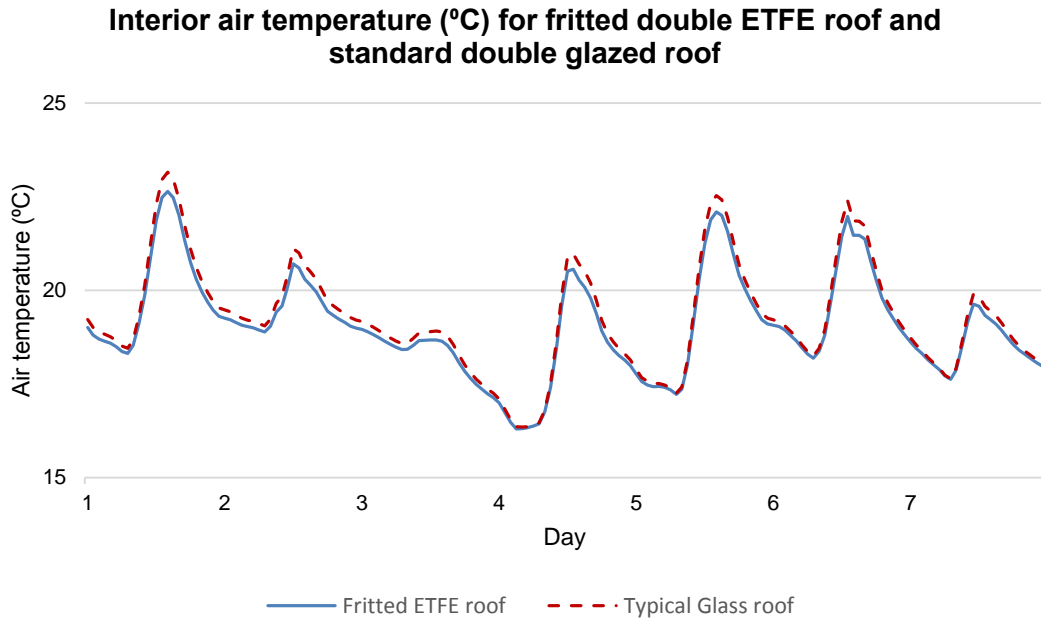


Figure 6.25: Simulated East Building atrium air temperature: comparison between a fritted double ETFE and a standard double glazed roof

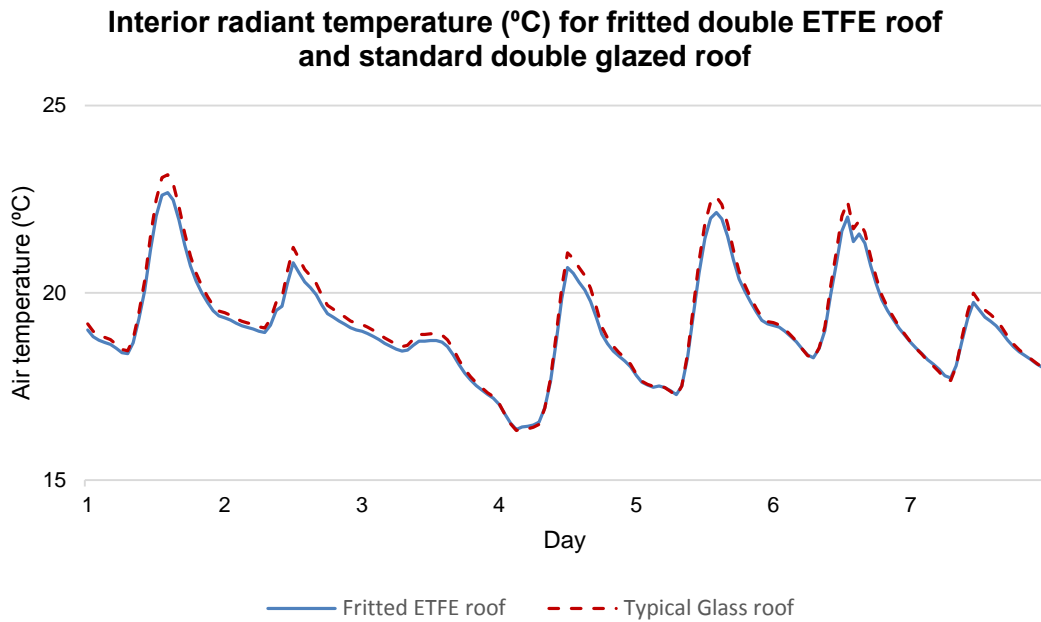


Figure 6.26: Simulated East Building atrium radiant temperature: comparison between a fritted double ETFE and a standard double glazed roof

Figure 6.27 shows the energy consumption due to heating and Figure 6.28 the energy consumption due to cooling simulated for the two notional buildings. The fritted double ETFE-covered building was predicted to consume similar energy to the standard double glass-covered building for heating. In summary, the annual space heating consumption of 1003102 kWh simulated for the fritted double ETFE-covered building was 0.1% more than the equivalent 1001752 kWh predicted for the standard double glass-covered building.

However, the building with the fritted ETFE roof was associated with lower energy consumption due to cooling than the building with the standard glass roof. The annual space cooling consumption of 491935 kWh estimated for the fritted double ETFE-covered building was 13.7% less than the 570133 kWh estimated for the standard double glass-covered building.

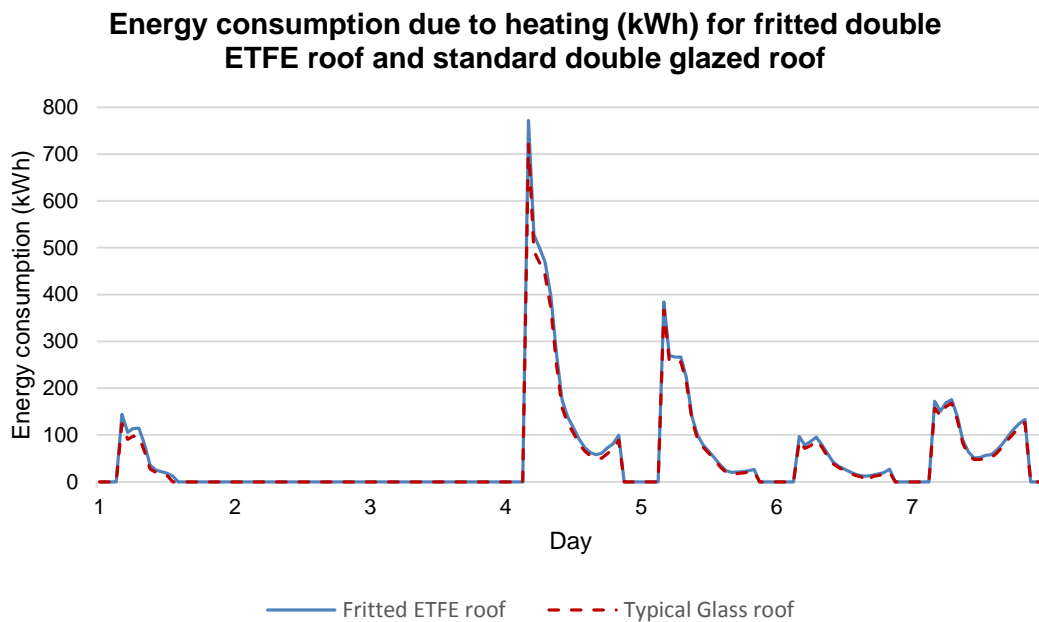


Figure 6.27: Simulated East Building atrium energy consumption due to heating: comparison between a fritted double ETFE and a standard double glazed roof

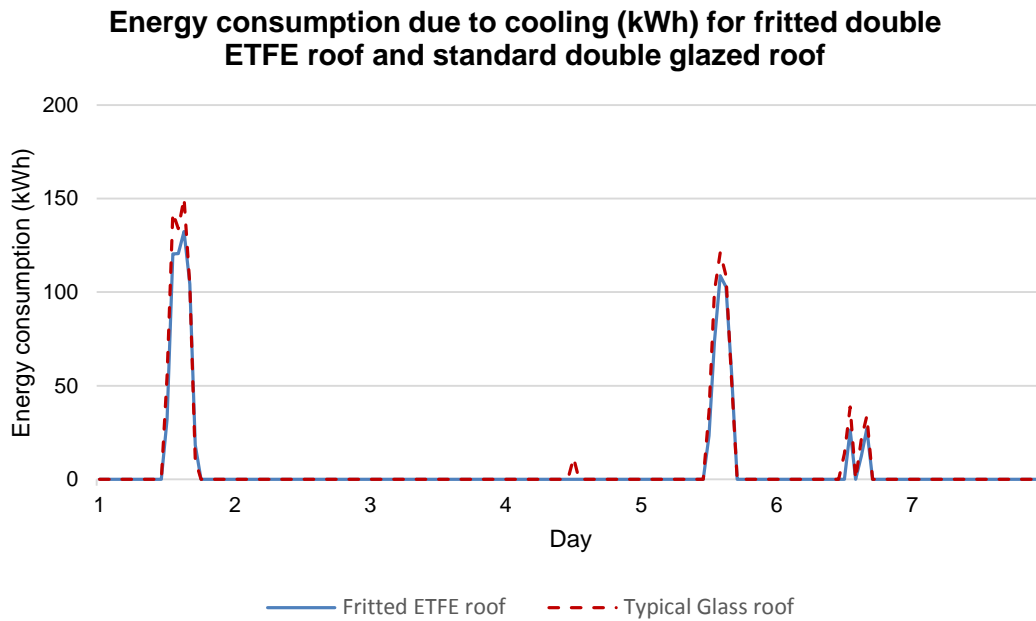


Figure 6.28: Simulated East Building atrium energy consumption due to cooling: comparison between a fritted double ETFE and a standard double glazed roof

6.3.6 Results analysis

The fritted double ETFE cover exhibited close thermal behaviour to the standard double glazed cover. Figure 6.29 demonstrates the relationship between the interior air and radiant temperature differences and the downward long-wave radiation, for the fritted double ETFE-covered building and standard double glass-covered building under clear sky conditions during night-time.

**Interior air and radiant temperature differences (°C) between
fritted double ETFE roof and standard double glazed roof in
relation to clear L_{\downarrow} values (W/m^2)**

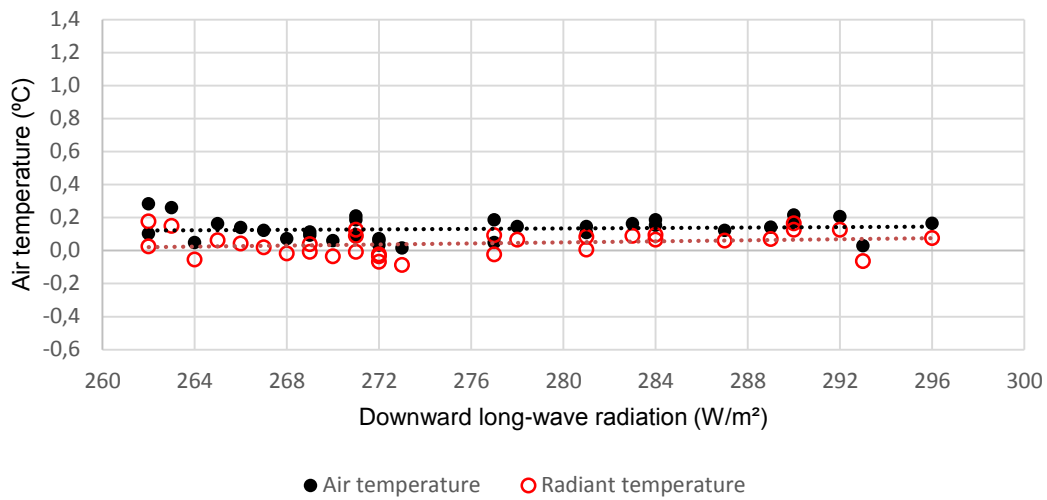


Figure 6.29: Simulated interior air and radiant temperature differences (°C) between the fritted double ETFE-covered building and standard double glass-covered building under clear sky L_{\downarrow} (W/m^2)

Figure 6.30 shows the relationship between the interior air and radiant temperature differences and downward long-wave radiation for the fritted double ETFE covered-building and standard double glass-covered building under overcast conditions.

**Interior air and radiant temperature differences (°C) between
fritted double ETFE roof and standard double glazed roof in
relation to overcast L_{\downarrow} values (W/m^2)**

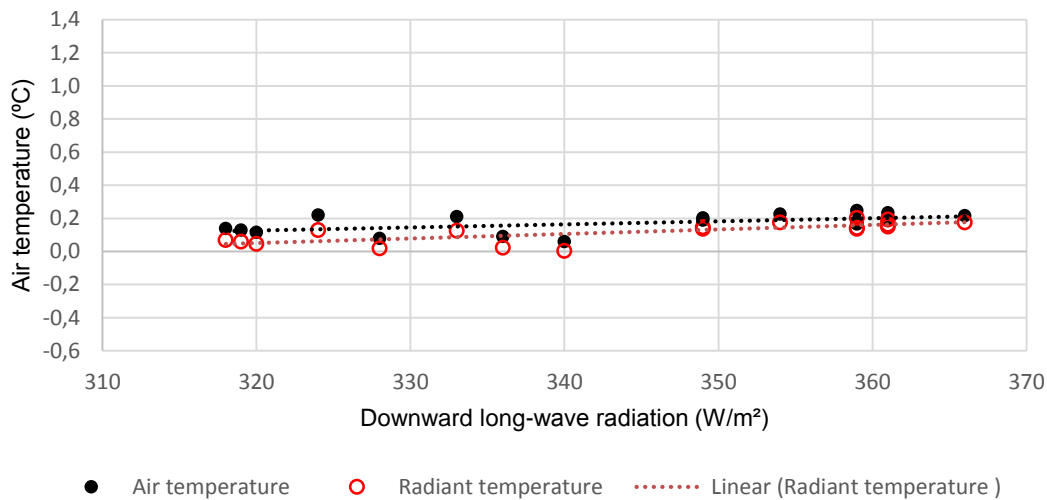


Figure 6.30: Simulated interior air and radiant temperature differences (°C) between the fritted double ETFE-covered building and standard double glass-covered building under overcast sky L_{\downarrow} (W/m^2)

The positive temperature differences occur when higher air and radiant temperatures were predicted for the standard double glass-covered building, whereas the negative temperature differences occur when higher air and radiant temperatures were predicted for the fritted double ETFE-covered building.

There is an average difference between air and radiant temperatures of $0.09^{\circ}C$ under clear sky conditions and $0.05^{\circ}C$ under overcast sky conditions. These differences are above the estimated margin of error, which is $0.02^{\circ}C$ for air temperatures and $0.01^{\circ}C$ for radiant temperatures under both clear sky and overcast sky. However, these figures are deemed very small to make clear conclusions based on the simulated results.

The results were examined in more detail regarding the simulated heating and cooling operation under clear sky conditions. Figure 6.31 shows the relationship between the heating energy consumption of the fritted double ETFE-covered building and the standard double glass-covered building to downward long-wave radiation, while Figure 6.32 shows the relationship between the cooling energy consumption to long-wave radiation.

Heating energy consumption difference (kWh) between fritted ETFE roof and standard double glazed roof in relation to clear L_{\downarrow} values (W/m^2)

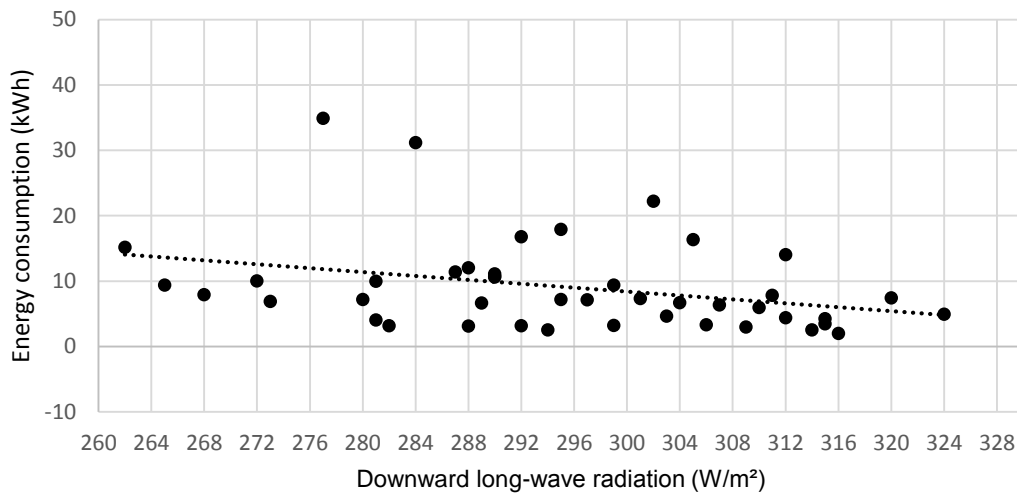


Figure 6.31: Simulated heating energy consumption difference (kWh) between the fritted double ETFE-covered building and standard double glass-covered building under clear sky L_{\downarrow} (W/m^2)

Cooling energy consumption difference (kWh) between fritted ETFE roof and standard double glazed roof in relation to clear L_{\downarrow} values (W/m^2)

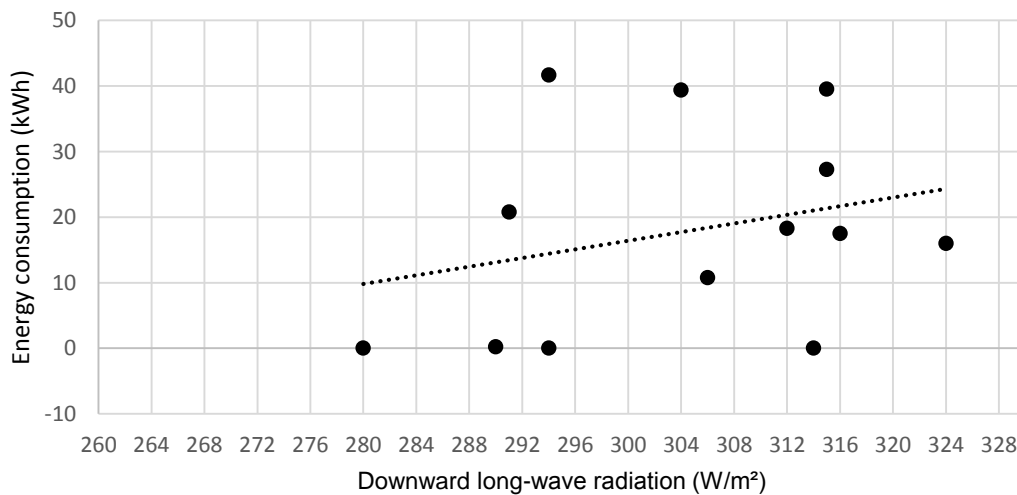


Figure 6.32: Simulated cooling energy consumption difference (kWh) between the fritted double ETFE-covered building and standard double glass-covered building under clear sky L_{\downarrow} (W/m^2)

The positive values indicate that the fritted double ETFE-covered building consistently exhibited higher energy consumption than the standard double glass-covered building for heating, whereas the relationship was reversed for cooling. The difference between the predicted energy consumption for the two buildings due to heating had a tendency to decrease with cloud presence by 9.3 kWh, which is above the margin of error of 9.1 kWh. The difference between the predicted energy consumption due to cooling did not present a correlation to long-wave radiation, as any noted association between the two values fell within the margin of error. In synopsis, the fritted double ETFE cover exhibits a worse energy performance than the standard double glass cover under cold weather conditions but better under warm weather. However, its performance is closer to the standard double glass cover than the low-E double glass cover.

6.3.7 Performance comparison of fritted double ETFE-covered notional building to low-E double glass-covered notional building

The fritted double ETFE cushion roof was consequently compared to the low-E double glazed roof to determine the effect of the two material treatments on internal conditions and energy consumption of the buildings. A low emissivity coating applied to glass typically allows shortwave radiation through, while inhibiting long-wave radiation, thus trapping most of it inside the building. This is beneficial under cold weather conditions, when heat retention is desirable, but less so under summer solar gain causing overheating of the enclosed space. For this reason low-E double glazing is typically expected to be used in conjunction to a shading device or solar treatment of the glass (CWCT, 2010). Conversely, ETFE foil allows a large amount of long-wave radiation through, while the frit reflects shortwave radiation. This property was demonstrated using the FTIR spectrometer to examine the range of radiation that the membrane and the frit allow through, as was described in Chapter 3.

Using IES modelling to reproduce the thermal behaviour of each material, the fritted double ETFE-covered building constantly demonstrated lower temperatures than the low-E double glazed building, as it can be seen in Figures 6.33 and 6.34.

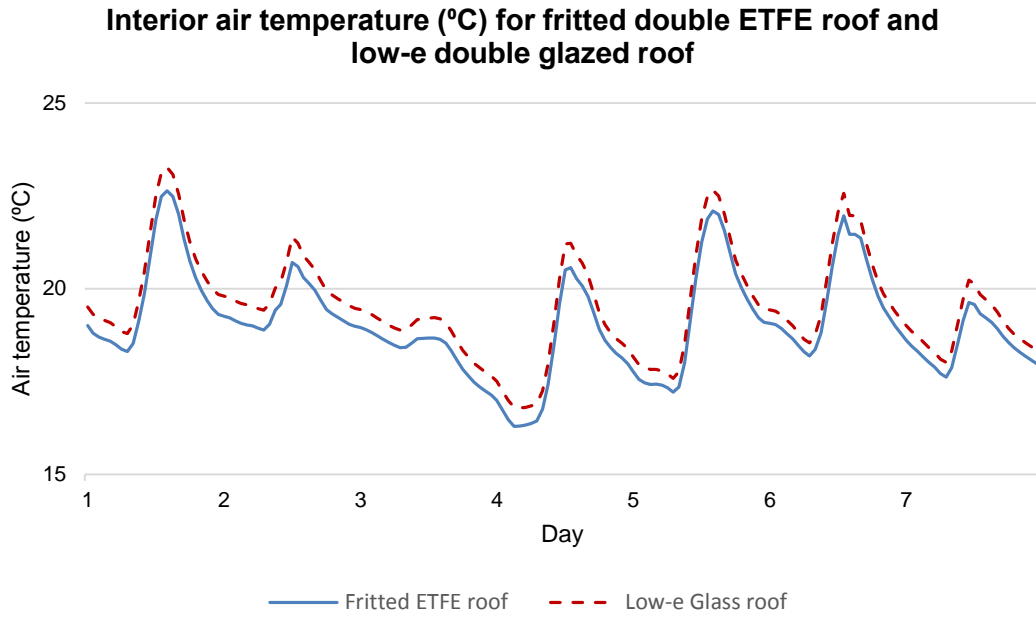


Figure 6.33: Simulated East Building atrium air temperature: comparison between a fritted double ETFE and a low-E double glazed roof

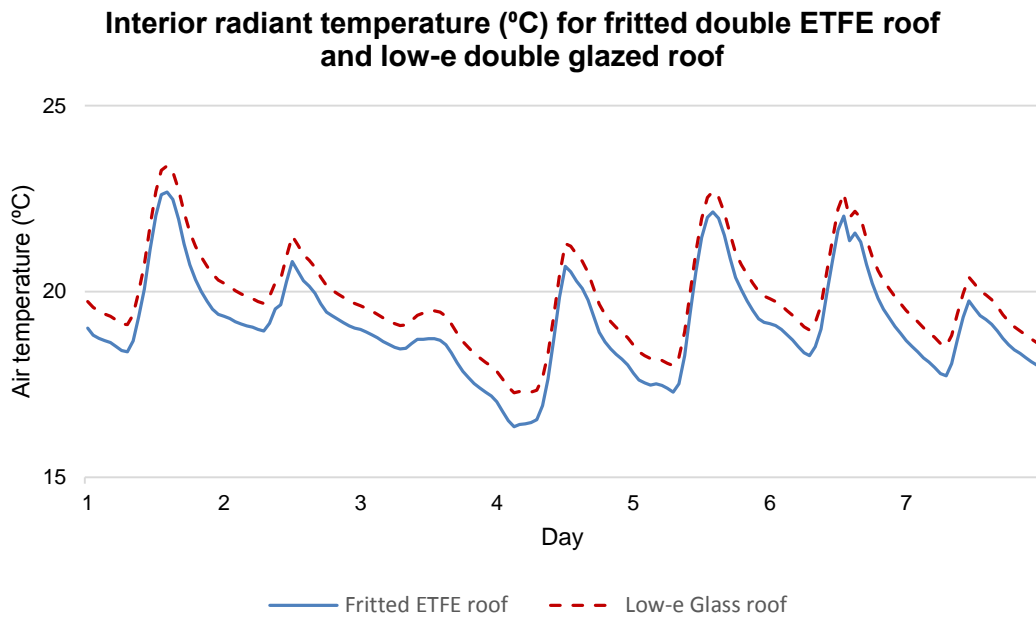


Figure 6.34: Simulated East Building atrium radiant temperature: comparison between a fritted double ETFE and a low-E double glazed roof

Figure 6.35 shows the energy consumption due to heating and Figure 6.36 the energy consumption due to cooling of the two notional buildings. The simulations for the fritted double ETFE-covered building showed greater space heating consumption than the low-E double glass-covered building. In summary, the fritted double ETFE-covered building was predicted to consume an annual total of 1003102 kWh, 5% more energy than the 955443 kWh predicted for the low-E double glass-covered building.

The fritted double ETFE-covered building was also predicted to consume less space cooling energy than the low-E double glass-covered building. In total, the building with the fritted ETFE cushion roof was estimated to consume an annual amount of 491935 kWh, 8.5% less energy than the building with the low-E glass roof and the estimated energy consumption of 537657 kWh.

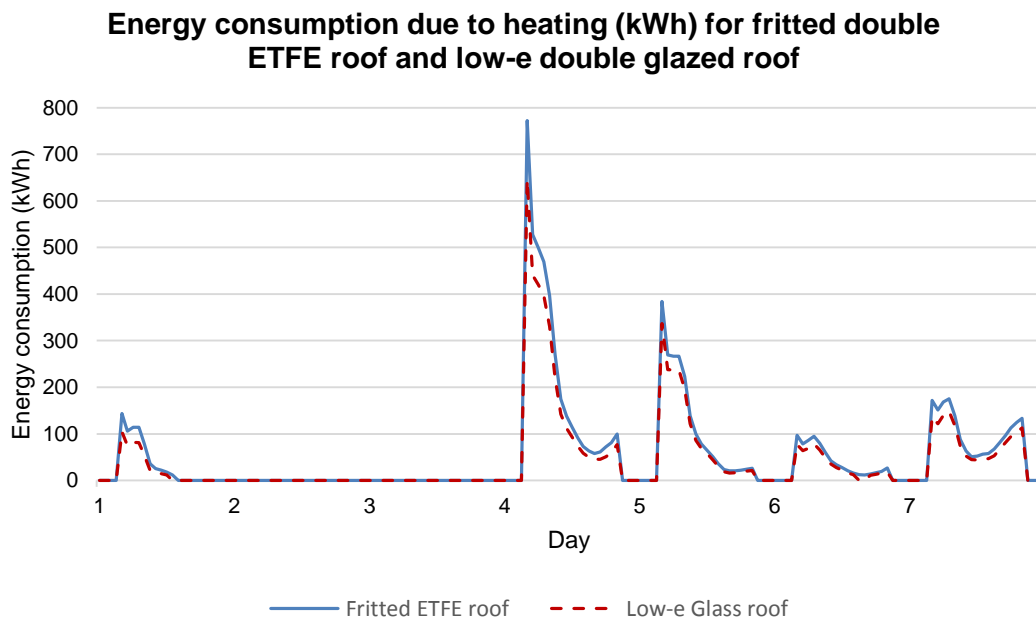


Figure 6.35: Simulated East Building atrium energy consumption due to heating: comparison between a fritted double ETFE and a low-E double glazed roof

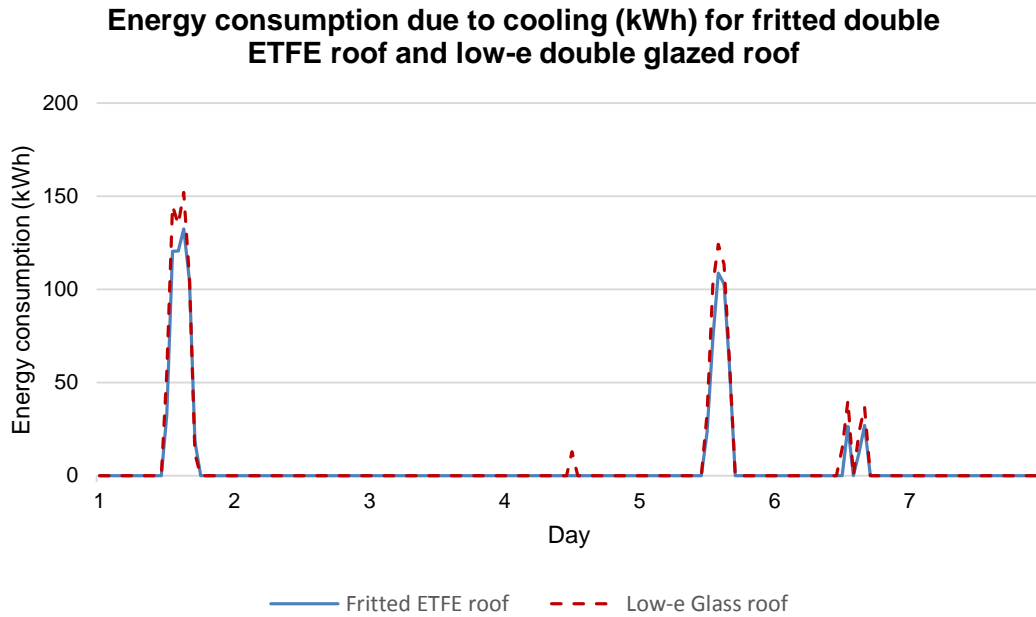


Figure 6.36: Simulated East Building atrium energy consumption due to cooling: comparison between a fritted double ETFE and a low-E double glazed roof

6.3.8 Results analysis

The simulated air and radiant predicted temperatures were constantly higher for the low-E double glass-covered building. In the presence of solar gain the frit assisted in keeping internal temperatures of the atrium at a lower level than the low-E treatment of the glazed units. In the absence of solar gain the frit did not help to contain heat inside the atrium, while the membrane itself allowed long-wave radiation to escape through the building cover. In summary, the fritted double ETFE-covered building was estimated to be more successful than the low-E double glass-covered building in maintaining comfortable interior conditions under warm weather but less successful under cold weather surroundings.

A more detailed examination was undertaken on the interior conditions predicted for the two models during night hours, to avoid the effect of overheating. Figure 6.37 presents the relationship between air and radiant temperature differences to downward long-wave radiation respectively, for the fritted double ETFE-covered building and low-E double glass-covered building under clear sky conditions.

**Interior air and radiant temperature differences (°C) between
fritted double ETFE roof and low-e double glazed roof in
relation to clear L_{\downarrow} values (W/m^2)**

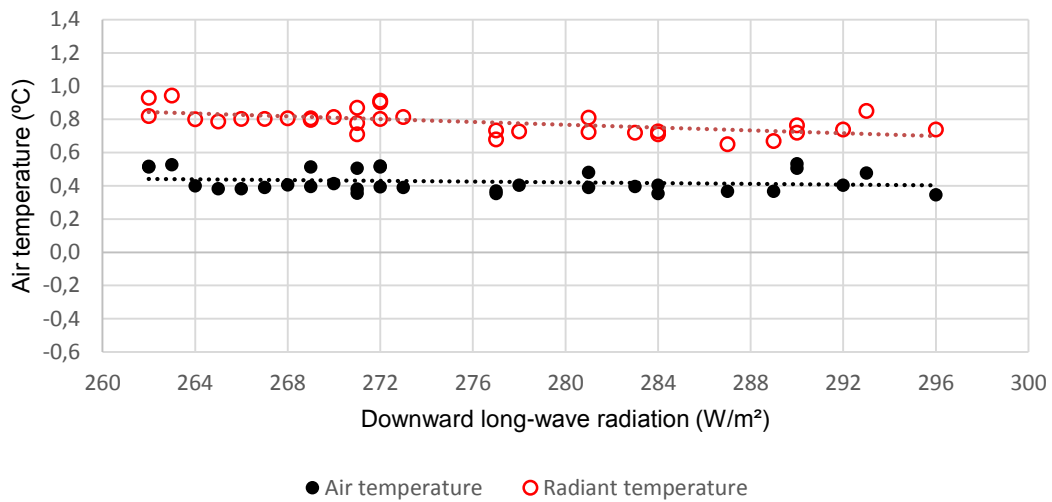


Figure 6.37: Simulated interior air and radiant temperature differences (°C) between the fritted double ETFE-covered building and low-E double glass-covered building under clear sky L_{\downarrow} (W/m^2)

Figure 6.38 presents the relationship of air and radiant temperature differences to downward long-wave radiation between the fritted double ETFE-covered building and low-E double glass-covered building under overcast sky conditions.

Interior air and radiant temperature differences (°C) between fritted double ETFE roof and low-e double glazed roof in relation to overcast L_{\downarrow} values (W/m^2)

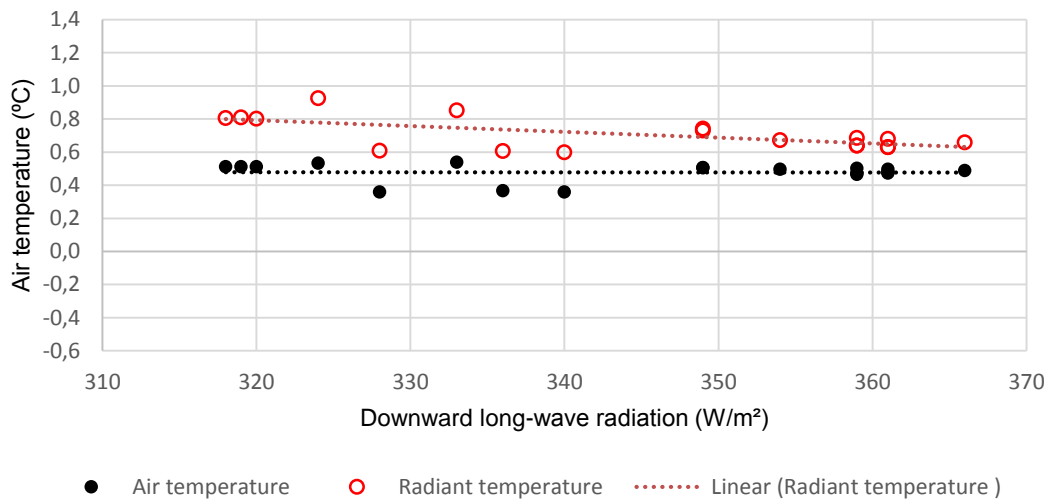


Figure 6.38: Simulated interior air and radiant temperature differences (°C) between the fritted double ETFE-covered building and low-E double glass-covered building under overcast sky L_{\downarrow} (W/m^2)

The positive temperature differences demonstrate that higher air and radiant temperatures were predicted for the low-E double glass-covered building. The difference between air and radiant temperatures can be explained by the nature of the low-E glass, which contains part of the long-wave radiation and raises the interior radiative temperatures higher than the equivalent temperatures under the fritted ETFE cover, which reflects shortwave radiation and obstructs the natural heating of the space.

The difference in the air temperature predicted for the two materials remained constant under both clear and overcast sky conditions. The difference in radiant temperature associated with the two covering materials presented a tendency to decrease as cloud presence increased by 0.19° C under clear sky and 0.17° C under overcast sky conditions. These values are above the estimated margin of error, which is 0.05° C and 0.04° C respectively. This tendency for radiant temperature difference to decrease with cloud increase can be explained by the fact that radiative heat loss is greater under a clear sky, in which case the low-E treatment was most effective in maintaining higher interior temperatures than the ETFE frit treatment.

Regarding the notional buildings' energy consumption due to space treatment, Figures 6.39 and 6.40 show the difference in simulated energy consumption for heating and cooling respectively between the fritted double ETFE-covered building and the low-E double glass-covered building. The analysis focuses on clear sky data only, as no energy consumption was recorded under overcast sky conditions for the period of time under examination.

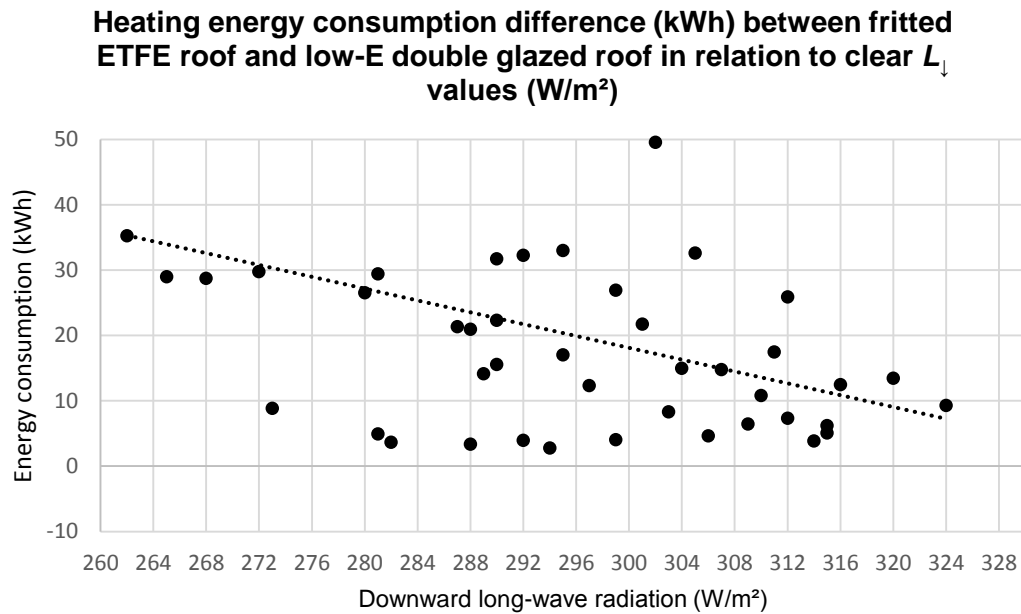


Figure 6.39: Simulated heating energy consumption difference (kWh) between the fritted double ETFE-covered building and low-E double glass-covered building under clear sky L_{\downarrow} (W/m^2)

Cooling energy consumption difference (kWh) between fritted ETFE roof and low-E double glazed roof in relation to clear L_{\downarrow} values (W/m^2)

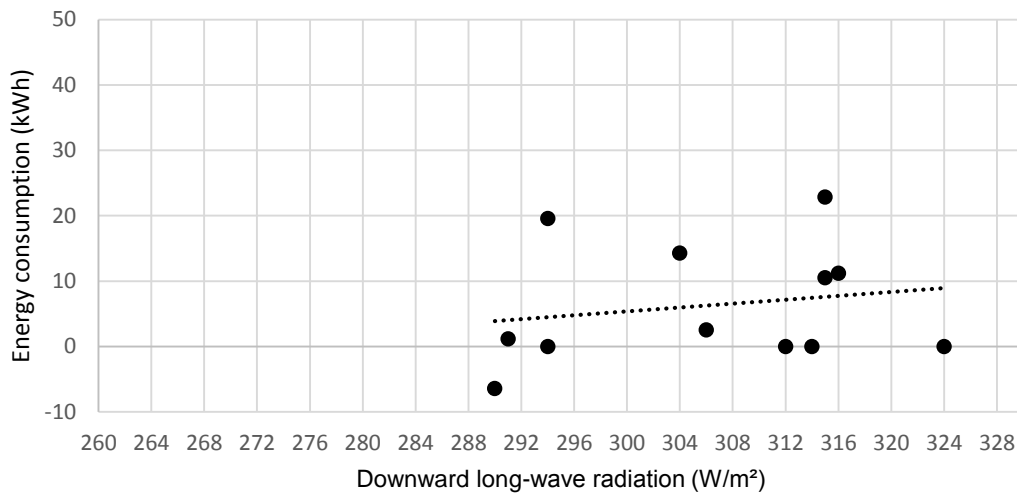


Figure 6.40: Simulated cooling energy consumption difference (kWh) between the fritted double ETFE-covered building and low-E double glass-covered building under clear sky L_{\downarrow} (W/m^2)

The positive temperature difference in the simulated energy consumption due to heating for the two buildings shows that the fritted double ETFE-covered building consumed more energy than the low-E double glass-covered building. This can be traced back to the radiative properties of the ETFE membrane, which allow most long-wave radiation to go through compared to the low emissivity treated glass, which contains heat in the building interior.

The positive temperature difference values in the energy consumption due to cooling show that the fritted double ETFE roof was associated with less energy than the low-E double glass roof. This is due to the fact that the radiative nature of the ETFE surface treatment reflected shortwave radiation and, therefore, prevented natural overheating of the building.

The difference between the predicted energy consumption for the two buildings due to heating had a tendency to decrease with cloud presence by 28.1 kWh, which is above the margin of error of 20.2 kWh. The difference between the predicted energy consumption due to cooling did not present a correlation to long-wave radiation, as any noted association between the two values fell within the margin of error.

This concludes the description and comparison of different types of covering materials. There is a broad range of both glass and ETFE treatments available for use, however, it was decided to narrow down the number of simulations to the most representative and most commonly used instances of each material for the purposes of brevity and clarity. The following – and final – section of this chapter will summarise and classify the examined covers based on their predicted performance.

6.4 Summary and conclusions

The current chapter used the design of an existing building with an ETFE-covered atrium as the basis to perform simulations on a realistic scale. This round of simulations allowed a comparison between the thermal and energy performance of the most commonly employed types of ETFE cushions (clear and fritted) to the most representative equivalent glazed options (standard and low-E double glazing).

- Regarding the thermal performance of the examined covers Table 6.3 summarizes the examined materials in estimated increasing order of comfort, first under cold weather and then under warm weather conditions. Cold weather conditions were marked as the period during which heating operated (24 September – 30 April) and warm weather conditions the period during which cooling operated (6 April – 13 October). The materials classification for the cold weather conditions is based on a descending order, as the higher the estimated temperature, the closest it is to the interior set temperature of 19 °C. The materials classification for the warm weather conditions is based on an increasing order, as the lower the estimated temperature, the easier it becomes to achieve the set interior temperature of 23 °C.

-

Table 6.3: Materials classification according to average interior air and radiant temperatures under cold and warm weather conditions

Material	Average interior air temperature (°C)	Average interior radiant temperature (°C)
Cold weather conditions		
Low-E double glazing unit	17.28	17.61
Clear double ETFE cushion	17.26	17.28
Standard double glazing unit	16.96	16.96
Fritted double ETFE cushion	16.88	16.96

Warm weather conditions		
Fritted double ETFE cushion	27.75	27.83
Standard double glazing unit	28.93	28.94
Low-E double glazing unit	28.96	29.30
Clear double ETFE cushion	30.30	30.32

Table 6.4 summarizes the examined materials in increasing order of comfort, under all weather conditions, as resulting from an entire year's data. As heating requirements dominated the overall energy consumption for space treatment, this classification takes place in a descending order, characterising as more successful the estimated temperature that is closest to the interior temperature of 19 °C.

Table 6.4: Materials classification according to average interior air and radiant temperatures under all weather conditions throughout an entire year

Material	Average interior air temperature (°C)	Average interior radiant temperature (°C)
Fritted double ETFE cushion	22.13	22.21
Standard double glazing unit	22.72	22.73
Low-E double glazing unit	22.91	23.25
Clear double ETFE cushion	23.53	23.54

To recap, clear double ETFE cushions were more successful than standard double glass in maintaining more desirable interior conditions under both clear and overcast sky circumstances in cold weather conditions. This is due to the insulating effect of the air trapped inside the clear double ETFE cushions. As it was discussed in section 6.2 on the preparation of secondary modelling using IES, the cushions' thickness was not represented to its realistic depth; however, its thickness was, in fact, significantly increased in relation to the glass units' thickness (ETFE air thickness: 175 mm, glass air thickness: 12 mm). On the contrary, clear double ETFE cushions were less successful than standard double glass in maintaining comfortable conditions under both clear and overcast sky in warm weather conditions. By allowing a slightly higher amount of shortwave radiation than standard double glass, the clear ETFE cushions caused the atrium to overheat.

Clear double ETFE cushions were not as successful as low-E double glass at providing desirable interior temperatures under both cold and warm weather conditions. This demonstrates that the insulating performance of the low-E coating of the double glass cover due its radiative properties exceeds the insulating performance of the air trapped in the clear double ETFE cover. More specifically, the thermal performance of the clear double ETFE cushions resulted in more desirable interior conditions under overcast sky circumstances, whereas the low-E double glass cover gave more desirable interior conditions under a clear sky.

Similarly, fritted double ETFE cushions were not as successful at maintaining desirable conditions compared to standard double glazing under cold weather conditions. The presence or absence of a frit on ETFE foil had no effect on the transmission of long-wave radiation. However, the thermal behaviour of the double fritted ETFE cushion was affected by the reflective properties of the frit towards shortwave radiation, which caused a thermal performance of the fritted double ETFE cover that was closer to the desirable temperatures under warm weather conditions.

Finally, the fritted double ETFE cushions presented a worse thermal performance than low-E double glass under both clear and overcast skies in cold weather conditions. The frit of the double ETFE cover did not assist in retaining long-wave radiation inside the building, in contrast to the low-E treatment of the double glass cover. However, the frit did reflect shortwave radiation, which maintained more comfortable conditions than the low-E double glass roof under warm weather conditions.

- Regarding the overall energy consumption that was estimated in relation to the materials used in these simulations, they are classified in increasing order, as shown in Table 6.6, first under cold weather and then under warm weather conditions.

Table 6.5: Materials classification according to overall energy consumption under cold and warm weather conditions

Material	Overall energy consumption (kWh)
Cold weather conditions – overall heating load (kWh)	
Low-E double glazing unit	955443
Clear double ETFE cushion	974007
Standard double glazing unit	1001752
Fritted double ETFE cushion	1003102

Warm weather conditions – overall cooling load (kWh)	
Fritted double ETFE cushion	491935
Low-E double glazing unit	537657
Standard double glazing unit	570133
Clear double ETFE cushion	652815

Table 6.6 shows the classification of materials first based on their overall annual energy consumption due to space heating and cooling combined, in descending order and then based on their overall energy consumption under clear and overcast sky conditions.

Table 6.6: Materials classification according to overall annual energy consumption

Material	U-value (W/m²K)	Overall energy consumption (kWh)
All weather conditions		
Low-E double glazing unit	2.03	1493099
Fritted double ETFE cushion	2.60	1495037
Standard double glazing unit	3.01	1571885
Clear double ETFE cushion	2.94	1626822
Clear sky conditions		
Low-E double glazing unit		781189
Fritted double ETFE cushion		782068
Standard double glazing unit		824137
Clear double ETFE cushion		853601
Overcast sky conditions		
Low-E double glazing unit		277940
Fritted double ETFE cushion		281833
Standard double glazing unit		291315
Clear double ETFE cushion		296870

In total, the building with the clear double ETFE cushion roof was predicted to consume 3.5% more energy for space treating than the building with the standard double glass roof and 9% more than the building with the low-E double glass roof. The building with the fritted double ETFE cushion roof was estimated to consume 4.9% less energy for space treating than the building with the standard double glass roof and 0.1% more than the building with the low-E double glass roof.

A disagreement can be noticed between the U-value classification and the energy consumption sorting of the examined covers in Table 6.6. The U-values describe the amount of heat loss through each cover, therefore indicating their insulating capacity. However, the simulated energy consumption of the East Building for each of the examined covers is not influenced solely by their U-value, but also by the radiative properties of each cover - which are not part of the U-value. More specifically, the disagreement between the U-value of the clear ETFE cushion roof being lower than that of the standard glass roof and the fact that the building with the clear ETFE roof was estimated to consume more energy than the building with the standard glass roof indicates that the clear double ETFE cushions should, in fact, have a higher U-value.

The total energy consumption for heating and cooling related to the clear double ETFE cushions is higher than that related to the standard double glazing unit, which is inconsistent with the order of the U-values of the two materials. This demonstrates that the lack of surface treatment of the clear double ETFE cushion was not sufficient to maintain internal long-wave radiation at desirable levels under cold weather conditions and repel shortwave radiation in order to prevent overheating under warm weather conditions.

The total energy consumption associated with the clear double ETFE cushions was also higher than the energy associated with the low-E double glazed unit for both heating and cooling. This can be explained by the U-value of the low-E double glazed unit - the lowest among the examined building covers - in combination to its radiative properties, which allowed the roof to contain long-wave radiation under cold weather conditions and also present high insulating properties under warm weather conditions.

The total energy consumption related to the fritted double ETFE cushions is higher than both the standard and the low-E double glazed covers for heating requirements. The excessive energy consumption due to heating associated with the fritted ETFE cover was interpreted to result from the repulsion of solar gain that the frit provided and the related protection from natural heating during daytime, allowing the building to

cool down sooner than clear double ETFE and standard and low-E double glazing. However, due to its radiative nature, the fritted ETFE roof reflected shortwave radiation and prevented the building from overheating, causing a lower energy consumption due for cooling than both the standard and the low-E double glass roofs.

To summarise, this round of simulations demonstrated that clear double ETFE cushions can be beneficial in a cold environment, where heating requirements are dominant, while fritted double ETFE proved an efficient alternative under a warm environment, where cooling requirements prevail.

This classification provided information that can be used by designers who are in the process of selecting a suitable transparent roofing material among the most common types of double ETFE cushions and double glass, based on either their thermal or energy performance. The classification completes the contents of this chapter and finalises this research. The following Chapter 7 will examine the contents of the thesis; the aims and objectives that were initially set and the degree to which each was met. Furthermore, the impact and significance of this work will be discussed, before providing a summary and presenting the conclusions resulting from this thesis.

7 Conclusions

7.1 Aims and objectives, and degree to which each was met

The main goal of this thesis was to examine the amount of thermal transfer through ETFE foil and cushions. The intended outcome was to provide an accurate description of the response of ETFE membranes and cushions to cold external conditions and the associated heating requirements, as well as offer direction on how to successfully model this response using dynamic simulation programs.

A number of objectives and the related research methodology had been identified at the start of the thesis. Upon completion of this research, the following section describes the method of objective execution, the caveats by which results should be interpreted, as well as the degree of success to which each objective was met. The caveats describe the conditions under which each objective should be considered.

- Review ETFE foil and cushions as a suitable replacement for glass.

Current practice in ETFE membranes and cushions was examined through review of journals, conference proceedings, books and product information material. Plastics were evaluated in relation to glass cladding and ETFE was identified as the optimum representative of its materials family during this process.

There is a plethora of plastic materials that could be adopted as an alternative to glass. Out of these, the most promising and well researched materials were selected from an abundance of options. The selection criteria entailed the plastic materials' visual performance, solar and thermal transmittance, as well as overall engineering performance, durability, strength, chemical stability and weight. As this thesis is a finite work, it could not examine every existing plastic as a possible cladding substitute.

- Characterise dynamic thermal response of ETFE cushions.

Existing research on the thermal behaviour of films, glass and ETFE cushions was investigated through review of journals, conference proceedings, books, product information material, as well as government and industry documents. The thermal response of ETFE membrane was analysed regarding heat transfer mechanisms – conduction, convection and radiation, placing an emphasis on the latter.

The available published scientific material on the thermal behaviour of ETFE membranes and cushions is limited – which is what this research attempted to address. This lack of published information instigated the experimentation and computer simulations herein.

- Review standards on heat transfer measurement.

The methods for the measurement of heat transfer were described, as established by standards and research bodies, either in a laboratory or an in-situ real life setup. This was done through review of journals and government documents.

The selected method for the measurement of heat transfer through ETFE membranes and cushions was through an in-situ setup, with a methodology not officially verified by a governmental or research facility by the time of this investigation. Therefore, the developed methodology had to be based on similar performed experiments found in literature.

- Quantification of radiative transfer of different types of single ETFE membrane.

A Fourier Transform Infra-Red (FTIR) spectrometer was used to determine the shortwave and long-wave radiation transmitted through five samples of single ETFE foil – clear, clear fritted, matt, white and white fritted.

The laboratory-based results resolved the existing ambiguity regarding the radiative properties of ETFE found in literature. However, further experimentation was required to comprehensively characterise the thermal behaviour of the material.

- Thermal characterisation of a two-layer ETFE cushion compared to a double pane glass unit.

The experiment used a two-layer cushion and a double glazed unit in the hot box method and in-situ real life conditions. The thermal behaviour of each material was examined as they responded to external conditions, using air and radiant temperatures.

There was some unaccounted heat loss due to infiltration. A calibration process was performed to offset the effects of this undesired heat loss.

- Appraise available models for the classification of sky types, in particular the detailed estimation of long-wave radiation (L) and sky emissivity (ϵ).

Research performed for the classification of clear, partly cloudy or overcast skies through review of journals, conference proceedings and books. Existing models were examined; one was selected as the most suitable to simulate long-wave radiation based on ground measurements and the proposed experimental procedure.

Experimental measurements were used to reproduce calculated results and validate the chosen long-wave and emissivity model. This goal was not fulfilled successfully, as the investigated models were based on experimental data that were found to be unsuitable for the gathered dataset in this research. A satisfactory method to estimate long-wave radiation from on-ground measurements was not found through literature.

- Analyse thermal behaviour of a fritted double-layer ETFE cushion against a standard double pane glass unit.

Experimental data was divided in clear and overcast sky data-sets. The correlation between energy consumption of experimental boxes and air temperature, shortwave and long-wave radiation was determined.

The examined datasets regarded heating conditions only, to limit the focus of the search around an area that seemed feasible. The examined fritted ETFE cushion still appeared to present issues with overheating. Further research might be useful in the future, focussing on the thermal and energy performance of ETFE foil in relation to cooling requirements.

- Devise design template for the optimal deployment of architectural ETFE cushions.

Integrated Environmental Solutions (IES) building simulation program was used to reproduce the measured performance of the experimental boxes. The necessary modifications and considerations to achieve agreement between recorded and simulated performance were examined. Guidance was provided for designers who attempt to model thermal and energy performance of an ETFE cushion.

The weather file conversion used in the IES simulations was a long and detailed process. Furthermore, an extensive calibration process took place to reach an agreement between the IES estimated and the actual measured thermal and energy

response of both experimental units. These facts indicated that for IES to deliver accurate results, it requires extensive fine-tuning at initial design stages.

- Quantify energy saving potential of different types of double ETFE cushions compared to different types of double glazing.

An existing building case study was modelled in IES to examine the comfort and heating energy saving potential of double ETFE cushion covers compared to double glass covers for a typical configuration in-use. The examined clear and fritted double ETFE cushions and standard and low-e double glass were classified according to their thermal and energy behaviour.

The building was modelled to a limited level of accuracy due to lack of detailed information regarding wall and glazing material properties. It was accepted that excessive precision would not offer any added benefit to the focus of the study. Although not necessarily representative for all buildings and all double ETFE cushion sizes and number of layers, the modelling was still able to provide a general understanding of the energy saving potential of a double ETFE cushion configuration.

7.2 Impact and significance of work

The following discussion concerns the impact and significance of the thesis in various fields:

- Data statistical significance and accuracy

Regarding the accuracy and statistical significance of data that was gathered through the laboratory based experiments, the measurements were performed three times each to ensure that the results were in agreement and accurate. As the measurements were done in a highly controlled environment and using a precise instrument, they can be replicated by other researchers.

Regarding the data gathered throughout the in-situ experiment, a large amount of external and internal environmental data was collected. The analysed sample size was narrowed down to the most representative weather conditions to facilitate the writer and the reader in viewing and understanding the analysis of the results. Due to the fact that the experiments were performed outside a controlled laboratory environment, the collected data cannot be replicated under the same conditions and using the same apparatus. However, the results were successfully reproduced digitally through

computational modelling, which verified their statistical significance for future reference in other research.

- Technical applicability

The main goal of this thesis was to resolve the ambiguity related to thermal loss through the ETFE membrane and its energy saving potential for space heating. One of the outcomes of this research was a methodology on how to digitally simulate the thermal and energy performance of ETFE cushions. This methodology includes both the geometrical representation of ETFE cushions, as well as the creation of a digital material profile. This technical knowledge is useful to designers who wish to use computer simulation to evaluate the suitability of the membrane as an alternative cladding material in comparison to other established options, such as glass.

- Energy savings

A number of environmental benefits are associated with the use of ETFE cushions. Primarily, with ETFE membrane being a very light cladding material with the ability to cover a large area, the supporting structure requires much smaller diameters and can reach longer spans, lowering material use in construction for structural support. Due to the membrane's low mass, ETFE cushions require little material to cover an area in relation to standard glass, lowering the embodied energy of the structure. The low mass is also associated with ease of transportation. Furthermore, due to its high levels of light transmission, ETFE cushions can be associated with energy savings in relation to lighting requirements.

In addition to these environmental benefits, this research demonstrated that clear double ETFE cushions are also capable of providing with heating energy savings. Therefore, for a cold climate, the employment of clear double ETFE cushions can increase the sustainability of a construction.

- Comfort impact

As the research demonstrated, clear double ETFE cushions are capable of providing comfortable internal thermal conditions, due to their insulating properties, particularly under cold weather conditions. The performed experiments and simulations established that clear double ETFE cushions are associated with overheating in the presence of solar input, making it necessary to accompany their use with a shading strategy. The application of fritting proved to be less beneficial than initially expected,

which is why it is the author's suggestion to combine the use of clear double ETFE cushions with an external shading system rather than an embedded system or printed films.

- Limitations to work

The thesis focused on the thermal and energy behaviour of ETFE cushions in relation to heating requirements, in moderately cold weather conditions. The performed experiments and simulations were all limited in the geographical location and the climate conditions of Bath, in the South-West of the United Kingdom. On a number of occasions ETFE membrane was associated with overheating, which indicated that further research is required to cover experiments and simulations either in a different location or at another time of the year, in order to examine a cooling scenario and available passive solutions to the issue. Before excluding ETFE cushions as an unsuitable cladding option for a hot climate, it is important to investigate alternatives that could improve its performance. However, due to finite time limitations and the need to narrow down the research focus, the examination of the overheating scenario was not part of this thesis.

7.3 Summary and conclusions

ETFE cushions have been examined in the pursuit of a replacement to glazing, as a solution to the disadvantages associated with its use, such as its fragility, weight and behaviour towards heat transmission (Clarke et al., 1998; Robinson-Gayle et al., 2001). Glass presents high transmission of near Infra-Red radiation, causing an increase in heating requirements during cold weather, and a consequent need for cooling in warm conditions (Brauer, 1999). The excessive use of glazing also increases the embodied energy and the cost its support structure. Furthermore, the geometry of the building is often an obstacle to the use of glass.

ETFE cushions cannot be treated like glass while performing an energy study on the thermal performance of a building. At present there is no available information published for the quantification of the long-wave radiation transmission through ETFE cushions (Poirazis et al., 2010).

Following the research based on literature review, this study aimed to address this issue by performing laboratory-based measurements of the thermal transmission of different types of single ETFE foil (clear, clear fritted, matt, white and white fritted). In

synopsis, the average transmission values of the examined untreated ETFE foils (clear, matt and white) in the long-wave radiation range varied between 77-81%. The average transmission measured on treated areas of the ETFE foils (clear fritted and white fritted) varied between 37-39%. The analysis of the peak measurements for both treated and untreated types of the material showed that there was no obvious correlation between the radiative response of the examined membranes and their thickness or colouration. Further investigation was deemed necessary to better understand the thermal behaviour of the material.

This research continued by performing an in-situ based experiment to study the thermal response of a two-layered fritted ETFE cushion alongside a double glazed unit, each covering one of two experimental boxes exposed to the same external conditions and supported by the same interior condition regulating mechanism. To avoid the effects of incoming solar radiation and the consequent overheating of the boxes, the data under examination involved only night-time recordings.

The recorded thermal performance of the fritted double ETFE cushion was compared to that of the double glazed cover. The fritted double ETFE cushion proved capable of providing more comfortable interior conditions than double glass on a number of occasions, and more specifically under cold weather conditions and in the absence of solar input. Regarding the recorded energy performance of the two experimental devices, the glass-covered box consumed a total of 11.13 kWh, which is slightly more than the 11.07 kWh that was consumed by the fritted double ETFE-covered box. The study demonstrated that under the specific experimental conditions, fritted double ETFE cushions can successfully replace glass in buildings under cold weather settings, while offering a comfortable interior environment. The gain in the energy consumption was small (0.5 %) but not negligible, identifying fritted double ETFE cushions as a viable alternative to double glazing.

The thesis made use of the experimental findings by using Integrated Environmental Solutions (IES) to reproduce the experimental conditions and results. The outcome of this process was to determine the necessary adjustments that must be taken into account when using IES to estimate the energy consumption of a building using one or more ETFE cushions as cladding. The result was to offer guidance to designers on how to examine ETFE cushions as an option through preliminary energy saving calculations.

Instigating the digital modelling of the experimental devices, a calibration process was required to achieve accurate simulation results, using material properties to describe the double glass and fritted double ETFE covers based on information obtained through the literature review and from the material manufacturers. The modelling of the double fritted ETFE cushion geometry was investigated; concluding that the optimum way to its digital representation was by representing the two membranes as flat parallel surfaces, having the distance between them adjusted to match the expected U-value. Seven more models were examined, using different numbers of faceted trapezoid surfaces to represent the curved surface of the cushion, since IES did not allow the modelling of the cushion camber. The models used 9, 13, 17, 21, 29 and 33 surfaces respectively. However, the process of modelling the fritted double ETFE cushion using a number of faceted surfaces was eventually rejected as too time consuming and impractical.

Finally, this research used the knowledge on how to accurately model the thermal and energy performance of an ETFE cushion to run simulations using the geometry of an existing building with a clear double ETFE-covered atrium. Two types of double ETFE cushions (clear and fritted) were compared to two types of double glass (standard and low-e) used as the building cover. The simulations were performed using a realistic mode of heating operation to classify the examined materials based on thermal comfort and heating energy performance.

In relation to the estimated thermal comfort linked to each material under cold weather conditions, the classification of the materials went as follows, in ascending order: low-E double glass, clear double ETFE cushion, standard double glass and fritted double ETFE cushion (Figure 7.1, based on the contents of Table 6.4). In relation to the thermal comfort associated to each material under warm weather conditions, the classification of the materials went as follows: fritted double ETFE cushion, standard double glass, low-E double glass and clear double ETFE cushion (Figure 7.2, based on the contents of Table 6.4).

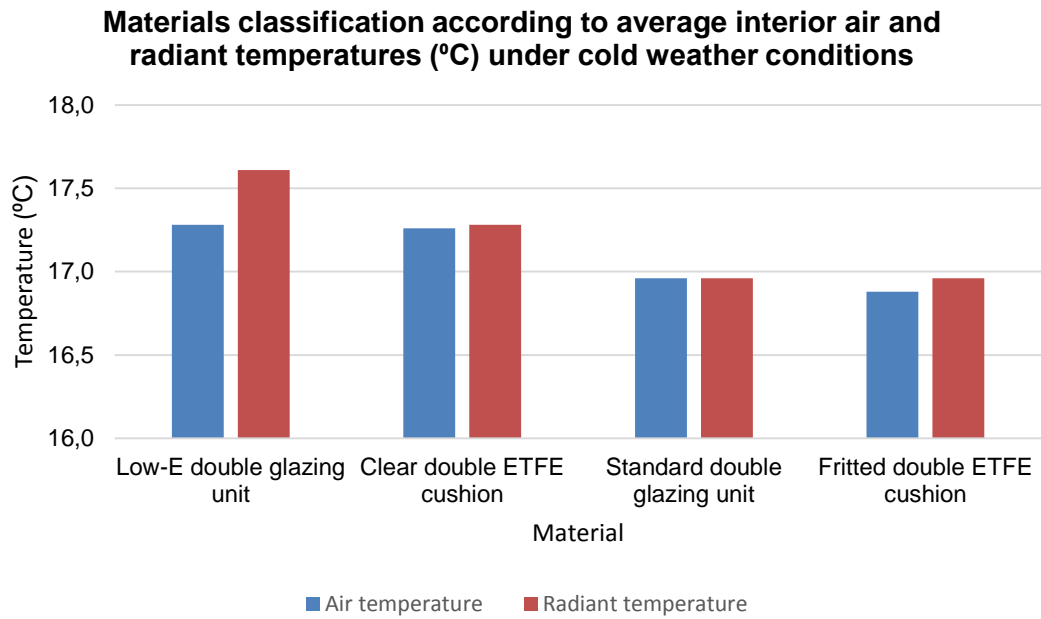


Figure 7.1: Materials classification according to average interior air and radiant temperatures under cold weather conditions

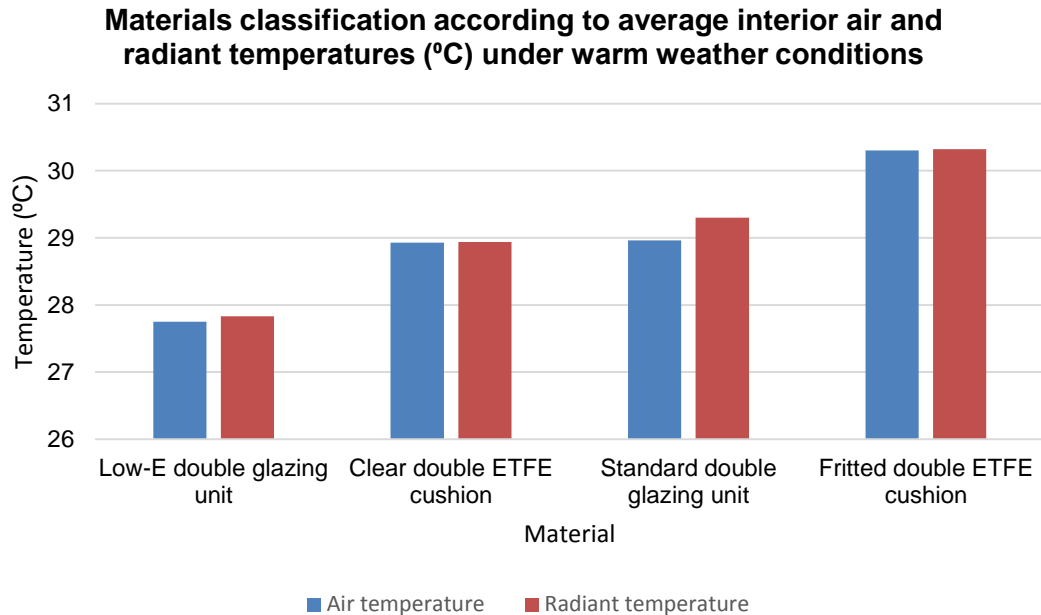


Figure 7.2: Materials classification according to average interior air and radiant temperatures under warm weather conditions

Regarding the estimated energy consumption associated with each covering material, the classification was as follows, in ascending order: fritted double ETFE cushion,

standard double glass, low-E double glass and clear double ETFE cushion (Figure 7.3, based on the contents of Table 6.6).

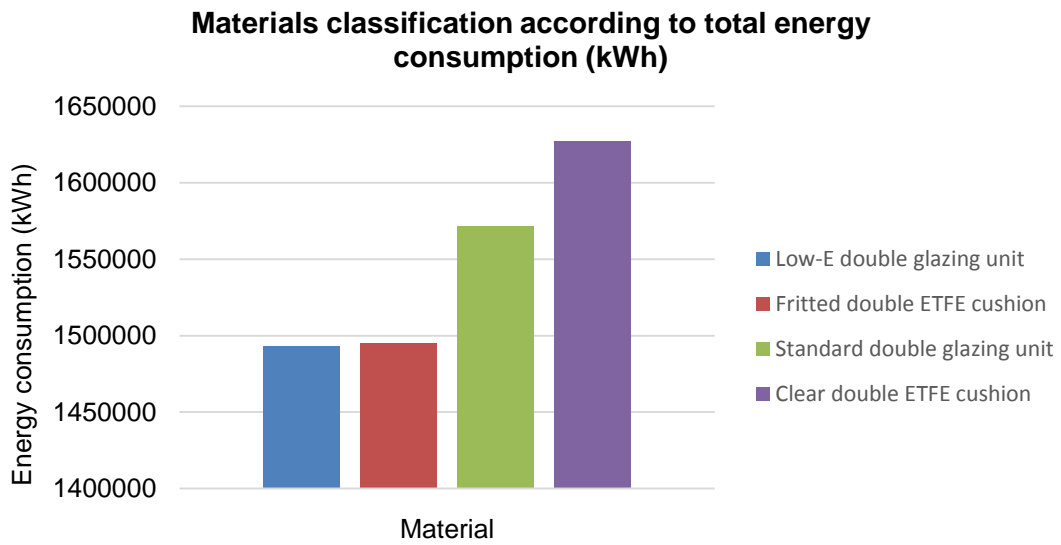


Figure 7.3: Materials classification according to total energy consumption

This classification facilitates material selection based on either on the desired interior conditions or heating energy saving requirements.

References

- 7345, E. I. (1995). Thermal insulation — Physical quantities and definitions (ISO 7345:1987). Brussels, European Committee for Standardization.
- AGC. (2013). "Fluon ETFE Film." from <http://www.agcce.com/ETFEFilmmain.asp>.
- Alados, I. (2012). "Estimation of downwelling longwave irradiance under all-sky conditions." International Journal of Climatology **32**(5): 781-793.
- Alamdari, F. & G. Hammond (1983). "Improved data correlations for buoyancy-driven convection in rooms." Building Services Engineering Research and Technology (4): 106-112.
- Ander, G. D. (2003). Daylighting performance and design New Jersey, USA, John Wiley and Sons.
- Ångström, A. (1916). "Über die Gegenstrahlung der Atmosphäre." Meteorologische Zeitschrift(33): 529-538.
- Antretter, F., W. Haupt & A. Holm (2011). "Thermal Transfer through Membrane Cushions Analyzed by Computational Fluid Dynamics."
- ApacheSim, I. (2013). ApacheSim Calculation Methods, Virtual Environment 6.3.
- Arasteh, D. (1989). An analysis of edge heat transfer in residential windows. ASHRAE/DOE/BTECC/CIBSE Conference on thermal performance of the exterior envelope of buildings IV. Orlando, USA.
- Arnfield, A. J. (1979). "Evaluation of empirical expressions for the estimation of hourly and daily totals of atmospheric longwave emission under all sky conditions." Quarterly Journal of the Royal Meteorological Society **105**(446): 1041-1052.
- Baille, A., J. C. López, S. Bonachela, M. M. González-Real & J. I. Montero (2006). "Night energy balance in a heated low-cost plastic greenhouse." Agricultural and Forest Meteorology **137**(1-2): 107-118.
- Bartle, N. J. & P. D. Gosling (2010). "Numerical formulations for the prediction of deformation, strain and stress of un-patterned ETFE cushions." Computers, Materials and Continua **20**(1): 19-62.
- Bath, U. o. (2014). "Energy, sustainability and the environment - East Building " Retrieved 2014, from <http://www.bath.ac.uk/estates/energy/eastbuildingbreeam.shtml>.
- Berdahl, P. & R. Fromberg (1982). "The thermal radiance of clear skies." Solar Energy **29**(4): 299-314.
- Berliand, M. E. & T. G. Berliand (1952). "Determining the net long-wave radiation of the Earth with consideration of the effect of cloudiness." Izvestiya Akademii Nauk SSSR Seriya Geofizicheskaya **1**.
- Berroug, F., E. K. Lakhal, M. E. Omari, M. Faraji & H. E. Qarnia (2011). "Numerical Study of Greenhouse Nocturnal Heat Losses." Journal of Thermal Science **20**(4): 377-384.
- Boedeker.com (2012). Polystyrene Specifications.
- Borgart, A. (2010). "An Approximate calculation method for air inflated cushion structures for design purposes." International journal of space structures **25**(2): 83-91.
- Brauer, G. (1999). "Large area glass coating." Surface & Coatings Technology **112**(1-3): 358-365.

- Brundt, D. (1932). "Notes on the radiation in the atmosphere." Quarterly Journal of the Royal Meteorological Society **58**(247): 389-418.
- Budyko, M. I. & D. H. Miller (1974). Climate and life. New York ; London, Academic Press
- Bugaev, S. P. & N. S. Sochugov (2000). "Production of large-area coatings on glasses and plastics." Surface and Coatings Technology **131**(1-3): 474-480.
- buildingskins (2010). Plastics + ETFE. Buildingskins's Blog.
- Burek, S. A. M., B. Norton & S. D. Probert (1989). "Transmission and forward scattering of insolation through plastic (transparent and semi-transparent) materials." Solar Energy **42**(6): 457-475.
- Callister, W. & D. Rethwisch (2011). Materials science and engineering, John Wiley.
- Campo, E. A. (2008). Selection of Polymeric Materials - How to Select Design Properties from Different Standards, William Andrew Publishing/Plastics Design Library.
- Capper, G., J. Matthews & S. Lockley (2012). Incorporating embodied energy in the BIM process. CIBSE ASHRAE Technical Symposium. Imperial College.
- Charbonneau, L., M. A. Polak & A. Penlidis (2014). "Mechanical properties of ETFE foils: Testing and modelling." Construction and Building Materials **60**: 63-72.
- Chen, B., J. Maloney, D. Clark, W. Ning Mei & J. Kasher (2013). Measurement of night sky emissivity in determining radiant cooling from cool storage roofs and roof ponds. Omaha, Nebraska, University of Nebraska at Omaha.
- Chen, X.-Y., W. Yuan, F. Ai, H. Li & L. Li (2012). "Melt rheological properties of ETFE: an attempt to illuminate the fluorine-substitution effect." Polymer bulletin **69**(3): 375-388.
- Chilton, J. (2013). "Lightweight envelopes: ethylene tetra-fluoro-ethylene foil in architecture " Proceedings of the Institution of Civil Engineers, Construction Materials **166**(CM6): 343-357.
- CIBSE (2004). Environmental performance toolkit for glazed facades CIBSE 2004. Heat transfer. United Kingdom.
- CIBSE (2006). Environmental Design CIBSE Guide A. Heat transfer. United Kingdom.
- Clarke, J. A., M. Janak & P. Ruyssevelt (1998). "Assessing the overall performance of advanced glazing systems." Solar Energy **63**: 231-241.
- Cremers, J. (2009). Integration of photovoltaics in membrane structures Detail, Das Architekturportal.
- Critten, D. & B. Bailey (2002). "A review of greenhouse engineering developments during the 1990s." Agricultural and Forest Meteorology(112): 1–22.
- CWCT (2010). Technical Note No. 61 Glass Types, Centre for Window and Cladding Technology.
- CWCT (2010). Technical Note No. 62 Specification of insulating glass units, Centre for Window and Cladding Technology.
- Daikin (2013). Neoflon EFEP RP-Series.
- DesignBuilder. (2014). from <http://www.designbuilder.co.uk/content/view/154/226/>.

- Desmarais, G., C. Ratti & G. S. V. Raghavan (1999). "Heat transfer modelling of screenhouses." Solar Energy **65**(5): 271-284.
- DuPont (2011). Tefzel® Properties Handbook.
- DuPont (2012). DuPont Teflon films for photovoltaic modules.
- Eames, P. (2009). Multi-foil Insulation BD2768. D. f. C. a. L. Government. United Kingdom.
- EcoTect, A. (2014). from <http://usa.autodesk.com/ecotect-analysis/>.
- Energy, P. N. I. O. f. t. U. S. D. o. (1978). Annual Report on the Characterization of High-Level Waste Glasses.
- Energy, U. D. o. (2012). Estimating Appliance and Home Electronic Energy Use.
- Energy, U. D. o. (2014). "Building Energy Software Tools Directory." from http://apps1.eere.energy.gov/buildings/tools_directory/software.cfm/ID=391/pagename_submenu=energy_simulation/pagename_menu=whole_building_analysis/pagename=subjects.
- EnergyPlus (2012). EnergyPlus Engineering Reference - The Reference to EnergyPlus Calculations, U.S. Department of Energy.
- EnergyPlus (2013). Weather Data, U.S. Department of Energy.
- ESP-r. (2014). from <http://www.esru.strath.ac.uk/Programs/ESP-r.htm>.
- Espi, E. (2006). "New ultrathermic films for greenhouse covers." Journal of plastic film and sheeting **22**(1): 59-68.
- Fantronix. (2013). "Silenta Extractor Fan - 100mm 4". 2013, from http://www.fantronix.com/acatalog/Silent_Toilet_Extractor_Fan_100mm.html.
- Fermilab (2013). Material Emissivity Properties, U.S. Department of Energy.
- Feuilleley, P. & G. Issanchou (1996). "Greenhouse Covering Materials Measurement and Modelling of Thermal Properties Using the Hot Box Method, and Condensation Effects." Journal of Agricultural Engineering Research **65**(2): 129-142.
- Foiltec, V. (2011). 2011, from <http://www.vector-foiltec.com/en/home.html>.
- Galli, C. (2004). "Radiative energy partition and cloud radiative forcing at a Po valley site." Atmospheric research **72**(1): 329-351.
- Galliot, C. & R. H. Luchsinger (2011). "Uniaxial and biaxial mechanical properties of ETFE foils." Polymer Testing **30**(4): 356-365.
- Geoola, F., Y. Kashti, A. Levi & R. Brickman (2009). "A study of the overall heat transfer coefficient of greenhouse cladding materials with thermal screens using the hot box method." Polymer Testing **28**(5): 470-474.
- Ghoshdastidar, P. S. (2004). Heat transfer. New Delhi ; Oxford Oxford University Press.
- Gorokhovskiy, A., H. I. Escalante Garcia & V. Gorokhovskiy (2000). "Mechanical strength of float glass: test results analysis and the nature of differences." Glass Science and Technology: Glastechnische Berichte **73**(11): 344-350.
- Government, H. (2012). Energy Efficiency Statistical Summary D. o. E. a. C. Change. London, UK.
- Greve, A. & M. Bremer (2010). Thermal Design and Thermal Behaviour of Radio Telescopes and their Enclosures, Springer.

- Griffths, P. R. (1983). "Fourier Transform Infrared Spectrometry." Science **222**(4621): 297-302.
- Herrero, J. & M. J. Polo (2012). "Parameterization of atmospheric longwave emissivity in a mountainous site for all sky conditions." Hydrology and earth system sciences **16**(9): 3139-3147.
- Hessenkemper, H. (2002). "The improvement of mechanical strength during the glass forming process." International Glass Journal **122**.
- Hinz, S. (2007). "Automatic reconstruction of shape evolution of ETFE-foils by close-range photogrammetric image analysis." International Archives of Photogrammetry, Remote Sensing and Spatial Information Sciences **36**.
- Holman, J. P. (1963). Heat Transfer, McGraw-Hill Book Co.
- Hottel, H. C. (1954). Radiant Heat Transmission. New York McGraw-Hill.
- Hu, J., W. Chen, B. Zhao & H. Song (2014). "Experimental studies on summer performance and feasibility of a BIPV/T ethylene tetrafluoroethylene (ETFE) cushion structure system." Energy and Buildings **69**: 394-406.
- IDES (2013). NEOFLON EFEP RP-4020 I. Prospector.
- IES-VE (2013). ApacheSim calculation methods I. E. S. V. E. 6.4.
- Incopera, F. P. & D. P. DeWitt (1985). Introduction to Heat Transfer. Canada, John Wiley & Sons Inc.
- InfraredServicesInc (2013). Emissivity Values for Common Materials.
- Iziomon, M. G., H. Mayer & A. Matzarakis (2003). "Downward atmospheric longwave irradiance under clear and cloudy skies: Measurement and parameterization." Journal of Atmospheric and Solar-Terrestrial Physics **65**(10): 1107-1116.
- Jian, J. (2010). Development of a Mathematical Model for Simulating the Energy Performance of ETFE in Building Applications. Department of Architecture and Civil Engineering. Bath, University of Bath. **MEng**.
- Johnson, T. (1991). Low-E glazing design guide. Boston, USA Butterworth Architecture
- Jones, H. (2000). Radiation Heat Transfer, Oxford University Press.
- Kenmore (2013). Kenmore 50-pt. Dehumidifier
- Kimball, B. A., S. B. Idso & J. K. Aase (1982). "A MODEL OF THERMAL-RADIATION FROM PARTLY CLOUDY AND OVERCAST SKIES." Water resources research **18**(4): 931-936.
- Kipp&Zonen (2010). CGR 3 Pyrgeometer Instruction Sheet. Delft.
- Kipp&Zonen (2012). Kipp & Zonen Pyranometers.
- Kipp&Zonen (2012). Kipp & Zonen Pyrgeometers.
- Knippers, J., J. Cremers, M. Gabler & J. Lienhard (2011). Construction Manual for Polymers and Membranes. Basel, Switzerland, Birkhauser.
- Kopeliovich, D. (2011). "Polymer materials." Substances and Technologies, from http://www.substech.com/dokuwiki/doku.php?id=polymer_materials_introduction.
- Korner, W. (2011) "Measurement and Calculation of the Solar and Thermal Properties of ETFE layers."

- La Mantia, F. P. (1996). Recycling of PVC and Mixed Plastic Waste, ChemTec Publishing.
- Lampert, C. M. (1981). "Heat mirror coatings for energy conserving windows." Solar Energy Materials **6**(1): 1-41.
- LBNL (2013). Optics 6 U.S. Department of Energy.
- LeCuyer, A., I. Liddell, S. Lehnert & B. Morris (2008). ETFE, Technology and Design. Basel, Switzerland, Birkhauser Verlag AG.
- Li, D. H. W., C. C. S. Lau & J. C. Lam (2004). "Standard skies classification using common climatic parameters." Journal of solar energy engineering **126**(3): 957-964.
- Longo, G. A. & A. Gasparella (2012). "Comparative experimental analysis and modelling of a flower greenhouse equipped with a desiccant system." Applied Thermal Engineering **47**(0): 54-62.
- Lucas, J., A. Krombholz, M. Petersilge, R. Shauble & A. Heilmann (2007). "Einfluss der Materialeigenschaften auf das Einsatzverhalten von pneumatisch stabilisierten ETFE-Membrankissen
(Material properties and mechanical behaviour of pneumatically stabilized ETFE membrane cushions)." VDI- Gesellschaft Bautechnik: Bauen mit Innovativen Werkstoffen **1970**: 269-274.
- Mainini, A. G., T. Poli, R. Paolini, M. Zinzi & L. Vercesi (2014). Transparent multilayer ETFE panels for building envelope: thermal transmittance evaluation and assessment of optical and solar performance decay due to soiling. . SHC 2013, International Conference on Solar Heating and Cooling for Buildings and Industry Freiburg, Germany, Energy Procedia. **48**: 1302-1310.
- Mangonon, P. L. (1999). The principles of materials selection for engineering design. London, Upper Saddle River, N.J. : Prentice Hall; London : Prentice-Hall International
- Masters. (2013). "Gravity Louvred Wall Vent 100mm." 2013, from <http://www.masters.com.au/product/900007149/gravity-louvred-wall-vent-100mm>.
- Max, J. F. J., G. Reisinger, T. Hofmann, J. Hinken, H.-J. Tantau, A. Ulbrich, S. Lambrecht, B. von Elsner & U. Schurr (2012). "Glass–film-combination: Opto-physical properties and energy saving potential of a novel greenhouse glazing system." Energy and Buildings **50**(0): 298-307.
- Michalsky, J., E. Dutton, M. Rubes, D. Nelson, T. Stoffel, M. Wesley, M. Splitt & J. DeLuisi (1999). "Optimal Measurement of Surface Shortwave Irradiance Using Current Instrumentation." Journal of Atmospheric and Oceanic Technology **16**(1): 55-69.
- Minamisawa, R. A., V. Abidzina, A. d. Almeida, S. Budak, I. Tereshko, I. Elkin & D. Ila (2007). "Radiation effects on ETFE polymer exposed to glow discharge." Nuclear Instruments and Methods in Physics Research(B 261): 715–718.
- Miskeen, R. (2009). Vision 2020 with ETFE - Better understanding of the material and its advancing technologies. Architecture and Civil Engineering. Bath, Univeristy of Bath. **Master of Science Degree In Façade Engineering**.
- Miskeen, R. (2009). Vision 2020 with ETFE - Better understanding of the material and its advancing technologies Architecture and Civil Engineering. Bath, Univeristy of Bath. **Master of Science Degree In Façade Engineering**: 173.

- Modest, M. (2003). Radiative Heat Transfer. Amsterdam ; Boston, Academic Press.
- Mohelnikova, J. (2009). "Materials for reflective coatings of window glass applications." Construction and Building Materials **23**(5): 1993-1998.
- Monteith, J. L. (1973). Principles of environmental physics. London, Edward Arnold.
- Newborough, M. & P. Augood (1999). Demand-side management opportunities for the UK domestic sector. Generation, Transmission and Distribution, IEE.
- NOVUM, S. (2011). ETFE Information. NOVUM Structures.
- NPL (2012). Thermal Transmittance, National Physical Laboratory.
- Oshima, A., S. Ikeda, T. Seguchi & Y. Tabata (1997). "Temperature effect on radiation induced reactions in ethylene and tetrafluoroethylene copolymer (ETFE)." Radiation Physics and Chemistry **50**(5): 519-522.
- Papadakis, G., D. Briassoulis, G. Scarascia Mugnozza, G. Vox, P. Feuilloy & J. A. Stoffers (2000). "Radiometric and Thermal Properties of, and Testing Methods for, Greenhouse Covering Materials." Journal of Agricultural Engineering Research **77**(1): 7-38.
- Perez, R., R. Seals & J. Michalsky (1993). "All-weather model for sky luminance distribution--Preliminary configuration and validation." Solar Energy **50**(3): 235-245.
- PerkinElmer (2005). Spectrum 100 Series, User's Guide. PerkinElmer. Bucks, United Kingdom.
- PerkinElmer (2008). Spectrum 100 Optica. Demonstrating the accuracy of transmittance measurements for high refractive index materials. Technical Note - Infrared Spectroscopy. PerkinElmer.
- Plexiglas (2011). Plexiglas properties handbook. A. INTERNATIONAL.
- Poirazis, H., M. Kragh & C. Hogg (2010). Energy modelling of ETFE membranes in building applications - Gathering material properties. XI International IBPSA Conference. Glasgow, ARUP.
- Read, F. H. (1985). Electromagnetic radiation, John Wiley & Sons.
- ReoTEMP. (2014). from <http://reotemp.com/thermocoupleinfo/thermocouple-accuracies.htm>.
- Robert, S. & H. J. R (1981). Thermal radiation heat transfer. USA, Hemisphere Publishing Corporation
- Robertson, T. (2011). "Forsyth barr stadium - Dunedin, New Zealand - A new fully roofed rugby stadium for otago." The structural engineer **89**(17): 14-22.
- Robinson-Gayle, S., M. Kolokotroni, A. Cripps & S. Tanno (2001). "ETFE foil cushions in roofs and atria." Construction and Building Materials **15**(7): 323-327.
- Robinson, L. (2005). Structural opportunities of ETFE (ethylene tetra fluoro ethylene). Massachusetts Institute of Technology, Dept. of Civil and Environmental Engineering. Massachusetts, University of Massachusetts. **M. Eng.:** 54.
- Schöne, L. (2007). "Bauen mit ETFE-Folien – Ein Praxisbericht." Stahlbau **76**(5): 305-313.
- Schween, T. & S. Lehnert (2007). "Dach-und Wandgestaltung mit pneumatisch vorgespannten Kissen aus ETFE

- (Roof and Wall Claddings made of pneumatically prestressed ETFE Foil Cushions)." VDI Berichte **1970**: 129-140.
- Scigiene, C. (2013). Infrared Thermometer Emissivity tables.
- Sedlar, J. & R. Hock (2009). "Testing longwave radiation parameterizations under clear and overcast skies at StorglaciÅren, Sweden." The Cryosphere **3**(1): 9.
- Siegel, R. & J. R. Howell (1972). Thermal Radiation Heat Transfer. USA Hemisphere Publishing Corporation
- Smith, G. B., S. Dligatch & F. Jahan (1998). "Angular selective thin film glazing." Renewable Energy **15**(1-4): 183-188.
- SOLARNEXT. (2013). "PV Flexibles Integrated in ETFE Foil Construction ", from <http://www.solarnext.eu/eng/ref/envelopeprojects.shtml>.
- Standards, B. (1997). BS ISO 15469:1997 Spatial distribution of daylight - CIE standard overcast sky and clear sky, BSI Standards Publication.
- Standards, B. (2004). BS ISO 15469:2004 Spatial distribution of daylight - CIE standard general sky, BSI Standards Publication.
- Standards, B. (2007). BS ISO 20473:2007 Optics and photonics - Spectral bands.
- Standards, B. (2012). BS EN ISO 22007-1:2012, Plastics – Determination of thermal conductivity and thermal diffusivity Part 1: General principles (ISO 22007-1:2009), BSI Standards Publication.
- Star, E. (2012). Energy Star Products - Dehumidifiers
- Statistics, N. (2005). Monthly Statistics of Building Materials and Components. D. o. T. Industry. Essex, United Kingdom, Tudorseed Construction Limited.
- Statistics, N. (2010). Monthly Statistics of Building Materials and Components. I. S. Department for Business. London, United Kingdom, Construction Statistics.
- Stensrud, D. J. (2007). Parameterisation schemes: Keys to understanding numerical weather prediction models, Cambridge University Press.
- Stephens, G. (2012). "The global character of the flux of downward longwave radiation." Journal of Climate **25**(7): 2329-2340.
- Stine, W. B. & R. W. Harrigan (1985). Solar energy fundamentals and design, John Wiley & Sons, Incorporated.
- Tanno, S. (1997). ETFE foil cushions as an alternative to glass for atriums and rooflights. The International Conference on Building Envelope Systems and Technologies. London, United Kingdom: 358-362.
- Tas, E. (2014). from <http://www.edsl.net/main/>.
- Tefzel®210, D. (2012). DuPont Tefzel® 210 Product Information
- Thermometrics. (2014). "Precision Temperature Sensors." from <http://www.thermometricscorp.com/thertypk.html>.
- Toolbox, E. (2013). Heat radiation from a black body - surroundings absolute zero.
- Toyoda, M. (2010). Rainfall noise from ethylene/tetrafluoroethylene aircushion-membrane structures
- 39th International Congress on Noise Control Engineering 2010, INTER-NOISE 2010.

- Toyoda, M. & D. Takahashi (2013). "Reduction of rain noise from Ethylene/TetraFluoroEthylene membrane structures." Applied Acoustics(74): 1309–1314.
- TRNSYS. (2014). from <http://sel.me.wisc.edu/trnsys/features/features.html>.
- Tsilingiris, P. T. (2003). "Comparative evaluation of the infrared transmission of polymer films." Energy Conversion and Management **44**(18): 2839-2856.
- UDEL (2014). University of Delaware, 2014, Department of Geography.
- Umwelt, I. B. u. (2011). Environmental Product Declaration – Texlon System. Königswinter, Germany.
- University of Missouri, D. o. A. (1993). Active Solar Collectors for Farm Buildings - Table 2: Radiant energy absorption and emittance for several surface materials.
- Vector (2012). Texlon material properties data sheet. E. A. Dimitriadou.
- Vector (2013). Texlon: Thermal Properties.
- Wang, L., M. R. Kamal & A. D. Key (2001). "Light transmission and haze of polyethylene blown thin films." Polymer Engineering and Science **41**(2 SPEC. ISS): 358-372.
- Ward, T. I. & S. M. Doran (2005). The thermal performance of multi-foil insulation. United Kingdom, BRE.
- Wong, L. T. & W. K. Chow (2001). "Solar radiation model." Applied Energy **69**: 191–224.
- Wu, H. & J. Fan (2008). "Measurement of radiative thermal properties of thin polymer films by FTIR." Polymer Testing **27**(1): 122-128.
- Wu, M., Y. Wu & J.-Y. Kim (2011). "ETFE foil spring cushion structure and its analytical method." Thin-Walled structures.
- WUFI. (2013). "WUFI wiki - Conversation of Radiation Data for other Directions." 2013, from <http://www.wufi-wiki.com/mediawiki/index.php5/Details:LongWaveExchange>.
- Yin-ping, Z. & G. Xin-shi (1995). "A new method for determination of the optical constants and thermal radiation properties of semi-transparent films." Solar Energy Materials and Solar Cells **37**(3-4): 379-387.
- Zhang, D. & X. Gao (2012). "The Performance of Tensile Properties of ETFE Membranes at Different Temperatures Sustainable Development of Urban Environment and Building Material." Advanced Materials Research **374-377**: 1800-1804.
- Zhang, Y., L. Gauthier, D. de Halleux, B. Dansereau & A. Gosselin (1996). "Effect of covering materials on energy consumption and greenhouse microclimate." Agricultural and Forest Meteorology **82**(1-4): 227-244.
- Zheng, Y., E. K. Yanful & A. S. Bassi (2005). "A Review of Plastic Waste Biodegradation." Critical Reviews in Biotechnology **25**(4): 243-250.

Appendix A: Trade values for construction materials and components

Table A. 1: Value of overseas trade for the United Kingdom in materials and components for constructional use: Imports (cost, insurance, freight) & Exports (freight on board) in thousand Pounds (Statistics, 2005; Statistics, 2010)

	1998	1999	2000	2001	2002	2003
Plastic building products						
Imports	47,829	54,727	66,374	72,944	76,035	87,149
Exports	83,971	100,106	84,347	96,746	85,262	82,280
Flat glass						
Imports	70,756	76,654	70,897	63,022	74,026	67,804
Exports	52,036	42,102	42,631	52,468	36,149	41,547
	2004	2005	2006	2007	2008*	
Plastic building products						
Imports	105,632	116,565	133,409	148,828	149,234	
Exports	93,460	99,630	100,498	115,008	117,408	
Flat glass						
Imports	58,092	53,410	55,900	71,800	61,062	
Exports	44,772	51,502	67,141	83,174	107,783	

*The available data for 2008 covered the first 10 months of the year. In reality, the presented numbers would be expected to be slightly higher for the entire year.

Appendix B: Long-wave radiation and emissivity

The available models generally tend to underestimate L_{\downarrow} values, and model accuracy is higher for clear skies, followed in precision classification by completely overcast and lastly by partially cloudy skies. More specifically, the available models tend to agree for downward long-wave values between 260 and 300 W/m², demonstrating a small deviation of the prediction model from measured results. In particular, clear sky models tend to overestimate results for clear daytime and underestimate results for night-time. To resolve this issue correction factors have been developed, which are, again, experimentally determined (Alados, 2012). An underestimation of approximately -5 W/m² is observed for L_{\downarrow} values varying between 310 and 350 W/m² and an underestimation of -10 to -15 W/m² for downward long-wave values above 350 W/m², (Sedlar *et al.*, 2009).

Kimball *et al.* (1982) developed a model of thermal radiation from partly cloudy and overcast skies involving an empirical constant k , varying with cloud type in combination with the fractional area of sky that is covered by clouds. Arnfield (1979) discussed on the various cloud types in relation to the k empirical constant and Stephens (2012) on the height of cloud layers in relation to mean long-wave values.

Bruntt (1932) developed Equation 4.9 through investigating the association between the net long-wave radiation under a clear sky and the temperature and humidity of the air, which was expressed in the Equation B.1.

$$L_o = \varepsilon_o * \sigma * T_a^4 * (a - b * \sqrt{e}) \quad \text{Equation B.1}$$

L_o : Long-wave radiation under a clear sky (W/m²)

ε_o : Clear sky emissivity, the average value of which is defined here as 0.7

σ : Stefan-Boltzmann constant ($5.67 \cdot 10^{-8}$ W/m²K⁴)

T_a^4 : Air temperature (K)

a, b : Experimentally derived coefficients

e : Water vapour pressure (mm Hg) (where mm Hg=133.32 Pascal)

More specifically, clear sky emissivity ε_o was later experimentally defined by Berdahl *et al.* (1982) as in Equation B.2.

$$\varepsilon_o = 0.741 + 0.0062 * T_{dp} \quad \text{Equation B.2}$$

ε_o : Clear sky emissivity

T_{dp} : Dew point temperature (°C)

To estimate T_{dp} (NOAA, 2013):

$$e_s = 6.112 * e^{\frac{17.67 * T_a}{T_a + 243.5}}$$

$$e = \frac{RH * e_s}{100}$$

$$T_{dp} = \frac{243.5 * \ln\left(\frac{e}{6.112}\right)}{17.67 - \ln\left(\frac{e}{6.112}\right)}$$

e_s : Saturated water vapour pressure

e : Actual vapour pressure

RH : Relative humidity

Equation B.2 was applied to the data set described previously in this chapter, with the intention of then inserting the clear sky emissivity values in Equation B.1. Results for clear sky emissivity ranged between 0.69 and 0.73. The average value for ε_o was found to be 0.71, close to the suggested value of 0.7 by Sedlar (2009). However, as an empirically defined formula, there was a concern that the range of results provided by Equation B.2 was too wide.

Further research by Chen *et al.* (2013) focused on developing a relationship between night sky emissivity and dew point temperatures. The findings of this research also indicate that the formula provided by Berdahl *et al.* (1982) does not necessarily match all data groups. Nonetheless, Equation B.2 is often referenced in bibliography and frequently cited in research papers.

Following the formula of Brundt (Equation 4.9), Berliand *et al.* (1952) defined the dependence of clear sky net long-wave radiation upon air temperature and humidity as following (Equation B.3):

$$L_o = \delta * \sigma * T_{air}^4 * (0.39 - 0.058 * \sqrt{e}) \quad \text{Equation B.3}$$

L_o : Long-wave radiation under a clear sky (W/m²)

δ : Coefficient whose value varies little for different surfaces. Therefore, its mean value 0.95 is used for calculations

σ : Stefan-Boltzmann constant (5.67*10⁻⁸ W/m²K⁴)

T_{air} : Air temperature (K)

e : Water vapour pressure (mm Hg) (where 1 bar = 750.06 mm Hg)

Water vapour pressure has been alternatively formulated as an expression of dew point temperature, as in the following Equation B.4 (Budyko *et al.*, 1974).

$$e = \exp\left(20.386 - \frac{5132}{T_{dp}}\right) \quad \text{Equation B.4}$$

e : Water vapour pressure (mm Hg)

T_{dp} : Dew point temperature (°C)

To take into account the presence of clouds, net long-wave radiation is influenced by the amount of clouds detected and the temperature difference between the surface and the air. Equation B.5 expresses the effect of cloudiness on net long-wave radiation (Budyko *et al.*, 1974; Kimball *et al.*, 1982).

$$L_{net} = L_o * (1 - n * \zeta) \quad \text{Equation B.5}$$

L_{net} : Net long-wave radiation with the presence of clouds (W/m²)

L_o : Long-wave radiation under a clear sky (W/m²)

n : Cloud fraction, the amount of cloud presence in percentage of unity

ζ : Experimentally defined coefficient

Berliand *et al.* (1952) estimated the mean latitudinal value of ζ for 50 °N (close to the geographical latitude 51.38 °N for Bath, UK) to be 0.72, whereas Ångström (1916) found the overall average value of ζ to be 0.75.

The ζ coefficient was examined and estimated for the particular location at the University of Bath to be 0.78. The coefficient was derived through Equation B.5, using measured net long-wave radiation data throughout 2011 and 2013 under an overcast sky with a cloud fraction $n = 1$. However, as the cloud fraction n is a parameter based on observation and not measurements, the calculated coefficient could not be used to estimate L_{net} for the case of this experiment.

Clouds are responsible for a significant amount of radiation fluxes (Galli, 2004). The study of Galli *et al.* (2004) provided with the seasonal variation of downward long-wave radiation as a function of the cloud fraction n with their variances. However, the results of this particular research will not be mentioned in detail as they concern a different geographical location. There was no attempt to adjust the relationship of L_{\downarrow} to n , since

the same issue of an inability to determine the cloud fraction n occurred, as with Equation B.5.

Another way to determine the amount of cloud in the sky is through the clearness factor. The clearness factor defines the amount of cloud above a certain location, describing how many eighths of the sky is covered by clouds. The range lies between 0 Oktas for a clear sky to 8 Oktas for an overcast (Li *et al.*, 2004). The calculation of sky emissivity in relation to the clearness factor is expressed by Equation B.6 (Alados, 2012; Herrero *et al.*, 2012; Iziomon *et al.*, 2003).

$$\varepsilon = \varepsilon_0(1 + q * N^2) \quad \text{Equation B.6}$$

ε : Emissivity ($0 < \varepsilon < 1$)

ε_0 : Emissivity under a clear sky

q : Coefficient proposed by Morgan *et al.* (1971), originally set to 0.22

N : Clearness factor (Okta)

Unsworth *et al.* (1975) also determined an empirical expression for the estimation of atmospheric long-wave emission under a cloudy sky (Equation B.7) (Arnfield, 1979). Due to the influence of clouds, the effective clear sky temperature is consistently cooler than the effective overcast sky temperature (Greve *et al.*, 2010).

$$\varepsilon = \varepsilon_o + n * (1 - \varepsilon_o) * \left(\frac{T_c}{T_{air}}\right)^4 \quad \text{Equation B.7}$$

n : Cloud fraction, the amount of cloud presence in percentage of unity

T_c : Average cloud base temperature (°C)

T_{air} : Air temperature (°C)

However, there is a lack of recorded data in this case that would be required to perform calculations that are related to cloud presence. To resolve this issue, a number of methods were examined that have been developed in an attempt to estimate downward long-wave radiation from surface-observed data (Stensrud, 2007). These offer an alternative to an empirical approach, which, again, leads to less accurate results but is the best available option for this experiment. The simplest model is that by Monteith *et al.* (1975), as derived from observations taken in the English Midlands, where μ and ν are experimentally derived coefficients (Equation B.8).

$$L_{\downarrow} = \mu + \nu * \sigma * T_b^4 \quad \text{Equation B.8}$$

μ : -119±16 W/m²

ν : 1.06±0.004 W/m²

The model was tested against a large data set of recorded data throughout 2011 and 2013 for the duration of the experiment and was calibrated for the location of Bath producing Equation B.9 to match the trend of the results.

$$L_{\downarrow} = 55.15 + \mu + \nu * \sigma * T_b^4 \quad \text{Equation B.9}$$

For the same μ : -119±16 W/m²

ν : 1.06±0.004 W/m²

The dataset presented previously to describe exterior long-wave radiative conditions was used to examine the accuracy of this model. Figure B.1 demonstrates the converted downward long-wave radiation for the period under examination against the measured long-wave radiation. The model presented here is based on the average values of the coefficients μ and ν .

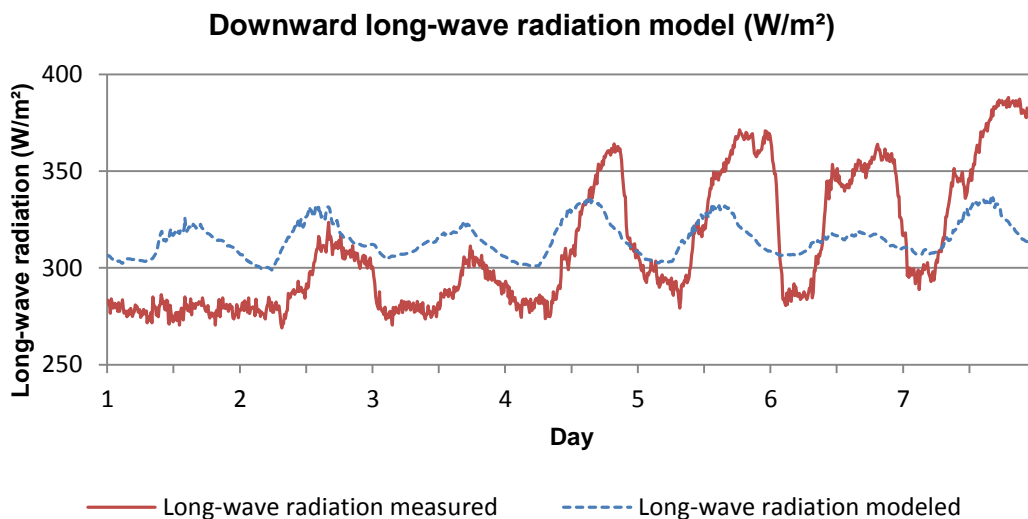


Figure B.1: Downward long-wave radiation (W/m²) model

The trend created by the model could not accurately predict downward long-wave radiation based on ground measurements; therefore the model was discounted as it overestimates clear sky values and underestimates overcast sky values. The values provided by Equation B.9 could be only be used to produce a rough approximation of

long-wave radiation through ground-based measurements for use in environmental condition modelling and analysis, such as the one that was performed using IES in Chapter 5. As a result, these outcomes are not used in the simulations performed by this research, as it is important to employ accurate radiative conditions to explore and model successfully, the thermal nature of the ETFE membrane. The above referenced long-wave data remain only for the validation of the models found in the literature.

Appendix C: Detailed measurements of experimental interior conditions

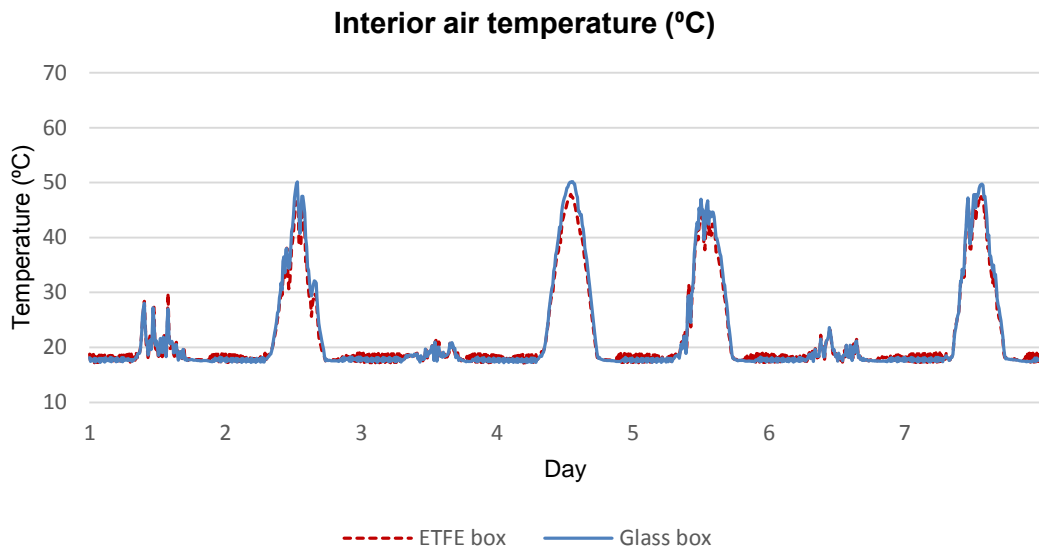


Figure C. 1: Interior air temperature (°C) for both boxes in ten minute intervals

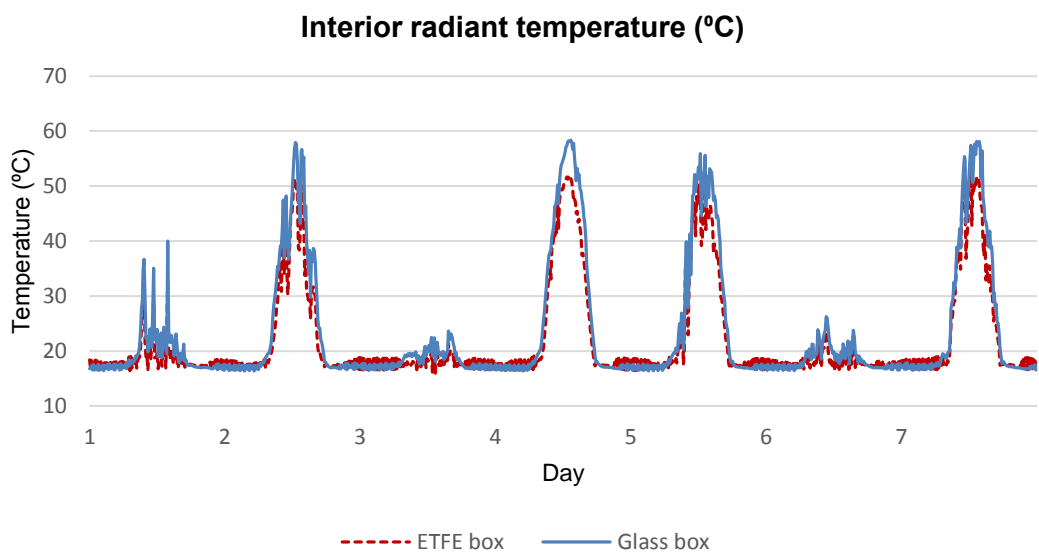


Figure C. 2: Interior radiant temperature (°C) for both boxes in 10 minute intervals

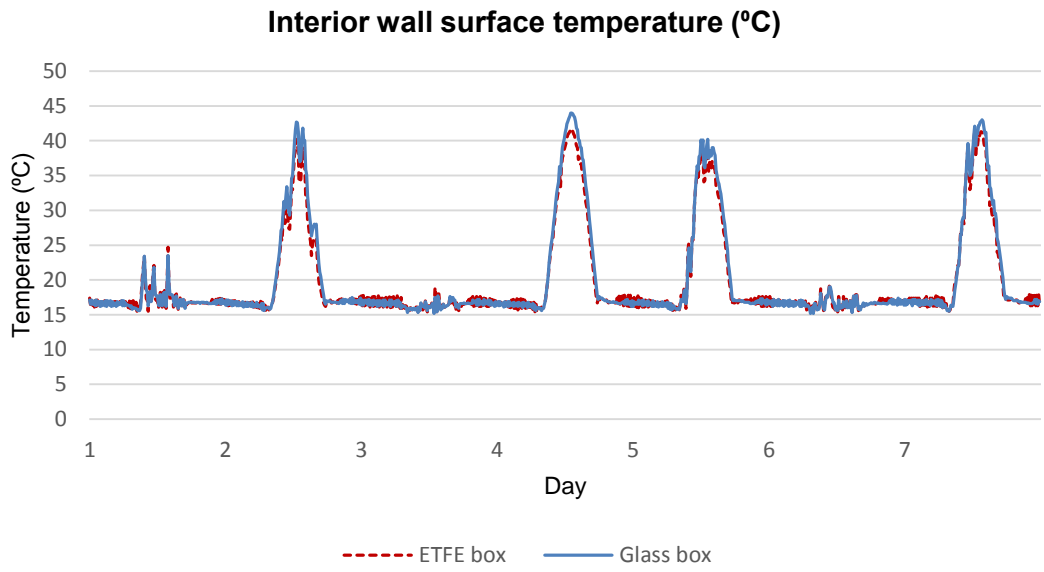


Figure C. 3: Interior wall surface temperature (°C) for both boxes in 10 minute intervals

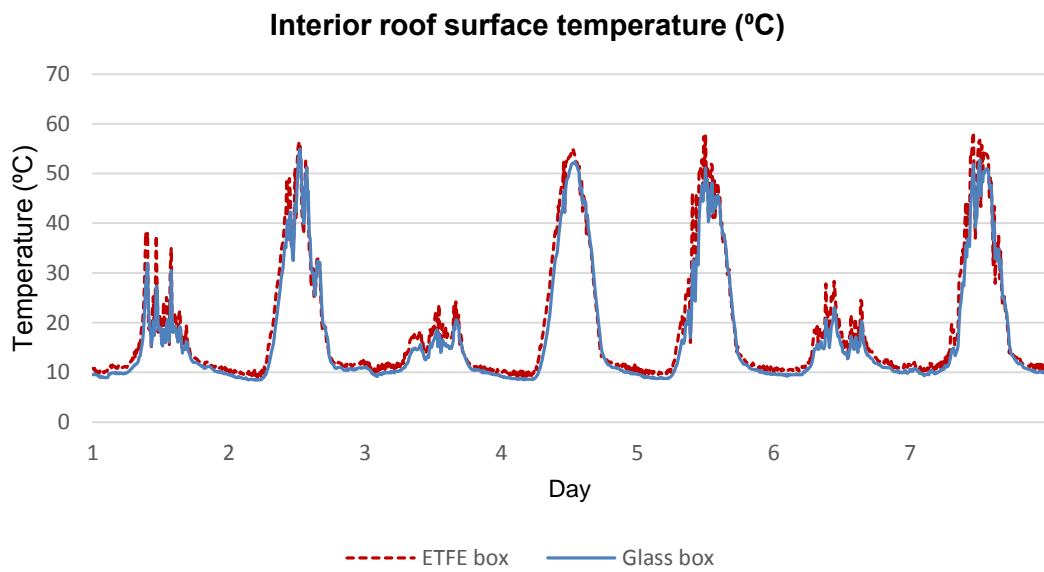


Figure C. 4: Interior roof surface temperature (°C) for both boxes in 10 minute intervals

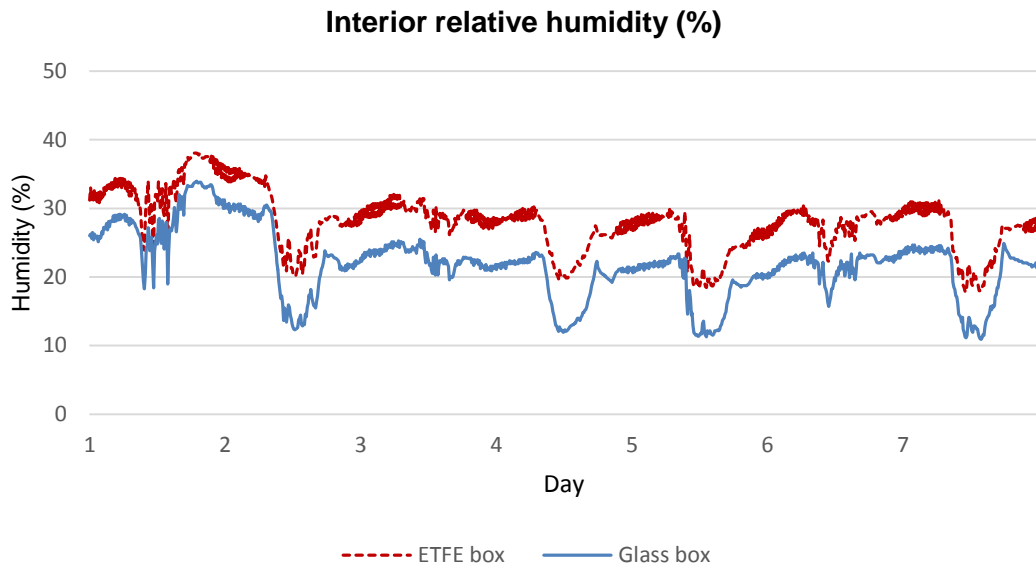


Figure C. 5: Interior relative humidity (%) for both boxes in 10 minute intervals

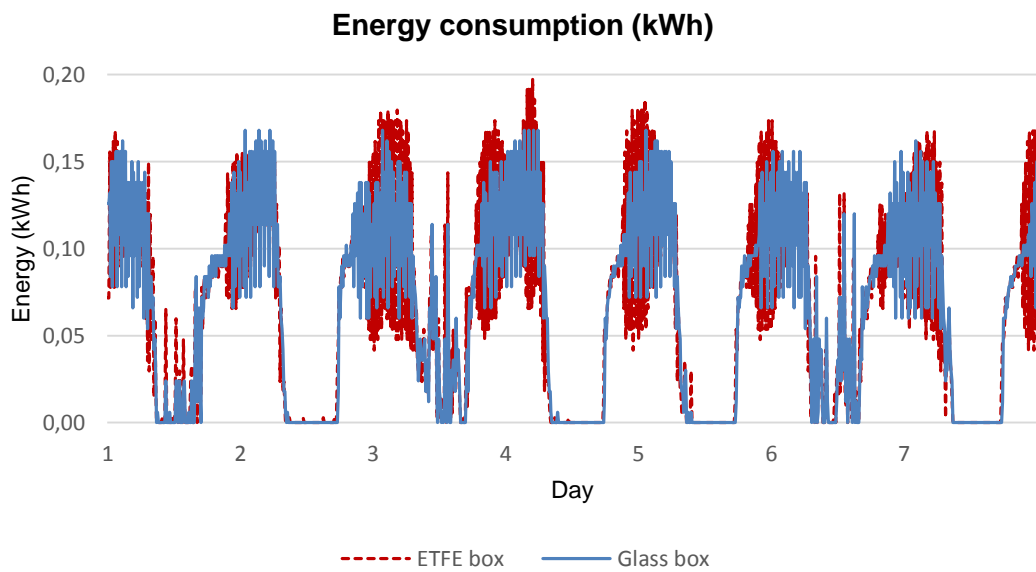


Figure C. 6: Energy consumption (kWh) for both boxes in 10 minute intervals

Appendix D: Calculation of the U-value of the two-layered ETFE cushion

The calculation of the U-value for the ETFE cushion, based on BS EN 673-2011 (2011) on the calculation of the U-value for glass, results to Equation D.1:

$$\frac{1}{U} = \frac{1}{h_e} + \frac{1}{h_b} + \frac{1}{h_i} \quad \text{Equation D.1}$$

Where h_e and h_i are external and internal heat transfer coefficients and h_b is the thermal conductance coefficient of the air trapped inside the ETFE cushion.

To perform calculations according to the Standard, it is assumed that the layers of the ETFE cushion are flat and parallel to each other, as in the case of a glass unit. Furthermore, when referring to the thickness of the air trapped inside the cushion, it will be described using an average value of 100 mm to cover the difference between 0 (around the cushion edges) and 200 mm (at the cushion's maximum camber). Finally, each material is considered to be thermally homogeneous.

As there are several unknown factors that are needed to calculate h_b with accuracy – such as the mean absolute temperature of the air inside the cushion and the temperature difference between the ETFE surfaces bounding the air space; an assumption is made and a pre-estimated value is used for the thermal conductance of air. According to Table 2 of BS EN 6946 (the standard on calculation of thermal resistance and transmittance) (2007), the thermal resistance of an unventilated air layer with high emissivity surfaces for an (average) thickness of 100mm and an upward direction of heat flow is given as $R_b = 0.16 \text{ m}^2 \text{ K/W}$. This results to a thermal conductance coefficient of air: $h_b = \frac{1}{R_b} = \frac{1}{0.16} = 6.25 \text{ W/(m}^2\text{K)}$.

According to BS EN 6946 (2007), the external heat transfer coefficient is a function of the wind speed near the ETFE membrane, the emissivity and other climatic factors, such as the temperature of the surface and its surroundings (Equation D.2):

$$h_e = h_{ce} + h_{re} \quad \text{Equation D.2}$$

h_{ce} is the external convective coefficient and h_{re} is the external radiative coefficient, where:

$$h_{ce} = 4 + 4v$$

Where v is the wind speed adjacent to the surface, in m/s. Throughout the experiment, for an internal-external temperature difference of 10 K, the wind speed varied between 1.5-5.8 m/s. The average wind speed 3.1 m/s will be used, which gives an external convective coefficient of:

$$h_{ce} = 4 + 4 * 3.1 = 16.23 \text{ W}/(\text{m}^2\text{K})$$

To estimate the radiative heat transfer coefficient h_{re} , BS EN 6946 provides the following equation:

$$h_{re} = \varepsilon h_{r0} \quad \text{Equation D.3}$$

Where h_{r0} is the radiative coefficient for a black-body surface:

$$h_{r0} = 4\sigma T_m^3$$

σ : Stefan-Boltzmann constant [$5.67 * 10^{-8} \text{ W}/(\text{m}^2\text{K}^4)$]

T_m : mean thermodynamic temperature of the surface and of its surroundings, in K.

Using the experimental data, for an internal-external temperature difference of 10 K, the external mean thermodynamic temperature of the ETFE surface and its surroundings was 286.7 K (or 12.5 °C) (the internal ETFE foil surface temperature was used, in the absence of an external surface temperature), which gives us an h_{re0} value of:

$$h_{re0} = 4 * 5.67 * 10^{-8} * 286.7^3 = 5.34 \text{ W}/(\text{m}^2\text{K})$$

BS EN 6946 recommends an approximate value of $\varepsilon = 0.9$ as appropriate for internal and external surfaces. For such an emissivity value, h_{re} results to:

$$h_{re} = 0.9 * 5.34 = 4.81 \text{ W}/(\text{m}^2\text{K})$$

The resulting external heat transfer coefficient then becomes:

$$h_e = 16.23 + 4.81 = 21 \text{ W}/(\text{m}^2\text{K})$$

According to BS EN 6946, the internal heat transfer coefficient is defined following Equation D.2, as Equation D.4:

$$h_i = h_{ci} + h_{ri} \quad \text{Equation D.4}$$

h_{ci} is the internal convective coefficient and h_{ri} is the internal radiative coefficient, where:

$$h_{ci} = 5.0 \text{ W/(m}^2\text{K)} \text{ for an upwards heat flow}$$

To estimate the radiative heat transfer coefficient h_{ri} , we will use the same equation as for the external radiative heat transfer coefficient. Using the experimental data, for an internal-external temperature difference of 10 K, the corresponding internal mean thermodynamic temperature of the surface and of its surroundings was 291.7 K (or 17.5 °C), giving the following outcome:

$$h_{ri0} = 4 * 5.67 * 10^{-8} * 291.7^3 = 5.63 \text{ W/(m}^2\text{K)}$$

For an approximate value of $\varepsilon = 0.9$ for internal and external surfaces, h_{ri} becomes:

$$h_{ri} = 0.9 * 5.63 = 5.07 \text{ W/(m}^2\text{K)}$$

The resulting internal heat transfer coefficient then becomes:

$$h_i = 5 + 5.07 = 10.07 \text{ W/(m}^2\text{K)}$$

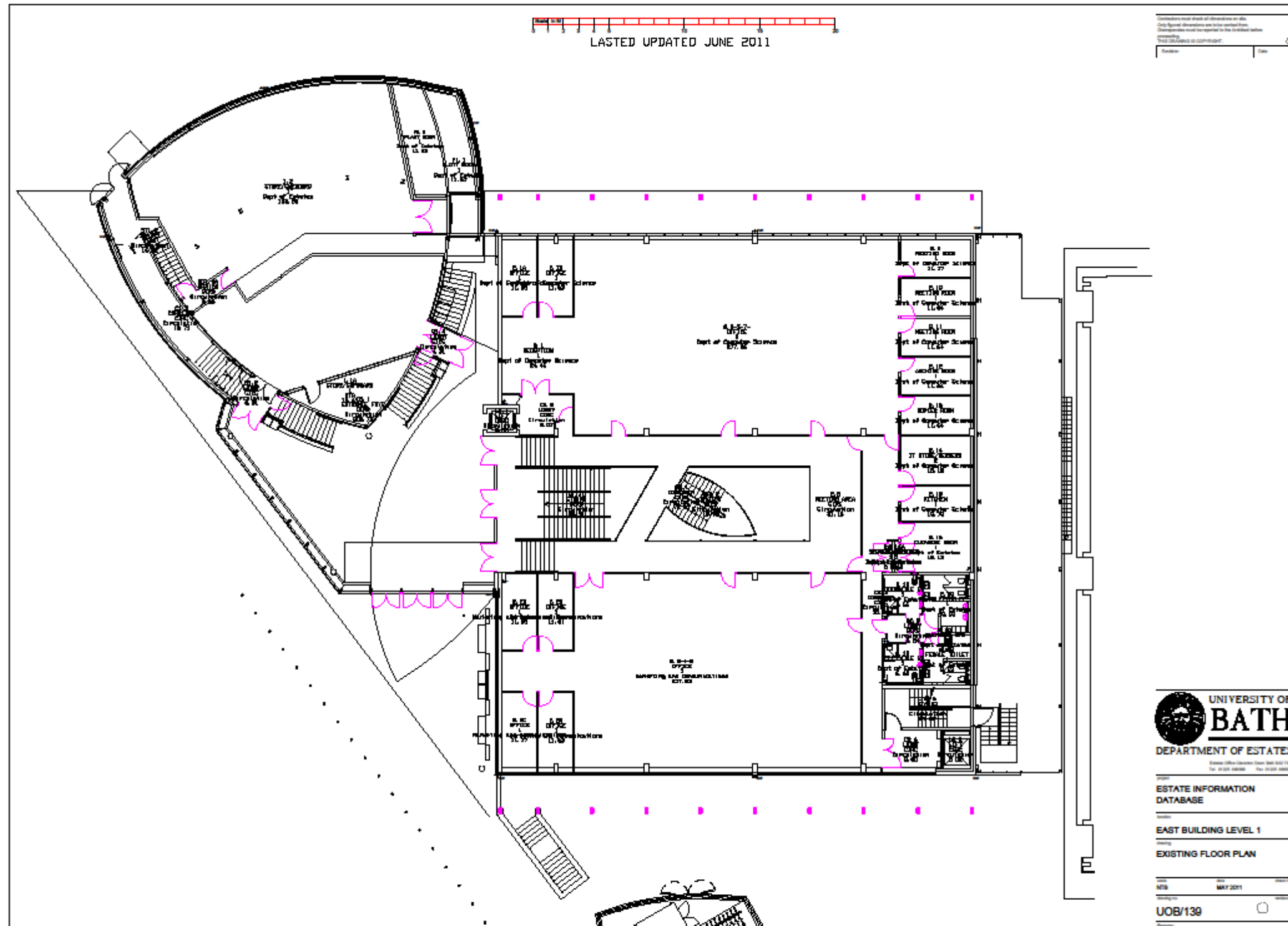
Therefore, the U-value for the ETFE cushion results to:

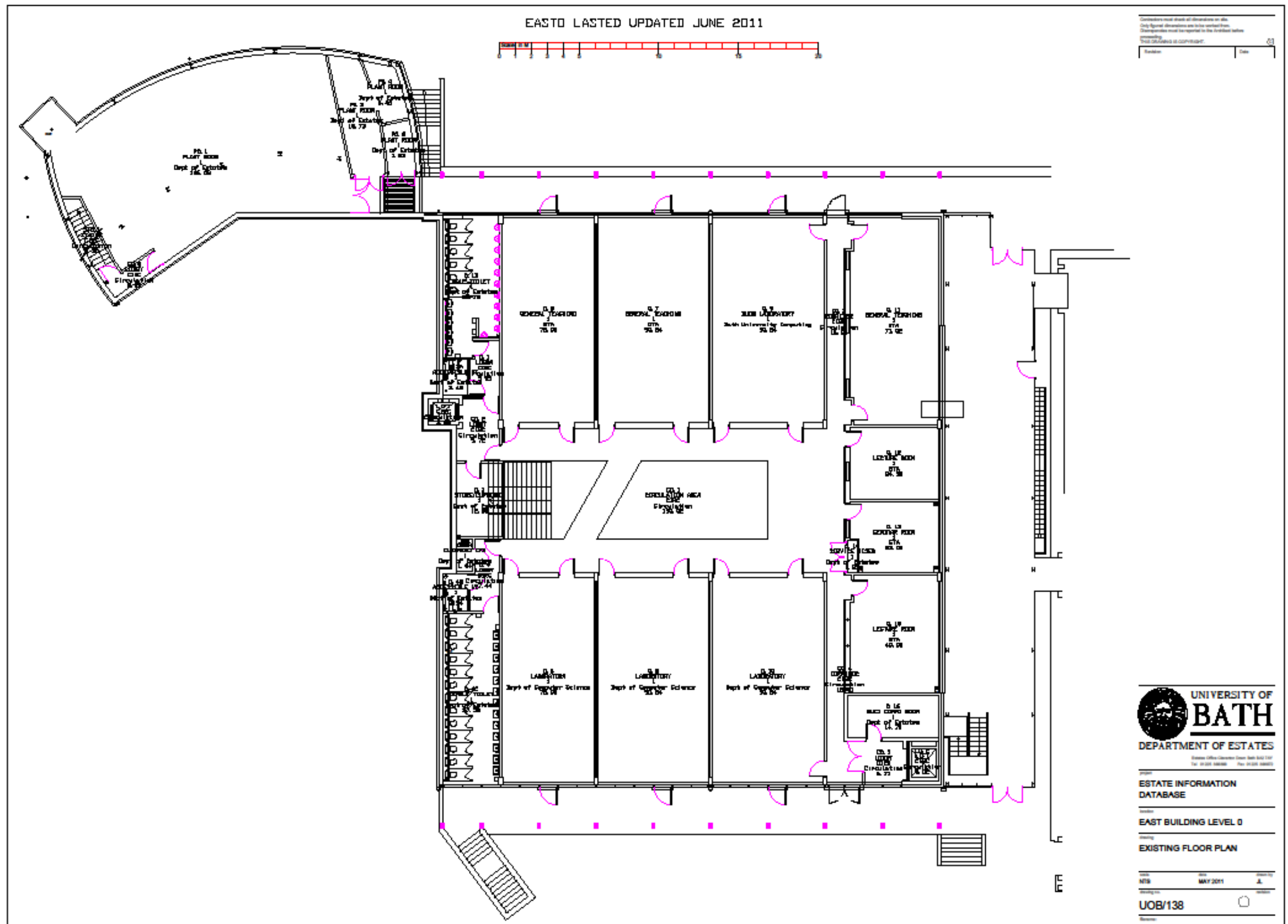
$$\frac{1}{U} = \frac{1}{h_e} + \frac{1}{h_b} + \frac{1}{h_i} = \frac{1}{21} + \frac{1}{6.25} + \frac{1}{10.07} = 0.053 + 0.16 + 0.099 = 0.31 \text{ m}^2\text{K/W}$$

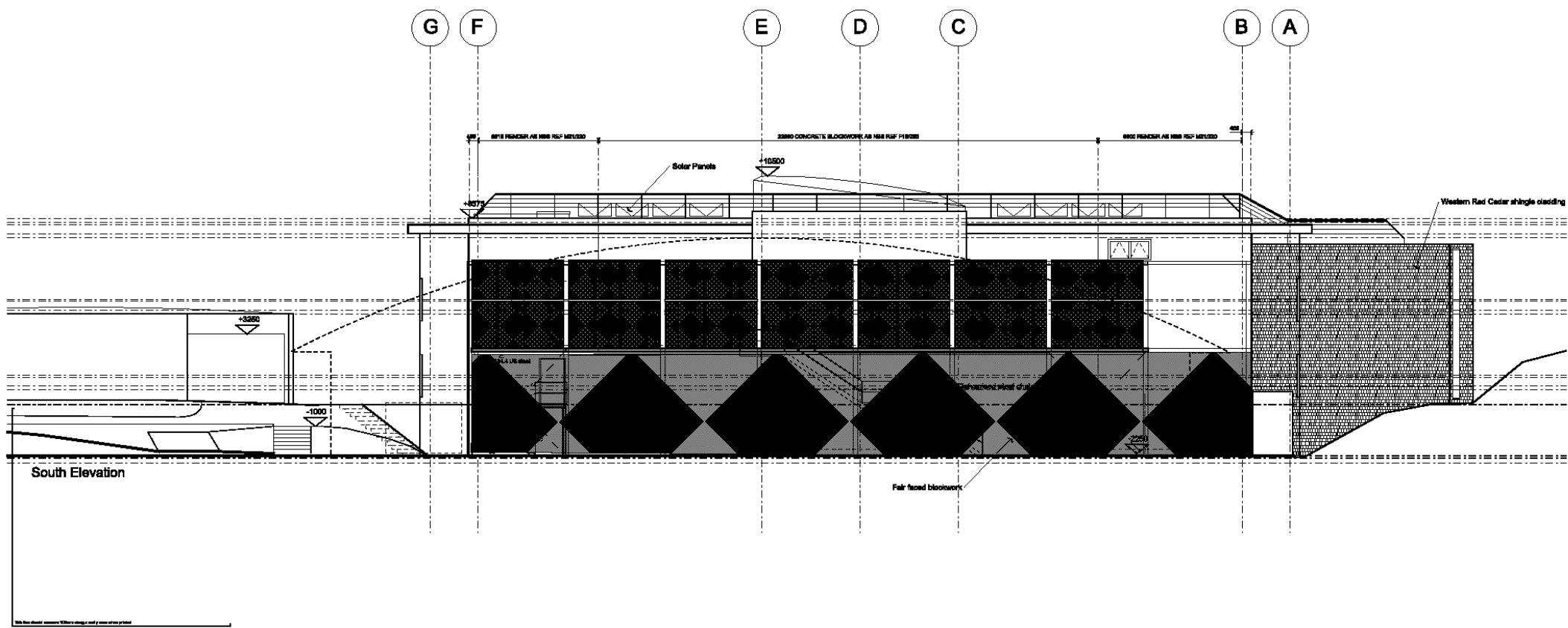
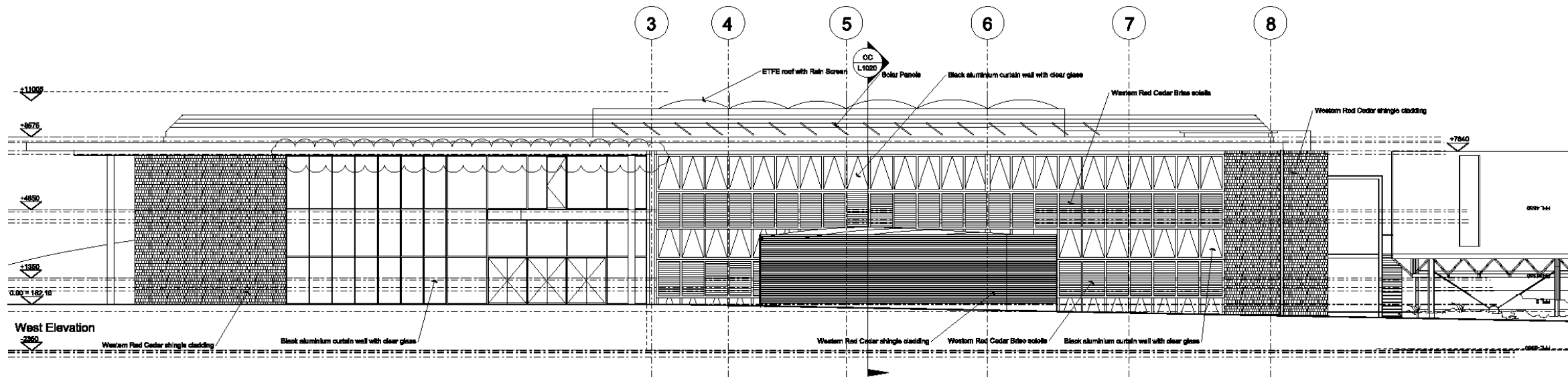
$$U = \frac{1}{0.31} = 3.2 \text{ W/(m}^2\text{K)}$$

The standard deviation was estimated between the U-value derived from each set of measurements and the estimated mean U-value for the given temperature difference, resulting to an error of 0.16 W/(m²K).

Appendix E: East Building drawings, IES default material properties and weather conditions







Revision	Date	Description	By	Appr'd
A	20.03.09	Issued for construction	lab	lab
B	20.03.09	Revised for construction	lab	lab
C	20.03.11	Revised for construction	lab	lab

CONSTRUCTION ISSUE

East Building
University Of Bath

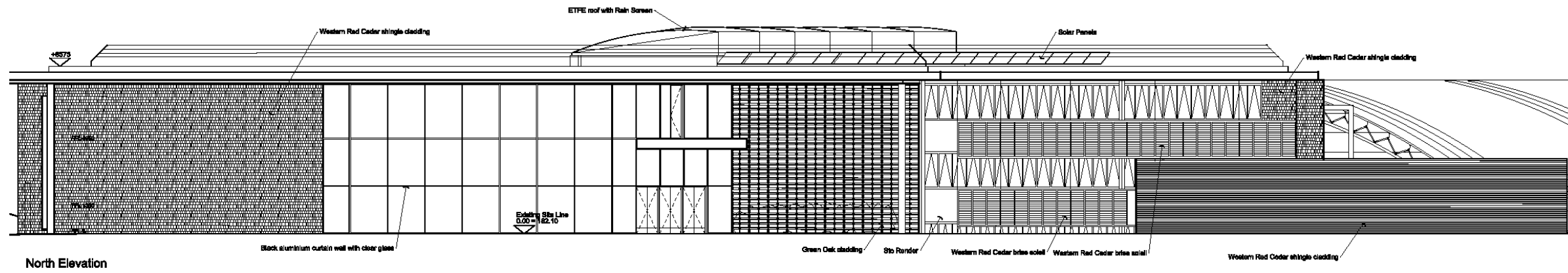
Works for
West & South Elevations
Line Drawing

Check all dimensions and verify in situ. Report any errors or omissions

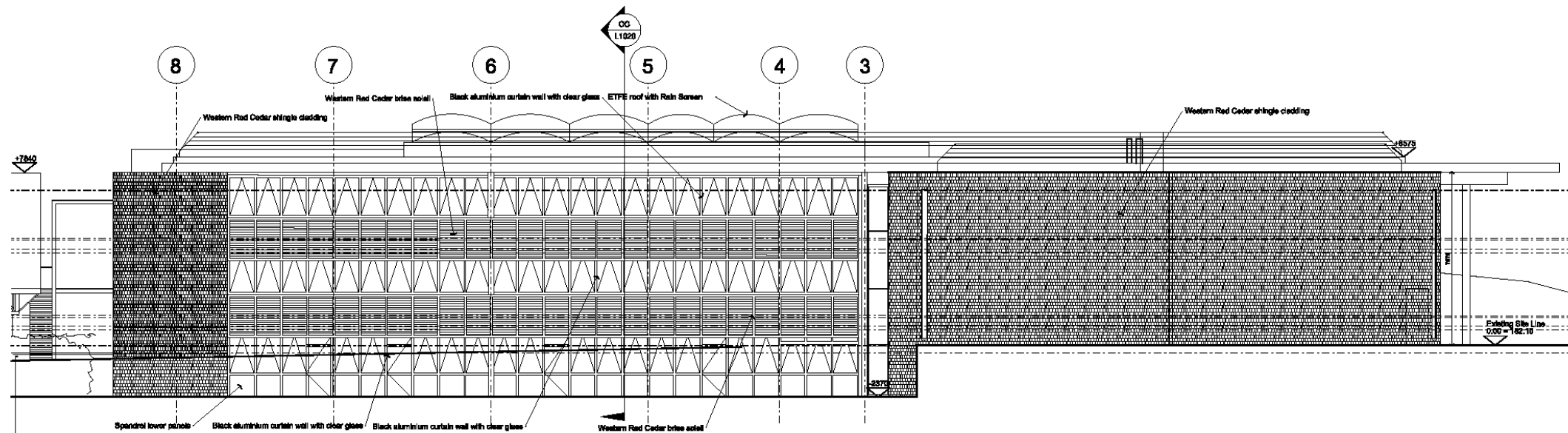
Date issued: 20.03.09
 Drawn by: lab
 Drawing number: A1
 Scale: 1:100
 Checked by: lab
 Job name: BTH7
 Drawing sheet path: L
 Drawing number: 1010
 Building: C



Headed Honor
 20, Woodland
 Bath BA2 9LN
 T +44(0) 1225 644990
 F +44(0) 1225 644991
 www.acp-architects.co.uk



North Elevation




East Elevation

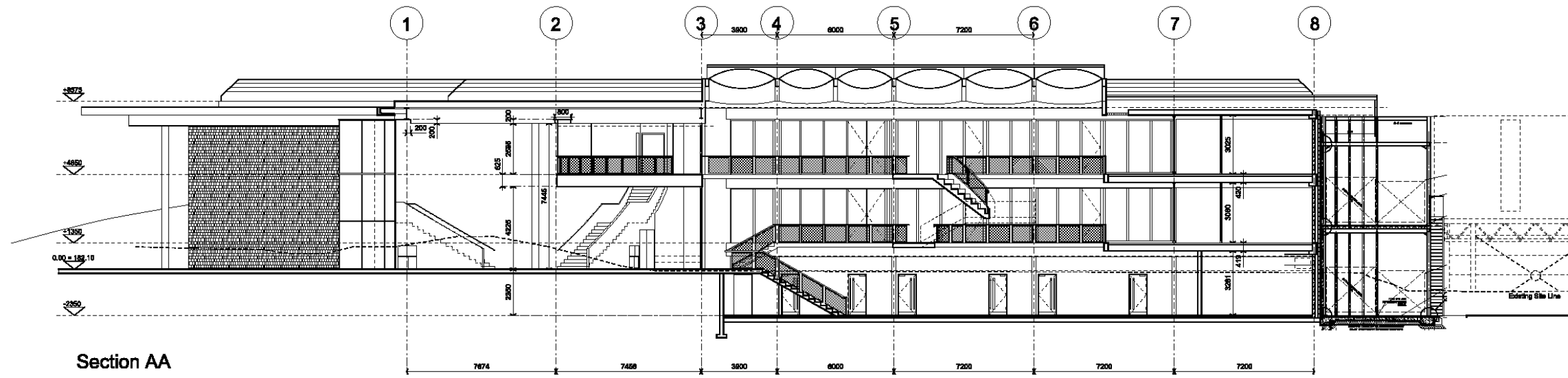
Revision	Date	Author	Checked	Approved
A	20.03.09	ASB/ML	ASB/ML	ASB/ML
B	20.03.09	ASB/ML	ASB/ML	ASB/ML
C	20.03.09	ASB/ML	ASB/ML	ASB/ML

AS BUILT
 East Building
 University Of Bath
 Existing Site Line
 0.00 = 182.10
 East & North Elevations

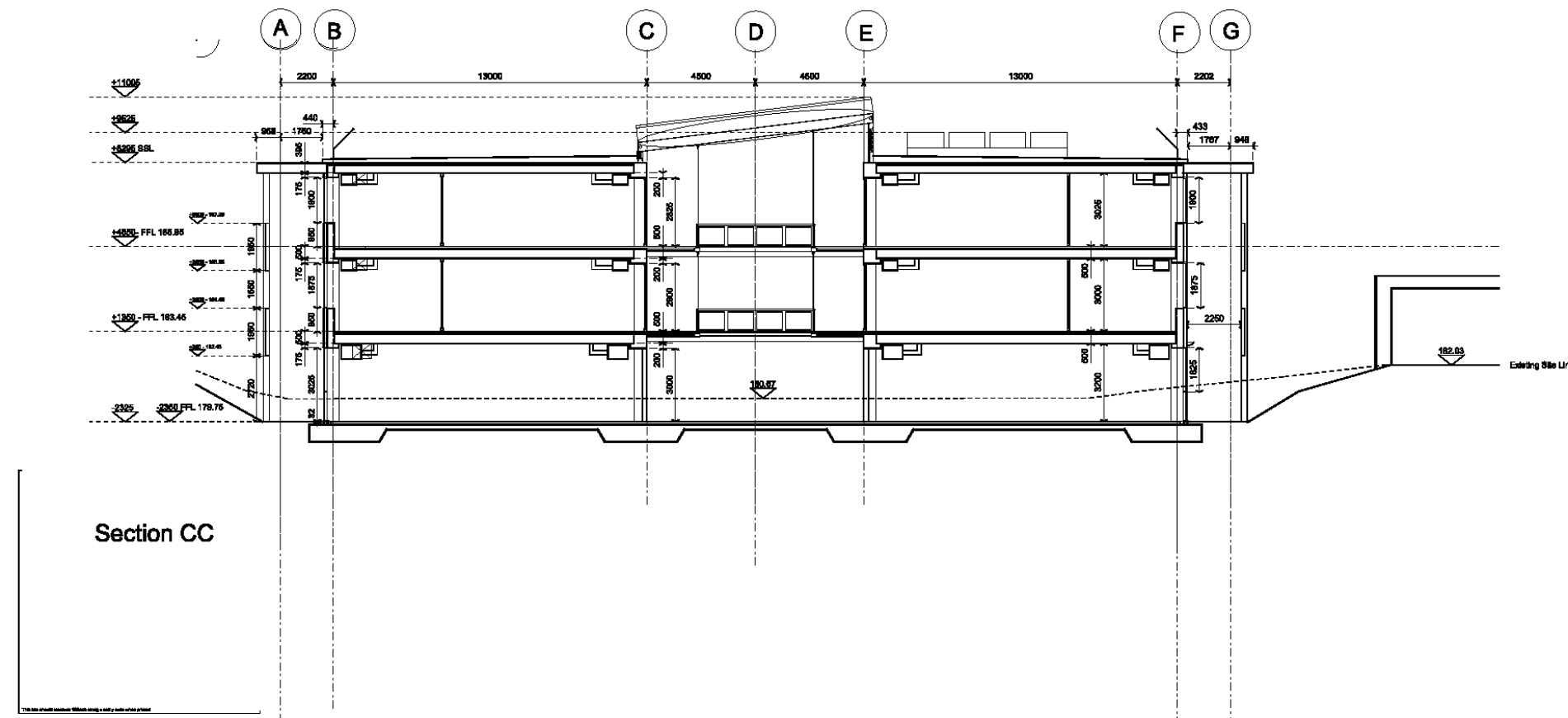
Check all dimensions and verify on site. Report any errors or omissions

Date issued	20.03.09
Drawn by	lob
Checked by	A1
Scale	1:100
Issued by	lob
Job code	BTH7
Drawing number prefix	L
Drawing number	1011
Revision	C


 Qualified Member
 20 Henfield
 Taverham Road, Norwich
 Norfolk, NR11 1JH
 Tel: +44 (0)1603 254410
 Fax: +44 (0)1603 254411
 www.acp.org.uk



Section AA



Section CC

Revision	Date	Author	Check
PA	06.12.08	Structural assessment	DC LOB
PB	08.01.09	Building Plan/Outline	DC LOB
PC	04.03.09	Plant Space Updated	DC LOB
PD	18.03.09	Asium Updated	DC LOB
	17.04.09	Traverse issue	DC LOB
A	07.08.08	Finalize levels added	LOB LOB
B	17.08.08	Finalize finished	DC LOB
C	06.08.10	Structural updated	LOB LOB
D	03.06.10	Drawn revised	LOB LOB
E	02.01.11	As BUILT	LOB LOB

AS BUILT

East Building
University Of Bath

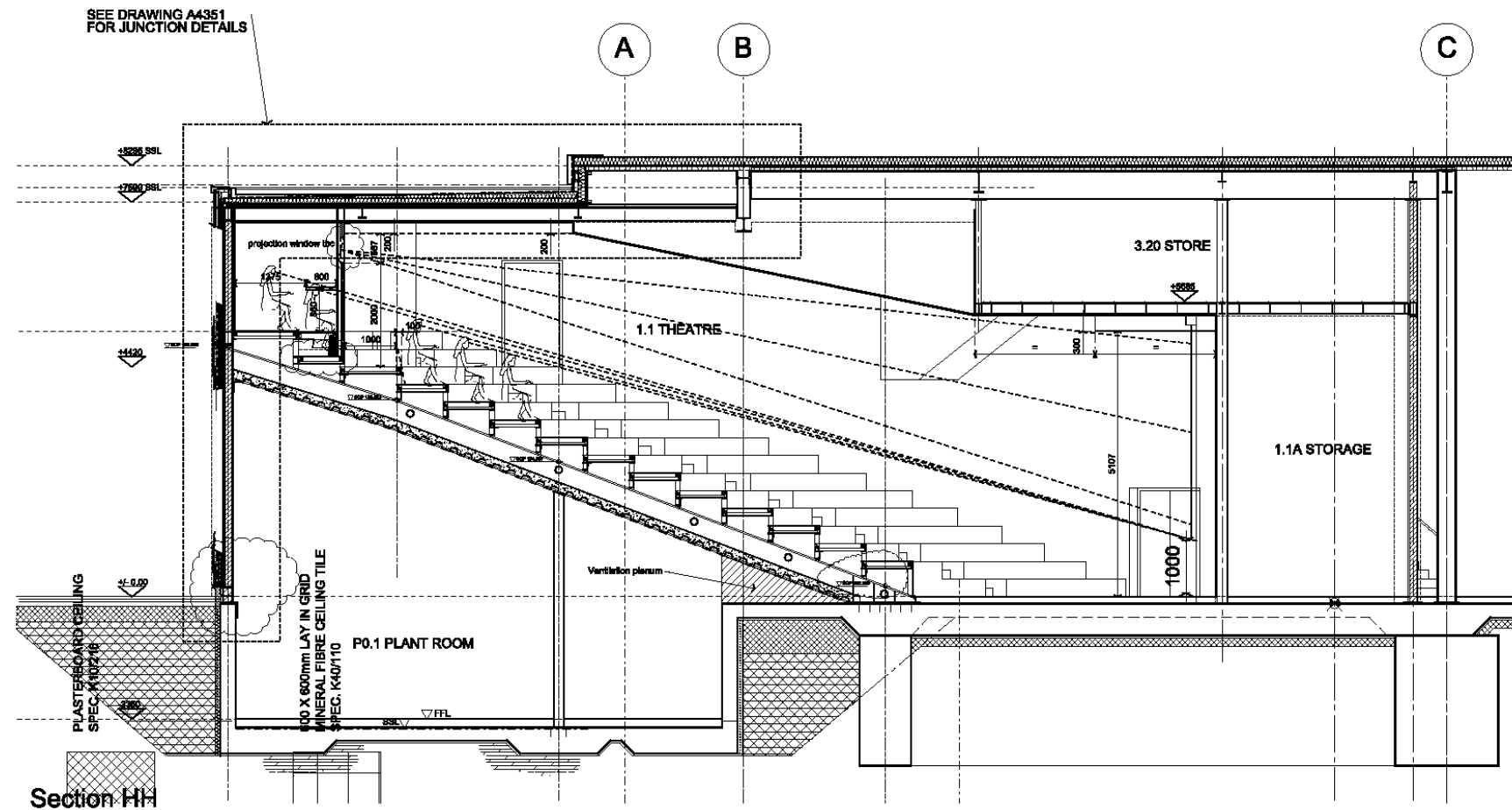
Cross Sections
AA and CC

Check all dimensions and verify on site. Report any errors or omissions

Date: 06.03.09
 Drawn by: dc
 Drawing sheet: A1
 Scale: 1:100
 Issued by: lab
 Job no: BTH7
 Drawing number: L
 Drawing number: 1020
 Scale: E



Upward Manor
 13, Southfield
 Tisbury, Wiltshire BA13 1UN
 T: +44(0) 1753 64483
 F: +44(0) 1753 64483
 info@upwardmanor.co.uk
 www.upwardmanor.co.uk



Revision	Date	Description	By	App'd
A	08.09.09	Colling updated	dc	lo
B	08.09.09	Colling updated and structural steel details added	dc	lo
C	08.09.09	Colling updated and structural steel details added and window glass type corrected	dc	lo
D	08.09.09	All steel 7.50mm	dc	lo

AS BUILT ISSUE

East Building
University Of Bath

Section HH
Grid 2

Check all dimensions and verify on site. Report any errors or omissions

Date issued: 14.09.09
 Drawn by: dc
 Drawing number: A1
 Scale: 1:50
 Reported by: loj
 Job code: BTH7
 Drawing number prefix: L
 Drawing number: 1024
 Revision: E



Headford Moore
33 Broad Street
Bath BA1 1RN
T: +44 (0) 1225 444410
F: +44 (0) 1225 444411
www.headfordmoore.co.uk

Table E. 1 East Building IES model default material properties

	Thickness (mm)	Conductivity (W/m*K)	Density (kg/m³)	Specific heat capacity (J/kg*K)	U-value (W/m²*K)
External walls (standard wall construction 2002 regs)					
Brickwork (outer leaf)	0.1000	0.8400	1700	800	0.3495
Dense EPS slab insulation (like Styrofoam)	0.0585	0.0250	30	1400	
Concrete block (medium)	0.1000	0.5100	1400	1000	
Gypsum plastering	0.0150	0.4200	1200	837	
Internal partitions (13 mm pll 105 mm bri 13 mm pll)					
Plaster (lightweight)	0.0130	0.1600	600	1000	1.6896
Brickwork (inner leaf)	0.1050	0.6200	1700	800	
Plaster (lightweight)	0.0130	0.1600	600	1000	
Exposed floor (standard floor construction 2002 regs)					
London clay	0.7500	1.4100	1900	1000	0.2499
Brickwork (outer leaf)	0.2500	0.8400	1700	800	
Cast concrete	0.1000	1.1300	2000	1000	
Dense EPS slab insulation (like Styrofoam)	0.0635	0.0250	30	1400	
Chipboard	0.0250	0.1500	800	2093	
Synthetic carpet	0.0100	0.0600	160	2500	
Roof (flat roof 2002 regs)					
Stone chippings	0.0100	0.9600	1800	1000	

Felt / bitumen layers	0.0050	0.5000	1700	1000	0.2497
Cast concrete	0.1500	1.1300	2000	1000	
Glass – fibre quilt	0.1345	0.0400	12	840	
Cavity	0.1000				
Ceiling tiles	0.0100	0.0560	380	1000	

Ceiling (Carpeted 100 mm reinforced-concrete ceiling)

Synthetic carpet	0.0100	0.0600	160	2500	2.2826
Cast concrete (dense)	0.1000	1.4000	2100	840	

Wooden doors

Pine (20% moist)	0.0400	0.1400	419	2720	2.1944
------------------	--------	--------	-----	------	--------

	Thickness (mm)	Conductivity (W/mK)	Transmission	Outside reflectance	Inside reflectance	Refractive index	U-value (W/m ² K)
--	----------------	---------------------	--------------	---------------------	--------------------	------------------	------------------------------

Internal glazing (4 mm Pilkington single glazing)

Clear float 4 mm	0.0040	1.0600	0.820	0.070	0.070	1.526	4.2025
------------------	--------	--------	-------	-------	-------	-------	--------

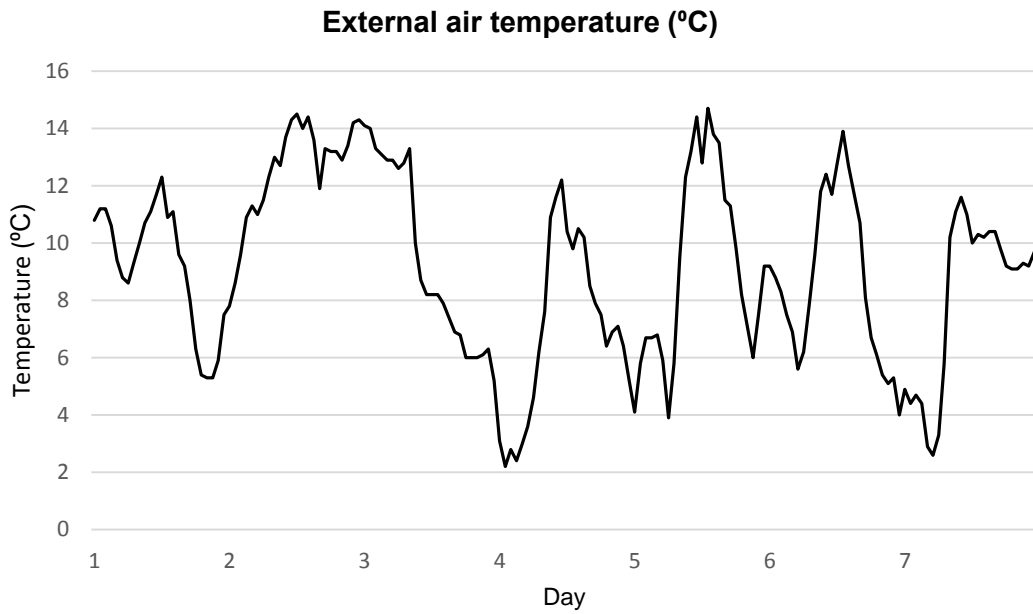


Figure E. 1: External air temperature (°C) for East building modelling

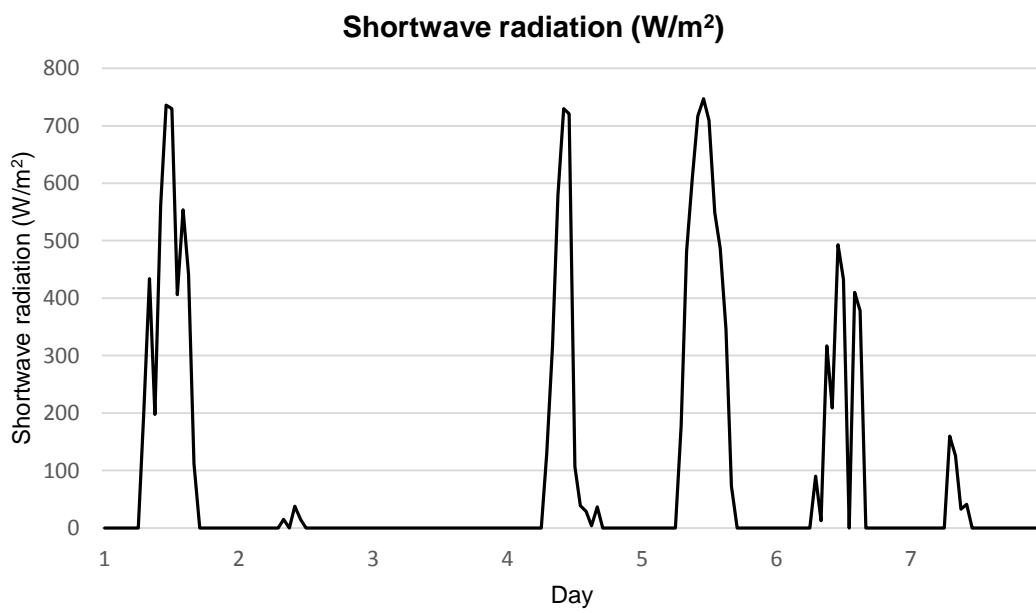


Figure E. 2: Shortwave radiation (W/m²) for East building modelling

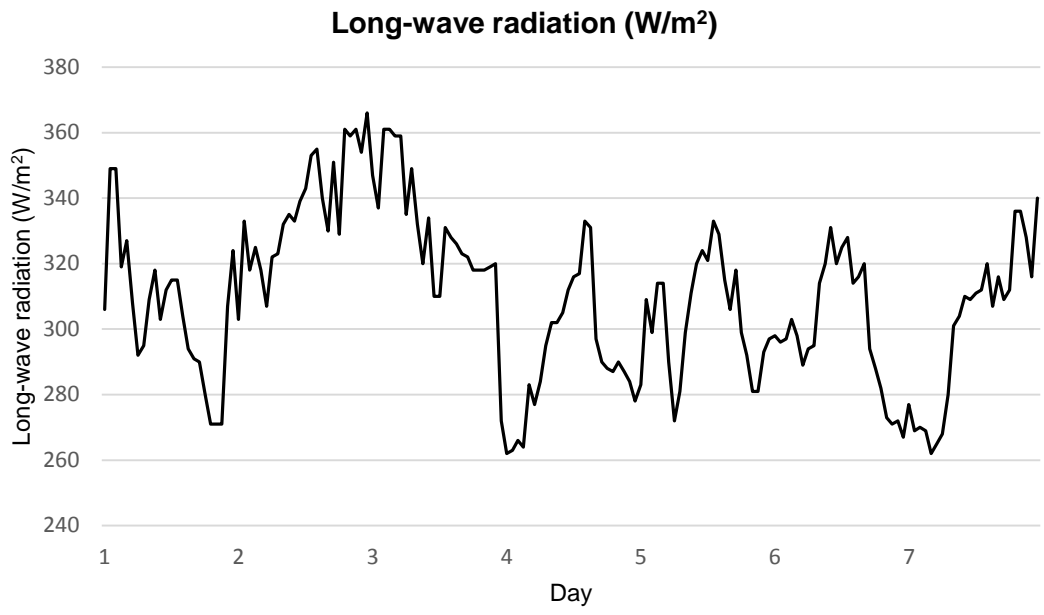


Figure E. 3: Long-wave radiation (W/m²) for East building modelling